520

JOURNAL OF RESEARCH

OF THE U.S. GEOLOGICAL SURVEY

MARCH–APRIL 1977
VOLUME 5, NUMBER 2

Scientific notes and summaries of investigations in geology, hydrology, and related fields

U.S. DEPARTMENT OF THE INTERIOR

UNITED STATES DEPARTMENT OF THE INTERIOR
CECIL D. ANDRUS, Secretary
GEOLOGICAL SURVEY
V. E. McKelvey, Director

For sale by Superintendent of Documents, U.S. Government Printing Office, Washington, DC 20402. Annual subscription rate, $18.90 (plus $4.75 for foreign mailing). Make check or money order payable to Superintendent of Documents. Send all subscription inquiries and address changes to Superintendent of Documents at above address.

Purchase single copy ($3.15) from Branch of Distribution, U.S. Geological Survey, 1200 South Eads Street, Arlington, VA 22202. Make check or money order payable to U.S. Geological Survey.

Library of Congress Catalog-card No. 72-600241.

The Journal of Research is published every 2 months by the U.S. Geological Survey. It contains papers by members of the Geological Survey and their professional colleagues on geologic, hydrologic, topographic, and other scientific and technical subjects.

Correspondence and inquiries concerning the Journal (other than subscription inquiries and address changes) should be directed to Anna M. Orellana, Managing Editor, Journal of Research, Publications Division, U.S. Geological Survey, 321 National Center, Reston, VA 22092.

Papers for the Journal should be submitted through regular Division publication channels.

The Secretary of the Interior has determined that the publication of this periodical is necessary in the transaction of the public business required by law of this Department. Use of funds for printing this periodical has been approved by the Director of the Office of Management and Budget through June 30, 1980.

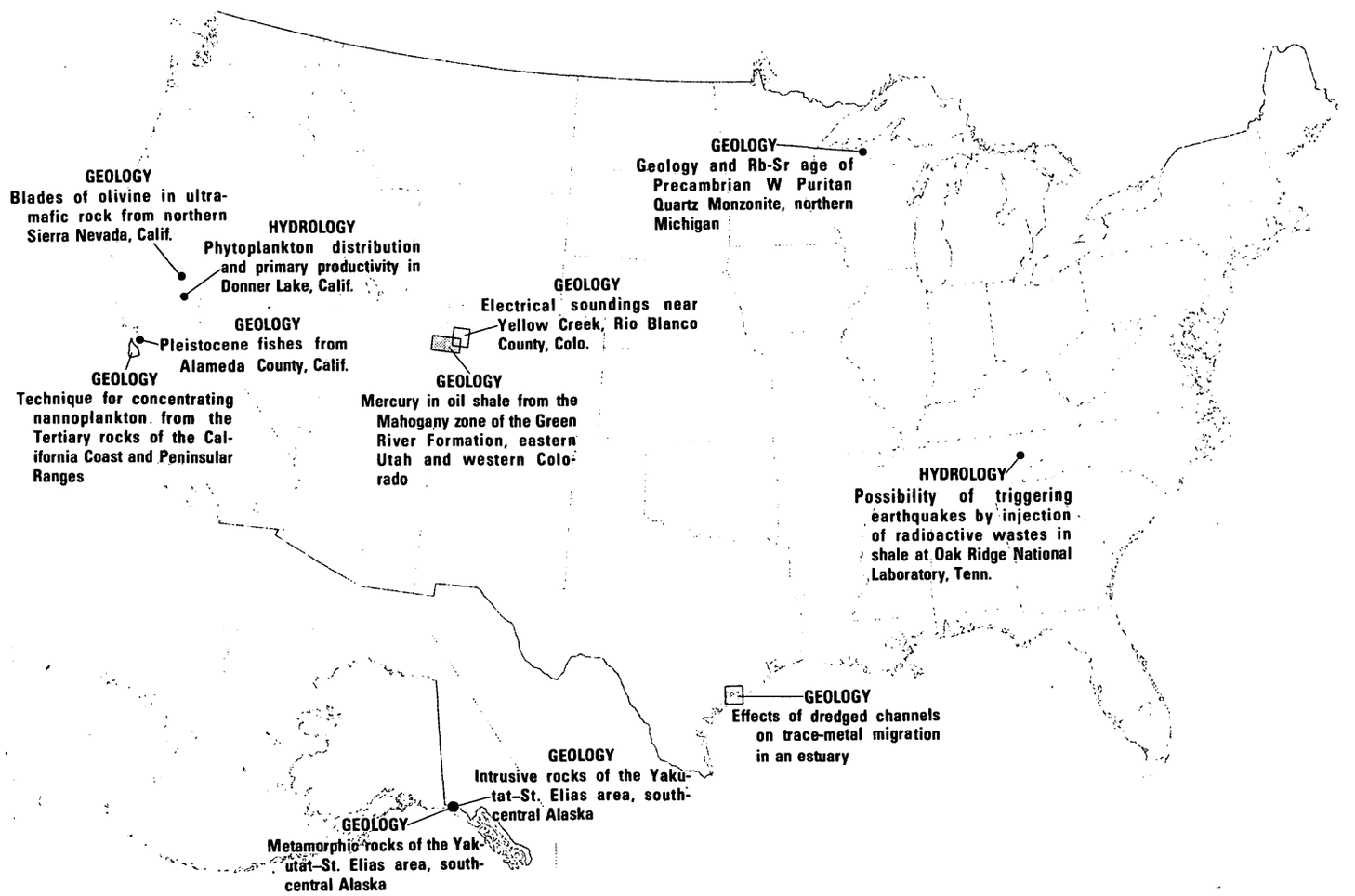

GEOGRAPHIC INDEX TO ARTICLES

See "Contents" for articles concerning areas outside the United States and articles without geographic orientation.

JOURNAL OF RESEARCH

of the

U.S. Geological Survey

Vol 5 No. 2 Mar.–Apr. 1977

CONTENTS

SI units and U.S. customary equivalents II

GEOGRAPHIC STUDIES

Land use and land cover changes—A framework for monitoring ..... *J. R. Anderson* 143

GEOLOGIC STUDIES

Intrusive rocks of the Yakutat–St. Elias area, south-central Alaska ..... *Travis Hudson, George Plafker, and M. A. Lanphere* 155

Metamorphic rocks of the Yakutat–St. Elias area, south-central Alaska ..... *Travis Hudson, George Plafker, and D. L. Turner* 173

Geology and Rb–Sr age of Precambrian W Puritan Quartz Monzonite, northern Michigan ..... *P. K. Sims, Z. E. Peterman, and W. C. Prinz* 185

Electrical soundings near Yellow Creek, Rio Blanco County, Colo ..... *D. L. Campbell* 193

Technique for concentrating nannoplankton from the Tertiary rocks of the California Coast and Peninsular Ranges ..... *S. W. Moore, E. E. Brabb, and A. D. Warren* 207

Pleistocene fishes from Alameda County, Calif ..... *R. W. Casteel and D. P. Adam* 209

Blades of olivine in ultramafic rock from northern Sierra Nevada, Calif ..... *Anna Hietanen* 217

Mercury in oil shale from the Mahogany zone of the Green River Formation, eastern Utah and western Colorado ..... *J. R. Donnell and V. E. Shaw* 221

Activity-product constants of brucite from 10° to 90°C ..... *K. A. McGee and P. B. Hostetler* 227

Removal of fluorine and lithium from hectorite by solutions spanning a wide range of pH ..... *H. C. Starkey, Wayne Mountjoy, and J. M. Gardner* 235

Effects of dredged channels on trace-metal migration in an estuary ..... *C. W. Holmes* 243

HYDROLOGIC STUDIES

Possibility of triggering earthquakes by injection of radioactive wastes in shale at Oak Ridge National Laboratory, Tenn ..... *R. J. Sun* 253

The quantitative determination of chlorophylls *a* and *b* from freshwater algae without interference from degradation products ..... *W. T. Shoaf and B. W. Lium* 263

Phytoplankton distribution and primary productivity in Donner Lake, Calif ..... *A. E. Dong and R. C. Averett* 265

Recent publications of the U.S. Geological Survey ..... Inside of back cover

SI UNITS AND U.S. CUSTOMARY EQUIVALENTS

[SI, International System of Units, a modernized metric system of measurement. All values have been rounded to four significant digits except 0.01 bar, which is the exact equivalent of 1 kPa. Use of hectare (ha) as as alternative name for square hectometer (hm^2) is restricted to measurement of land or water areas. Use of liter (L) as a special name for cubic decimeter (dm^3) is restricted to the measurement of liquids and gases; no prefix other than milli should be used with liter. Metric ton (t) as a name for megagram (Mg) should be restricted to commercial usage, and no prefixes should be used with it. Note that the style of meter^2 rather than square meter has been used for convenience in finding units in this table. Where the units are spelled out in text, Survey style is to use square meter]

SI unit		U.S. customary equivalent	
Length			
millimeter (mm)	=	0.039 37	inch (in)
meter (m)	=	3.281	feet (ft)
	=	1.094	yards (yd)
kilometer (km)	=	0.621 4	mile (mi)
	=	0.540 0	mile, nautical (nmi)
Area			
centimeter^2 (cm^2)	=	0.155 0	inch^2 (in^2)
meter^2 (m^2)	=	10.76	feet^2 (ft^2)
	=	1.196	yards^2 (yd^2)
	=	0.000 247 1	acre
hectometer^2 (hm^2)	=	2.471	acres
	=	0.003 861	section (640 acres or 1 mi^2)
kilometer^2 (km^2)	=	0.386 1	mile^2 (mi^2)
Volume			
centimeter^3 (cm^3)	=	0.061 02	inch^3 (in^3)
decimeter^3 (dm^3)	=	61.02	inches^3 (in^3)
	=	2.113	pints (pt)
	=	1.057	quarts (qt)
	=	0.264 2	gallon (gal)
	=	0.035 31	foot^3 (ft^3)
meter^3 (m^3)	=	35.31	feet^3 (ft^3)
	=	1.308	yards^3 (yd^3)
	=	264.2	gallons (gal)
	=	6.290	barrels (bbl) (petroleum, 1 bbl=42 gal)
	=	0.000 810 7	acre-foot (acre-ft)
hectometer^3 (hm^3)	=	810.7	acre-feet (acre-ft)
kilometer^3 (km^3)	=	0.239 9	mile^3 (mi^3)
Volume per unit time (includes flow)			
decimeter^3 per second (dm^3/s)	=	0.035 31	foot^3 per second (ft^3/s)
	=	2.119	feet^3 per minute (ft^3/min)

SI unit		U.S. customary equivalent	
Volume per unit time (includes flow)—Continued			
decimeter^3 per second (dm^3/s)	=	15.85	gallons per minute (gal/min)
	=	543.4	barrels per day (bbl/d) (petroleum, 1 bbl=42 gal)
meter^3 per second (m^3/s)	=	35.31	feet^3 per second (ft^3/s)
	=	15 850	gallons per minute (gal/min)
Mass			
gram (g)	=	0.035 27	ounce avoirdupois (oz avdp)
kilogram (kg)	=	2.205	pounds avoirdupois (lb avdp)
megagram (Mg)	=	1.102	tons, short (2 000 lb)
	=	0.984 2	ton, long (2 240 lb)
Mass per unit volume (includes density)			
kilogram per meter^3 (kg/m^3)	=	0.062 43	pound per foot^3 (lb/ft^3)
Pressure			
kilopascal (kPa)	=	0.145 0	pound-force per inch^2 (lbf/in^2)
	=	0.009 869	atmosphere, standard (atm)
	=	0.01	bar
	=	0.296 1	inch of mercury at 60°F (in Hg)
Temperature			
temp kelvin (K)	=	[temp deg Fahrenheit (°F)+459.67]/1.8	
temp deg Celsius (°C)	=	[temp deg Fahrenheit (°F)−32]/1.8	

Jour. Research U.S. Geol. Survey
Vol. 5, No. 2, Mar.–Apr. 1977, p. 143–153

LAND USE AND LAND COVER CHANGES—A FRAMEWORK FOR MONITORING

By JAMES R. ANDERSON, Reston, Va.

Abstract.—Information on the rate and kind of change in the use of land resources is essential to the proper planning, management, and regulation of the use of such resources. Starting in 1975, the U.S. Geological Survey has been engaged in mapping and inventory of land use and land cover at a scale of 1:250 000 with plans to change to new 1:100 000 base maps as they become available. Such scales are appropriate for acquiring benchmark or baseline data on land use and land cover on a nationwide basis with a reasonable degree of standardization and accuracy, within a practical time frame of 6 to 7 years, and at a reasonable level of detail in categorization. Changes in land use and land cover occur at highly variable rates from place to place. Thus variations in the intervals between updates of land use and land cover data should be carefully evaluated in order to provide an appropriate frame of reference for the systematic updating of such data. A methodological framework is needed for monitoring changes in land use and land cover that will be timely, relatively inexpensive, and appropriate for widely varying needs at national, interstate-regional, state, multicounty, county, and city levels. In this article a partial framework for monitoring land use and land cover changes is provided with opportunity to extend its use to greater levels of detail in categorization and shorter intervals of frequency when needed for selected areas.

Information on the rate and kind of change in the use of land resources is essential to the proper planning, management, and regulation of the use of such resources. Before land use and land cover changes can be effectively measured and evaluated, a benchmark or baseline mapping and inventory of land use and land cover should be carried out. Starting in 1975, the U.S. Geological Survey has been engaged in the mapping and inventory of land use and land cover at a scale of 1:250 000. As new 1:100 000 maps become available, land use and land cover mapping will be done on that base. These scales are appropriate for acquiring such baseline data on a nationwide basis with a reasonable degree of standardization and accuracy within a practical time frame of 6 to 7 years, and at a reasonable level of detail in categorization (Anderson and others, 1976).

Knowledge about existing land use and rates and trends of change is essential if the Nation is to overcome the problems associated with haphazard and uncontrolled growth; declining environmental quality; loss of prime agricultural lands; destruction of wetlands by industrial, agricultural, residential, and recreational development; and strip mining of coal as a much needed source of energy.

One of the prime requisites for better use of land is information on existing land use and changes in land use with time. The present distribution of agricultural, recreational, and urban land; knowledge of how and where urbanization and other development has been occurring; and data on the proportions of a given area recently devoted to different uses are used by legislators and State and local officials to determine land use policy and by planners to project transportation demand, to identify areas where future development pressure will be greatest, to estimate future infrastructure requirements, and to develop more effective plans for regional development (Anderson and others, 1976).

Information on existing land use and changes in land use is needed for water-resource planning. As land is changed from agricultural or forestry uses to urban uses, surface-water runoff increases in magnitude, flood peaks become sharper, surface- and groundwater quality deteriorates, and water-use increases, thereby reducing water availability. By monitoring and projecting land use trends, it will be possible to develop more effective plans for flood control, water supply, and waste-water treatment.

Land use information must be current. For example, the assessment of recreational needs and opportunities requires knowledge of the location and extent of urban areas and potential recreational lands. This information is used to forecast demand, identify potential solutions, and develop recreation plans. Comprehensive inventories of existing uses of public lands plus the existing and changing uses of adjacent private lands can improve the management of the public lands. Other Federal uses of land use data include assessing the impact of energy-resource development and of water-resource and river-basin planning, managing wildlife

resources, studying changes in the use of lands in the migratory bird flyways, and preparing national overviews of changes in the use of land for national policy formulation.

Another application of land use data is in assessing the impact of natural disasters such as floods. Statistics on the acres of agricultural, urban, and other types of land inundated by floodwaters would be invaluable in estimating damages, future crop losses, and consequent economic impacts.

Many differing viewpoints exist about the role of land use planning and the need to regulate land use at local, State, and Federal levels. Regardless of these differences of opinion, there is a basic need to know how the Nation is currently using its land resources and what changes in land use are occurring. Unless an objective assessment of the current land use situation is made, and unless a process for measuring change is initiated, no one will have the necessary facts to evaluate trends and problems associated with the use of land resources.

PROBLEMS IN MONITORING CHANGES

Changes in land use and land cover occur at highly variable rates from place to place. Some kinds of change also take place in a much shorter time frame than do others. For example, natural reversion of cropland and pasture to forest land in the New England or Great Lakes States occurs over a much longer period of time than change from cropland and pasture to pine plantation in the South. The development of a new residential subdivision or the strip mining of coal in a given location generally takes place within a few months and is easily identified from remotely sensed data. Thus variations in rate of change should be carefully evaluated in order to provide an appropriate frame of reference for the systematic updating of land use and land cover data.

Some changes in land use and land cover are harder to reverse than others or cannot be reversed at all, and hence need to be evaluated differently from those changes in land use and land cover that can be reversed easily. For example, once a city is built up on prime agricultural land, it is quite unlikely that such an area will ever be returned to agricultural uses. Areas that are strip mined can be revegetated and restored but at considerable cost and generally with some loss in productivity for agricultural and forestry uses. The plow-up of rangeland and pasture for cropland in the western Great Plains in recent years in response to high wheat prices can be reversed by reseeding to rangeland or pasture but at some cost and after soil loss has occurred during periods of drought.

Marked changes in land cover and land use that may occupy a relatively small area often have an impact far beyond the area where an actual change in cover or use takes place. A new residential development with increased demands for urban services may result in higher taxes over an entire county and the viability of agricultural activities in that county may be severely damaged as a result. Interstate highways that have been built over the past 20 years occupy only about 0.8 million hectares (2 million acres) of land but have created a strong impetus for land use changes involving new alinements of residential, commercial, and industrial activities, development of campgrounds and campsites, and the creation of new recreational opportunities in formerly remote areas.

METHODOLOGICAL FRAMEWORK NEEDED

A methodological framework is needed for monitoring changes in land use and land cover that will be timely, relatively inexpensive, and appropriate for widely varying needs at national, interstate-regional, state, multicounty, county, and city levels. Recognition of the need for varying levels of information about land use and land cover is essential if local, State, and Federal users of such information are to avoid excessive duplication in the acquisition of basic information about land resources and their use.

The rapidly developing technology of remote sensing offers an efficient and timely approach to the mapping and collection of basic land use data. Such technology offers a wide range of capabilities at the present time and it is likely that more sophisticated techniques will be available in the future. Capabilities at the present time include:

1. Multispectral scanner data available from Landsat over extensive areas on a repetitive basis that may be as frequent as every 9 to 18 days.
2. High-resolution color-infrared aerial photography being acquired from high-altitude platforms such as the U–2. Such photography is generally being acquired on any given flight for areas of only several thousand square miles and at frequencies ranging from 1 to 10 years or longer.
3. Panchromatic, color-infrared, and color aerial photography is being obtained by using relatively low altitude flights that generally cover a county or less on any one mission or contract. Black-and-white photography has been acquired by the Agricultural Stabilization and Conservation Service of the U.S. Department of Agriculture

(1975) for agricultural and some adjacent areas generally at intervals of 7 years or more. Photography has also been acquired from flights funded by the U.S. Geological Survey and other Federal agencies, by State and local agencies, as well as by private corporations and individuals for a wide variety of specific purposes.

Given this range in the availability and characteristics of remotely sensed data, the methodological framework for monitoring land use and land cover changes should be designed to make maximum use of these complementary sources of data. It is also extremely important to recognize that remotely sensed data will not provide all the land use information that may be wanted by a specific user. Supplemental sources of information are available and should be used when land use and land cover data are being collected. Even expensive field mapping may be necessary for some purposes.

Remote sensing technology alone is not adequate for the efficient and timely generation of land use and land cover maps and data. A geographically oriented information system employing a wide range of sophisticated computer technology must also be recognized as a major asset by many but not necessarily all users of land use and land cover information. For the user who wants a land use map and land use statistics for a limited area on a one-time basis, the computer technology now available is likely to be of limited value. For the user who is faced with the problem of developing a set of baseline maps and data pertaining to land use and land cover, must update such maps and data from time to time, and must relate several sets of data about land and its use (soils, slope, value, taxation rates, and so forth), the use of an information system with the capability for inputting, storing, retrieving and manipulating data spatially or geographically on an electronic computer will be an invaluable asset.

The approach to the monitoring of changes in land use and land cover taking place over time follows in general the basic approaches to the baseline mapping and collection of land use and land cover data previously cited (Anderson and others, 1976).

HISTORICAL PERSPECTIVE

Great diversity existed in the natural or relatively undisturbed vegetation of the United States at the time settlement by Europeans began to occur. Forest, grassland, and desert shrub were the three major divisions of natural vegetation. The relative area of the original major divisions of vegetation in what now comprises the 48 conterminous States is shown in table 1.

TABLE 1.—*Natural vegetation: original areas of the major divisions*
[From Shantz and Zon, 1924]

Type of vegetation	Acres (millions)		Square miles (thousands)		Percentage
Forest:					
Hardwood	400		625		21
Coniferous	419		655		22
Woodland (arid)	95		148		5
		914		1428	48
Grassland:					
Tall Grass (Prairie)	304		475		16
Shortgrass (Plains)	267		417		14
Other Grasses	152		238		8
		723		1130	38
Desert:					
Northern Desert Shrub	190		297		10
Southern Desert Shrub	76		119		4
		266		416	14
Total		1903		2974	100

This original pattern of natural vegetation has undergone tremendous change since early European settlement, and today the original land cover that has remained relatively undisturbed has shrunk considerably. Clearing land for agricultural and for urban and built-up uses has been continuous since colonial times. The original forests of the United States covered an estimated 331 million hectares (819 million acres), not including 38 million hectares (95 million acres) of arid and other woodland. Only about 10 million hectares (25 million acres) were cleared before the American Revolution. Over the next 100 years about 61 million hectares (150 million acres) of forest land in the eastern part of the United States had been cleared for agricultural uses. Since 1880, at least another 40 million hectares (100 million acres) of forest land have been cleared for farming. In the West, 2 to 3 million hectares (6 to 7 million acres) of arid woodland were cleared for irrigated agriculture, and another 10 to 12 million hectares (25 to 30 million acres) of forest land in the West were cleared for nonirrigated agriculture. At least 12 to 16 million hectares (30 to 40 million acres) of cleared forest land are now used for cities, roads, and other built-up or developed areas.

Altogether about 136 to 142 million hectares (335 to 350 million acres) of originally forested land were cleared for farming and other nonforest uses. Probably as much as 30 million hectares (75 million acres) of formerly cleared land have reverted to forest and brush and hence are no longer in agricultural uses (U.S. Department of Agriculture, 1958, p. 409–415). Much land has been cleared more than one time.

Natural grasslands have also shrunk greatly in extent due to the plow-up for agricultural purposes, particularly for the production of corn, soybeans, and wheat and other small grains. Approximately 97 million hectares (240 million acres) of the original 293 million hectares (723 million acres) of grassland are now being used as cropland (based on estimated area

of present cropland located in areas of original grassland). Additional areas of natural grassland have also been converted to pasture with introduced grasses. Desert areas have also been irrigated for agricultural production. In the early 1970's cropland reseeded to rangeland and pasture cover in the 1950's and 1960's and earlier has been replowed and converted to cropland.

In Alaska the original natural vegetation was very much as it is today, as shown in table 2. In 1969 the Economic Research Service reported less than 40 000 hectares (100 000 acres) being used in Alaska as cropland and less than 121 000 hectares (300 000 acres) in urban areas and transportation uses (Frey, 1973).

In Hawaii the potential natural vegetation consisted of (1) sclerophyllous forest, shrubland, and grassland, (2) guava mixed forest, (3) ohia lehua forest, (4) lama manele forest, (5) koa forest, (6) koa mamani parkland, and (7) microphyllous shrubland. Barren lava areas were, and are, also present (Kuchler, 1970). Within the past 100 years, sugarcane and pineapple plantations have replaced extensive areas of natural vegetation. Urban or built-up uses of land have also expanded considerably, particularly on Oahu since 1940.

During the first half of the present century, changes in land use and land cover continued to take place. Cropland area increased in some regions, but declined markedly in others. Major reversions of cropland to forest land occurred particularly in New England, Appalachia, and the southern Piedmont. Urbanization absorbed cropland during this period, but not nearly as much as was reverting to forest land and not at nearly so rapid a pace as after 1950. Cropland also reverted to grassland over extensive areas of the Great Plains after disastrous drought conditions in the 1930's.

Since the 1940's, land use and land cover changes of several kinds have been occurring. Some of the more significant of these changes are listed in table 3. Table 4 and figure 1 show the extent and regional distribution of changes in the very important cropland base of the Nation on which we depend heavily for food and fiber production for domestic consumption as well as for export to other nations in exchange for petroleum, minerals, pulp and paper, foodstuffs, and other products. It is obvious from the data presented in table 4 and figure 1 that there is much variation in the increases and decreases of the cropland base that are taking place within and among the major farm production regions of the United States (figure 2). The monitoring of such changes is a significant component of keeping land use and land cover data current at the present time.

Urbanization since World War II has resulted in significant shifts in land use and land cover in some parts of the country while having very little impact in other parts. Although the actual total area of expansion in urban or built-up land is not as great as many believe it to be, the impact of urban development generally reaches far beyond the actual area being built up (Zeimetz and others, p. 24). Most but not all of the expansion involving urban or built-up land is occurring in metropolitan areas. Counties included in the Standard Metropolitan Statistical Areas are shown as figure 3.

TABLE 2.—*Land and water cover in Alaska, 1973*
[From Joint Federal-State Land Use Planning Commission for Alaska, 1973]

	Acres (millions)		Square miles (thousands)		Percentage
Forest Land:					
Coastal Western Hemlock–Sitka Spruce	23		35		6
Bottomland Spruce–Poplar	18		28		5
Upland Spruce–Hardwood	65		101		17
Lowland Spruce–Hardwood	35		55		9
		140		219	37
Tundra:					
Moist	66		102		17
Wet	33		51		9
Alpine	85		133		23
		183		286	49
Brush Land:					
High Brush	18		28		5
Low Brush, Muskeg-Bog	10		16		3
		28		44	8
Glaciers and Ice Fields	11		17		3
Lakes	5		8		1
Riverine Areas	8		12		2
Total	375		586		100

TABLE 3.—*Significant kinds of changes in land use and land cover occurring since the 1940's*

From	*To*
Agricultural Land	Wetland.
	Rangeland.
	Forest Land.
	Reservoirs.
	Strip Mines, Quarries, and Gravel Pits.
	Urban or Built-Up Land.
Forest Land	Cropland and Pasture, Orchards, Groves, Vineyards, and so forth.
	Reservoirs.
	Strip Mines, Quarries, and Gravel Pits.
	Urban or Built-Up Land.
Rangeland	Cropland and Pasture, Orchards, Groves, Vineyards, and so forth.
	Reservoirs.
	Strip Mines, Quarries, and Gravel Pits.
	Urban or Built-Up Land.
Wetland	Cropland and Pasture.
	Reservoirs.
	Urban or Built-Up Land.
Barren Land	Reservoirs.
	Urban or Built-Up Land.

TABLE 4.—*Total cropland, change in cropland, and number of counties showing changes by regions, 1944–64*
[From Krause (1970, p. 6)]

Region	Total cropland in millions of acres		Increase		Decrease [1]		Regional net change in millions of acres
	1944	1964	Number of counties	Acres (millions)	Number of counties	Acres (millions)	
Northeast	22.7	15.8	4	0.1	240	7.0	−6.9
Lake States	41.3	39.5	72	1.2	169	2.9	−1.8
Corn Belt	80.9	82.1	288	4.6	208	3.3	+1.3
Northern Plains	92.3	93.5	132	4.7	188	3.5	+1.2
Appalachian	26.7	18.8	20	.1	450	8.1	−8.0
Southeast	24.5	15.0	35	1.0	304	10.6	−9.5
Delta	18.7	15.1	42	1.6	179	5.2	−3.6
Southern Plains	45.4	38.3	78	2.8	253	9.9	−7.1
Mountain	30.5	36.9	150	8.0	127	1.5	+6.4
Pacific	20.2	21.4	47	2.6	86	1.4	+1.2
48 States	403.2	376.5	868	26.7	2,204	53.5	−26.8

[1] Or no change.

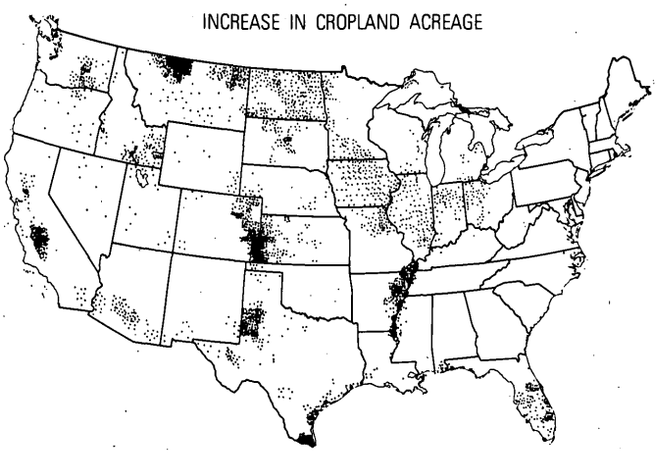

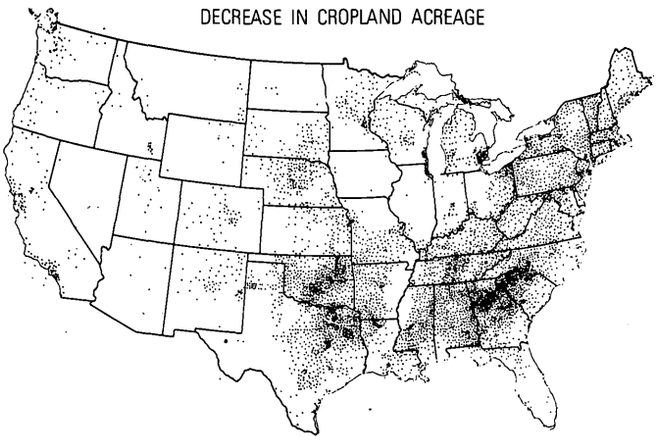

FIGURE 1.—Cropland acreage changes, 1944–64. Cropland acreage includes cropland harvested, failed, summer fallowed, idle, or in soil improvement crops only and excludes cropland pasture. One dot indicates a 10 000-acre increase or decrease in counties which had a net increase or decrease in cropland acreage. Source of cropland acreage data taken from the "U.S. Census of Agriculture" for 1944 and 1964. From Krause (1970, p. 7).

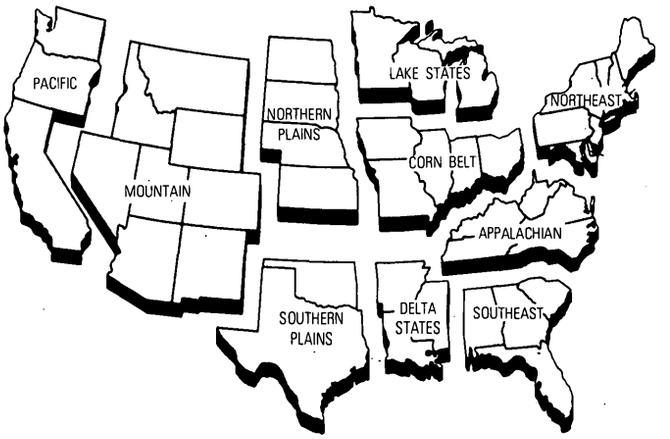

FIGURE 2.—Farm production regions. From Otte (1974, p. 2).

In tables 5 and 6 indication of the regional distribution of the amount of land in urban or built-up areas and the kind of changes that took place between 1950 and 1970 are shown. Such changes continue to occur and are worthy of careful and selective monitoring now and in the future. For many purposes a much more detailed monitoring of the changes that are occurring is needed. Not only do changes between additional categories of land use and land cover need to be monitored, but the location of such changes needs to be identified for some planning, management, and regulatory purposes.

SOME GENERAL GUIDELINES FOR MONITORING CHANGES IN LAND USE AND LAND COVER

Many differences in need exist among users of land use and land cover data for the updating of such data, but the following guidelines should be helpful in providing more timely and useful monitoring of land use

and land cover changes at less cost per unit of area being monitored.

1. More reliance ought to be placed on using remote sensing technology for the primary land use and land cover mapping and data-collection process because of the economies that can be realized in the mapping and acquisition of such data. Such an approach to mapping and data collection can be effectively complemented by use of other data sources if a carefully developed plan for the integration of data from different sources is developed in advance. For relatively small areas, field mapping may be a preferable approach.
2. Use of different kinds of remote sensor data may provide the best approach to monitoring of changes in land use and land cover, particularly over extensive areas. At the present time in the U.S. Geological Survey, experimental studies are being undertaken to determine how data acquired from Landsat and high-altitude aircraft can be interfaced for the efficient updating of land use and land cover mapping that is now being done by that agency.
3. The seasonal selection of remotely sensed data for mapping and measuring changes in land use and land cover will vary from place to place and from one type of change to another. For example, strip-mining activity will probably be most appropriately monitored in late autumn or early spring in West Virginia, but in western coal regions the seasonal selection might also include summer months.
4. The minimum unit selected for the mapping and collection of land use and land cover data and the level of detail in categorizing land use ought to be kept at the smallest scale compatible with survey needs in order to minimize time and cost of data collection and updating.
5. Many users of land use and land cover data have a need for knowing what kind of land use or cover change has occurred—that is, what was the land use before and after the change. This need argues strongly for a complete or 100-percent selective updating of only a few categories. However, such a guideline is much more applicable in some situations than others. For example, the recent change from rangeland and pasture to cropland in the western Great Plains dominates so completely the kind of land cover changes taking place that other changes are relatively unimportant. On the other hand, the diversity of significant changes likely to occur within a metropolitan area makes complete monitoring more desirable for most users of land use and land cover data in such areas.
6. Qualitative or quantitative review (if complementary data sources exist) of the kind and relative importance of changes likely to be expected should precede detailed land use and land cover mapping and data collection. Such review may consist of low-altitude light-aircraft reconnaissance or ground traverses of areas such as cities, counties, or Standard Metropolitan Statistical Areas.

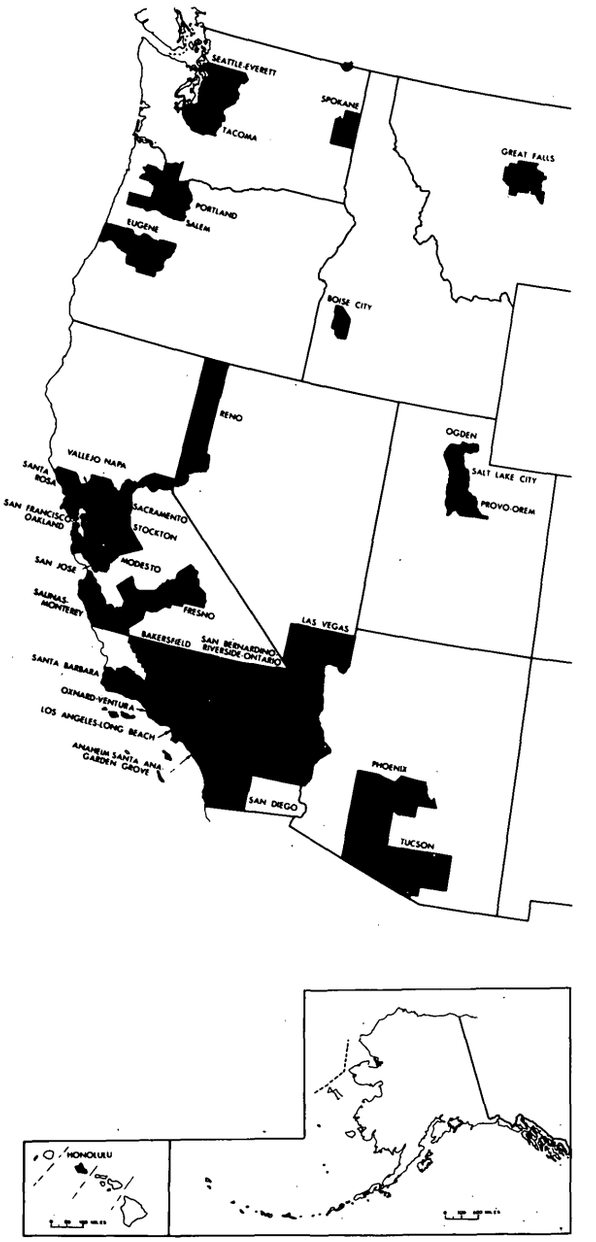

FIGURE 3.—Standard Metropolitan

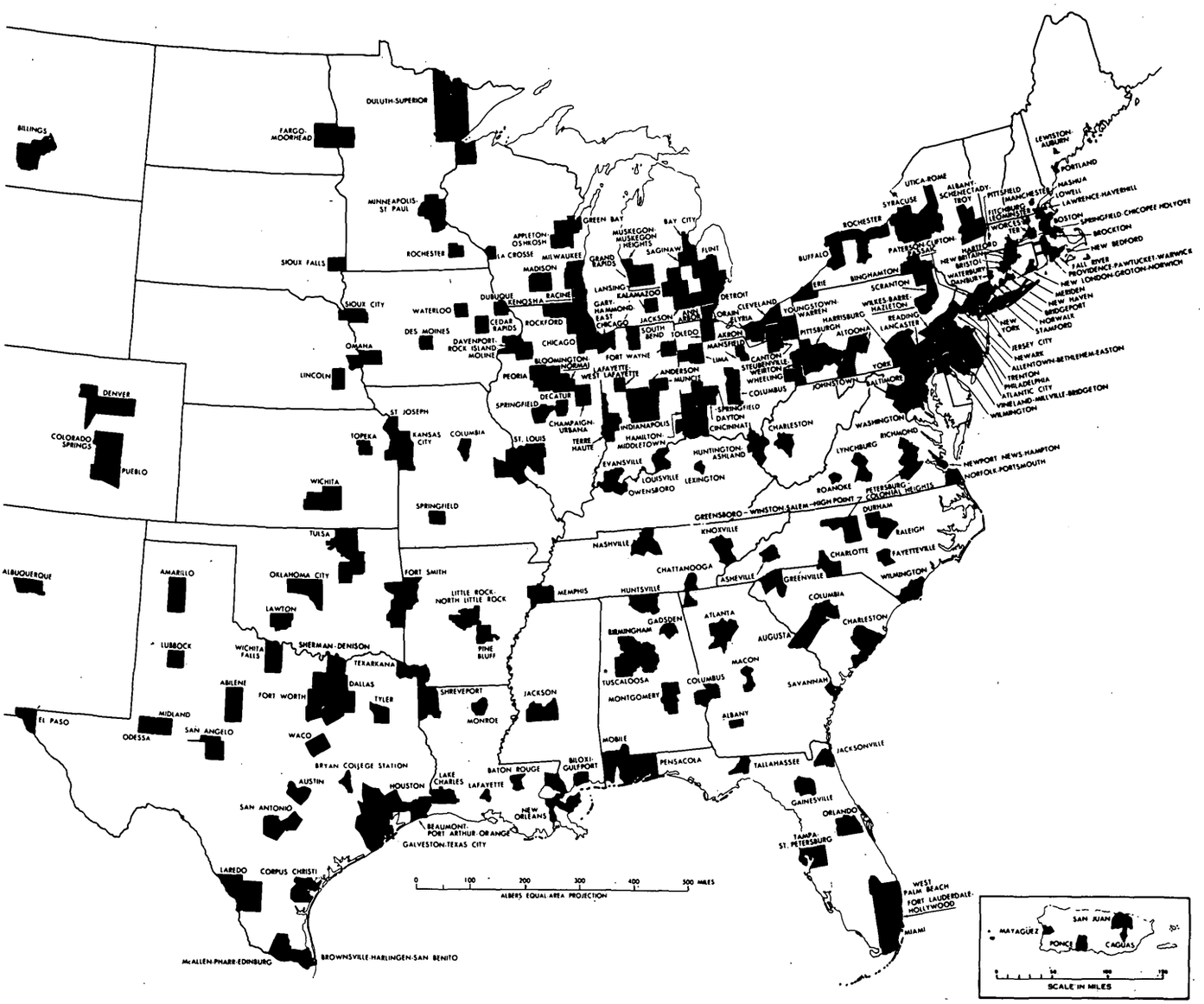

Statistical Areas; areas defined by Office of Management and Budget, February 1971. From Otte (1974, p. 4).

7. For those applications which require information about the nature of changes and the degree of change, but not necessarily the exact spatial location in which all individual changes occur, sampling ought to be considered as an alternative to complete detailed compilation. Acceptable statistical estimation may be adequate for specific applications, and use of such sampling procedures may also offer an effective method for the selection of areas needing much more detailed attention.

8. Careful selection of the minimum mapping unit most appropriate for the level of categorization and the kind of land use and land cover changes being monitored is important.

9. Only those areas actually undergoing change from one land use or land cover type to another need to be mapped. Mapping of changes is less costly than complete remapping. In figure 4, a part of the map of the Washington, D.C., area showing changes in land use by type of change from 1970

TABLE 5.—*Area, in thousands of acres, for selected urban and built-up uses, by Farm Production Regions, 1950–70*

[From Wooten, 1953a; Wooten 1953b, p. 33–36; Frey, 1973, p. 37–38. N.A., data not available]

Region [1]	1950			1970		
	Urban areas	Highways and railroads [2]	Farmsteads [2]	Urban areas	Highways and railroads [2]	Farmsteads, farm roads, and lanes [3]
Northeast	4 126	1 921	799	7 282	2 037	386
Lake States	1 784	2 769	1 330	3 040	3 008	1 008
Corn Belt	2 950	3 467	2 334	5 594	3 727	2 067
Northern Plains	514	4 033	1 174	833	3 495	1 135
Appalachian	1 330	1 713	1 115	3 022	2 109	842
Southeast	1 876	1 566	655	3 832	2 318	522
Delta States	841	1 061	699	1 432	1 182	595
Southern Plains	1 269	1 800	925	3 288	2 305	767
Mountain	867	2 848	616	1 736	3 597	578
Pacific	2 722	1 702	631	4 331	1 927	495
48 States	18 279	22 880	10 278	34 390	25 705	8 395
Alaska	N.A.	N.A.	N.A.	59	208	3
Hawaii	N.A.	N.A.	N.A.	141	40	22
50 States	N.A.	N.A.	N.A.	34 590	25 953	8 420

[1] Data are also available by State from Wooten (1953b) and Frey (1973).
[2] Rural areas only.
[3] Data for 1950 and 1970 are not exactly comparable.

TABLE 6.—*Increases in selected urban and built-up uses, by Farm Production Regions, 1950–70*

[Wooten, 1953b, p. 9–11, 33–36; Frey, 1973, p. 23–24, 37–38. N.A., data not available]

Region [1]	Total increase in urban areas 1950–70 (thousands of acres)	Percentage of total land area in the region in urban and transportational use		Average annual rate of change 1950–70 (thousands of acres)
		1950	1970	
Northeast	3 156	5	8	158
Lake States	1 256	3	4	63
Corn Belt	2 644	3	5	132
Northern Plains	319	2	2	16
Appalachian	1 692	2	4	85
Southeast	1 956	2	4	98
Delta States	591	2	2	30
Southern Plains	2 019	1	2	101
Mountain	869	1	1	44
Pacific	1 609	2	3	81
48 States	16 111	2	3	806
Alaska	N.A.	N.A.	(2)	N.A.
Hawaii	N.A.	N.A.	4	N.A.
50 States	N.A.	N.A.	2	N.A.

[1] Data are also available by State from Wooten (1953b) and Frey (1973).
[2] Less than 0.1 of 1 percent.

to 1972 illustrates this approach to mapping of land use and land cover changes.

10. Thorough and careful documentation of the initial compilation of land use and land cover data from remote sensor sources as well as of the identification of land use and land cover changes is essential for accurate and useful mapping and data acquisition from such sources.

TEMPORAL AND REGIONAL GUIDELINES FOR MONITORING CHANGES IN LAND USE AND LAND COVER

It is impossible to establish temporal and regional guidelines for monitoring land use and land cover changes that will be satisfactory for all users. However, information presented in tables 4, 5, and 6, and figures 1 and 3, along with information from other sources provides general guidelines as presented in tables 7 and 8 (Averitt, 1970, p. 23; Clawson, 1972, p. 154–156; U.S. Department of Agriculture, 1974, p. vii). At municipal and county levels many diverse factors will dictate the need and capability for monitoring land use and land cover changes.

The guidelines presented in table 7 are based mainly on the historical and regional patterns of change since World War II and on projected national patterns to the year 2000 (U.S. Department of Agriculture, 1974, p. vii). In some instances regional variations based on historical patterns are not the same as those likely to be significant in the future. The accelerated stripping of coal in western coal regions has been recognized in table 8, for example. Changes in the significance of urbanization. which is likely to accelerate in the Southeast and Southwest and is slowing down in the Northeast and Midwest, are also reflected in the table.

The time between updating the mapping and measurement of land use and land cover changes shown in table 8 may vary with time. For example, in the 1950's, citrus acreage was expanding rapidly in central Florida and annual changes were watched closely. In the 1960's, the area in citrus groves stabilized and a longer time between updating became acceptable. In the 1950's, after severe drought in parts of the Great Plains, conversion of cropland to rangeland accelerated markedly with annual monitoring needed for some purposes. In the 1960's, little change occurred. As wheat prices soared in the 1970's a plow-up of rangeland brought a resurgence of interest in land use changes along the western margin of the Plains. When

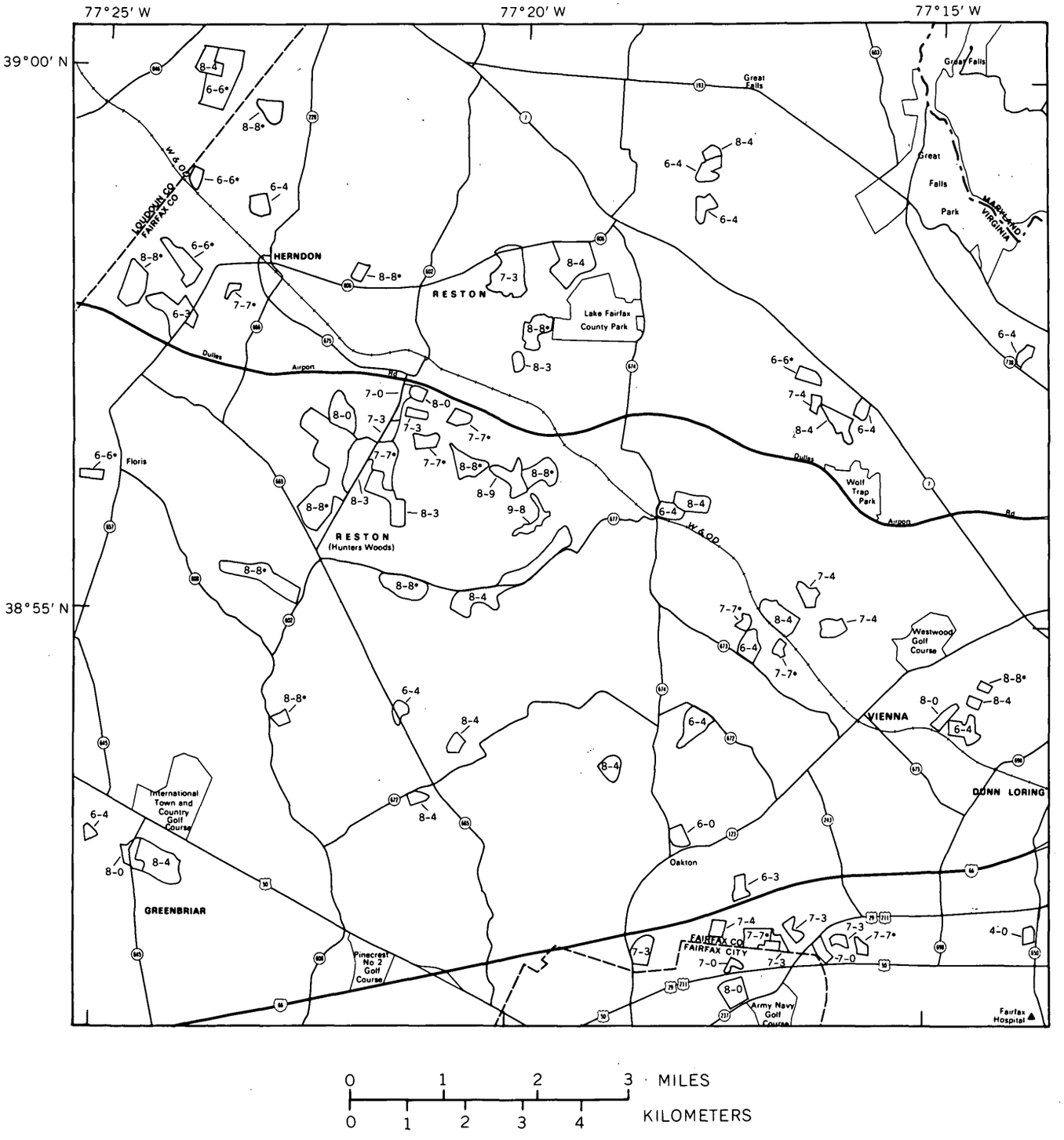

FIGURE 4.—Selected area within Fairfax County, Va., taken from the map of Washington urban area, District of Columbia, Maryland, and Virginia, showing land use and land cover change between 1970 and 1972. Modified from U.S. Geological Survey (1975).

the kinds of changes indicated in table 8 are related to economic and environmental concerns, the frequencies suggested for mapping and measuring land use and land cover changes appear to be reasonable in relation to the available capability to monitor such changes.

The potential value of Landsat data for consistent mapping and measuring spatial and temporal changes in land use and land cover for a wide range of users has not been fully demonstrated at this time. However, the need for a remote sensor capable of periodically

TABLE 7.—*Significance of land use and land cover changes by Farm Production Regions, 1950–70*

[1, regionwide significance; 2, multicounty significance; 3, locally significant; 4, little or no significance]

Land use and land cover changes														
From	To	Northeast	Lake States	Corn Belt	Northern Plains	Appalachian	Southeast	Delta States	Southern Plains	Mountain	Pacific	Alaska	Hawaii	50 States
Agricultural land	Wetland	3	3	4	4	4	3	3	4	4	4	4	4	4
	Rangeland	4	4	4	2	4	4	4	2	2	4	4	4	4
	Forest Land	1	2	2	4	1	2	2	2	4	4	3	4	2
	Reservoirs	3	3	3	2	3	3	2	2	4	4	4	4	3
	Strip Mines, Quarries, and Gravel Pits.	3	3	2	3	3	3	4	3	3	4	4	4	3
	Urban or Built-Up Land	2	2	2	4	2	2	3	2	3	2	4	2	2
Forest Land	Cropland and Pasture, Orchards, Groves, Vineyards, and so forth.	4	4	3	4	4	2	2	4	4	4	4	4	3
	Reservoirs	3	3	3	4	2	2	2	3	3	3	4	4	3
	Strip Mines, Quarries, and Gravel Pits.	3	3	3	4	2	3	4	4	4	4	4	4	3
	Urban or Built-Up Land	2	2	2	4	3	2	3	3	4	3	4	4	3
Rangeland	Cropland and Pasture, Orchards, Groves, Vineyards, and so forth.	4	4	4	3	4	4	4	2	2	2	4	4	3
	Reservoirs	4	4	4	2	4	4	4	2	3	3	4	4	3
	Strip Mines, Quarries, and Gravel Pits.	4	4	4	3	4	4	4	3	3	4	4	4	4
	Urban or Built-Up Land	4	4	4	4	4	4	4	3	3	3	4	4	4
Wetland	Cropland and Pasture	4	4	2	2	4	2	2	4	4	4	4	4	3
	Reservoirs	4	4	4	4	4	3	3	4	4	4	4	4	4
	Urban or Built-Up Land	4	4	4	4	4	3	3	4	4	4	4	4	4
Barren Land	Reservoirs	4	4	4	4	4	4	4	4	3	3	4	4	4
	Urban or Built-Up Land	4	4	4	4	4	4	4	4	3	3	4	4	4

TABLE 8.—*Guidelines for monitoring frequency of land use and land cover changes*

Land use and land cover changes		Nationwide, interstate, regional, and statewide changes		Standard Metropolitan Statistical Areas and other selected intrastate regional areas		
From	To	5–7 years	8–12 years	Less than 4 years	5–7 years	8–12 years
Agricultural Land	Wetland		×			×
	Rangeland		×			×
	Forest Land		×			×
	Reservoirs		×		×	
	Strip Mines, Quarries, and Gravel Pits.	×		×		
	Urban or Built-Up Land	×		×		
Forest Land	Cropland & Pasture, Orchards, Groves, Vineyards, and so forth.		×			×
	Reservoirs		×		×	
	Strip Mines, Quarries, and Gravel Pits.	×		×		
	Urban or Built-Up Land	×		×		
Rangeland	Cropland & Pasture, Orchards, Groves, Vineyards, and so forth.		×			×
	Reservoirs		×		×	
	Strip Mines, Quarries, and Gravel Pits.	×		×		
	Urban or Built-Up Land	×		×		
Wetland	Cropland and Pasture		×		×	
	Reservoirs		×		×	
	Urban or Built-Up Land	×		×		
Barren Land	Reservoirs		×		×	
	Urban or Built-Up Land	×		×		

scanning extensive areas for such changes is becoming more obvious as the costs and problems of collecting information about land use and land cover from enumeration, ground surveys, and low-altitude high-resolution aerial photography continue to mount. Use of a lower resolution remote sensor to complement the use of high-resolution remote sensor data for selecting areas where higher resolution remote sensors are most needed for obtaining land use and land cover data must now be more carefully evaluated. If land use and land cover data are to be maintained at a reasonable level of currency in a cost-effective manner, more research is needed to assure that appropriate use is made of the wide range of remote sensing technology now available. Research is currently underway on the use of Landsat data for land use and land cover mapping and for the monitoring of land use change.

SUMMARY

This report has focused on providing a framework for monitoring land use and land cover changes rather than a plan for undertaking a systematic monitoring of such changes. Some of the major constraints have been indicated; the need for differing intervals of time for monitoring changes depending on the dynamics of land use and the need to change the degree of emphasis in the monitoring of the various categories of land use and land cover have been stressed. Emphasis has also been placed on the need to recognize practical consid-

erations of obtaining suitable remotely sensed data for the monitoring of land use and land cover changes. Further research on this problem will be needed to provide efficient and systematic approaches to the monitoring of changes in land use and land cover.

REFERENCES CITED

Anderson, J. R., Hardy, E. E., Roach, J. T. and Witmer, R. E., 1976, A land use and land cover classification system for use with remote sensor data: U.S. Geol. Survey Prof. Paper 964, 28 p.

Averitt, Paul, 1970, Stripping-coal resources of the United States—January 1, 1970: U.S. Geol. Survey Bull. 1322, 34 p.

Clawson, Marion, 1972, America's land and its uses, *in* Resources for the Future, Inc.: Baltimore, Johns Hopkins Press, 166 p., refs., index.

Frey, H. T., 1973, Major uses of land in the United States—summary for 1969: U.S. Dept. Agriculture Econ. Rept. 247, 42 p.

Joint Federal-State Land Use Planning Commission for Alaska, 1973, Major ecosystems of Alaska: Anchorage, Joint Federal-State Land Use Planning Comm. for Alaska, text and map, scale 1:2,500,000.

Krause, O. E., 1970, Cropland trends since World War II—regional changes in acreage and use: U.S. Dept. Agriculture Econ. Rept. 177, 15 p.

Kuchler, A. W., 1970, Potential natural vegetation of Hawaii, *in* National Atlas of the United States of America: U.S. Geol. Survey, map, scale 1:7,500,000, p. 92.

Otte, R. C., 1974, Farming in the city's shadow—urbanization of land and changes in farm output in Standard Metropolitan Statistical Areas, 1960–1970: U.S. Dept. Agriculture Econ. Rept. 250, 13 p.

Shantz, H. L., and Zon, Raphael, 1924, The physical basis of agriculture—natural vegetation, *reprinted in* Baker, O. E., ed., Atlas of American agriculture, 1936: U.S. Dept. Agriculture, 26 p.

U.S. Department of Agriculture, 1958, Land: The yearbook of agriculture: U.S. Dept. Agriculture, 605 p.

———1974, Our land and water resources: current and prospective supplies and uses: Econ. Research Service, Misc. Pub. 1290, 54 p., refs., tables, figs.

———1975, Comprehensive listing of aerial photography: Agr. Stabilization and Conserv. Service, 145 p.

U.S. Geological Survey, 1975, Land use change map, 1970–1972, Washington urban area, D.C., Md., and Va.: U.S. Geol. Survey Misc. Inv. Map I–858–D, scale 1:100,000 [1976].

Wooten, H. H., 1953a, Major uses of land in the United States: U.S. Dept. Agriculture Tech. Bull. 1082, 100 p.

———1953b, Major uses of land in the United States: U.S. Dept. Agriculture Tech. Bull. 1082, Supp., 78 p.

Zeimetz, K. A., Dillon, Elizabeth, Hardy, E. E., and Otte, R. C., 1976, Dynamics of land use in fast growth areas: U.S. Dept. Agriculture Agr. Econ. Report 325, 48 p.

Jour. Research U.S. Geol. Survey
Vol. 5, No. 2, Mar.–Apr. 1977, p. 155–172

INTRUSIVE ROCKS OF THE YAKUTAT–ST. ELIAS AREA, SOUTH-CENTRAL ALASKA

By TRAVIS HUDSON, GEORGE PLAFKER, and M. A. LANPHERE

Menlo Park, Calif.

Abstract.—Twenty-three plutons, exposed over a total area of nearly 1200 km², have been studied in the Alaska part of the St. Elias Mountains between long 138° and 141°W. Results of potassium-argon age determinations combined with field relations, petrography, and major- and trace-element chemistry suggest six major intrusive events: (1) late Paleozoic gabbro to quartz diorite intruded Paleozoic metamorphic rocks that are probably equivalent to the Kaskawulsh Group in adjacent areas of Canada, (2) Triassic quartz diorite formed one small pluton in undated metamorphic rocks near Mt. St. Elias, (3) Jurassic tonalite and granite intruded upper Paleozoic(?) and lower Mesozoic(?) metamorphic rocks, (4) Late Cretaceous or Tertiary altered tonalite formed three widely separated plutons in metasedimentary rocks of Jurassic(?) and Cretaceous age in the Yakutat Group, (5) Eocene granodiorite and granite, and (6) late Cenozoic tonalite and granodiorite intruded both the Yakutat Group and upper Paleozoic(?) and lower Mesozoic(?) metamorphic rocks. The Paleozoic, Jurassic, and Cretaceous or Tertiary plutonic suites are restricted to particular geologic terranes, and the Jurassic and Eocene suites correlate with regional plutonic belts present elsewhere in southern Alaska. The distribution of the Tertiary plutons does not require large-scale horizontal displacements along the Fairweather and other major high-angle faults. The available data indicate that the mineral resource potential of the Yakutat–St. Elias area is low for those deposits that are generally related to magmatic processes.

Twenty-three larger plutons and numerous dikes, sills, and plugs have been sampled and mapped in the Yakutat and Mt. St. Elias quadrangles (Plafker, 1976). This paper summarizes the field, petrographic, major- and trace-element, and potassium-argon age data available on the intrusive rocks. Metamorphic rocks are discussed in a companion paper by Hudson, Plafker, and Turner (1977). Field occurrences, physical and chemical characteristics, and ages help identify six plutonic suites. Some of these suites, and the geologic terranes in which they occur, have correlatives elsewhere in the Border Ranges of southern Alaska.

The Yakutat–St. Elias area includes approximately 16 000 km² (square kilometers) in the Yakutat and Mt. St. Elias quadrangles between the Canadian border and the Gulf of Alaska (fig. 1). It extends eastward to the Alsek River drainage (long 138°W.) and westward to the vicinity of Mt. St. Elias (long 141°W.). Except for a low and relatively level coastal foreland, relief in the area is exceptionally rugged. Glaciers extend to sea level, and individual peaks such as Mt. St. Elias reach elevations of 5500 meters (m) only 30 km inland from the coast. At higher elevations bedrock exposures are limited to nunataks, many of which are not accessible for sampling.

Acknowledgments.—E. M. MacKevett, Jr., and Michael Perkins participated in parts of the fieldwork and mapped and sampled many of the igneous rocks. Phillip Frame stained rock slabs, made modal point counts, and separated many of the minerals that were used for potassium-argon dating. Kenneth Williams assisted in examination of polished sections. Three of the potassium-argon determinations were kindly provided by D. L. Turner, University of Alaska.

METHODS OF STUDY

We examined the intrusive rocks megascopically to determine physical and structural characteristics, and determined modal proportions by point counting on slabs stained for potassium feldspar and plagioclase following procedures outlined by Norman (1974). The silicate minerals and their textural relations were determined in thin sections, and, for several samples, opaque minerals were studied in polished sections. Plagioclase compositions have been estimated by measurement of the maximum extinction angles of albite twin lamellae in sections oriented normal to (010) (Winchell and Winchell, 1967, p. 287–288). The lithologic and petrographic data are summarized in table 1. This report uses the nomenclature suggested by the International Union of Geological Sciences' Subcommission on the Systematics of Igneous Rocks (Geotimes, 1973) for the plutonic rocks and that of Irvine and Baragar (1971) for fine-grained rocks.

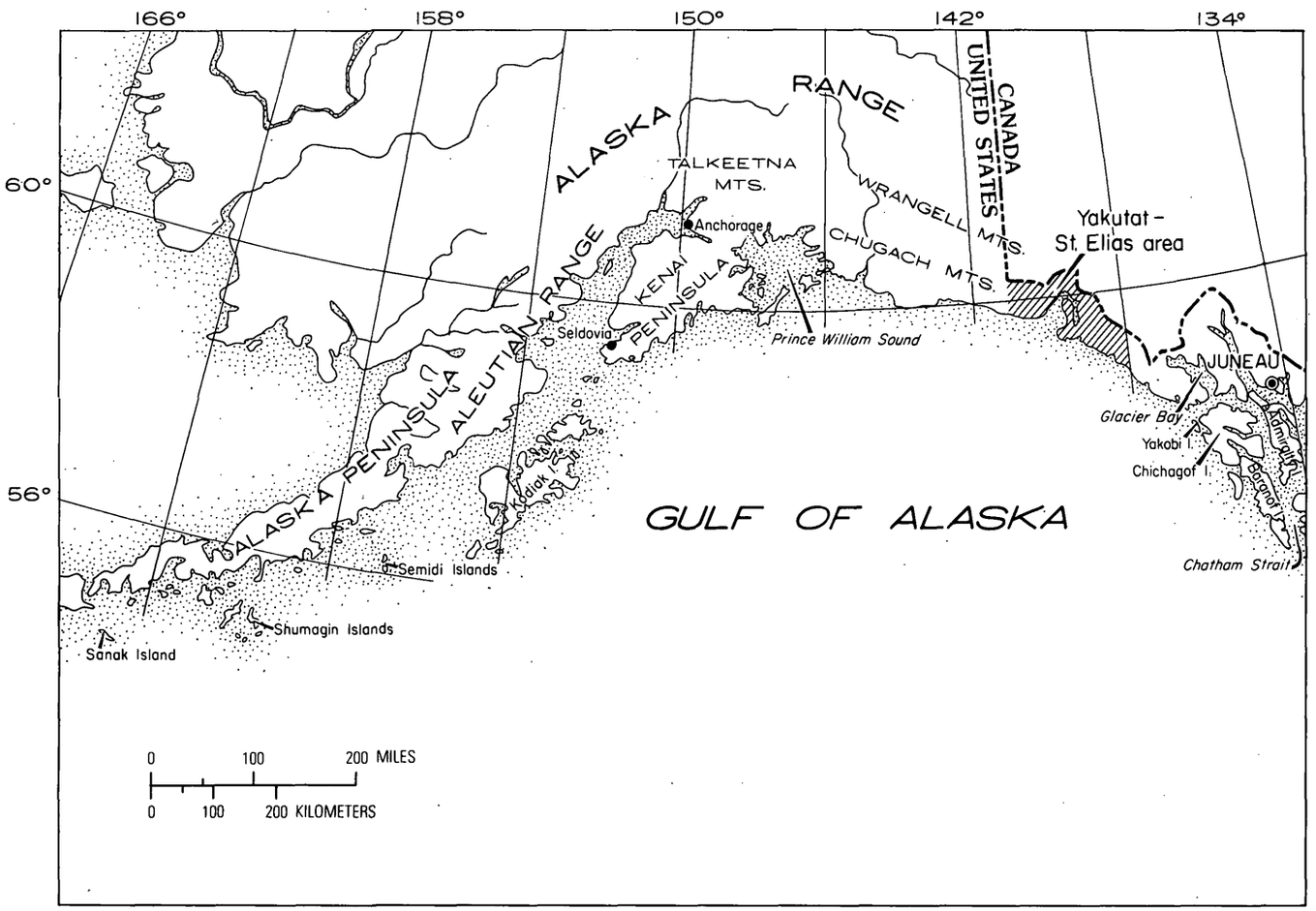

FIGURE 1.—Index map of south-central Alaska showing location of study area.

The major- and trace-element compositions of many whole-rock samples have been determined by standard techniques in the analytical laboratories of the U.S. Geological Survey. Major oxides in individual samples are listed in table 2, and all trace elements generally present in amounts above detection limits are included in the compilation shown in figure 2. Norms were calculated according to the C.I.P.W. method.

Potassium-argon ages were measured on minerals separated from 19 samples of intrusive rocks. Argon analyses were done by isotope dilution using equipment and techniques described by Dalrymple and Lanphere (1969). The argon measurements were made on a Nier-type 15-centimeter-radius rare-gas mass spectrometer. Potassium was determined by flame photometry using a lithium metaborate fusion technique (Suhr and Ingamells, 1966; Ingamells, 1970). The plus-or-minus value assigned each age measurement (table 3) is an estimate of the standard deviation of analytical precision according to the method of Cox and Dalrymple (1967) together with an estimate of accuracy based on uncertainties in the isotopic composition and concentration of the argon-38 tracer and the concentration of the flame photometer standards. Three of the determinations were done by D. L. Turner of the University of Alaska, following procedures described elsewhere (Turner and others, 1973).

GEOLOGIC SETTING

The area contains four broadly distinctive bedrock terranes that trend subparallel to the structural grain of the mountains and the Gulf of Alaska margin. The terranes are the Hubbard, Fairweather–Art Lewis, Yakutat, and coastal lowland (fig. 3). The age of the sedimentary and metamorphic rocks within them generally increase in a northerly direction at angles to the major structures.

Hubbard terrane

The Hubbard terrane consists of undated mafic metavolcanic rocks, associated marbles, and some mica

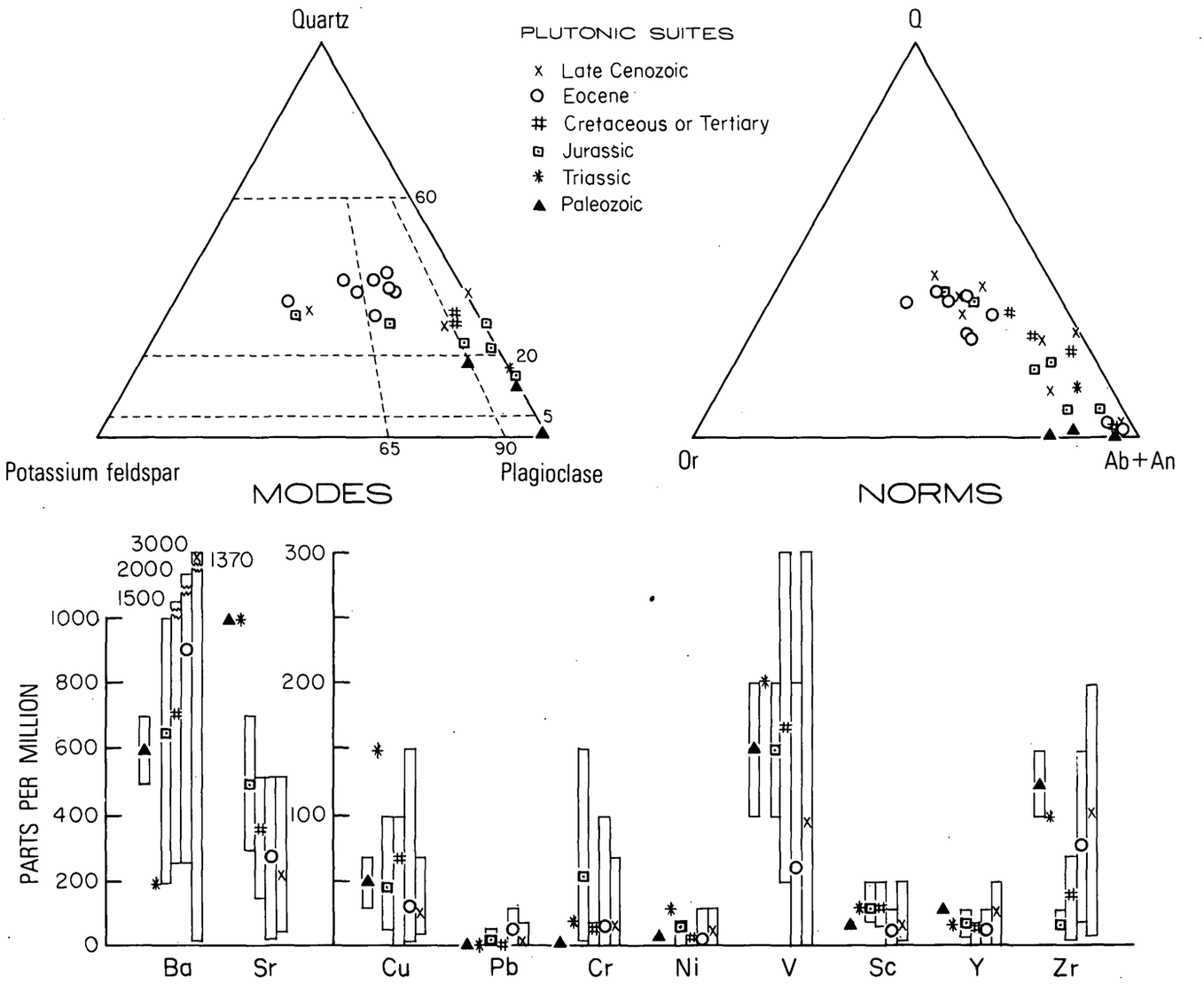

FIGURE 2.—Summary of the modal, normative, and trace-element data available for the six plutonic suites recognized in the Yakutat–St. Elias area. Average trace-element values are indicated by the location of the identifying symbol for each suite, and the range in a set of reported values is indicated by a vertical bar. The number of separate analyses used in the compilation of the trace-element data is: Paleozoic, 3; Triassic, 1; Jurassic (tonalites only), 4; Cretaceous or Tertiary, 3; Eocene, 9; and late Cenozoic, 6. Trace elements determined by semiquantitative spectrographic procedures described in Meyers, Havens, and Dunton (1961); Chris Heropoulos, analyst.

schists. These rocks are probably part of the dominantly middle Paleozoic terrane found just east of the map area in the Canadian part of the St. Elias Mountains (Campbell and Dodds, 1975). Ninety kilometers to the northeast of the map area, the middle Paleozoic sequence is composed mostly of low-grade metasedimentary, mainly carbonate, rocks which were originally named the Kaskawulsh Group by Kindle (1952, p. 29). They are considered part of the Alexander terrane (Berg and others, 1972, p. D2), a terrane believed to extend southeast through Glacier Bay (MacKevett and others, 1971) at least to Chichagof Island (Loney and others, 1975) and northwest to the eastern extremities of the Wrangell Mountains (MacKevett and others, 1974).

Fairweather–Art Lewis terrane

The Fairweather–Art Lewis terrane is a metamorphic belt composed of greenschist- to amphibolite-grade metavolcanic and metasedimentary rocks of unknown age. Following the suggestion of Berg, Jones, and Richter (1972), rocks of this belt are tentatively considered higher grade equivalents of the Skolai Group of Smith and MacKevett (1970) but they have

TABLE 1.—*Summary of the lithologic and petrographic data available for the intrusive rocks of the Yakutat–St. Elias area*

[NA, not available]

	Letter on fig. 4	Pluton(s)	Principal lithology	Granularity, texture, and structure	Mineralogy*			Plagioclase characteristics	Color index	Remarks
					Essential	Accessory	Secondary			
TERTIARY		Plugs, dikes and sills.	Andesite and basalt.	Fine-grained, porphyritic, ophitic, trachytoid, vesicular, and amygdaloidal. Chilled borders common.	Plagioclase, unknown mafic, hornblende, quartz, K-feldspar.	Apatite, magnetite.	Epidote, actinolite(?), chlorite, sericite, calcite, +iron hydroxide, ±prehnite.	Subhedral to euhedral phenocrysts with oscillatory zoning in intermediate compositions. Thin elongate laths in basalts.	NA	Patchy oxidation and alteration of groundmass. Vesicles variably filled with combinations of quartz, chlorite, calcite, and prehnite.
LATE CENOZOIC	A	Mt. Owen	Rhyolite porphyry and granite.	Quite variable granularity, porphyritic with plagioclase, K-feldspar, and quartz phenocrysts and glomeroporphyritic aggregates. Granite is fine-grained, hypidiomorphic, and equigranular.	Quartz, k-feldspar, plagioclase, +biotite, ±hornblende.	Apatite, ±pyrite, ±zircon.	±Calcite, ±white mica, ±chlorite, ±epidote, ±actinolite, ±iron hydroxide.	Phenocrysts are unzoned and simply twinned. Others normal and oscillatory zoning to An_{24} rims. Overgrowths of K-feldspar common.	NA	Alteration variable and patchy, calcite usually in veinlets.
	B	Brabazon	Granodiorite	Fine- to medium-grained, equigranular to seriate, hypidiomorphic. Weak to moderate foliation defined by orientation of mafic grains.	Plagioclase, hornblende quartz, biotite, K-feldspar.	Augite, apatite, ilmenite, pyrite, ±zircon.	Chlorite, epidote group, ±white mica.	An_{36}-An_{26}, normal to very strongly oscillatory zoning, some patchy zoned interiors, complex twinning.	12-32	Clinozoisite veinlets, chlorite replacing biotite, hornblende replacing augite, variable saussuritization of plagioclase, variable mafic : quartz ratio.
	C	Mt. Foresta	Granodiorite(?)	NA	NA	NA	NA	NA	NA	No samples available.
	D	Valerie Glacier.	Tonalite.	Fine- to medium-grained, seriate, hypidiomorphic; foliate with oriented hornblende and faint compositional banding.	Plagioclase, quartz, hornblende.	Epidote, apatite, ilmenite, hematite, pyrite, zircon(?).	White mica	An_{39}, dominantly unzoned and complexly twinned, minor patchy interior and normal zoning.	16	Epidote occurs as primary accessory mineral.
	E	Mt. Seattle	Granite	Fine- to medium-grained, equigranular, hypidiomorphic; weakly foliate with oriented biotite.	Plagioclase, quartz, K-feldspar, biotite, muscovite.	Garnet	Epidote(?), chlorite	NA	2	No thin sections available; epidote in fractures parallel to foliation, chlorite secondary after biotite.
	F	Butler Glacier	Granodiorite(?)	NA	NA	NA	NA	NA	NA	No samples available.
EOCENE	G	Mt. Vancouver.	Granodiorite	Fine-grained, equigranular, hypidiomorphic; myrmekite common; foliate with oriented biotite and faint compositional banding.	Plagioclase, quartz, microcline, biotite, muscovite.	Apatite, allanite(?), zircon(?), opaque.	Chlorite, clinozoisite, sericite.	An_{28}-An_{20}, generally normally zoned, saussuritized cores, some fuzzy oscillatory zoning.	5	Chlorite after biotite, plagioclase : quartz : K-feldspar ratios probably variable.
	H	Mt. Stamy	Granodiorite	Medium-grained, equigranular to seriate, hypidiomorphic; myrmekite common; foliate with oriented biotite, hornblende, and plagioclase.	Plagioclase, quartz, microcline, biotite hornblende.	Augite, apatite, zircon, +ilmenite, ±pyrrhotite.	Epidote, ±calcite, ±sericite, ±chlorite, ±prehnite.	An_{47}-An_{28}, patchy zoned interiors with oscillatory zoning outward to strongly normal zoned rims, simple twinning.	19	Augite-bearing samples are from more mafic and foliate border zones of the pluton where K-feldspar may be absent; interior zones are more massive and leucocratic; chlorite and prehnite after biotite.
	I	Mt. Draper	Granite and granodiorite.	Fine- to medium-grained, equigranular to seriate; some coarse and semi-poikilitic K-feldspar, myrmekite common; massive to moderately foliate.	Plagioclase microcline quartz, biotite, muscovite.	Apatite, zircon(?), chalcopyrite(?).	Epidote, chlorite, ±calcite.	An_{38}, patchy zoning in the interiors with oscillatory zoning in outer margins, simple twinning.	6-12	Minor saussuritization of plagioclase and chloritization of biotite.
	J	Grand Plateau Glacier.	Granite	Medium- to coarse-grained, equigranular to seriate, hypidiomorphic; massive to foliate with oriented biotite.	Quartz plagioclase, microcline, biotite.	Garnet, zircon, magnetite.	Chlorite, sericite, iron hydroxide.	An_{20}-An_{10}, patchy zoned and slightly altered interiors with fine oscillatory zoning outwards; simple twinning.	11	Probably a composite pluton; minor chlorite after biotite and sericite in plagioclase cores.
CRETACEOUS OR TERTIARY	K	Chamberlain Glacier.	Tonalite	Fine- to medium-grained equigranular to seriate, hypidiomorphic; foliate with oriented mafic minerals; fractured, veined, and sheared.	Plagioclase, biotite, ±hornblende, quartz, ±K-feldspar.	Apatite, pyrrhotite, +ilmenite ±chalcopyrite.	Epidote, prehnite, sericite, chlorite, quartz(?), iron hydroxide.	An_{38}-An_{32}, normal to oscillatory zoning, complex twinning.	23	Abundant and distinctive secondary mineral development.
	L	Russel Fiord	do.	Medium-grained, equigranular, hypidiomorphic; foliate with oriented mafic minerals; fractured, veined, and sheared.	Plagioclase, quartz, microcline, biotite, ±hornblende.	Apatite	Epidote, prehnite, chlorite, quartz(?), iron hydroxide.	An_{37}, oscillatory zoning in outer margins, simple to complex twinning.	10[1]	Do.
	M	Mt. Cook	Diorite(?) and quartz diorite(?).	Medium-grained, equigranular, hypidiomorphic; fractured, veined, and sheared. Secondary minerals obscure original relations.	Plagioclase, unknown mafic.		Calcite, chlorite, epidote, prehnite, sericite, albite.	Pervasively altered but simple twinning still evident.	15-20[1]	Do.

See footnotes at end of table.

TABLE 1.—*Summary of the lithologic and petrographic data available for the intrusive rocks of the Yakutat–St. Elias area*—Continued

	Letter on fig. 4	Pluton(s)	Principal lithology	Granularity, texture, and structure	Mineralogy* Essential	Accessory	Secondary	Plagioclase characteristics	Color index	Remarks
JURASSIC	N	Novatak Glacier.	Tonalite	Fine- to medium-grained, equigranular to seriate, hypidiomorphic; foliate with oriented mafic minerals.	Plagioclase, quartz, biotite, hornblende.	Apatite, ±ilmenite.	Epidote group, chlorite, sericite, iron hydroxide.	An_{46}, not obviously zoned, complexly twinned.	31-33	Pluton is more mafic and foliate near borders; late crystallizing minerals include fine-grained plagioclase, quartz, and interstitial to poikilitic hornblende.
	O	Alsek River.	Granite	Medium-grained, equigranular, hypidiomorphic; myrmekite common; foliate with oriented and deformed biotite and plagioclase; fractured and variably sheared.	Quartz, plagioclase, microcline, biotite, muscovite.	Garnet, ±chalcopyrite, ±apatite, ±monazite, ±zircon.	Chlorite, ±iron hydroxide, white mica, epidote group.	An_{38}-An_{29}, patchy interior zoning; marginal hazy to well-defined oscillatory zoning.	3-25	Dikes and borders of the pluton are more mafic; secondary minerals minor to absent, textures indicate much post-emplacement deformation.
	P	Marble Point.	Tonalite	Fine- to medium-grained, seriate, hypidiomorphic; originally massive to foliate(?), veining and shearing present.	Plagioclase, quartz, hornblende, biotite, K-feldspar.	Sphene, apatite, pyrite.	Epidote, chlorite, prehnite, sericite, calcite.	An_{43}, extensively sericitized, some saussuritized cores, some oscillatory zones.	18	Pluton is tectonically emplaced; prehnite and chlorite occur in veinlets and replace biotite.
TRIASSIC	Q	Mt. St. Elias	Quartz diorite	Fine- to medium-grained, seriate, hypidiomorphic. Foliate with oriented mafic minerals. Weak to strong deformation features with some shearing.	Plagioclase, hornblende, quartz, biotite.	Apatite, zircon, magnetite, pyrite, ±chalcopyrite.	Epidote, chlorite, sericite.	An_{37}-An_{25}, weak normal and oscillatory zoning to distinct rims, complex twinning.	32	Minor secondary mineral development.
PALEOZOIC	R	Mt. Hubbard	Diorite and quartz diorite.	Fine- to medium-grained, equigranular to seriate, hypidiomorphic. Myrmekite common, massive to strongly foliate with all minerals oriented. Shearing, veining, and strain features present.	Plagioclase, hornblende, biotite, quartz, K-feldspar.	Apatite, ilmenite, pyrite, ±zircon ±sphene, ±chalcopyrite.	Sphene, epidote group, white mica, prehnite, ±actinolite, ±chlorite.	An_{47}-An_{27}, saussuritized cores with patchy zoning. Normal or oscillatory zoning to distinct rims. Generally simple twinning.	27-31	Opaque minerals and apatite each present in amounts more than 1%.
	S	Art Lewis Glacier.	do.	Medium- to coarse-grained, equigranular, hypidiomorphic. Foliate with oriented mafic minerals. Some shearing.	Plagioclase, unknown mafic.	Apatite, magnetite, pyrite.	Epidote, actinolite, muscovite, chlorite, iron hydroxide.	An_{47}, extensively saussuritized.	40-54	Pluton cut by abundant, fine-grained, leucocratic dikes and simple granitic pegmatites. Up to 5% apatite.
UNKNOWN	T	Mt. Alverstone.	NA	NA	NA	NA	NA	NA	NA	No samples available; pluton is leucocratic and has sharp contacts; is probably younger than nearby Paleozoic intrusive rocks.

*Listed in order of decreasing abundance as estimated by visual inspection; bracketed (]) when relative position(s) interchangeable.
]Visual estimate.

have not yet been traced through the remote and rugged Canadian part of the St. Elias Mountains that lies between this belt and the known Skolai Group to the west. The Skolai Group is considered to be of Pennsylvanian and Permian age on the basis of its contained fossils (Smith and MacKevett, 1970; Richter and Dutro, 1975).

The St. Elias block is lithologically and structurally similar to the Fairweather–Art Lewis terrane in most respects and is tentatively considered to be an allocthonous fragment of that terrane. Unpublished data from the adjacent Bering Glacier quadrangle to the west suggest that this block of metamorphic rocks extends for 35 km west of the map area into the Cugach Mountains.

Yakutat terrane

The Yakutat terrane is underlain mainly by the Yakutat Group, a eugeosynclinal sequence of bedded Jurassic(?) and Cretaceous sedimentary and volcanic rocks that in part are characterized by chaotic structure and tectonically intermixed fragments or blocks of competent rocks of widely diverse origins and ages (Plafker, 1973). This group is generally metamorphosed to prehnite-pumpellyite facies, but in the eastern Mount Cook block, the Boundary-Fairweather block, and the southern Yakutat foothills, rocks of higher grade are present. The Yakutat Group is similar in age and general lithology to the areally extensive Valdez Group to the west (Plafker and MacNeil, 1966; Clark, 1972) and to the Sitka Graywacke and related rocks on Chichagof and Baranof Islands south-

TABLE 2.—*Chemical analyses of Yakutat–St. Elias area intrusive rocks*

[Analytical procedure described in Shapiro and Brannock (1962) supplemented by atomic absorption; Gillison Chloe, P. L. D. Elmore, J. L. Glenn, James Kelsey, and Hezekiah Smith, analysts]

Field number	Pluton(s)	SiO_2	Al_2O_3	Fe_2O_3	FeO	MgO	CaO	Na_2O	K_2O	H_2O+	H_2O-	TiO_2	P_2O_5	MnO	CO_2	Total	Remarks
68APr27B	Plugs, dikes, and sills.	67.0	16.1	0.8	2.6	1.5	1.5	5.7	2.6	1.4	0.24	0.40	0.17	0.04	<0.05	100	Andesite plug, plagioclase and hornblende megacrysts, sericitized plagioclase, and minor secondary epidote.
68APr68D	do.	43.8	16.8	1.3	14.0	6.1	2.9	3.5	1.6	5.8	.49	2.2	.31	.28	.18	99	Altered diabase with abundant secondary chlorite, epidote, and calcite.
69APr59C3	do.	55.2	14.3	1.4	5.8	5.2	10.4	2.5	0.34	1.8	.79	1.2	.23	.18	.30	100	Amygdaloidal basalt with quartz megacrysts and secondary chlorite, calcite, quartz, and prehnite.
68APs47B	do.	45.0	14.7	4.2	2.9	1.0	12.8	5.6	1.1	1.7	.61	1.9	0.34	.07	8.0	100	Amygdaloidal and veined basalt with abundant secondary calcite, epidote, and chlorite.
69APr44C	Mt. Owen	74.2	12.4	.18	1.2	.17	1.4	4.0	3.7	.89	.05	.14	.00	.00	.44	99	Rhyolite porphyry with potassium feldspar, plagioclase, and quartz megacrysts.
69APr35C	do.	72.4	13.7	1.2	2.1	.31	1.7	4.1	3.3	.77	.06	.32	.04	.00	< .05	100	Fine-grained granite with potassium feldspar overgrowths and minor secondary actinolite, sericite, epidote, and chlorite.
69APr34D1	do.	76.0	12.7	.26	1.4	.21	.72	3.4	4.1	.75	.08	.13	.00	.00	.10	100	Rhyolite porphyry with 40% megacrysts, some sedimentary inclusions, and minor secondary minerals.
67APr94B	Brabazon	65.9	16.0	.63	3.7	1.4	4.1	4.5	1.6	1.1	.11	.69	.13	.04	< .05	100	Biotite hornblende granodiorite with chloritized biotite, minor saussuritized plagioclase, accessory pyroxene, and clinozoisite veinlets.
68APs64B*	do.	58.2	16.2	.78	6.2	3.7	6.9	3.7	1.7	1.3	.12	.90	.17	.09	< .05	100	Hornblende granodiorite with minor biotite, chlorite after biotite, and saussuritized plagioclase.
69APr40A*	Mt. Foresta	66.3	16.0	.74	3.6	2.4	3.0	2.8	3.4	.94	.16	.63	.22	.05	< .05	100	Sheared and granulated muscovite-biotite granodiorite with secondary clinozoisite and minor accessory garnet.
67APr78A*	Valerie Glacier.	63.9	17.1	1.5	3.2	1.8	6.4	4.1	.20	.80	.13	.73	.15	.00	< .05	100	Hornblende tonalite with accessory epidote (?).
69APr42D	do.	51.0	20.7	.44	6.6	4.5	10.9	2.5	.23	2.1	.05	.67	.03	.10	.09	100	Hornblende diorite (metadiorite?) with interstitial quartz and minor carbonate.
69APr32A*	Mt. Vancouver	73.1	14.7	.18	1.2	.32	1.9	3.4	4.1	.79	.04	.17	.02	.00	< .05	100	Biotite granodiorite with 2% muscovite and minor secondary sericite, clinozoisite, and chlorite.
69APr32B	do.	51.6	20.4	2.5	6.3	3.3	9.0	3.4	.70	.85	.04	1.1	.22	.11	< .05	100	Do.
68APs41G	Mt. Draper	73.2	15.7	.00	.84	.14	1.8	4.8	2.9	.41	.08	.02	.02	.00	< .05	100	Muscovite biotite granodiorite with minor secondary chlorite.
67APr42B1*	do.	74.1	13.7	.00	1.4	.20	1.1	2.8	5.7	.35	.12	.17	.03	.00	< .05	100	Muscovite biotite granite with minor secondary minerals.
67APr66B	do.	66.2	16.2	.47	3.3	1.2	3.3	3.2	3.8	1.2	.18	.61	.19	.00	< .05	100	Muscovite-biotite granodiorite with minor saussuritized plagioclase and chloritized biotite.
69APr21B	Mt. Stamy	65.8	15.4	.46	4.4	1.3	3.8	3.1	3.7	.72	.10	.81	.17	.04	< .05	100	Hornblende-biotite granodiorite with accessory augite and minor secondary minerals.
67APr42A*	do.	53.1	19.5	.46	5.4	5.7	10.7	3.0	.40	1.1	.13	.42	.04	.07	< .05	100	Hornblende diorite with accessory quartz and minor secondary minerals.
67APr83C	do.	51.1	21.8	.24	5.6	3.3	12.1	3.0	.38	.49	.12	1.5	.11	.05	< .05	100	Diorite with 20% diopside and accessory quartz. Secondary minerals very minor.
68APr77D*	Grand Plateau Glacier.	72.9	14.7	.18	2.2	.25	1.7	3.8	3.3	.48	.13	.18	.08	.03	< .05	100	Biotite granite with accessory garnet, minor sericite, and chlorite.
69APr92D	do.	71.9	14.3	.26	2.4	.72	1.7	3.0	4.1	1.0	.08	.37	.17	.00	< .05	100	Biotite granite with minor secondary minerals.
68APr108B	Chamberlain Glacier.	62.4	15.4	1.0	5.1	2.9	3.3	3.9	1.5	2.8	.28	.58	.08	.07	< .05	100	Biotite tonalite with extensive sericitization and chloritization. Some chlorite-prehnite veinlets.
68APr98A	do.	58.5	15.8	1.1	5.6	3.2	6.8	3.2	.60	3.6	.24	.63	.11	.09	.07	100	Biotite tonalite, sheared and extensively altered secondary chlorite, epidote, white mica, prehnite, and calcite.
69APr110A	Russel Fiord	69.3	15.2	.72	2.8	1.3	1.3	4.9	2.0	1.7	.15	.38	.10	.07	< .05	100	Biotite tonalite with moderate sericitization and chloritization.
69APr40C1	Mt. Cook	49.4	20.1	1.0	6.6	4.0	9.5	2.8	.51	3.9	.18	.58	.02	.11	.55	99	Tonalite with completely chloritized mafic grains and extensively saussuritized plagioclase, some prehnite veinlets.
63APr196*	Marble Point	60.5	16.4	1.0	4.9	3.0	4.8	3.9	1.4	1.9	.31	.73	.13	.07	< .05	99	Biotite-hornblende tonalite with abundant secondary chlorite, sericite, epidote, and prehnite.
68APr85B	Alsek River	74.9	14.4	.00	.96	.04	.81	3.9	4.1	.71	.13	.00	.08	.00	< .05	100	Muscovite-biotite granite with accessory garnet sheared but only minor secondary chlorite and sericite.
67APr94C*	do.	73.1	14.4	.00	1.8	.28	1.5	4.2	3.2	1.0	.13	.14	.06	.00	< .05	100	Muscovite-biotite granite, some shearing and minor chlorite, epidote, and sericite.
68APr103B*	Novatak Glacier.	60.0	17.2	.64	5.6	3.4	5.8	3.0	1.9	1.1	.15	.81	.14	.09	< .05	100	Hornblende-biotite tonalite with minor secondary chlorite, epidote, and sericite.
68AMk108*	do.	77.4	9.0	.64	3.6	2.3	1.7	1.5	1.5	1.3	.20	.60	.21	.00	< .05	100	Biotite-albite quartz pegmatite dike in tonalite.
68APr82D	do.	55.2	18.4	.52	6.8	4.9	6.0	3.4	1.5	2.0	.25	.53	.27	.11	< .05	100	Biotite-hornblende quartz diorite in border migmatite, mafic minerals partially chloritized.
69APr54A*	Mt. St. Elias.	55.2	17.6	2.7	5.6	3.9	8.1	3.3	.88	.91	.02	1.3	.27	.11	< .05	100	Biotite-hornblende quartz diorite with minor secondary minerals and 3% accessory magnetite.
69APr31A2	Mt. Hubbard	55.8	18.5	1.5	5.1	2.9	5.7	4.9	2.6	1.0	.15	1.3	.38	.07	< .05	100	Biotite-hornblende quartz diorite, minor saussuritized plagioclase.
69APr31B*	do.	53.2	17.0	3.6	6.1	3.1	6.6	4.7	1.7	.83	.15	1.9	.38	.11	< .05	99	Hornblende quartz diorite, sheared, partly uralitized and sericitized.
68APr69C*	Art Lewis Glacier.	40.1	16.8	6.5	8.2	5.8	11.2	2.6	.55	2.5	.20	2.5	2.1	.18	< .05	99	Diorite with actinolitic amphibole, extensive saussuritization, and abundant apatite and magnetite.

*Radiometrically dated sample; see table 3.

TABLE 3.—*Potassium-argon ages and analytical data*

[Potassium analyses by H. C. Whitehead and L. B. Schlocker; argon analyses by M. A. Lanphere, J. Von Essen, and E. H. McKee; decay constants for ^{40}K: $\lambda_\epsilon = 0.585 \times 10^{-10}$ year^{-1}; $\lambda_\beta = 4.72 \times 10^{-10}$ year^{-1}. Atomic abundance of $^{40}K = 1.19 \times 10^{-4}$. σ, standard deviation]

No. (fig. 4)	Field No.	Lat (N)	Long (W)	Mineral	Percent K_2O	Average K_2O (percent)	^{40}Ar rad (10^{-10} mol/g)	$\frac{^{40}Ar_{rad}}{^{40}Ar\ total}$	Apparent age ± 1σ m.y.
1	63 APr 196	59°56'	144°24'	Hornblende	0.829, 0.830	0.8295	2.041	0.73	160±3.5
2	69 APr 23A	59°49.65'	139°17'	do.	.316, .322	.319	.09456	.18	20.0±2
3	68 APr 77D	59°00.15'	138°01.45'	Biotite	8.47, 8.48	8.475	6.118	.16	48.2±6
4	67 APr 42A	59°52.75'	139°08.1'	Hornblende	.279, .282	.280	.2148	.43	51.1±3
5	67 APr 42B	59°45.5'	139°06.2'	Muscovite	10.50, 10.55	10.525	7.631	.64	48.4±2
				Biotite	---	8.37	5.341	.41	42.7±2
6	68 APs 64B	59°19.95'	138°21'	do.	7.82, 7.75	7.785	2.791	.16	24.1±3
7	69 APr 54A	60°17'	140°53'	do.	9.11, 9.13	9.12	12.02	.84	87.2±3
				Hornblende	.363, .370	.366	1.072	.69	188±6
8	69 APr 32A	60°18.1'	139°36.1'	Muscovite	10.53, 10.43	10.48	7.338	.74	46.8±1
				Biotite	8.37, 8.41	8.39	5.978	.63	44.6±1
9	69 APr 40A	60°13.3'	139°31'	do.	9.43, 9.41	9.42	4.293	.92	30.6±1
10	67 APr 78A	60°07.6'	139°28.5'	Muscovite	8.29, 8.44	8.365	2.591	.17	20.9±3
				Hornblende	---	.423	.1159	.37	18.5±1
11	68 APr 103B	59°37'	138°31'	do.	.668, .658	.663	.6074	.63	61.0±2
12	68AMk 108	59°31.8'	138°23.5'	Biotite	---	8.43	3.174	.47	25.3±1
13	67 APr 94C	59°25.5'	138°00'	do.	8.68, 8.67	8.675	22.10	.92	165±5
14	67 APr 94D	59°36.2'	138°04.8'	Hornblende	.472, .478	.475	1.083	.75	148±4
15	69 APr 31B	60°17.2'	139°11.9'	do.	.632, .633	.632	2.812	.89	279±8
16	68 APr 69C	59°49.3'	138°44.7'	do.	.305, .306	.3055	.6358	.52	136±4
17*	67 APr 57B1	59°52.1'	138°58.8'	Muscovite	8.852, 8.849	8.850	3.092	.177	23.5±0.7
18*	69 APr 30B	59°51.9'	138°45'	Hornblende	.310, .330	.320	1.132	.896	225±6
19*	69 APr 31C2	60°20.1'	139°12.6'	do.	1.350, 1.350, 1.365, 1.360	1.356	6.153	.949	284±7

*Determinations provided by D. L. Turner, University of Alaska.

east of the map area (Loney and others, 1975). Sedimentary rocks of Tertiary age unconformably overlie the Yakutat Group in the western part of the Mt. Cook block and in the Malaspina foothills.

Coastal lowland

The coastal lowland consists of unconsolidated glacial, alluvial, and shallow marine deposits of Quaternary age. Tertiary and Cretaceous bedded rocks equivalent to those exposed in the western Yakutat terrane have been penetrated by exploratory wells drilled for oil on the Yakutat Foreland and along the margin of the Malaspina Glacier (Plafker, 1967). The Tertiary rocks are part of a sequence of near-shore marine and nonmarine sediments of Eocene to Pliocene age that extended along the continental margin from Kodiak Island at least as far east as Palma Bay in Glacier Bay National Monument.

INTRUSIVE ROCKS

Intrusive igneous rocks are widely distributed in all the principal geologic terranes. Dikes, sills, and plugs of mafic to intermediate composition commonly intrude both the Tertiary and older rocks, but larger plutons have only been found emplaced in rocks of late Mesozoic or older age. Some of the plutonic suites are apparently restricted to particular geologic terranes as plutonic rocks of Tertiary age are the only intrusive rocks known to be in more than one of the geologic terranes.

The plutonic rocks underlie approximately 1200 km² of the Yakutat–St. Elias area. They are char-

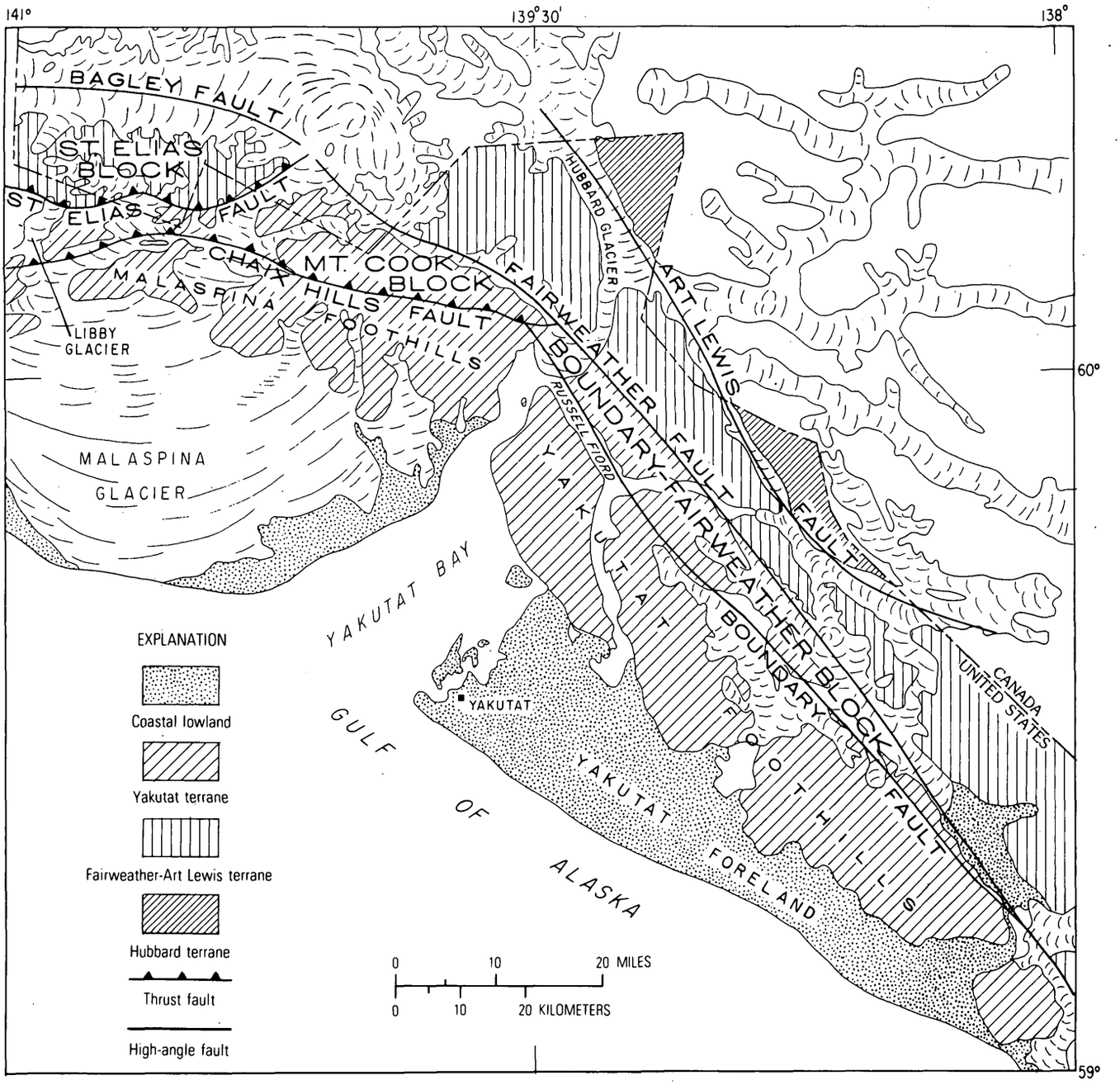

FIGURE 3.—Index map of the Yakutat–St. Elias area showing major fault boundaries, structural blocks, and geologic terranes.

acterized by diverse compositions and field relations and are exposed in 23 separate bodies that range in age from Paleozoic to Miocene (fig. 4). Most of these plutons display some degree of conformity to the regional structural grain and, at levels now exposed, indicate emplacements in epizonal and mesozonal environments. There is a general shift in composition from mafic and intermediate in the older plutons to felsic in the Tertiary plutons. The plutons have been divided into six suites largely on the basis of apparent or inferred potassium-argon age differences. The different suites are referred to in this paper as the Paleozoic, Triassic, Jurassic, Cretaceous or Tertiary, Eocene, and late Cenozoic suites. Important general characteristics of each suite are discussed below. Sills, dikes, and plugs that are not directly related to the

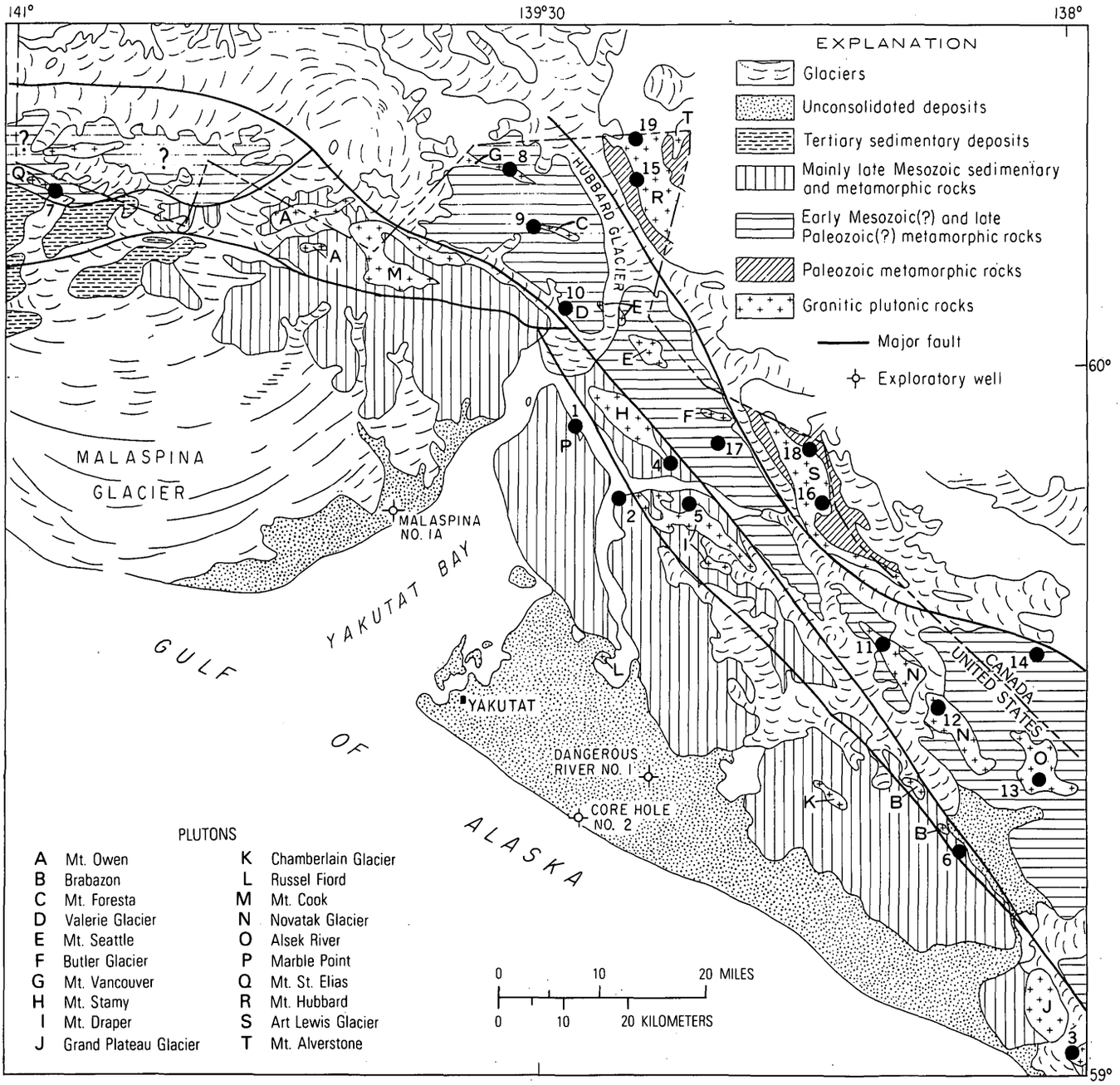

FIGURE 4.—Generalized geologic map of the Yakutat–St. Elias area showing locations of larger plutons (lettered) and radiometrically dated igneous rock samples (numbered dots) relative to the major rock sequences and structural features. Letters refer to table 1 and numbered dots to table 3. Fault names are shown in figure 3. The plutons are named after prominent geographic features in their vicinity.

larger plutons are discussed separately. Table 1 summarizes the lithologic and petrographic data for each of the larger plutons.

Paleozoic suite

The Paleozoic suite includes the Mt. Hubbard and Art Lewis Glacier plutons (plutons R and S, fig. 4). These plutons are large, elongate bodies that intrude mafic metavolcanic rocks (amphibolite) and subordinate associated marble and mica schist in the Hubbard terrane. The contact relations are locally complex and are sharp and crosscutting as well as gradational. Gradational contacts typify diorite-amphibolite transitions and are characterized by numerous dioritic

dikes and sills and coarse-grained hypidiomorphic textures in amphibolites near the main intrusive masses. Pendants and inclusions of country rocks are common.

The plutons are dominantly foliate, medium-grained biotite-hornblende diorite and quartz diorite. Biotite, hornblende, and plagioclase (An_{27-47}) commonly constitute 90 percent or more of individual specimens. Quartz and potassium feldspar form small, anhedral, interstitial grains if they are present. Alteration is common and includes saussuritization of plagioclase, development of actinolitic amphibole, chlorite replacement of mafic minerals, and prehnite veinlets. Some altered specimens contain up to 5 percent intergranular apatite and almost as much opaque minerals. The opaque minerals are magnetite and subordinate ilmenite and pyrite.

The compositional data shown in figure 2 are not abundant but serve to illustrate the general mafic character of the suite. Much of the normative orthoclase variation is due to biotite. The suite as a whole contains average to low contents of most trace elements with two exceptions, zirconium and strontium. Values for both of these elements are particularly high and possibly divergent enough from values for most other suites to be helpful in correlating similar but undated or undatable rocks.

The ages of two samples from the Mt. Hubbard pluton (Nos. 15 and 19, fig. 4) agree very well at about 280 m.y. (million years). Two ages from the Art Lewis Glacier pluton (Nos. 16 and 18), which probably is the same age as the Mount Hubbard pluton, are significantly lower. The Art Lewis Glacier pluton, partly bounded on the west side by the Art Lewis fault, is generally more altered and deformed than the Mount Hubbard pluton. The dated samples from the Art Lewis Glacier pluton contain actinolitic amphibole, chlorite, and much apatite, and clearly have undergone secondary changes. The Mt. Alverstone pluton (pluton T) is located in the northeast corner of the map area near the Mt. Hubbard pluton. It is not accessible for sampling, but it appears from close aerial observation to be leucocratic and to have sharp contacts, suggesting that it is probably much younger than the larger Paleozoic intrusive body located nearby.

Triassic suite

The only pluton in the Triassic suite is the Mt. St. Elias pluton (pluton Q, fig. 4) located in the St. Elias block and exposed on the sheer south face of Mt. St. Elias at elevations between 3000 and 4600 m. Close aerial inspection indicates that the pluton is lensoid in outline and grossly conformable, although the contacts appear to be sharp.

The pluton is inaccessible, but one sample, clearly derived from the pluton, was collected from the moraine of Libbey Glacier. It is a foliate, fine- to medium-grained, biotite-hornblende quartz diorite with fine-grained, hypidiomorphic inclusions rich in mafic minerals. Accessory magnetite is abundant (3–4 percent) and there is no potassium feldspar. Quartz forms small interstitial grains. Deformation features in the specimen, such as wavy biotite, broken and granulated plagioclase, and strained quartz, probably reflect movement on the nearby St. Elias thrust fault. Alteration includes minor replacement of plagioclase cores by epidote and sericite and slight chloritization of some mafic grains.

Chemically, the sample is similar in many respects to the Paleozoic suite; however, it has barium and copper abundances markedly different from values for any of the other intrusive suites. Like the Paleozoic suite, its strontium content is much higher than in the younger intrusive bodies.

The biotite and hornblende age determinations (No. 7, table 3 and fig. 2) are strongly discordant and suggest a minimum age of 188 m.y. for the pluton. The crystallization age of this pluton cannot be established from this single discordant pair of ages, but it seems unlikely that it is as old as the Paleozoic suite. Consequently, we have assigned a Triassic age to the Mt. St. Elias pluton.

Jurassic suite

The Jurassic suite includes the Marble Point, Alsek River, and Novatak Glacier plutons (plutons P, O, and N, fig. 4). The small Marble Point pluton is believed to be part of an exotic block in a melange complex exposed along the west side of Russell Fiord. The Alsek River and Novatak Glacier plutons intrude amphibolite and quartzofeldspathic schists in the southern part of the Fairweather-Art Lewis terrane. These plutons are elongate and generally conformable, and have steeply dipping, gradational and migmatitic contact zones. Intrusive rocks in or near the contact zones are strongly foliate, have abundant inclusions of metamorphic rocks, and are generally more mafic than rocks in interior parts of the plutons. As now exposed, the Novatak Glacier pluton is actually a zone of numerous, small granitic intrusions whose borders are complex zones of diking.

The two principal lithologies in the Jurassic suite are granite and tonalite. The Alsek River pluton is dominantely composed of strongly foliate, medium-

grained muscovite-biotite granite with accessory garnet. Muscovite is both intergranular and interleaved with biotite. Deformation features such as distorted plagioclase, strained and partially polygonized quartz, and wavy biotite are commonly present. Alteration is minor and includes saussuritization of plagioclase and chloritization of biotite. The Marble Point and Novatak Glacier plutons are dominantly foliate fine- to medium-grained hornblende-biotite tonalite. Both quartz and potassium feldspar form small interstitial grains but potassium feldspar is absent in many samples. Some chloritization of mafic minerals is common, and prehnite replaces some biotite.

The modal and normative ratio for two samples from the Alsek River pluton are far removed from the ratios for the tonalites (fig. 2) and emphasize the more felsic nature of this pluton relative to the others of Jurassic age. Trace elements in the Alsek River pluton are grossly similar to those in the more felsic Tertiary plutons, and they are not included in the summary of trace-element abundances in figure 2. The chemical data for the Jurassic tonalites include one sample of a dike in the contact zone of the Novatak Glacier pluton (68APr82D, table 2). This sample is more mafic than the others and plots modally as a quartz diorite without potassium feldspar. The Jurassic tonalites have intermediate trace-element contents except for zirconium which is present in a narrow range of low concentrations.

The Marble Point and Alsek River plutons have both yielded Jurassic potassium-argon ages. In addition, an age of 148 m.y. was measured on a tonalite sample from a large body exposed in Canada (No. 14, table 3 and fig. 4). This pluton has not been mapped, but its identification broadens the area with known Jurassic plutons. One sample from the Novatak Glacier pluton has yielded an apparent potassium-argon age of 61.0±2 m.y. on hornblende (No. 11, table 3 and fig. 4). The 61 m.y. apparent age may be due to resetting during Tertiary time of a hornblende that originally crystallized in Jurassic time because the 61 m.y. date is not near the ages of any of the other recognized plutonic suites and because the Novatak Glacier pluton is similar in lithology and composition to tonalitic plutons in the Jurassic suite. This interpretation is tentative but is also supported by the gross differences in lithology and composition between the Novatak Glacier pluton and the plutons of known early Tertiary age. If resetting probably took place, it was probably during the Miocene Epoch when many of the country rocks in the vicinity of the Novatak Glacier pluton were recrystallized (Hudson and others, 1977) and the pluton was intruded by many dikes including a biotite-albite-quartz pegmatite that has been dated at 25.3±1 m.y. (No. 12, table 3 and fig. 4).

Cretaceous or Tertiary suite

Because of similarities in composition and occurrence, the Chamberlain Glacier, Russell Fiord, and Mt. Cook plutons (plutons K, L, and M, fig. 4) are traced as a separate plutonic suite. No radiometric dates are available for these plutons because of widespread alteration. However they intrude rocks of the late Mesozoic Yakutat Group in the Yakutat foothills and the eastern Mt. Cook block and are considered to be of Cretaceous or Tertiary age. The Chamberlain Glacier and Russell Fiord plutons intrude prehnite-pumpellyite-facies metasediments and have sharp but grossly conformable contacts and well-developed thermal aureoles. Marginal zones of these plutons locally contain numerous inclusions of country rock. The Mt. Cook pluton is the least well exposed of the three included in this suite. It intrudes sheared and chaotically deformed metasedimentary rocks in the low greenschist facies. Near the contact the country rocks are apparently thermally metamorphosed, and they locally weather reddish brown from oxidation of disseminated sulfide. Dikes are locally abundant in the contact zone, and inclusions and septa of country rocks are present in the pluton. A a whole, the plutons of the Cretaceous or Tertiary suite appear to have been emplaced in middle to lower epizonal environments.

The plutons are dominantly sheared and highly altered hornblende-biotite tonalite, with 15 percent or more quartz and up to 5 percent potassium feldspar. One specimen from the Mt. Cook pluton is a diorite that may represent a more mafic marginal facies of the pluton. The most conspicuous characteristics of these rocks are extensive deformation and alteration. Most specimens have been sheared along fractures, and secondary mineral veining, dominantly by prehnite, is common. Saussuritization of plagioclase and chloritization of primary mafic minerals generally obliterate details of the original textures and mineralogy.

The normative variation (fig. 2) is in accord with the relative variation of primary mineral abundances that was estimated from hand specimens and thin sections. Regular modal analysis was generally inappropriate because of alteration. The effects of alteration appear to be due primarily to hydration and oxidation; the ratios of H_2O+ to H_2O- have been increased and the ratios of the FeO to Fe_2O_3 decreased. Trace elements are present in intermediate amounts

with the possible exception of copper, which on the average is more abundant than in rocks from most of the other suites.

The intrusive relations of these plutons to the Yakutat Group establish their lower age limit as Cretaceous. If the plutons are related to any of the other intrusive suites in the area, it would probably be to those of Tertiary age (Eocene and late Cenozoic) However, comparison of lithology and composition (modal, major and trace elements, fig. 2) indicates there is little in common between these plutons and those of known Tertiary age. Thus, we interpret these plutons as a separate intrusive suite on the basis of their field occurrence, compositions, characteristic alteration, and probable age. They were possibly intruded sometime during the Cretaceous or earliest Tertiary Period when the host rocks were still wet and poorly lithified sediments. Much of the water involved in the alteration of the plutons may have been derived from the country rocks, and the deformation and alteration of the plutons may have occurred during or shortly after the episode of complex deformation that affected the Yakutat Group and before emplacement of the Eocene plutons.

Eocene suite

Plutons of the Eocene suite include the Grand Plateau Glacier, Mt. Draper, Mt. Stamy, and Mt. Vancouver plutons (plutons J, I, H, and G, fig. 4). They are widely distributed and as a group have complex contact relations suggesting both mesozonal and epizonal emplacement environments. The Grand Plateau Glacier pluton intrudes the southernmost part of the Yakutat foothills. It has sharp contacts and a well-developed hornfels aureole. Attitudes in the country rocks near the contact conform to the margins of the pluton. The Mt. Draper and Mt. Stamy plutons are large and elongate intrusions in the central Boundary-Fairweather block that have transitional contacts on their south ends and sharp, crosscutting contacts at their north ends. The transitional contacts exhibit injection gneisses, dioritized amphibolites, abundant country rock inclusions, and hybrid border facies. The country rocks adjacent to the northern contacts consist of garnet- and staurolite-bearing biotite-rich schists within a well-defined thermal aureole. The Mt. Vancouver pluton is a narrow elongate body that straddles the international boundary in the northern part of the Fairweather–Art Lewis terrane. Contacts are steeply dipping, and there are marginal zones of complex dike intrusion into the country rocks.

The Eocene suite is dominantly muscovite-biotite granodiorite and granite. Overall, the Grand Plateau Glacier pluton is the most felsic. It is clearly epizonal and the presence of marked textural variations suggests that it may be composite. The other plutons characteristically have more massive and leucocratic rocks in their northern and wider parts and more foliate and mafic rocks in their narrower southern parts. Typically, plagioclase exhibits well-developed zoning in marginal bands around calcic cores, potassium feldspar is microperthitic, and muscovite is a late but primary mineral. Accessory mineral content is low; apatite is the most abundant accessory mineral. The relatively mafic rocks characteristically have more calcic plagioclase, hornblende, some garnet, and minor augite. The augite is replaced to various degrees by green amphibole. Development of the more mafic facies is probably due in large part to contamination that resulted from assimilation of mafic country rocks.

The general felsic nature of the suite is illustrated by both the modal and normative ratios plotted in figure 2. The more mafic compositions are from samples of marginal facies of plutons, and indications of contamination are present in most of them. There is considerable range in most individual trace-element abundances, but this suite, in keeping with its general felsic nature, has less strontium and vanadium and more barium than the older, and characteristically more mafic, intrusive suites.

Potassium-argon ages have been measured for all of the plutons in the Eocene suite. The field relations and compositions of the Eocene and late Cenozoic suites are similar in some respects, and in places it is difficult to distinguish between the two suites. Generally the Eocene plutons are exposed over larger areas and to deeper levels than the late Cenozoic plutons. There may be some differences in trace-element abundances between the two suites, but this is not demonstrable with the data now available (fig. 2).

Late Cenozoic suite

The late Cenozoic suite contains 10 small and widely distributed intrusive bodies. These include the Brabazon plutons (plutons B, fig. 4) in the Boundary-Fairweather block, the Butler Glacier, Mt. Seattle, Valerie Glacier, and Mt. Foresta plutons in the Fairweather–Art Lewis terrane, (plutons F, E, D, and C), and the Mt. Owen plutons in the Mt. Cook block (pluton A). Contacts of these plutons are grossly concordant and both transitional and sharp. Mixed dike and country-rock zones characterize the transitional contacts, and well-developed hornfels has been recognized adjacent only to the Brabazon plutons. In transitional contact zones, the intrusive rocks are more foliate and mafic, much like the Eocene plutons in similar environ-

ments. Most late Cenozoic plutons appear to have been emplaced in mesozonal environments. Their characteristic small outcrop areas indicate that they have not been deeply exposed. The Mt. Owen plutons, the only hypabyssal plutons known in the entire area, have sharp crosscutting contacts and have thermally metamorphosed the nearby country rocks. Oxidation of disseminated sulfides, mainly pyrite, produces conspicuous rust-stained zones in this contact aureole, but the thermal metamorphism was intense only in a narrow zone adjacent to the contact.

The late Cenozoic plutons are dominantly muscovite-biotite granodiorite, but most of the samples represent the more mafic border zones where biotite-hornblende quartz diorite and tonalite are common. The lithologic and petrographic data are minimal (table 1), but it appears that the late Cenozoic suite is grossly similar to the Eocene suite in general composition and mineralogy.

The felsic compositions from this suite shown in the modal and normative diagrams of figure 2 are from samples of the composite Mt. Owen plutons, which are composed of rhyolite porphyry and fine-grained granite. The variability of the trace-element contents results from the inclusion of the data from the Mt. Owen plutons in the compilation shown in figure 2. The three analyzed samples from these plutons have consistently high barium and zirconium and low strontium, copper, chromium, nickel, vanadium, and cobalt contents.

Only two of the larger plutons in the late Cenozoic suite have been radiometrically dated (Valerie Glacier and Mt. Foresta plutons, fig. 4). The Mt. Foresta pluton has yielded an Oligocene age of 30.6 m.y., and the possibility that it is an older, partially reset, Eocene pluton cannot be discounted. Correlation of the undated plutons with this suite is quite tentative and is based on similarities in their occurrence or their proximity to dated intrusions that are mostly of Miocene age (fig. 5). The Brabazon plutons for example, are inferred to be Miocene, because they are felsic and have sharp crosscutting contacts, and a 24.1-m.y. potassium-argon age was obtained from float of a nearby granodiorite dike (68APs64B, tables 1 and 2). The Mt. Owen plutons are an exception. Because they are composite hypabyssal bodies, their exposure in the highest parts of the mountain range suggests that they are young. They are included here simply because the late Cenozoic suite represents the youngest recognized plutonic episode in the area. The other undated plutons, if not actually of late Cenozoic age, were probably emplaced during the Eocene episode of plutonism.

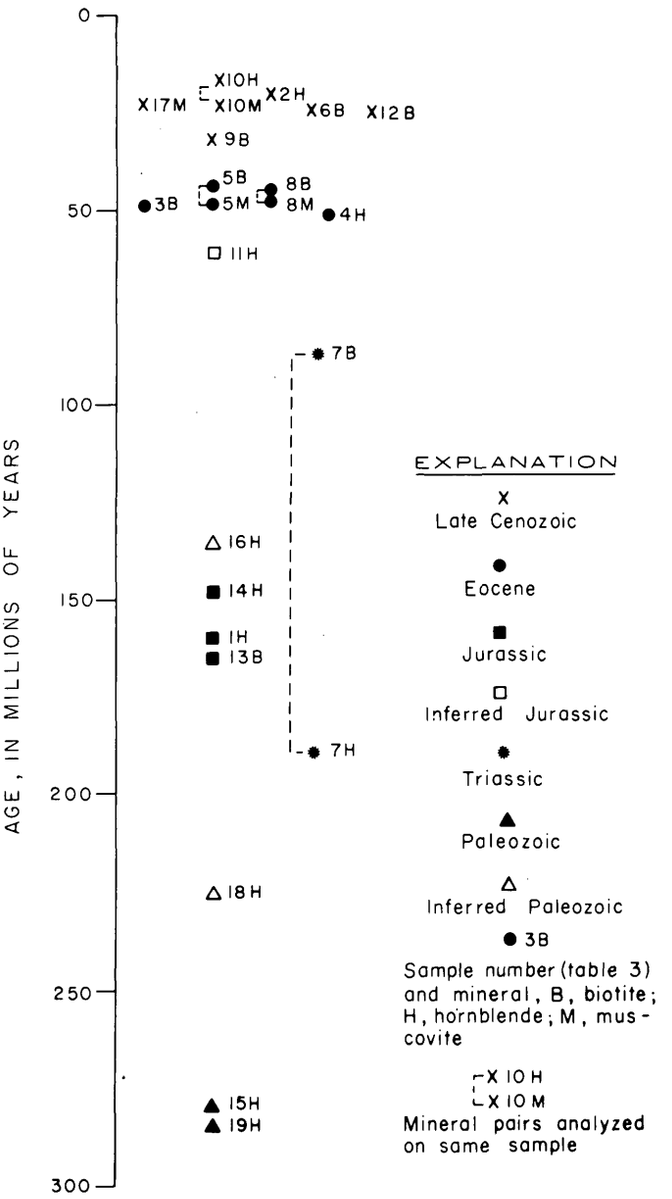

FIGURE 5.—Diagrammatic representation of apparent potassium-argon ages of the intrusive rocks discussed in this report.

Dikes sills, and plugs

Dikes, sills, and plugs of mafic, intermediate, and felsic composition are widespread in the area. Those discussed together here are not directly related to larger plutons and are probably all of Tertiary age. Only bodies that have been radiometrically dated are located on figure 4.

Felsic dikes are common throughout the Fairweather–Art Lewis and Hubbard terranes. They are most abundant in a complex stockwork of irregularly oriented, interconnected dikes that intrude the Art

Lewis Glacier pluton (fig. 4). These dikes are generally fine grained and leucocratic, but they also include simple biotite-albite-quartz pegmatites. Some of the fine-grained dikes are trondhjemitic. Two radiometric dates (Nos. 12 and 17, table 3, and fig. 4) on pegmatites from the Fairweather–Art Lewis terrane date them as early Miocene (fig. 5). They apparently are related to the Miocene thermal event that was accompanied by plutonic emplacement and widespread recrystallization (Hudson and others, 1977). The relation of these Miocene pegmatites to the leucocratic dikes east of the Art Lewis fault is not known.

Andesitic plugs and dikes locally intrude the Yakutat Group, and possibly cogenetic lamprophyre dikes intrude rocks in and around the Mt. Hubbard and St. Elias plutons (fig. 4). One small plug exposed on the shore of Russell Fiord is a porphyritic andesite with phenocrysts of plagioclase, hornblende, and quartz. The plug has sharply chilled margins, and potassium-argon dating of the hornblende has yielded an early Miocene age (No. 2, table 3, fig. 4). Compositionally similar mafic and lamprophyric dikes that intrude the Yakutat Group in the Russel Fiord area have been described by Tarr and Butler (1909, p. 176–177) and have been penetrated in the Malaspina 1A well (fig. 4) at a depth of 12 400–12 450 ft (feet) within what is probably an Eocene continental sequence.

Basaltic plugs and dikes intrude lower Tertiary strata at several localities in the western part of the Malaspina foothills. They are generally amygdaloidal and vesicular, may have flow structures such as oriented plagioclase laths, and commonly contain many secondary minerals including prehnite, calcite, quartz, epidot, and chlorite. Olivine-bearing basalt that may be intrusive was also found within the Tertiary sequence on the Yakutat Foreland (fig. 3) in the Dangerous River No. 1 well (1390–1720 ft) and in Core Hole No. 2 (4500–4600 ft) (fig. 4). These basaltic rocks may be correlative with the basaltic and andesitic submarine flows and pyroclastic rocks that are intercalated with clastic sedimentary rocks in the middle Tertiary Cenotaph, Poul Creek, and Katalla Formations elsewhere along the Gulf of Alaska margin (Plafker, 1971, 1974).

COMPOSITIONAL VARIATIONS

The plutonic rocks of the area can be divided into two broad compositional groups. The differences between these are most evident in the modal ratios shown in figure 2. Compositions in the first group are dependent primarily on plagioclase-quartz variation and characterize the Mesozoic and older intrusive rocks. These rocks are composed principally of mafic minerals and plagioclase with less abundant quartz and little or no potassium feldspar. Both the quartz and potassium feldspar form relatively small interstitial grains. The second compositional group is composed of more typical hypidiomorphic equigranular rocks in which intergranular quartz, potassium feldspar, and plagioclase produce the principal compositional variations. Rocks of the second group characterize the Tertiary plutons. The major shift in composition is not as clear in the plot of the normative ratios in figure 2 because many of the analyzed samples from the Tertiary plutons are from more mafic border facies.

The trace-element data are very limited, and the range of values for individual elements within rocks of a particular suite commonly overlaps the concentrations for the element in other suites. Nonetheless, the data suggest that some trace-element abundances might be helpful in distinguishing particular intrusive suites:

Paleozoic suite.—The strontium content is high, in the Paleozoic suite, over twice the average (440 parts per million) for high-calcium granitic rocks compiled by Turekian and Wedepohl (1961).

Triassic suite.—The one sample from the Triassic suite has the same strontium content as rocks in the Paleozoic suite, but the barium content is much lower. The barium content is less than half the average (420 ppm) for high-calcium granitic rocks compiled by Turekian and Wedepohl (1961). The sample also has a high copper content.

Jurassic suite.—The low and relatively uniform zirconium content may be characteristic of the tonalities in the Jurassic suite. The chromium values of the tonalites are, on the average, much higher than in the other suites.

The trace-element abundances in the younger suites are quite variable, and significant distinctions between the suites on the basis of trace elements are not obvious. In a general way, the shift to more felsic compositions in the Tertiary Period is evidenced by the higher barium and lower strontium and vanadium contents of rocks in the Eocene and late Cenozoic suites.

PLUTONISM AND MINERALIZATION

The Yakutat–St. Elias area was studied because the complex geology of the crystalline terrane was considered to be favorable for mineralization and because beach placers in the coastal areas contain deposits of gold, magnetite, ilmenite, and platinum (Tarr and Butler, 1909; Thomas and Berryhill, 1962; Wright, 1972; Reimnitz and Plafker, 1976) thought to have

been derived from the igneous and metamorphic rocks in the central part of the mountains.

Reconnaissance mapping and geochemical sampling of the crystalline terrane disclosed numerous small anomalous concentrations of many metals, but none that appear to have economic significance (MacKevett and Plafker, 1970). Furthermore, there are no known lode mineral prospects or previously mined lode deposits in the area. Simple pegmatite dikes are locally common, but late-stage and near-surface crystallization or thermal processes that characterize many mineral deposits associated with granitic rocks are poorly developed or absent. Contact zones locally contain some disseminated sulfide, but it is dominantly pyrite. The small bodies of sheared serpentinite along some of the larger faults are not associated with mineralization, and layered gabbro complexes, similar to those described by Rossman (1963) and Plafker and MacKevett (1970) in the Fairweather Range to the southeast, have not been identified. The available data suggest that the mineral resource potential of the Yakutat–St. Elias area is low for mineral deposits related to magmatic processes.

REGIONAL CORRELATIONS

Some of the plutonic suites are possibly correlative with intrusive rocks found elsewhere in southern Alaska on the basis of lithology or age:

Paleozoic suite.—Potassium-argon ages have been obtained on the Ahtell pluton in the eastern Alaska Range (Richter and others, 1975) and on intrusive rocks in the southeast McCarthy quadrangle (MacKevett, oral commun., 1975) that are near to the ages of the plutons in the Paleozoic suite of the Yakutat–St. Elias area. These complexes are not similar in detail, but consist mainly of quartz monzonite and monzonite with more mafic marginal facies (typically of granodiorite or syenodiorite and monzodiorite) whereas in the Yakutat–St. Elias area the plutons are chiefly composed of diorite and quartz diorite. This suggests that the plutons in the Paleozoic suite of the Yakutat–St. Elias area may not be part of the plutonic event that resulted in the emplacement of the other intrusive complexes to the northwest, even though all the complexes are apparently of similar age.

Triassic suite.—Plutonism possibly correlative with the Triassic suite has not been clearly identified in south-central Alaska. Upper Triassic andesitic volcanicastic rocks in the Seldovia area on the southern Kenai Peninsula (Martin and others, 1915, p. 55) indicate that local volcanism, and probably plutonism, occurred along the Gulf of Alaska margin during this time. The Seldovia area rocks are structurally on strike with and are a part of the regional geologic terrane that includes the Fairweather–Art Lewis terrane in the Yakutat–St. Elias area (Paleozoic and early Mesozoic bedded rocks of Plafker, 1969, p. 46; Taku-Skolai terrane of Berg and others, 1972). As the St. Elias block is considered to be correlative with the Fairweather–Art Lewis terrane, the Mt. St. Elias pluton (fig. 4) may be a part of an intrusive suite that is unrecognized elsewhere and cogenetic with the local Upper Triassic volcaniclastic rocks in south-central Alaska.

Jurassic suite.—The Jurassic is similar in age and lithology to parts of large intrusive complexes found west of the area in the northern Chugach Mountains (MacKevett, oral commun., 1975), in the Talkeetna Mountains (Grantz and others, 1963), and in the Alaska-Aleutian Range batholith (Reed and Lanphere, 1973). Similar Jurassic plutons have been identified to the southeast on Chichagof and Baranof Islands (Loney and others, 1967). In the Alaska and Aleutian Ranges and in the Talkeetna Mountains the Jurassic plutons define a curvilinear belt spatially associated with Early Jurassic andesitic volcanic rocks. This plutonic belt probably represents the lower levels of a Mesozoic magmatic arc (Reed and Lanphere, 1973, p. 2606). Farther east, the Jurassic plutons are not known to be directly associated with coeval or precursor volcanism.

Cretaceous or Tertiary suite.—Large plutons, composed of altered and deformed granitic rocks of intermediate composition, intrude the Mesozoic flysch sequences southeast of the map area in the Lituya District (George Plafker and Travis Hudson, unpub. data, 1975) and are believed to be correlative with the plutons in the Cretaceous or Tertiary suite of the Yakutat–St. Elias area. Other plutonic rocks are present in this southeastern extension of the Yakutat terrane, but the greenish-gray, altered tonalites of the Cretaceous or Tertiary suite are distinctive. The consistent geologic setting, occurrence, and lithologies of these intrusive rocks throughout the foothills belt help to establish that they represent a distinct plutonic event of regional extent.

Eocene suite.—The Eocene plutons are part of a distinctive belt of intermediate and felsic intrusive bodies that parallels the Pacific margin from Sanak Island, adjacent to the Alaska Peninsula nearly 1,600 km southwest of the Yakutat–St. Elias area, to Baranof Island, 390 km to the southeast. Plutons are exposed along this belt at Sanak Island (Moore, 1974), the Shumagin and Semidi Islands (Burk, 1965), Kodiak Island and Prince William Sound (Lanphere,

1966), eastern Chugach Mountains (Plafker and Lanphere, 1974), Yakutat–St. Elias area (this report), and Baranof Island (Loney and others, 1967). For the most part, these plutons occur between the central part of the Pacific Border Ranges and the coast, and most of them intrude late Mesozoic and early Tertiary flysch. There is a considerable range in their ages; in the western part of the belt the plutons are Paleocene (56–64 m.y.), in western Prince William Sound they are Oligocene (34–36 m.y.), and from eastern Prince William Sound to Chatham Strait they are Eocene (41–52 m.y.). Two important exceptions in the belt are the mafic and intermediate intrusive complexes, located on Yakobi and western Chichagof Islands, that are associated with nickel deposits (Reed and Dorr, 1942; Pecora, 1942). These complexes are apparently of Tertiary age, as they intrude the deformed Mesozoic flysch sequence, but they are not similar in composition or crystallization style to other plutons in the belt.

Except for the Oligocene plutons of eastern Prince William Sound which seem to be compositionally more heterogeneous than others in the belt (R. Tysdal, oral commun., 1975), the plutons share several characteristics: (1) they usually have sharp and crosscutting contacts and appear to have been emplaced in lower to middle epizonal environments, (2) they generally have simple felsic compositions and are mainly composed of biotite granodiorite and granite, and (3) they are locally foliate and typically have homogeneous medium-grained, seriate to equigranular, hypidiomorphic textures. The general textural and compositional homogeneity in these plutons indicates that they have simple crystallization histories.

The similarities in petrology, occurrence, and geologic setting of these plutons implies that they are similar in origin. The localization of these felsic plutons within accreted flysch terranes along the continental margin suggests that they are the result of anatectic processes within a thickened and deformed sediment pile. Under these conditions, the magma temperatures might not exceed that of the lower melting range, and the melts would be emplaced and crystallized in environments relatively close to their source regions. This would lessen the chance that individual plutons would undergo extended crystallization histories at high crustal levels and may help to explain why those types of mineralization and alteration that can be related to plutonic processes are absent in the coastal belt.

Late Cenozoic suite.—Late Cenozoic potassium-argon ages have been reported for some plutonic rocks on Baranof Island (Loney and others, 1967), but other temporal or lithologic correlatives of the late Cenozoic suite are not presently known in nearby areas. Effects of a major thermal influx, evidenced by mostly Miocene plutonism and metamorphism in the Yakutat–St. Elias area, should probably be expected elsewhere along the Gulf of Alaska continental margin.

SUMMARY AND DISCUSSION

The intrusive rocks of the Yakutat–St. Elias area consist of six suites of late Paleozoic, Triassic, Jurassic, Late Cretaceous or Tertiary, Eocene, and late Cenozoic age. The different suites have been identified on the basis of their field relations, petrology, radiometric age, and some aspects of their major- and trace-element chemistry. Although this study was reconnaissance in scope, it has clarified much of the plutonic history of the area and provided insight into the following important regional geologic relations:

1. The complexity of the plutonic history of the relatively small Yakutat–St. Elias area is due in large part to the structural juxtaposition of geologic terranes that differ distinctly in age, original geologic environment, and tectonic history. These terranes have been sandwiched into less than a 50-km wide zone, whereas elsewhere in southern Alaska, such as the Kodiak Island–Alaska Peninsula area, the terranes have an exposed width commonly greater than three times this distance.
2. The older plutonic suites tend to be restricted in their distribution to particular geologic terranes; the Paleozoic suite has only been identified in the Hubbard terrane, the Jurassic suite in the Fairweather–Art Lewis terrane, and the Cretaceous or Tertiary suite in the foothills belt.
3. The Tertiary plutons are more generally distributed and overall more felsic than the older plutons. Simple crystallization histories apparently characterize the Tertiary plutons, and their potential for generating significant mineralization is believed to be low.
4. Plutons of the Jurassic and Eocene suites are both parts of curvilinear plutonic belts that parallel the continental margin from the Alaska Peninsula to Baranof Island, but they are totally dissimilar in origin. The Jurassic suite appears to be part of an eastward extension of the Jurassic magmatic arc of the Alaska–Aleutian Range batholith, although coeval or precursor volcanic rocks are not known to be associated with the Jurassic plutons east of the Talkeetna Mountains.

The Eocene suite is part of an early Tertiary belt that has apparently formed as a result of anatectic processes in the deeper parts of an accreted flysch terrane.

5. The late Cenozoic suite is composed of many small plutons that are widely distributed and not deeply exposed. Most of them have not been dated directly, and their ages are in large part inferred. However, intrusive activity, mostly of Miocene age, was widespread in the area and, in addition to the granitic plutons, it included many dikes, sills, and plugs, both mafic and felsic. These intrusions were accompanied by widespread recrystallization of the metamorphic rocks of the area.
6. The distribution of the Tertiary plutons does not directly indicate the sense or amount of displacement on any of the major faults. Their distribution does not require large-scale horizontal displacements and could be accounted for by dominantly vertical movements along the throughgoing high-angle faults.

REFERENCES CITED

Berg, H. C., Jones, D. L., and Richter, D. H., 1972, Gravina-Nutzotin Belt—Tectonic significance of an upper Mesozoic sedimentary and volcanic sequence in southern and southeastern Alaska, *in* Geological Survey research 1972: U.S. Geol. Survey Prof. Paper 800–D, p. D1–D24.

Burk, C. A., 1965, Geology of the Alaska Peninsula—Island arc and continental margin: Geol. Soc. America Mem. 99, pt. 1, 250 p.

Campbell, R. B., and Dodds, C. J., 1975, Operation St. Elias, Yukon Territory: Canada Geol. Survey Paper 75–1, pt. A, p. 51–53.

Clark, S. H B., 1972, Reconnaissance bedrock geologic map of the Chugach Mountains near Anchorage, Alaska: U.S. Geol. Survey Misc. Field Studies Map MF–350.

Cox, Allen, and Dalrymple, G. B., 1967, Statistical analysis of geomagnetic reversal data and the precision of potassium-argon dating: Jour. Geophys. Research, v. 72, p. 2603–2614.

Dalrymple, G. B., and Lanphere, M. A., 1969, Potassium-argon dating—Principles, techniques, and applications to geochronology: San Francisco, W. H. Freeman, 258 p.

Geotimes, 1973, Plutonic Rocks—Classification and nomenclature recommended by the IUGS Subcommission on the systematics of igneous rocks: Geotimes, v. 18, no. 10, p. 26–30.

Grantz, Arthur, Thomas, Herman, Stern, T. W., and Sheffey, N. B., 1963, Potassium-argon and lead-alpha ages for stratigraphically bracketed plutonic rocks in the Talkeetna Mountains, Alaska, *in* Short papers in geology and hydrology: U.S. Geol. Survey Prof. Paper 475–B, p. B56–B59.

Hudson, Travis, Plafker, George, and Turner, D. L., 1977, Metamorphic rocks of the Yakutat–St. Elias area, south-central Alaska: U.S. Geol. Survey Jour. Research, v. 5, no. 2, p. 173.

Ingamells, C. O., 1970, Lithium metaborate flux in silicate analysis: Anal. Chim. Acta, v. 52, p. 323–334.

Irvine, T. N., and Baragar, W. R. A., 1971, A guide to the chemical classification of the common volcanic rocks: Canadian Jour Earth Sci., v. 8, p. 523–548.

Kindle, E. D., 1952, Dezadeash map-area, Yukon Territory: Canada Geol. Survey Mem. 368, 68 p.

Lanphere, M. A., 1966, Potassium-argon ages of Tertiary plutons in the Prince William Sound region, Alaska, *in* Geological Survey research 1966: U.S. Geol. Survey Prof. Paper 550–D, p. D195–D198.

Loney, R. A., Brew, D. A., and Lanphere, M. A., 1967, Post-Paleozoic radiometric ages and their relevance to fault movements, northern southeastern Alaska: Geol. Soc. America Bull., v. 78, p. 511–526.

Loney, R. A., Brew, D. A., Muffler, L. J. P., and Pomeroy, J. S., 1975, Reconnaissance geology of Chicagof, Baranof, and Kruzof Islands, southeastern Alaska: U.S. Geol. Survey Prof. Paper 792, 105 p.

MacKevett, E. M., Jr., Brew, D. A., Hawley, C. C., Huff, L. C., and Smith, J. G., 1971, Mineral resources of Glacier Bay National Monument, Alaska: U.S. Geol. Survey Prof. Paper 632, 90 p.

MacKevett, E. M., Jr., Hudson, Travis, and Tysdal, R. G., 1974, Relationship between the Taku-Skolai and Alexander terranes in the McCarthy quadrangle, *in* Carter, Claires, ed., United States Geological Survey Alaska Program, 1974: U.S. Geol. Survey Circ. 700, p. 51.

MacKevett, E. M., Jr., and Plafker, George, 1970, Geochemical and geophysical reconnaissance of parts of the Yakutat and Mount St. Elias quadrangles, Alaska: U.S. Geol. Survey Bull. 1312–L, p. L1–L12.

Martin, G. C., Johnson, B. L., and Grant, U. S., 1915, Geology and mineral resources of Kenai Peninsula, Alaska: U.S. Geol. Survey Bull. 587, 243 p.

Moore, J. C., 1974, Geologic and structural map of the Sanak Islands, southwestern Alaska: U.S. Geol. Survey Misc. Geol. Inv. Map I–817.

Myers, A. T., Havens, R. G., and Dunton, P. J., 1961, A spectrochemical method for the semiquantitative analysis of rocks, minerals, and ores: U.S. Geol. Survey Bull. 1084–I, p. 207–229.

Norman, M. B., II, 1974, Improved techniques for selective staining of feldspar and other minerals using amaranth: U.S. Geol. Survey Jour. Research, v. 2, no. 1, p. 73–79.

Pecora, W. T., 1942, Nickel-copper deposits on the west coast of Chichagof Island, Alaska: U.S. Geol. Survey Bull. 936–I, p. 221–243.

Plafker, George, 1967, Geologic map of the Gulf of Alaska Tertiary province: U.S. Geol. Survey Misc. Geol. Inv. Map I–484.

——— 1969, Tectonics of the March 27, 1964 Alaska earthquake: U.S. Geol. Survey Prof. Paper 543–I, p. I1–I74.

——— 1971, Pacific margin Tertiary basin, *in* Future petroleum provinces of North America: Am. Assoc. Petroleum Geologists Mem. 15, p. 120–135.

——— 1973, Yakutat Group, an upper Mesozoic flysch and melange sequence in southern Alaska [abs.]: Am. Assoc. Petroleum Geologists Bull., v. 57, no. 4, p. 800.

——— 1974, Preliminary geologic map of Kayak and Wingham Islands, Alaska: U.S. Geol. Survey Open-File Map 74–82.

——— 1976, Preliminary reconnaissance geologic map of the Yakutat and Mount Saint Elias quadrangles, Alaska: U.S. Geol. Survey open-file rept.

Plafker, George, and Lanphere, M. S., 1974, Radiometrically dated plutons cutting the Orca Group, *in* Carter, Claire, ed., United States Geological Survey Alaska Program, 1974: U.S. Geol. Survey Circ. 700, p. 53.

Plafker, George, and MacKevett, E. M., Jr., 1970, Mafic and ultramafic rocks from a layered pluton at Mount Fairweather, Alaska, *in* Geological Survey research 1970: U.S. Geol. Survey Prof. Paper 700–B, p. B21–B26.

Plafker, George, and MacNeil, F. S., 1966, Stratigraphic significance of Tertiary fossils from the Orca Group in the Prince William Sound region, Alaska, *in* Geological Survey research 1966: U.S. Geol. Survey Prof. Paper 550–B, p. B62–B68.

Reed, B. L., and Lanphere, M. A., 1973, Alaska—Aleutian Range batholith—Geochronology, chemistry, and relation to circum-Pacific plutonism: Geol. Soc. America Bull., v. 84, p. 2583–2610.

Reed, J. C., and Dorr, J. V. N., 2d, 1942, Nickel deposits of Bohemia Basin and vicinity, Yakobi Island, Alaska: U.S. Geol. Survey Bull. 931–F, p. 105–138.

Reimnitz, Erk, and Plafker, George, 1976, Marine gold placers along the Gulf of Alaska: U.S. Geol. Survey Bull. 1415, 30 p.

Richter, D. H., and Dutro, J. T., Jr, 1975, Revision of the type Mankomen Formation (Pennsylvanian and Permian), Eagle Creek area, eastern Alaska Range, Alaska: U.S. Geol. Survey Bull. 1395–B, 25 p.

Richter, D. H., Lanphere, M. A., and Matson, N. A., Jr., 1975, Granitic plutonism and metamorphism, eastern Alaska Range, Alaska: Geol. Soc. America Bull., v. 86, p. 819–829.

Rossman, D. L., 1963, Geology and petrology of two stocks of layered gabbro in the Fairweather Range, Alaska: U.S. Geol. Survey Bull. 1121–F, 50 p.

Shapiro, Leonard, and Brannock, W. W., 1962, Rapid analysis of silicate, carbonate, and phosphate rocks: U.S. Geol. Survey Bull. 1144–A, p. A1–A56.

Smith, J. G., and MacKevett, E. M., Jr., 1970, The Skolai Group in the McCarthy B–4, C–4, and C–5 quadrangles, Wrangell Mountains, Alaska: U.S. Geol. Survey Bull. 1274–Q, p. Q1–Q26.

Suhr, N. H., and Ingamells, C. O., 1966, Solution technique for analysis of silicates: Anal. Chemistry, v. 38, p. 730–734.

Tarr, R. S., and Butler, B. S., 1909, The Yakutat Bay region, Alaska: U.S. Geol. Survey Prof. Paper 64, 183 p.

Thomas, B I., and Berryhill, R. V., 1962, Reconnaissance studies of Alaskan beach sands, eastern Gulf of Alaska: U.S. Bur. Mines Rept. Inv. 5986, 40 p.

Turekian, K. K., and Wedepohl, K. H., 1961, Distribution of the elements in some major units of the earth's crust: Geol. Soc. America Bull., v. 72, p. 175–192.

Turner, D. L., Forbes, R. B., and Naeser, C. W., 1973, Radiometric ages of Kodiak Seamount and Giacomini Guyot, Gulf of Alaska—Implications for circumpacific tectonics: Science, v. 182, p. 579–581.

Winchell, A. N., and Winchell, Horace, 1967, Elements of optical mineralogy: Pt. II–Description of minerals [4th ed.]: New York, John Wiley and Sons, Inc., 551 p.

Wright, F. F., 1972, Marine geology of Yakutat Bay, Alaska, *in* Geological Survey research 1972: U.S. Geol. Survey Prof. Paper 800–B, p. B9–B15.

Jour. Research U.S. Geol. Survey
Vol. 5, No. 2, Mar.–Apr. 1977, p. 173–184

METAMORPHIC ROCKS OF THE YAKUTAT–ST. ELIAS AREA, SOUTH-CENTRAL ALASKA

By TRAVIS HUDSON, GEORGE PLAFKER; and DONALD L. TURNER

Menlo Park, Calif.; Fairbanks, Alaska

Astract.—Metamorphic rocks in the Yakutat–St. Elias area range in grade from zeolite to amphibolite facies. Radiometric age determinations on selected metamorphic rocks have helped to identify two major metamorphic events, one in Late Cretaceous time that was characterized by penetrative deformation, and one in the Miocene Epoch that resulted in widespread recrystallization and igneous intrusions. Mapped facies units show many discontinuities across major faults, and their distribution indicates major differential uplift between several structurally bound crustal blocks within a strongly deformed mobile belt west of the Art Lewis fault. Late Cretaceous metamorphic gradients indicate that the blocks have been tilted to the west or northwest parallel to their general structural grain. As mineral assemblages that were recrystallized during Miocene time occur on both sides of the Fairweather fault, large-scale, post-Miocene strike-slip movement along the fault is not indicated.

Metamorphic rocks in a part of the Yakutat and St. Elias quadrangles in the St. Elias Mountains were mapped and sampled during a regional reconnaissance study of the area by Plafker (1976). This paper outlines the distribution and character of metamorphic facies units and reports the results of potassium-argon age determinations of metamorphic rocks. Intrusive rocks are discussed in a companion paper (Hudson and others, 1977).

The area discussed covers approximately 16 000 square kilometers in the rugged and mountainous parts of the Yakutat and Mt. St. Elias quadrangles between the Canadian border and the Gulf of Alaska (fig. 1). It extends eastward to long 138° W. and westward to long 141° W. Geologically, it is characterized by the structural juxtaposition of broadly distinctive geologic terranes along major fault boundaries (figs. 1 and 2). These terranes are: (1) a belt of greenschist-facies marble, metavolcanic rocks, and mica schist northeast of the Art Lewis fault (Hubbard terrane), (2) a belt of greenschist-to-amphibolite-facies metavolcanic rocks and schistose metasedimentary rocks between the Art Lewis and Fairweather faults (Fairweather–Art Lewis terrane) that is probably equivalent to epidote-amphibolite- and amphibolite-facies metavolcanic rocks and mica schist in the St. Elias block north of the St. Elias thrust fault, (3) a foothills belt composed mostly of zeolite- to greenschist-facies flysch and melange of the Yakutat Group (Mt. Cook block, Boundary-Fairweather block, Malaspina and Yakutat foothills), and (4) a coastal lowland that is extensively covered by surficial materials and underlain mainly by nonmetamorphosed Tertiary nearshore sediments that overlie low-grade rocks of the Yakutat Group.

The Art Lewis fault juxtaposes terranes of differing regional metamorphic character. Areas west of this fault are part of a mobile belt characterized by complex deformation and variable recrystallization with metamorphic grades generally increasing northeastward roughly perpendicular to the major structural trends. In contrast, the deformation and metamorphic grade diminish rather abruptly east of the Art Lewis fault, and much of the nearby rock in Canada is of low metamorphic grade (Kindle, 1952; Campbell and Dodds, 1975).

Acknowledgments.—E. M. MacKevett, Jr., and Michael Perkins participated in the fieldwork during 1968 and mapped and sampled many of the metamorphic rocks. Phillip Frame and Gary Winkler separated the minerals used for potassium-argon dating, and M. A. Lanphere provided a potassium-argon age determination on one of the amphibole separates.

METHODS OF STUDY

The reconnaissance field studies were supported by helicopter and carried out under the direction of Plafker during parts of the 1967, 1968, and 1969 field seasons. Petrographic studies and data compilation were done by Hudson, and most of the potassium-argon age determinations were provided by D. L. Turner.

Thin sections of the metamorphic rock sampled at localities shown in figure 2 were used to identify the metamorphic mineral assemblages and important textural relations. Facies assignments based on the as-

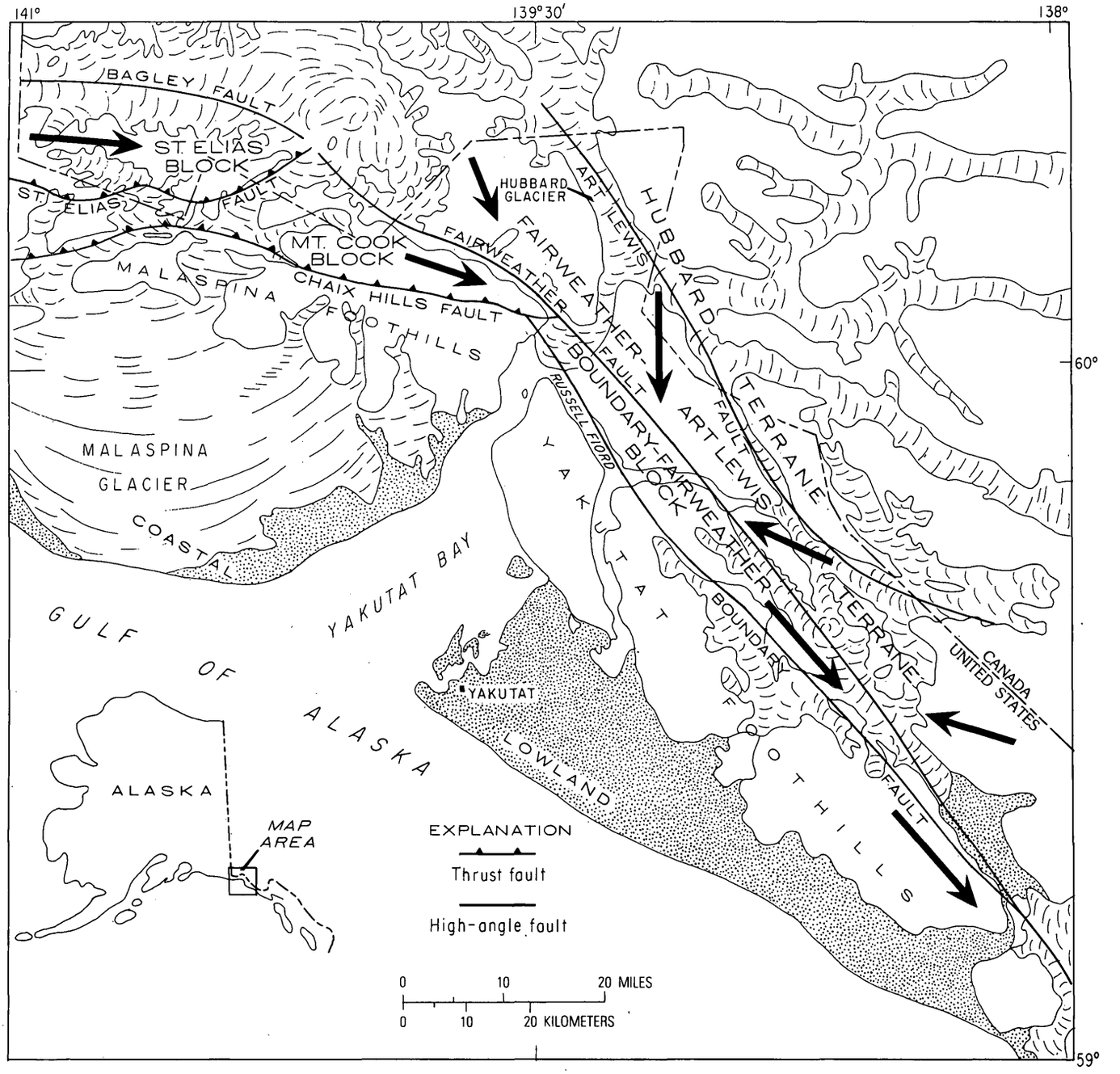

FIGURE 1.—Index map of Yakutat–St. Elias area showing major structural blocks and fault boundaries referred to in text. Arrows indicate general direction of increasing metamorphic grade.

semblages were made following the classification of Turner (1968). The plagioclase compositions were estimated (as An $_{<15}$, An $_{\geqslant 15}$, and An $_{>15}$) by comparison of the plagioclase refractive indices to that of the mounting medium of the thin sections (Lakeside thermoplastic cement, $n=1.537$). Extinction angles of elongate amphibole sections were used to differentiate actinolite and hornblende.

Fourteen biotite and amphibole mineral separates were analyzed to determine their apparent potassium-argon ages. Analytical techniques used have been described previously (Turner and others, 1973). The analytical data are listed in table 1, and petrographic descriptions of the analyzed samples are shown in table 2.

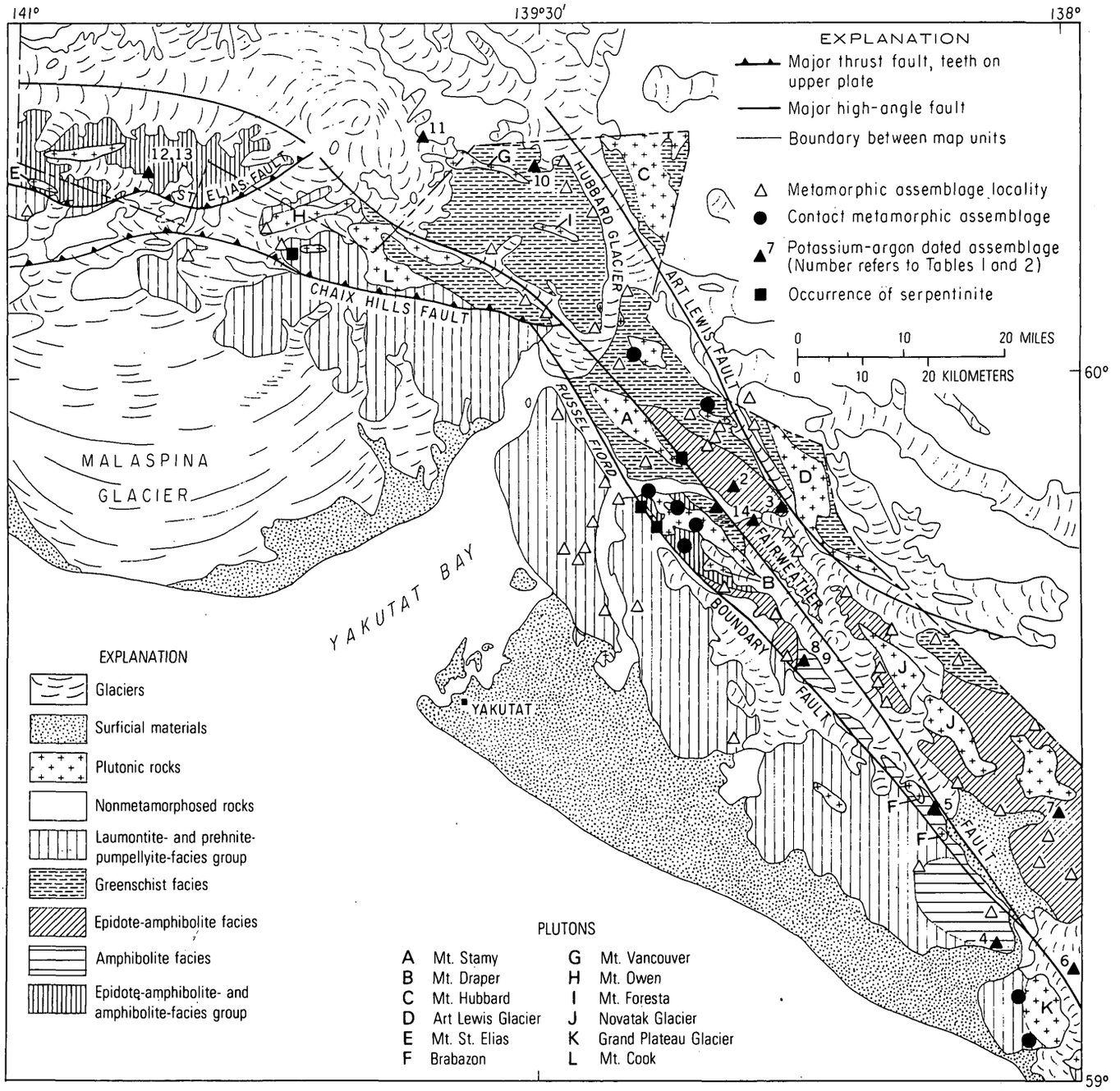

FIGURE 2.—Distribution of metamorphic facies units and assemblage localities in Yakutat–St. Elias area, south-central Alaska.

METAMORPHIC FACIES UNITS

It has been suggested (Zwart and others, 1967) that three standard facies series (Miyashiro, 1961; Hietanen, 1967) and four facies groups be used for the cartographic representation of metamorphic units, and some criteria have been outlined for distinguishing between them. Facies groups as proposed (Zwart and others, 1967, p. 58) and as used in this report are combinations of facies that are useful in defining map units because of difficulties in showing individual facies at the map scale used or because the data are insufficient to define the distribution of individual facies. Differences between the facies included in a facies group are largely due to variations in temperature and are independent of pressure. The recognition of a standard facies series is handicapped in the Yakutat–St. Elias area by the structural juxtaposition of rocks of different metamorphic grade and the resulting lack of continuous transitions between assemblages as well

TABLE 1.—*Potassium-argon ages and analytical data*

[Nos. 1-13 by D. L. Turner, Univ. of Alaska; No. 14 by M. A. Lanphere; σ, standard deviation; $\bar{x}$, sample mean]

No. (fig. 2)	Field No.	Lat (N)	Long (W)	Mineral	Percent K_2O	Average K_2O (percent)	^{40}Ar rad (10^{-10} mol/g)	$\frac{^{40}Ar\ rad}{^{40}Ar\ total}$	Apparent age ± 1σ (m.y.)
1	63 APr 219	59°49.6'	139°1.8'	Amphibole	0.024, 0.024	0.024	0.2303	0.444	63.8±1.9
2	67 APr 44B	59°51.1'	138°59.8'	do.	.061, .063	.062	.0626	.042	67.2±2.0
3	67 APr 45B	59°48.7'	138°48.8'	Biotite	9.080, 9.088	9.084	2.614	.774	19.4± .6
4	68 APs 57F	59°11.8'	138°12.7'	do.	8.990, 8.995	8.992	.5527 .4998	.219 .319	4.1± .12 3.8± .15 $\bar{x}$ = 3.95± .15
5	68 APs 65B	59°23.8'	138°24.6'	Amphibole	.660, .660	.660	.6489	.792	65.4±2.0
6	68 APr 78D1	59°8.4'	138°0.2'	do.	.220, .220	.220	.0604	.134	18.5± .6
7	68 APr 84A	59°22.2'	138°6.6'	Biotite	9.492, 9.527	9.509	3.299	.710	23.3± .7
8	68 APr 106A2	59°35.5'	138°46.3'	do.	8.279, 8.278	8.278	3.717	.802	30.1± .9
9	68 APr 106B	59°35.5'	138°46.3'	Amphibole	.094, .095	.094	.0665	.363	47.0±1.4
10	69 APr 37D	60°18.1'	139°31.9'	do.	.256, .256	.256	.2247	.443	58.5±1.7
11	69 APr 43B3	60°20.9'	139°50.0'	do.	.320, .322	.321	.2450	.710	51.0±1.5
				Biotite	8.802, 8.766	8.784	6.215	.885	47.3±1.4
12	69 APr 47C1	60°17.3'	140°40.5'	do.	7.948, 7.963	7.955	2.057	.740	17.4± .5
13	69 APr 47C2	60°17.3'	140°40.5'	Amphibole	.250, .250	.250	.0871	.173	23.4± .7
14	63 APr 205	59°48.2'	138°53.3'	do.	.279, .279	.279	.0909	.34	21.9±1.0

as by the fact that the metamorphic grades generally did not exceed the lower amphibolite facies. The absence of blueschist-facies rock in outcrop and of higher grade assemblages that contain kyanite or sillimanite suggests that the area has undergone dominantly low-pressure-facies series metamorphism.

Metamorphic rocks in the Yakutat–St. Elias area range from zeolite to amphibolite facies. The facies units that have been mapped (fig. 2) include: (1) laumontite and prehnite-pumpellyite-facies group, (2) greenschist facies, (3) epidote-amphibolite facies, (4) amphibolite facies, and (5) epidote-amphibolite- and amphibolite-facies group. The boundaries between facies units are approximate, and many changes in them, as well as in mapped units, would result from more detailed work. Nonetheless, the data are sufficient to identify regional metamorphic grades in a general way and to show relations between the metamorphic grades and the important structural elements in the area. The characteristics of the metamorphic map units are discussed below. Nonmetamorphosed rocks in the area have been described elsewhere (Plafker, 1976).

Laumontite- and prehnite-pumpellyite-facies group

Rocks assigned to the laumontite- and prehnite-pumpellyite-facies group are restricted to the eugeosynclinal sedimentary and related volcanic rocks of the Yakutat Group (Jurassic? and Cretaceous) in the western Mt. Cook block and the Malaspina and Yakutat foothills. In the southeastern part of the foothills belt, these rocks grade over a narrow interval into amphibolite-facies rocks, but the transitional facies units have not been shown on figure 2. In addition, cordierite-bearing hornfels is present in the Yakutat Group adjacent to the Grand Plateau Glacier pluton (pluton K, fig. 2) in the southeastern Yakutat foothills. It has not been possible to map zeolite-facies rocks separately from those of prehnite-pumpellyite facies because of the limited number of sample localities and because many of the observed assemblages are transitional between the two facies and contain both laumontite and prehnite.

Locally, these low-grade rocks are strongly sheared and complexly folded, but original sedimentary textures and structures are generally well preserved. The sandstones are feldspathic and tightly indurated, and associated argillite is slaty in many cases. The recog-

TABLE 2.—*Summary of petrographic data for age-dated metamorphic rocks*

No. (fig. 2)	Field No.	Lithology and composition	Metamorphic mineral assemblage*	Facies assignment	Remarks
1	63 APr 219	Amphibolite, mafic	Hornblende, plagioclase (An ≥15), chlorite (8%), magnetite, (garnet).	Epidote-amphibolite	Fine-grained schistose, partially segregated, porphyroblastic plagioclase, minor epidote.
2	67 APr 44B	do.	Hornblende, plagioclase (An >15), epidote, (sphene).	do.	Schistose, nonsegregated, semigranoblastic plagioclase, intergranular epidote (3%), minor opaque minerals.
3	67 APr 45B	Gneissic schist, quartzofeldspathic.	Quartz, plagioclase (An ≥15), biotite, muscovite, clinozoisite (4%), (garnet, sphene).	do.	Fine-grained, doubly foliated, compositionally banded, quartz with undulatory extinction, honey-brown biotite, intergranular anhedral clinozoisite.
4	68 APs 57F	Schist, quartzofeldspathic	Quartz, plagioclase (An >15), potassium feldspar, biotite, opaque minerals (garnet, apatite).	Amphibolite	Fine-grained semigranoblastic red-brown biotite, minor tourmaline and sphene.
5	68 APs 65B	Amphibolite, mafic	Hornblende, plagioclase (An ≥15), magnetite (6%), biotite, (apatite).	do.	Fine-grained, schistose, partially segregated, some crosscutting thin shear zones, incipient brown biotite after amphibole, dusty plagioclase.
6	68 APr 78D1	Greenstone, mafic	Actinolite, plagioclase (An ≥15), epidote (10%), magnetite (2%).	Greenschist	Schistose, partially segregated, clots of fine- to medium-grained green actinolitic amphibole, segregated magnetite and sphene stringers, intergranular epidote.
7	68 APr 84A	Schist, quartzofeldspathic	Quartz, plagioclase (An ≥15), biotite, hornblende, clinozoisite, (sphene, magnetite).	Epidote-amphibolite	Schistose but with semigranoblastic quartz and plagioclase, thin compositional banding, honey-brown biotite, intergranular clinozoisite, poikilitic hornblende to 2.4 mm long.
8	68 APr 106A2	do.	N.A.	N.A.	N.A.
9	68 APr 106B	Amphibolite, mafic	Hornblende, plagioclase (An >15), magnetite, (sphene, apatite).	Amphibolite	Schistose, segregated aggregates of anhedral poikilitic plagioclase, granular sphene and magnetite, some small granular epidote in plagioclase.
10	69 APr 37D	do.	Hornblende, plagioclase (An ≥15), quartz, epidote, chlorite, muscovite, magnetite.	Epidote-amphibolite	Schistose with very fine grained and granoblastic quartz and plagioclase domains, compositionally segregated, crosscutting epidote-prehnite veinlets; contact zone assemblage?
11	69 APr 43B3	Schist, feldspathic	Plagioclase (An ≥15), biotite, quartz, hornblende, magnetite, (garnet).	Amphibolite	Fine- and even-grained granoblastic plagioclase, bright red-brown biotite, quartz in segregation bands; contact zone assemblage?
12	69 APr 47C1	Schist, quartzofeldspathic	Plagioclase (An >15), biotite, quartz, opaque minerals (magnetite and sulfide), garnet, staurolite, muscovite.	do.	Doubly foliated with porphyroblasts of euhedral garnet and poikilitic staurolite.
13	69 APr 47C2	Amphibolite, mafic	Hornblende, plagioclase (An ≥15), quartz, magnetite, sphene.	do.	Fine-grained, schistose, partially segregated, cleanly crystallized.
14	63 APr 205	do.	Hornblende, plagioclase (An ≥15), epidote, quartz, sphene.	Epidote-amphibolite	Fine- to medium-grained, schistose, poorly segregated, green to brown hornblende, twinned and slightly warped plagioclase, granular epidote, fine-grained quartz with complex irregular boundaries.

* Listed in order of decreasing abundance. Parentheses indicate minerals present as minor constituents.

nized metamorphic mineral assemblage includes only minerals that are clearly of secondary origin, such as minerals that occur interstitially or in veinlets, and not those that are restricted to replacements of detrital mineral grains or lithic fragments. Twenty-three of 36 sandstone samples contain an assemblage diagnostic of the facies group, and the typical assemblage includes laumontite, prehnite, calcite, chlorite, and white mica. Laumontite, calcite, prehnite, and quartz occur interstitially and in veinlets, but chlorite and white mica occur mostly as interstitial grains. Quartz is considered part of the metamorphic assemblage even though its secondary origin is not always clear.

Generally laumontite does not occur without prehnite, although the reverse is not uncommon. Pumpellyite occurs interstitially but is dominantly restricted to lithic grains of mafic composition. A few specimens contain very fine grained, patchy, and granular epidote together with white mica and chlorite. This assemblage indicates that lower-greenschist-facies metamorphic conditions were reached locally within parts of the low-grade Yakutat Group rocks of the foothills belt.

Greenschist facies

Greenschist-facies rocks occur in the Hubbard terrane, the Fairweather–Art Lewis terrane, and in the Mt. Cook and Boundary-Fairweather blocks of the foothills belt. They display wide ranges in metamorphic texture, structure, and degree of recrystalli-

zation. Some, such as semischist and slate, have not been completely recrystallized, but they are mapped with the greenschist-facies unit because they do not contain mineral assemblages diagnostic of the next lower facies unit, and they grade into or are associated with, rocks of more typical greenschist-facies character. The greenschist-facies rocks generally grade into higher grade rocks or are structurally bound, but in the Mt. Cook block a westward transition to lower grade rocks is apparently present. This transition is confused by structural complications in melange and by large intrusive bodies at Mt. Cook and Mt. Owen (plutons L and H, fig. 2).

Greenschist-facies rocks of the foothills belt are dominantly slate, phyllite, and semischist inferred to be correlative with the Yakutat Group, and they retain many original features such as bedding and detrital textures. Typical assemblages contain white mica, chlorite, calcite, and some patchy very fine grained epidote. Incipient biotite is a local constituent.

In the Fairweather–Art Lewis terrane, the greenschist facies consists of metasedimentary and metavolcanic rocks. The metasedimentary rocks are semischist and schist that were derived from quartzofeldspathic sandstone and finer grained sedimentary rocks. They commonly contain white mica, chlorite, quartz, plagioclase (of variable composition), clinozoisite, and some biotite. The metavolcanic rocks are moderately abundant and were originally mainly intermediate to mafic volcaniclastic rocks. They are generally fine-grained and thinly banded schist that contains quartz, actinolite, calcite, albite, and epidote. In outcrop the epidote commonly forms conspicuous green bands and segregations.

In the Hubbard terrane, most of the nonplutonic rocks are metamorphosed to greenschist facies and include abundant coarsely crystalline marble, massive to thinly banded mafic metavolcanic rocks that are mainly typical greenschist, and mica schist. In the vicinity of the large Mt. Hubbard and Art Lewis Glacier plutons (plutons C and D, fig. 2), the rocks are of higher grade and amphibolites are common. Typical assemblages in the metavolcanic rocks contain actinolite, albite, epidote, and calcite. Mica schist interbedded with marble contains muscovite, chlorite, and quartz. The marble is light colored, foliated, and contains variable amounts of impurities ranging from disseminated graphite to thin discontinuous segregations of silicate minerals including pyroxene, tremolite, white mica, and plagioclase. The only specimen from the entire area that appears to be retrograded was collected near the Art Lewis Glacier pluton just south of the international boundary. It is a chlorite-quartz-muscovite schist with an incipient second foliation oblique to the primary schistosity. It contains almost completely chloritized garnet porphyroblasts, sericitized plagioclase grains, and aggregates of fine-grained chlorite, white mica, oqaque minerals, and sphene that have apparently replaced some preexisting mafic mineral (hornblende?).

The area mapped as greenschist facies immediately northeast of the Mt. Draper pluton (pluton B, fig. 2) includes a small higher grade amphibolite-diorite complex that is characterized by segregation and injection gneisses. Deformation features such as warped plagioclase, undulatory extinction in quartz, and granulated shear zones are common, as are exceptionally well crystallized rocks with clean unzoned plagioclase and interstitial to porphyroblastic amphibole. Typical assemblages are either plagioclase, tremolite, chlorite, and quartz, or hornblende, plagioclase, and quartz. Biotite and garnet are locally present. The variable metamorphic grade and complex textures suggest conditions intermediate between those of metamorphic and igneous environments, and the deformation features are undoubtedly due to displacement along the adjacent active Fairweather fault. This area, informally known as the Nunatak, probably represents the root zones of the Mt. Stamy pluton (pluton A, fig. 2) which broadens into a lensoid body along strike to the northwest.

Foliation is generally well developed in the greenschist-facies rocks and usually parallels original layering except near the axes of folds. In some rocks, less well developed secondary foliations produce lineations in the primary foliation plane. Such rocks are mainly located near the Art Lewis or Fairweather faults, and they contain strained quartz, distorted micas, and small shear zones and veinlets with secondary minerals. In many cases, the second foliation is probably due to deformation from the nearby major faults. An extreme example of this is a zone of orange-weathering, light-colored, fine-grained, and strongly mylonitized rocks on the east side of the Fairweather fault at Hubbard Glacier. Some rocks in this zone were originally granitic, but they now consist of granulated, elongated aggregates of polygonized quartz and plagioclase, wavy muscovite, and angular microcline grains with undulatory extinction.

Epidote-amphibolite facies

Rocks of epidote-amphibolite facies (greenschist-amphibolite transitional facies of Turner, 1968) occur in the southeast part of the map area west of the Art Lewis fault. They are generally structurally bound

or transitional with lower grade rocks of greenschist facies. The metamorphic grades within this facies vary widely, and although the rocks are completely recrystallized, they have variable granularity and schistosity and contain minerals characteristic of both amphibolite- and greenschist-facies environments. Judging from their textural development, the highest grade rocks in this facies are in parts of the amphibolite belt and in nearby schist in the central part of the Fairweather–Art Lewis terrane northeast of Russell Fiord.

In the Boundary-Fairweather block, the small area of epidote-amphibolite-facies rocks includes mafic metavolcanic rocks and quartzofeldspathic schist. The metavolcanic rocks are fine- to medium-grained strongly foliated amphibolites that contain epidote and hornblende. The schist contains plagioclase of variable composition, muscovite, biotite, quartz, and some partially chloritized garnet. The area includes some rocks of greenschist facies that contain chlorite, clinozoisite, and calcite.

A larger area of epidote-amphibolite-facies rocks occurs in the Fairweather–Art Lewis terrane and includes a belt of amphibolite adjacent to the Fairweather fault and quartzofeldspathic schist with intercalated metavolcanic rocks to the east and south. The metasedimentary rocks locally include metachert and marble. The amphibolite is fine to medium grained, variably segregated, and characteristically contains hornblende, plagioclase ($An_{\geqslant 15}$), epidote, some quartz, and locally chlorite. Hornblende is usually dark (almost black) in hand specimens and locally forms poikilitic porphyroblasts. The schist is variably banded, strongly schistose to semigranoblastic, and contains quartz, biotite, plagioclase ($An_{\geqslant 15}$ generally), muscovite, and garnet. In the immediate vicinity of the Novatak Glacier pluton (pluton J, fig. 2), the rocks are of slightly higher grade and include garnet-plagioclase ($An_{>15}$)-quartz-chlorite schist and quartz-plagioclase ($An_{>15}$)-hornblende amphibolite.

Amphibolite facies

Amphibolite-facies rocks have been mapped in the southern part of the Boundary-Fairweather block and in the nearby southern part of the Yakutat foothills.

The amphibolite-grade area in the Boundary-Fairweather block contains two lithologically distinct parts; the northern part is composed of quartzofeldspathic metasedimenetary rocks, and the southern part is dominantly mafic metavolcanic rocks. In the northern part, the original rocks were a layered, dominantly sandstone sequence that was probably part of the Yakutat Group. They are now very similar to the coarse grained amphibolite-facies metasedimentary rocks west of the Boundary fault, and the original bedding relations are generally clear. Typical quartzofeldspathic schist is fine to medium grained, semigranoblastic, and contains quartz, plagioclase (probably $An_{>15}$), biotite, and garnet.

In the southern part, the metavolcanic rocks are massive to thinly bedded and in large part volcaniclastic. They range from thinly laminated green to light-gray metatuff to massive porphyritic flow rocks. Interbedded wtih these are a variety of metasedimentary rocks including very fine grained pelitic rocks, metasandstone and conglomerate, and fine to coarsely crystalline gray-weathering marble. The schistosity is variable, and many of the more foliated rocks may be locally cataclastic. Slightly reddish, dense, and very fine grained hornfels is locally present. The dated specimen (no. 5, tables 1 and 2) is a typical amphibolite, but its proximity to the Brabazon plutons (plutons F, fig. 2) and the presence of incipient biotite suggest that it has been thermally recrystallized. Thermally induced recrystallization may be responsible for other higher grade rocks in this area, which probably contains assemblages ranging from greenschist to amphibolite facies. The metamorphic diversity of this southern area contrasts sharply with that of the more homogeneous northern area of quartzofeldspathic schist, and the contact between the two areas may be a fault that strikes northwestward, oblique to the Fairweather and Boundary faults in the vicinity of the mapped lithologic break (Plafker, 1976).

In the southern part of the Yakutat foothills, amphibolite-facies rocks from a broad northwest-plugging antiform and have a sharply transitional contact with zeolite- and prehnite-pumpellyite-facies group metasedimentary rocks of the Yakutat Group. The transition from low- to high-grade facies occurs over a horizontal distance commonly less than 1.5 km, and the distribution of intermediate facies is too narrow to be shown in figure 2. The amphibolite-facies rocks represent an interbedded sandstone-pelite sequence that has been thoroughly recrystallized, but the general bedding relations are still preserved. Quartzo-feldspathic schist contains quartz, plagioclase ($An_{>15}$), potassium feldspar, biotite, garnet, and locally minor tourmaline. Interbedded pelitic layers are very rich in biotite and also contain quartz, garnet, and locally andalusite porphyroblasts. The principal schistosity is parallel to compositional banding and is generally defined by the orientation and concentration of biotite. Semigranoblastic textures are well developed, and unstrained quartz and red-brown biotite are characteristic. The sharp facies gradient into the amphibolite-facies rocks,

the preserved bedding relations, the mineral assemblages containing andalusite, and the granoblastic texture suggest that this higher-grade area is largely the result of thermally induced recrystallization.

Epidote-amphibolite- and amphibolite-facies group

The St. Elias block and part of the Boundary-Fairweather block have been mapped as containing rocks of the epidote-amphibolite- and amphibolite-facies group. This unit was designated, because, near the Mt. Draper pluton (pluton B, fig. 2) the facies relations are complicated by an irregular contact aureole and because, north of the St. Elias thrust fault the field data and sampling collections are insufficient to distinguish individual facies units. Both areas contain some greenschist-facies rocks.

In the Boundary-Fairweather block, the Mt. Draper pluton (pluton B, fig. 2) intrudes metasandstone and interbedded fine-grained metasedimentary and mafic metavolcanic rocks of the Yakutat group. The facies distribution is complex near this pluton owing to the irregularity of the intrusive contact. The facies gradient is steep on the east side of the pluton where the contact is relatively continuous and steeply dipping, and only the distribution of greenschist-facies rocks can be shown at the scale of figure 2. On the west side, however, pendants and roof zone rocks containing epidote-amphibolite- and amphibolite-facies assemblages are exposed over a larger area. As these different facies are not systematically distributed with respect to the present exposed contacts of the pluton, the pluton must underlie much of this area irregularly. The recrystallized rocks are schistose, but they typically have semigranoblastic textures, and poikiloblastic and(or) porphyroblastic crystals are common. In the metasedimentary rocks, lower grade assemblages contain quartz, plagioclase, biotite, clinozoisite or epidote, and garnet. Higher grade assemblages contain quartz, plagioclase ($An_{>15}$), biotite, muscovite, garnet, and locally staurolite. Rocks of mafic composition are not abundant but do occur in some small pendants. They are semigranoblastic amphibolite with hornblende, plagioclase ($An_{>15}$), and less abundant opaque minerals, epidote-group minerals, and quartz.

The St. Elias block is a metamorphic terrane characterized by an east-west structural grain. It has been thrust southward over Tertiary strata and the zeolite and prehnite-pumpellyite facies of the Yakutat Group. Sampling in this area was minimal because it is exceptionally rugged and is largely in Canada. Most of the rocks sampled are dark greenish-black sulfide-bearing amphibolite and less abundant interbedded, reddish-weathering schist. Between these rocks and the St. Ellias thrust fault is a structurally conformable sequence of interbedded slate, phyllite, quartzite, feldspathic metasandstone, and minor stretched metaconglomerate. The sequence contains quartz veins and is intruded by leucocratic dikes. The amphibolite sequence contains some assemblages that are indicative of the amphibolite facies (Nos. 12 and 13, tables 1 and 2), but farther west along strike in the Bering Glacier quadrangle, some of the rocks are greenschist that contains abundant actinolite, chlorite, and epidote (Plafker, unpub. data, 1974). The higher grade assemblages (nos. 12 and 13, tables 1 and 2) may be the result of contact metamorphism, in which case the distribution of amphibolite-facies rocks within the St. Elias block would be limited. The apparent transition from lower grade metasedimentary rocks (slate, quartzite, metasandstone) northward to amphibolite-facies metavolcanic rocks may reflect either an exceptionally steep metamorphic gradient or alternatively structural juxtaposition of the amphibolite sequence southward over the lower grade metasedimentary rocks. The sparse data available are not adequate to resolve the issue. However, the same geologic relations occur in an area just north of the Fairweather fault at Hubbard Glacier, where there is good exposure and no evidence of faulting. This suggests that very steep local metamorphic gradients do exist in the area.

POTASSIUM-ARGON DATED METAMORPHIC EVENTS

Potassium-argon ages for the 14 dated metamorphic rocks from the Yakutat–St. Elias area (table 1, fig. 3) fall into four groups; (1) an older set of amphibole ages that ranges from 58.5 to 67 m.y. (million years), (2) a set of coexisting biotite and amphibole ages that are discordant ranging from 30 to 51 m.y., (3) a set of biotite and amphibole ages that are in part discordant ranging from 17 to 23 m.y., and (4) a single very young biotite age of 4 m.y. The older set gives a minimum age for the regional metamorphism that was largely dynamothermal and the principal cause of penetrative deformation throughout the area. This Late Cretaceous metamorphism accompanied the deformation and accretion of thick eugeosynclinal sequences of the late Mesozoic Valdez and Yakutat Groups throughout southern Alaska (Plafker, 1972; MacKevett and Plafker, 1974).

The two sets of discordant ages within the 30–51 m.y. range reflect the intrusion of an Eocene pluton and resetting during a major Miocene thermal event.

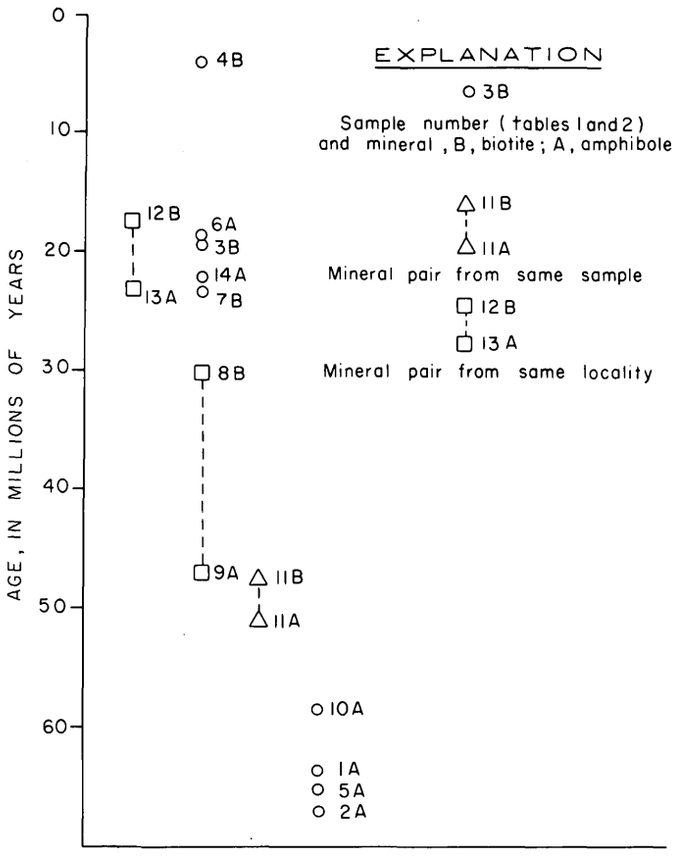

FIGURE 3.—Diagrammatic representation of apparent potassium-argon ages of metamorphic rocks dated in this report. Sample localities shown in figure 2.

The older discordant pair (no. 11, tables 1 and 2) is from a sample collected near the contact of the Eocene Mt. Vancouver pluton (pluton G, fig. 2) that straddles the international boundary in the north-central map area. The other pair (Nos. 8 and 9, tables 1 and 2) are from samples collected in the Boundary-Fairweather block. In these samples, biotite and probably the hornblende have been partially reset during the Miocene Epoch as discussed below.

The ages between 17 and 23 m.y. are the result of a major regional metamorphic event. This event, although not associated with extensive penetrative deformation, was accompanied by sufficiently high temperatures to reset or initially crystallize biotite and amphibole in metamorphic rocks throughout large areas. Semigranoblastic textures are common in the rocks that were recrystallized during this event. Thermal resetting, rather than cooling related to uplift, is suggested by discordances in age between amphiboles from the same amphibolite unit at localities less than 5 km apart (Nos. 2 and 14, fig. 2) and by striking discordances in age between dated minerals from metamorphic rocks and from nearby plutons that probably underwent the same uplift history.

One biotite separate from the amphibolite-facies rocks in the southern part of the Yakutat foothills yielded a remarkably young and consistent age of 4 m.y. (No. 4, fig. 2, tables 1 and 2). As discussed earlier, these amphibolite-facies rocks are semigranoblastic and texturally appear to have been recrystallized by thermal processes. The reason for the young potassium-argon age is unknown but some possible explanations are: (1) the age represents a very local contact metamorphism by an unrecognized intrusion, (2) the age is representative of the entire higher grade area and is due to recrystallization that has accompanied intrusion of a large unexposed pluton, or (3) the age represents the time at which the terrane was uplifted and passed through the critical biotite isotherm for argon retention. Even though the metamorphic nature of these higher grade rocks is apparently similar to that of the rocks recrystallized during Miocene time, the radiometric age suggests that their metamorphism may be unrelated to the Miocene event.

In summary, the potassium-argon age data document two major metamorphic events, one with a minimum age of about 65 m.y. and one that occurred about 20 m.y. ago. In one area, recrystallization appears to have occurred as recently as 4 m.y. ago. The effects of any regional metamorphism prior to 65 m.y. ago have not been recognized, although there is strong reason to believe that pre-Cretaceous metamorphism affected the Fairweather–Art Lewis terrane, the St. Elias block, and perhaps the Hubbard terrane.

Areas that may have been affected by metamorphism prior to 65 m.y. ago are those known to be of at least Jurassic age. The minimum ages of the older parts of the Yakutat–St. Elias area are known from the ages of the plutons that intrude them; the Fairweather–Art Lewis terrane is intruded by Jurassic plutons, the St. Elias block is cut by a pluton that is of at least Triassic age, and the Hubbard terrane contains late Paleozoic plutons (Hudson and others, 1976). To the northwest in Canada, and farther west in the northern Chugach Mountains, nonmetamorphosed Lower Cretaceous strata overlie metamorphic and plutonic rocks that are on strike with, and similar to, those in the Fairweather–Art Lewis terrane (Sharp and Rigsby, 1956, MacKevett and others, 1974). In the northern Chugach Mountains, the metamorphic rocks are part of the Skolai Group of Pennsylvanian and Permian age (Smith and MacKevett, 1970, Richter and Dutro, 1975). As the Lower Cretaceous sedimen-

tary rocks appear to have been deposited on the underlying metamorphosed terrane, a pre-Early Cretaceous metamorphism must have affected the upper Paleozoic rocks. If so, the same may be true for their probable correlatives in the Yakutat–St. Elias area which, in addition to the metamorphic rocks of the Fairweather–Art Lewis terrane, includes the rocks of the St. Elias block. This metamorphism probably accompanied a period of orogeny that took place in the Jurassic Period throughout a large part of southern Alaska (Plafker, 1969, p. I53).

During the reconnaissance study of the Yakutat–St. Elias area, the effects of a pre-Early Cretaceous metamorphism have not been identified, possibly because they were obscured by subsequent metamorphisms, but detailed work in the areas of older rocks might uncover evidence of an earlier metamorphism. The Paleozoic rocks of the Hubbard terrane may have also been affected by the suspected pre-Early Cretaceous metamorphism, but this possibility cannot now be substantiated because the timing and nature of the structural juxtaposition of this terrane against the distinctly different Fairweather–Art Lewis terrane are unknown.

GENERAL AREAS AFFECTED BY REGIONAL METAMORPHIC EVENTS

The distribution of dated metamorphic rocks, combined with the regional geologic relations, allows the definition of the general areas that were affected by the two recognized regional metamorphisms.

The Late Cretaceous metamorphic rock dates and rocks with discordant ages in the 30–51-m.y. range are in the Boundary-Fairweather block and the Fairweather–Art Lewis terrane. They clearly indicate that this central area of greenschist- to amphibolite-facies rocks, located on both sides of the Fairweather fault, was affected by the Late Cretaceous metamorphism. Most of the metamorphic rocks elsewhere in the Yakutat–St. Elias area are characterized by penetrative deformation. As this is considered to be indicative of the strongly dynamothermal Late Cretaceous metamorphic event, it is concluded that nearly all the metamorphosed rocks in the Yakutat–St. Elias area were affected by the Late Cretaceous regional metamorphism.

The metamorphic rocks that have been dated in the 17–23-m.y. range are not as widely or uniformly distributed as those with older dates. The dated rocks define areas of Miocene greenschist- to amphibolite-facies metamorphism east of Yakutat Bay in the Boundary-Fairweather block and the Fairweather–Art Lewis terrane. In addition, they also occur in at least part of the St. Elias block. It is difficult to identify other areas affected by the Miocene event because of its dominantly thermal nature and the lack of superimposed structures on rocks metamorphosed earlier.

However, as this metamorphism was accompanied by widespread emplacement of igneous rocks, the distribution of Miocene plutons and dikes provides additional data on areas affected by the Miocene thermal influx. Miocene intrusive rocks include andesitic dikes that intrude low-grade rocks of the Yakutat Group in the Yakutat foothills, pegmatites and related finer grained leucocratic dikes that intrude the Novatak Glacier pluton (pluton J, fig. 2), and numerous small granitic plutons that intrude greenschist-facies rocks in the central Fairweather–Art Lewis terrane. The hypabassal Mt. Owen pluton (pluton H, fig. 2) and leucocratic dikes in the slate sequences north of the St. Elias fault may indicate Miocene intrusion at shallow depth from Hubbard Glacier west to locations of the dated metamorphic rocks (Nos. 12 and 13, fig. 2, tables 1 and 2) in the St. Elias block. Although no metamorphic rocks have been dated east of the Art Lewis fault, leucocratic dike swarms in the vicinity of the Art Lewis Glacier pluton (pluton D, fig. 2) and the lamprophyre dikes near the Mt. Hubbard pluton (pluton C, fig. 2) suggest that Miocene intrusive activity affected this area. Although the recognizable effects of the Miocene resetting have a generally irregular and spotty distribution in the Yakutat–St. Elias area, it is probable that intrusive or metamorphic products related to it occur in all the principal geologic terranes. The apparent discontinuity of the affected areas is probably due to both the thermal nature of the metamorphic event and later tectonic displacements.

DISTRIBUTION OF METAMORPHIC FACIES UNITS

The facies boundaries within geologic terranes and structural blocks are transitional. In all the terranes, except the foothills belt, the easterly- and southeasterly-increasing metamorphic gradients are in dynamothermally metamorphosed rocks and appear to have developed during the Late Cretaceous metamorphism. Miocene recrystallization has locally decreased these gradients, as in the southern part of the Fairweather–Art Lewis terrane (Nos. 6 and 7, tables 1 and 2), but generally the results of this metamorphism are local increases in metamorphic grade (Nos. 3, 12, 13, and 14, tables 1 and 2). The boundaries between facies units in adjacent geologic terranes or structural blocks are the major faults (fig. 2), and the discontinuities of the facies units across these faults provide some

evidence concerning both the sense and relative amounts of vertical displacements between adjacent geologic terranes and structural blocks, and the post-Miocene displacements along the historically active Fairweather fault.

Within the mobile belt east of the Art Lewis fault there is evidence for differential uplift within and between the major structural blocks. Assuming that the grade of regional metamorphism can be roughly correlated with depth in the Earth's crust, it is apparent that the foothills belt, the Boundary-Fairweather block, and the Fairweather–Art Lewis terrane have all been uplifted, but by different amounts. In general, uplift in the foothills belt is less than within the Boundary-Fairweather block and Fairweather–Art Lewis terrane. The last two terranes have somewhat similar uplift histories, but the Boundary-Fairweather block appears to have been uplifted more along its south end. Uplift within each terrane is not uniform, and a general feature of each structural block within the mobile belt west of the Art Lewis fault is that the metamorphic grade, and by implication the vertical displacement, increases along the structural grain in an easterly or southeasterly direction. In other words, each block appears to have undergone a variable but significant amount of tilting toward the northwest.

The epizonal plutons within the Fairweather–Art Lewis terrane allow a crude estimate of the amount of regional uplift within it. These plutons, ranging in age from 19 to 31 m.y., are now exposed at elevations between 300 and 3300 m (Hudson and others, 1976; Plafker, 1976). This suggests that uplift in this block was on the order of several kilometers and may have been as much as 10 km or more since the plutons were emplaced.

The Fairweather fault has been historically active and recent movement along it has been dominantly right lateral strike slip (Tocher, 1960; Page, 1969). In the Yakutat–St. Elias area rocks that were recrystallized during Miocene time are close to each other on opposite sides of the Fairweather fault (Nos. 8, 9, 14, 5, and 7, fig. 2). This suggests that large-scale strike-slip movements since Miocene time are not required to account for the distribution of facies units across the fault, and that it can be adequately accounted for by dominantly vertical displacements.

DISCUSSION AND SUMMARY

This study of the metamorphic rocks exposed in the Yakutat–St. Elias area, although general in nature, has revealed the following relations and characteristics of the metamorphic history of this part of the continental margin:

1. Metamorphic rocks in the Yakutat–St. Elias area are dominantly products of zeolite- to lower amphibolite-facies regional metamorphism. Late Cretaceous or Cenozoic plutonism has caused local thermal recrystallization, and dynamic metamorphism is associated with major faults.
2. The results of potassium-argon dating of selected metamorphic rocks provides evidence of a Late Cretaceous (minimum age about 65 m.y.) regional metamorphism that was characterized by penetrative deformation and widespread but apparently spotty thermal recrystallization during the Miocene Epoch. This Miocene recrystallization was accompanied by the intrusion of many small basaltic and granitic plutons and dikes. A relatively small and apparently thermally recrystallized area within the late Mesozoic flysch sequence yielded a very young potassium-argon age of 4 m.y. Parts of the area, most notably the Fairweather–Art Lewis terrane, St. Elias block, and perhaps the Hubbard terrane, may have undergone a pre-Early Cretaceous metamorphism, but evidence of this has not been found, possibly because of the extensive overprinting by the younger metamorphic and plutonic events.
3. The recognized regional metamorphisms are quite different, but some general characteristics of the overall metamorphic environment of the area have been identified. Throughout the area the metamorphic grade does not exceed the lower amphibolite facies, and the lack of blueschist-facies assemblages suggests that the area has only undergone low-pressure-facies series metamorphism. Many relatively sharp facies gradients are present, but there are many sharp textural gradients as well. For example, it is common for thinly banded and strongly schistose amphibolite sequences to be intercalated with texturally lower grade metasedimentary rocks in which primary sedimentary features can still be recognized. An important aspect of the radiometric ages of crystalline rocks in the area is the striking discrepancy between some of the potassium-argon ages of the metamorphic rocks and those of apparently older plutons that intrude them. For example, within the Fairweather–Art Lewis terrane, Jurassic plutons are emplaced in host metamorphic rocks that yield Late Cretaceous and Tertiary ages. Evidently

the layered rocks are texturally and compositionally more susceptible to recrystallization than are the plutons.

4. The mapped distribution of facies units shows many discontinuities as a result of tectonic displacements along major faults. The facies distribution indicates variable but major uplift within a strongly deformed mobile belt west of the Art Lewis fault. The mobile belt contains several structurally bound crustal blocks that have been uplifted differentially with respect to each other and have been tilted parallel to their general structural grain in a westerly or northwesterly direction. The deepest structural levels of each of these blocks are now exposed along their eastern or southeastern edges. The metamorphic facies distribution and the metamorphic ages across the Fairweather fault do not require large strike-slip displacements during the last 20 m.y.

REFERENCES CITED

Campbell, R. B., and Dodds, C. J., 1975, Operation St. Elias, Yukon Territory: Canada Geol. Survey Paper 75–1, pt. A, p. 51–53.

Hietanen, Anna, 1967, On the facies series in various types of metamorphism: Jour. Geology, v. 75, p. 187–214.

Hudson, Travis, Plafker, George, and Lanphere, M. A., 1977, Intrusive rocks of the Yakutat–St. Elias area south-central Alaska: U.S. Geol. Survey Jour. Research, v. 5, no. 2, p 155.

Kindle, E. D., 1952, Dezadeash map-area, Yukon Territory: Canada Geol Survey Mem. 268, 68 p.

MacKevett, E. M., Jr., Hudson, Travis, and Tysdal, R. G., 1974, Preliminary results of investigations in the southeastern McCarthy quadrangle, *in* Carter, Claire, ed., U.S. Geological Survey Alaska Program, 1974: U.S. Geol. Survey Circ. 700, p. 51–52.

MacKevett, E. M., Jr., and Plafker, George, 1974, The Border Ranges fault in south-central Alaska: U.S. Geol. Survey Jour. Research, v. 2, no. 3, p. 323–329.

Miyashiro, A., 1961, Evolution of metamorphic belts: Jour. Petrology, v. 2, p. 277–311.

Page, R. A., 1969, Late Cenozoic movement on the Fairweather fault in southeastern Alaska: Geol. Soc. America Bull., v. 80, p. 1873–1878.

Plafker, George, 1969, Tectonics of the March 27, 1964 Alaska earthquake: U.S. Geol. Survey Prof. Paper 543–I, p. I1–I74.

——— 1972, Alaskan earthquake of 1964 and Chilean earthquake of 1960—Implications for arc tectonics: Jour. Geophys. Research, v. 77, no. 5, p. 901–925.

——— 1976, Preliminary reconnaissance geologic map of the Yakutat and Mount St. Elias quadrangles, Alaska: U.S. Geol. Survey open-file rept., scale 1:250,000.

Richter, D. H., and Dutro, J. T., Jr., 1975, Revision of the type Mankomen Formation (Pennsylvanian and Permian), Eagle Creek area, eastern Alaska Range, Alaska: U.S. Geol. Survey Bull. 1395–B, 25 p.

Sharp, R. P., and Rigsby, G. P., 1956, Some rocks of the central St. Elias Mountains, Yukon Territory, Canada: Am. Jour. Sci., v. 254, no. 2, p. 110–122.

Smith, J. G., and MacKevett, E. M., Jr., 1970, The Skolai Group in the McCarthy B–4, C–4, and C–5 quadrangles, Wrangell Mountains, Alaska: U.S. Geol. Survey Bull. 1274–Q, p. Q1–Q26.

Tocher, Don, 1960, The Alaska earthquake of July 10, 1958—Movement on the Fairweather fault and field investigation of southern epicentral region: Seismol. Soc. America Bull., v. 50, p. 396–404.

Turner, D. L., Forbes, R. B., and Naeser, C. W., 1973, Radiometric ages of Kodiak Seamount and Giacomini Guyot, Gulf of Alaska—Implications for circumpacific tectonics: Science, v. 182, p. 579–581.

Turner, Francis J., 1968, Metamorphic petrology—Mineralogical and field aspects: McGraw-Hill, San Francisco, 403 p.

Zwart, H. J., Corvalan, J., James, H. L., Miyashiro, A., Saggerson, E. P., Sobolev, U. S., Subramaniam, A. P., and Vallance, T. G., 1967, A scheme for the cartographic representation of regional metamorphic belts: Geol. Newsletter, v. 1967, no. 2, p. 57–72.

Jour. Research U.S. Geol. Survey
Vol. 5, No. 2, Mar.–Apr. 1977, p. 185–192

GEOLOGY AND Rb-Sr AGE OF PRECAMBRIAN W PURITAN QUARTZ MONZONITE, NORTHERN MICHIGAN

By P. K. SIMS, Z. E. PETERMAN; and W. C. PRINZ, Denver, Colo.; Reston, Va.

Abstract.—**The Puritan Quartz Monzonite, in the western part of the Upper Peninsula of Michigan, composes a batholith at least 50 kilometres long and as much as 20 km wide on the south side of the Gogebic iron range. It is associated with subaqueous metavolcanic rocks assigned to the Precambrian W Ramsey Formation and with a complex gneissic unit of the same age. The quartz monzonite has a Rb-Sr isochron age of 2,710±140 million years and an initial $^{87}Sr/^{86}Sr$ of 0.7015±0.0017. The scatter of data points in excess of analytical error is interpreted as indicating that minor cataclasis and retrograde metamorphism produced slight open-system behavior in Precambrian X (circa 1,800 m.y.) time. The Puritan Quartz Monzonite and associated volcanic rocks are equated with similar Precambrian W greenstone-granite complexes in northern Minnesota, and clearly are a part of the Precambrian W greenstone terrane, as defined previously for the Lake Superior region.**

Recent geologic mapping in Gogebic County in the western part of the Upper Peninsula of Michigan by the U.S. Geological Survey has shown that granitic rocks of similar mineralogical and chemical affinity compose a batholith at least 50 kilometres long and as much as 20 km wide on the south side of the Gogebic iron range. The batholith extends from the vicinity of Lake Gogebic, on the east, westward into Wisconsin for at least 6 km (fig. 1) (Dutton and Bradley, 1970). East of Ironwood, Mich., the granitic rocks are overlain unconformably by the Precambrian X Ironwood Iron-formation and associated sedimentary rocks; accordingly, the granitic rocks have been considered as Precambrian W in age. The southern margin of the batholith is poorly defined because of sparse exposures, but it is overlapped by and possibly is in fault contact with metasedimentary and metavolcanic rocks and intercalated lenticular iron-formations of Precambrian X age. Allen and Barrett (1915) referred to this belt of iron-formation and associated rocks as the Marenisco range.

The main purposes of this paper are to establish the time of emplacement of the granitic rocks and, indirectly, to define a minimum age for the older volcanic rocks that are intruded by the granitic rocks. Also, we discuss briefly the probable relationship of these rocks to the granite and associated metavolcanic and metasedimentary rocks that form the basement in northern Minnesota. Preliminary data indicated an age of about 2,600 million years for the granitic rocks at the eastern end of the batholith, north of Marenisco (Sims and Peterman, 1976).

The samples for this study were collected by Prinz and Sims in 1975 and by C. E. Fritts and V. A. Trent in 1965 and 1967. Petrographic descriptions of the analyzed samples are given in table 1.

Acknowledgments.—We thank G. T. Cebula and J. W. Groen for preparation of the samples, and Kiyoto Futa and Robert Hildreth for the chemical and mass spectrometric analytical work.

GEOLOGY

The granitic rocks composing the batholith are herein referred to as Puritan Quartz Monzonite, following the formal designation of these rocks in the Ironwood area by Schmidt (1976). Prinz and Hubbard (1975) extended this terminology to the granitic rocks in the Wakefield quadrangle, 20 km east of the type locality. Previously, the granitic rocks at the eastern end of the batholith were named Presque Isle Granite by Allen and Barrett (1915, p. 50–54) and this term was used by Trent (1973) and by Sims and Peterman (1976). However, the term Presque Isle is not used in this report because it also was applied previously to gneissic rocks associated with the granite, some of which are now known to be country rocks older than the granite. The granitic rocks at the extreme eastern end of the batholith were called granite near Nelson Creek by Fritts (1969).

Steeply dipping mafic lavas, which commonly are pillowed, and felsic to intermediate pyroclastic rocks are intruded by the Puritan Quarz Monzonite and are in contact with it from the vicinity of Wakefield eastward almost to the eastern end of the batholith (fig.

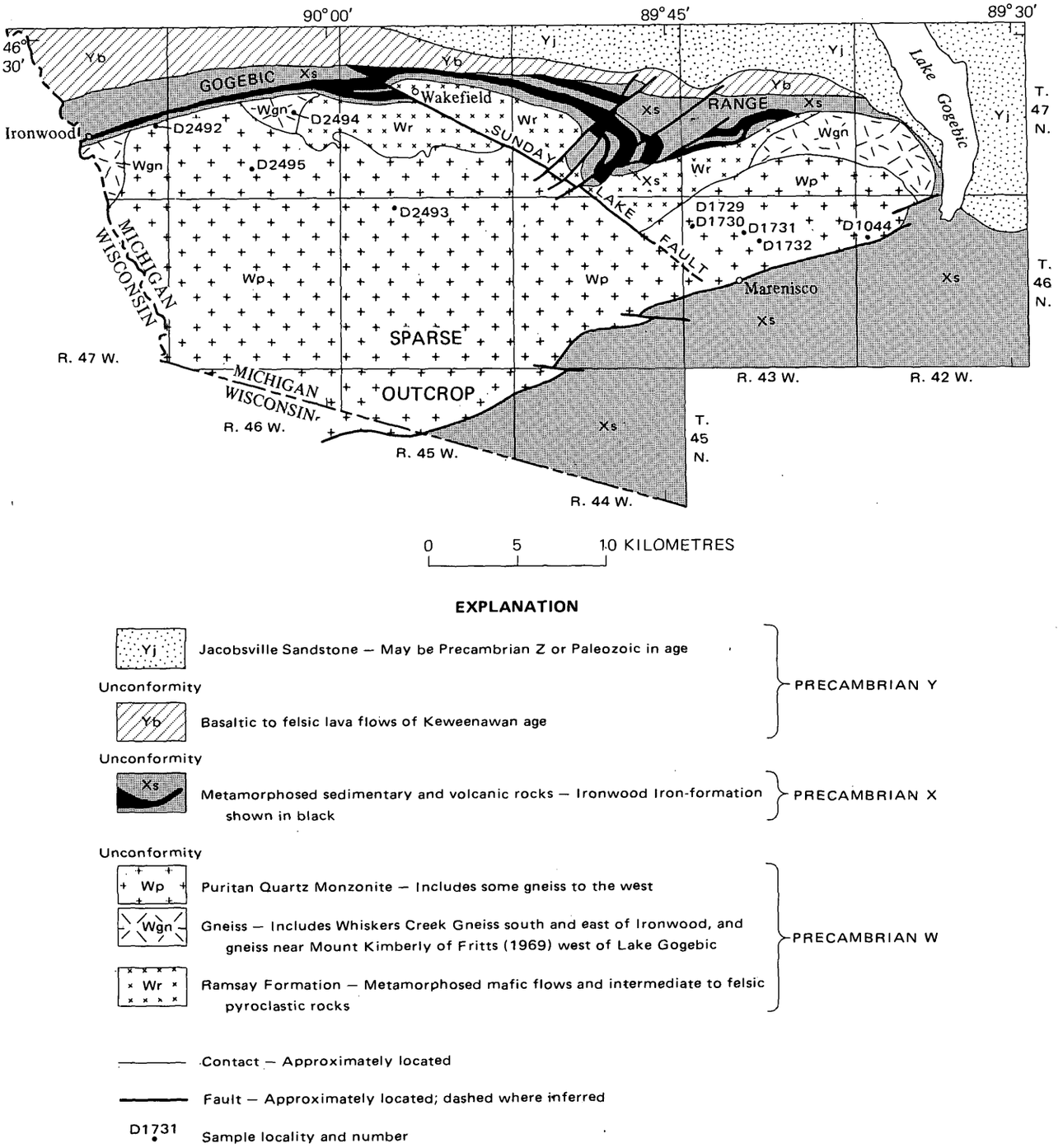

FIGURE 1.—Generalized geologic map of western part of Upper Peninsula of Michigan. Compiled by W. C. Prinz from Fritts (1969), Prinz and Hubbard (1975), Schmidt and Hubbard (1972), and Trent (1973).

1). The volcanic rocks have been assigned to the Precambrian W Ramsay Formation (Schmidt, 1976; and Prinz and Hubbard, 1975). The metamorphic grade of the volcanic rocks increases generally from chlorite grade (greenschist facies) to garnet grade (amphibolite facies) toward exposed granitic rocks (Prinz and others, 1975), suggesting that the metamorphism is related both spatially and genetically to intrusion of the Puritan Quartz Monzonite.

A complex gneissic unit is in contact with Puritan Quartz Monzonite south and east of Ironwood and west of Lake Gogebic. Near Ironwood, this unit has been

TABLE 1.—*Petrographic descriptions of samples*
[Sample localities are shown in fig. 1]

Sample No.		Collector and year	Sample locality			Description
Lab.	Field		Sec.	T. N.	R. W.	
Puritan Quartz Monzonite						
D1044	65–M–14	Fritts, 1965	7	46	42	Pinkish-gray, medium-grained, weakly foliated, equigranular, leucocratic quartz monzonite has allotriomorphic granular texture. Perthitic microcline (31 percent) embays and corrodes larger anhedral grains of moderately altered plagiocase (33 percent). Plagioclase has rims of albite and, locally, myrmekite adjacent to microcline grains. Biotite (3 percent) occurs in stubby aggregates associated with microcline and muscovite; these minerals are later paragenetically than plagioclase. Modal quartz is 33 percent.
D1729	VT–67–10	Trent, 1967	7	46	43	Pink, medium- to coarse-grained, leucocratic quartz monzonite with megacrysts of white and pink feldspar; has typical mortar structure; sodic plagioclase (43 percent), K-feldspar (22 percent), quartz (31 percent), and biotite (4 percent) are partly granulated and recrystallized; retrograde metamorphism, indicated by partial alteration of biotite to green chlorite, epidote, and opaque iron oxides, accompanied cataclasis. K-feldspar is perthitic microcline; it is poikilitic and includes sodic plagioclase with albite rims, quartz, and biotite; it embays and replaces plagioclase. Plagiocase is moderately altered to sericite and clay minerals.
D1730	VT–67–11	Trent, 1967	7	46	43	Pink, inequigranular leucocratic quartz monzonite; in part pegmatitic; moderate granulation. Similar to D1729. Quartz, 31 percent; sodic plagioclase, 40 percent; K-feldspar, 26 percent; biotite, 3 percent. K-feldspar is slightly perthitic microcline; it embays and poikilitically includes sodic plagioclase with albite rims. Biotite partly altered to chlorite and epidote.
D1731	VT–67–25	Trent, 1967	9	46	43	Pink, medium-coarse-grained granite pegmatite; has moderate granulation. Quartz, 30 percent; sodic plagioclase, 18 percent; K-feldspar, 50 percent; biotite, 2 percent. K-feldspar is slightly perthitic microcline; it poikilitically includes plagioclase.
D1732	VT–67–97	Trent, 1967	9	46	43	Pinkish-gray, fine-medium-grained, foliated biotite quartz monzonite. Texture is allotriomorphic granular. Quartz is highly strained. Similar to D1729. Quartz, 31 percent; sodic plagioclase, 31 percent; K-feldspar, 34 percent; biotite 4 percent.
D2492	M54	Prinz and Sims, 1975	24	47	47	Pale-red, medium- to coarse-grained, inequigranular, massive quartz monzonite. Has hypidiomorphic granular texture. Perthitic microcline (28 percent) and quartz (30 percent) embay blocky, subhedral crystals of moderately altered pagioclase (36 percent). The plagioclase has oscillatory concentric zoning and albitic rims adjacent to microcline. Biotite (5 percent) is largely altered to chlorite, muscovite, epidote, calcite, and opaque oxides. Quartz has strong strain shadows.
D2493	M55	Prinz and Sims, 1975	5	46	45	Grayish-pink, medium-grained, massive granodiorite. Similar petrographically to D2492. Quartz occurs partly as large amoeboid grains; it is locally fractured. Plagioclase, 52 percent; microcline, 23 percent; quartz, 20 percent; biotite, 5 percent.
D2495	M57	Prinz and Sims, 1975	28	47	46	Very light gray, fine- to medium-grained, inequigranular, foliated biotite quartz monzonite. Similar petrographically to D2492 but finer grained and less altered. Plagioclase, 49 percent; microcline, 12 percent; quartz, 33 percent; biotite, 6 percent.

TABLE 1.—*Petrographic descriptions of samples*—Continued

Sample No. Lab.	Sample No. Field	Collector and year	Sample locality Sec.	T. N.	R. W.	Description
		Whiskers Creek Gneiss				
D2494	M56	Prinz and Sims, 1975__	14	47	46	Pinkish-gray, mottled, medium- to coarse-grained, foliated hornblende granodiorite. Foliation given by alined aggregates of hornblende. Composed principally of sausseritized plagioclase (43 percent); green hornblende (22 percent); microcline (20 percent); and quartz (14 percent). Microcline and quartz are later interstitial minerals that embay and replace plagioclase.

called Whiskers Creek Gneiss (Schmidt, 1976); west of Lake Gogebic, it has been referred to informally as gneiss near Mount Kimberly (Fritts, 1969). The gneiss consists of two rock types, a layered phase and an intrusive phase. The layered phase consists of quartz-feldspar-hornblende gneiss, with or without biotite, and quartz-feldspar-biotite schist, and represents highly metamorphosed volcanic rocks of the Ramsay Formation. The intrusive phase consists of medium- to coarse-grained, pink to red, hornblende-rich quartz diorite. The quartz diorite is weakly to strongly foliated parallel with the foliation and layering in the host gneiss and schist. The intrusive phase contains inclusions of the gneiss and schist, and both are cut by dikes of typical Puritan Quartz Monzonite. The intrusive phase probably formed at an early stage of the magmatic episode that produced the Puritan batholith.

Puritan Quartz Monzonite consists predominantly of light-gray to buff to pale-red, medium- to coarse-grained, generally massive, leucocratic quartz monzonite. Both equigranular and porphyritic phases are present. The quartz monzonite in the eastern part of the batholith has a weak foliation or primary flow structure, defined mainly by biotite alinement.

The average modal composition for the major minerals of the Puritan Quartz Monzonite is 39 percent plagioclase, 25 percent microcline, and 31 percent quartz. Although the range in composition is large (19 to 60 percent plagioclase, 0 to 40 percent microcline, and 18 to 46 percent quartz), more than half the samples studied fall within 5 percent of the average. Compositionally, most of the unit is quartz monzonite with subordinate granodiorite. Puritan Quartz Monzonite contains 0 to 10 percent biotite or its alteration product, chlorite, and a few percent muscovite. Epidote and (or) clinozoisite are common accessory or alteration minerals, and most samples also contain accessory zircon, apatite, and, less commonly, allanite and opaque oxides. The texture of the rock is typically hypidiomorphic granular.

The plagioclase in Puritan Quartz Monzonite is subhedral or anhedral oligoclase, which is weakly to intensely altered to sericite, clay minerals, and clinozoisite (fig. 2). Most crystals show a conspicuous concentric zoning that is generally oscillatory or normal with more calcic cores; reversed zoning is less common. Some grains are rimmed by clear, unaltered albite.

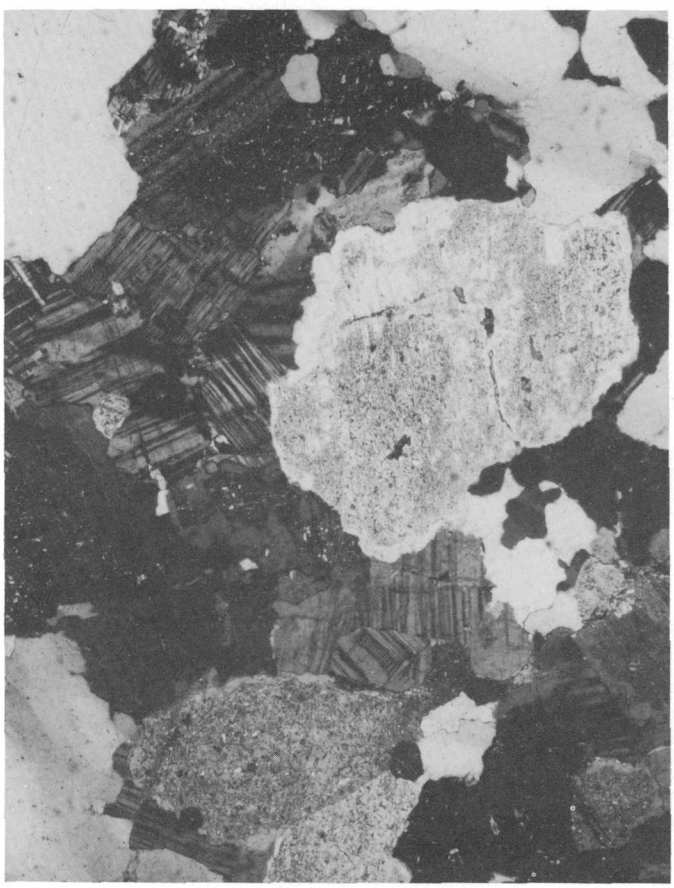

FIGURE 2.—Photomicrograph of Puritan Quartz Monzonite from locality D1044 (fig. 1). Moderately altered plagioclase grains with albite rims are surrounded by finer grained microcline. Note strain shadows in quartz. × 31, crossed nicols.

Myrmekitic textures are common. Perthitic microcline and quartz are interstitial to plagioclase and appear to have crystallized relatively late. The microcline is generally unaltered and poikilitic, containing small inclusions of plagioclase. Quartz shows conspicuous strain shadows but is rarely broken.

Granite pegmatite is widespread in Puritan Quartz Monzonite, mostly as dikes, schlieren, or irregular masses that may have either sharp or gradational contacts. Most bodies are only a few centimetres to several tens of metres in size, but at places large areas as much as 600 m across are entirely pegmatite (Prinz and Hubbard, 1975). Most of the pegmatite probably formed during the final stages of the magmatic cycle that produced the Puritan Quartz Monzonite, but as the following points out, some pegmatite is much younger.

Puritan Quartz Monzonite locally contains inclusions of quartz-feldspar-biotite schist, probably derived from the Ramsay Formation. The inclusions are generally less than 10 m long and are in sharp contact with the quartz monzonite.

Migmatitic gneiss, called Van Buskirk Gneiss by Schmidt (1976), occurs locally in Puritan Quartz Monzonite in T. 46 N., Rs. 46 and 47 W., and consists of an originally layered rock, now biotitic gneiss, which forms screens or inclusions in an igneous phase. The layered rock may have been derived either from the Ramsay Formation or from another unit. The igneous phase of the migmatite consists of medium- to coarse-grained quartz monzonite, identical to that in the main batholith, and of fine- to medium-grained granodiorite. The granodiorite is finer grained than the quartz monzonite and contains more biotite and less K-feldspar. Much of the igneous phase is concordant with layering in the host gneiss and is locally contorted with it. The granodiorite forms angular inclusions in the quartz monzonite, and wherever the two are in contact the coarser grained quartz monzonite cuts the finer grained granodiorite. This finer grained phase is moderately abundant in the western part of the batholith, even away from the gneissic patches. Like the quartz diorite in the Whiskers Creek Gneiss, it probably formed at an early stage of the magmatic cycle.

Cataclastic textures, expressed mainly by local mortar structure and bent or broken plagioclase crystals, are widespread in Puritan Quartz Monzonite, but are abundant only at the eastern end of the batholith east of the Sunday Lake fault. The cataclastic texture in this particular area was interpreted by Sims and Peterman (1976) as having resulted from reactivation of the granitic body in Precambrian X time, and probably was concomitant with doming of the overlying Precambrian X sedimentary rocks. At least some pegmatite was developed during reactivation, to account for scattered small bodies of granitic material in Precambrian X sedimentary rocks adjacent to the granitic body. One sample of pegmatite in this body has an apparent Rb-Sr age of 1,860 m.y. (Sims and Peterman, 1976).

Diabasic and gabbroic dikes of at least two ages cut the Puritan Quartz Monzonite and associated Precambrian W rocks. Precambrian W dikes are abundant in the area near Ironwood (Schmidt and Hubbard, 1972). The most abundant dikes in the eastern part of the batholith are Precambrian X in age, and provide evidence that the Puritan batholith was mildly and regionally metamorphosed (Prinz and others, 1975). The dikes cut units as young as Ironwood Iron-formation and are particularly abundant in the Puritan Quartz Monzonite in the eastern part of the batholith and in a belt extending from the southeastern part of T. 47 N., R. 45 W., west-southwestward across the northwestern quarter of T. 46 N., R. 45 W., and the northern half of T. 46 N., R. 46 W. The dikes contain typical greenschist-facies mineral assemblages that were formed during regional metamorphism in late Precambrian X (Penokean orogeny) time. The Precambrian W rocks intruded by the dikes, including Puritan Quartz Monzonite, must also have undergone low-grade regional metamorphism at this time. Abundant retrograde minerals were formed in amphibolitic rocks of the Ramsay Formation, but the only mineral changes in the Puritan Quartz Monzonite attributable to this metamorphism were the alteration of biotite to chlorite and the development of clinozoisite in plagioclase.

ANALYTICAL DATA AND DISCUSSION

Whole-rock samples weighing between 2 and 5 kilograms were collected from the Puritan Quartz Monzonite for Rb-Sr dating (table 2). Data for four of the samples used to develop the isochron were reported previously (Sims and Peterman, 1976), and these samples are identified in table 2. Isotope dilution techniques that pertain to the earlier data are described by Peterman, Doe, and Bartel (1967). The remaining data represent new samples that were analyzed in order to define more precisely the age of the Puritan Quartz Monzonite. Analytical techniques are similar to those previously described except that separate splits were used for Rb and Sr determinations. Sr concentrations and isotopic compositions were determined on the same split using an ^{84}Sr spike. Analytical uncertainties at one standard deviation are estimated at ± 1 percent for $^{87}Rb/^{86}Sr$ and 0.04 percent for $^{87}Sr/^{86}Sr$. The decay constant for ^{87}Rb used in the age calculation is 1.39×10^{-11} yr^{-1}. The regression method of McIntyre,

TABLE 2.—*Analytical data*

[Sample D2494 is Whiskers Creek Gneiss; all others are Puritan Quartz Monzonite. Samples D1044, D1729, D1730, and D1732 were reported in Sims and Peterman (1976) where rock was designated as Presque Isle Granite. Samples D2492–D2495 were analyzed by Kiyoto Futa (chemistry) and Robert Hildreth (mass spectrometry). ppm, parts per million]

Sample	Rb (ppm)	Sr (ppm)	$^{87}Rb/^{86}Sr$	$*^{87}Sr/^{86}Sr$
D1044	237	50.9	13.50	1.2033
D1729	119	180	1.93	.7793
D1730	118	174	1.97	.7775
D1732	54.4	79.7	1.99	.7816
D2492	233	158	4.13	.8503
D2493	104	640	.469	.7194
D2494	124	864	.417	.7172
D2495	127	245	1.51	.7591

*Normalized to $^{86}Sr/^{88}Sr = 0.1194$.

Brooks, Compston, and Turek (1966) was used to determine the slope and initial intercept of the isochron. Uncertainties in the age and r_i (initial $^{87}Sr/^{86}Sr$) are given at the 95-percent confidence level.

Regression of the data points (fig. 3) shows that some scatter exists in excess of that which can be explained by the assigned analytical uncertainty. Results of the regression follow:

Model	*Age (m.y.)*	r_i
I	2,700±39	0.7017±0.0006
II	2,706±144	0.7015±0.0017
III	2,607±85	0.7039±0.0042

Had the points fit an isochron within analytical untainty, the regression program would have stopped with the model–I fit of McIntyre and others (1966) but, instead, the program proceeds to increase the variance on the points until a fit is obtained. Model II increases the variance on $^{87}Sr/^{86}Sr$ values in proportion to the $(Rb/Sr)^2$, whereas model III increases the variance independently of the Rb/Sr ratios. It must be emphasized that these are only statistical manipulations which attempt to compensate for slight open-system behavior or conditions of nonuniform r_i values among the samples. Nevertheless, these calculations are useful in treating data that scatter slightly in excess of analytical error. The statistical assessment of the two models did not result in a clear choice between the two regressions, but we favor the model–II age for the following reasons: (1) The data points are rather unequally distributed along the isochron with sample D1044 being significantly removed from the other data points; model II, by increasing the variance in proportion to $(Rb/Sr)^2$, tends to minimize the influence of D1044 in determining a best fit, and (2) excluding D1044 from the regression results in a model–II fit with an age of 2,730 m.y. and an r_i of 0.7012.

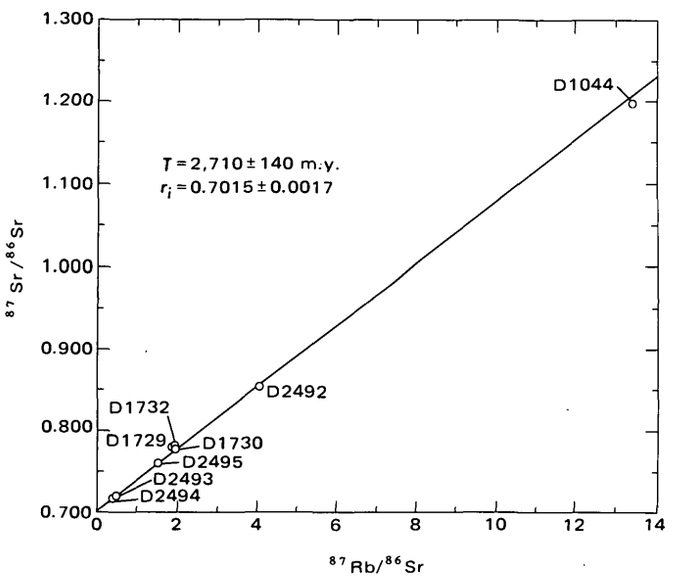

FIGURE 3.—Rb-Sr isochron plot for samples of Whiskers Creek Gneiss (D2494) and the Puritan Quartz Monzonite, northern Michigan. T, age; r_i, initial $^{87}Sr/^{86}Sr$.

The scatter of the data points in excess of analytical error probably results from the superimposed low-grade metamorphism and resultant mineralogical changes. Some samples show minor cataclasis and recrystallization, and nearly all show some retrograde alteration of plagioclase and biotite. Although minerals from the Puritan Quartz Monzonite have not been analyzed to determine the time of this metamorphism, it probably occurred about 1,800 m.y. ago, when older basement rocks to the south were reactivated and Precambrian X sedimentary rocks and mafic dikes were metamorphosed. Rb-Sr data for a pegmatite from the Puritan Quartz Monzonite gives a model age of about 1,860 m.y. (Sims and Peterman, 1976).

The possibility that the Rb-Sr isochron age may have been substantially reduced by the low-grade metamorphism is raised by the open-system behavior exhibited by some of the samples. Gross redistribution of radiogenic ^{87}Sr would likely have resulted in significant dispersion of the data points from a linear array as well as a lowered age and a raised r_i, such as observed in data for the highly deformed and recrystallized tonalitic gneiss at Watersmeet (Sims and Peter-

man, 1976). This possibility can be evaluated by determining an average total-rock point from the data and by estimating an age for this point using a minimum r_i of 0.700. This calculation results in an "age" of 2,770 m.y. for the average total-rock point. We conclude that the isochron age is probably correct within the assigned error.

Both the r_i and the age of the Puritan Quartz Monzonite are similar to those determined for granitic rocks in northern Minnesota and adjacent Ontario (Hanson and Goldich, 1972; Peterman and others, 1972; and Prince and Hanson, 1972).

CONCLUSIONS

1. The Rb-Sr data indicate that the Puritan Quartz Monzonite was emplaced approximately 2,700 m.y. ago. It intruded metabasalt and associated felsic to intermediate volcanic rocks of the Ramsay Formation. The low r_i of the granitic rocks argues against derivation from significantly older crustal rocks, and the Puritan Quartz Monzonite probably was derived directly or indirectly from the mantle.
2. The radiometric data support the field and petrographic data in indicating that the Puritan Quartz Monzonite was mildly metamorphosed and altered subsequent to its emplacement, probably at about 1,800 m.y. ago.
3. On the basis of these data, it seems certain that there are no granitic plutons of Precambrian X or younger age (Presque Isle Granite of Allen and Barrett, 1915) in the area encompassed by the Puritan batholith.

REGIONAL GEOLOGIC RELATIONSHIPS

Morey and Sims (1976) have shown that there are two markedly different, discrete sequences of Precambrian W rocks in Minnesota, a greenstone-granite terrane (circa 2,700 m.y. old) in northern Minnesota and a gneiss terrane (circa 3,500 m.y. old) in southern Minnesota, and they suggested that the same two sequences exist in northern Michigan and Wisconsin, on the east side of the Keweenawan rift system, marked by the Midcontinent gravity high. They proposed that the boundary between the two sequences in northern Michigan and Wisconsin is located a short distance south of the Gogebic iron range and that it projects eastward into Lake Superior about midway between the northern tip of the Keweenaw Peninsula and Marquette. Further studies have verified the existence of the two terranes in Michigan and Wisconsin and provide more specific information on the location of the boundary between the two Precambrian W terranes (Sims, 1976b). The new data indicate that the boundary is about 2.5 km south of the Puritan batholith at the longitude of Marenisco (see fig. 1) and that it projects eastward beneath the Marquette iron range, near Marquette, Michigan.

The association of 2,700 m.y.-old Puritan Quartz Monzonite and older subaqueous volcanic rocks of low- and intermediate-metamorphic grade, described in this study, is closely comparable to Precambrian W rock associations in the greenstone terrane of northern Minnesota (Sims, 1972; 1976a) and adjacent areas in Ontario, Canada (Peterman and others, 1972; Goldich, 1972). Accordingly, we interpret the greenstone-granite sequence in northern Michigan as being a part of the same greenstone terrane that occurs in northern Minnesota. Prior to the Precambrian Y (Keweenawan) rifting the two greenstone terranes (in Michigan and Minnesota) would have been in juxtaposition.

REFERENCES CITED

Allen, R. C., and Barrett, L. P., 1915, Contributions to the pre-Cambrian geology of northern Michigan and Wisconsin: Michigan Geol. Survey Pub. 18, Geol. Ser. 15, p. 13–164.

Dutton, C. E., and Bradley, R. E., 1970, Lithologic, geophysical, and mineral commodity maps of Precambrian rocks in Wisconsin: U.S. Geol. Survey Misc. Geol. Inv. Map I–631.

Fritts, C. E., 1969, Bedrock geologic map of the Marenisco-Watersmeet area, Gogebic and Ontonagon Counties, Michigan: U.S. Geol. Survey Misc. Geol. Inv. Map I–576.

Goldich, S. S., 1972, Geochronology in Minnesota, *in* P. K. Sims and G. B. Morey, eds., Geology of Minnesota—A centennial volume: Minnesota Geol. Survey, p. 27–37.

Hanson, G. N., and Goldich, S. S., 1972, Early Precambrian rocks in the Saganaga Lake—Northern Light Lake area, Minnesota-Ontario, Part II—Petrogenesis, *in* B. R. Doe and D. K. Smith, eds., Studies in mineralogy and Precambrian geology: Geol. Soc. America Mem. 135, p. 179–192.

McIntyre, G. A., Brooks, C., Compston, W., and Turek, A., 1966, The statistical assessment of Rb-Sr isochrons: Jour. Geophys. Research, v. 71, no. 22, p. 5459–5468.

Morey, G. B., and Sims, P. K., 1976, Boundary between two lower Precambrian terranes in Minnesota and its geologic significance: Geol. Soc. America Bull., v. 87, p. 141–152.

Peterman, Z. E., Doe, B. R., and Bartel, Ardith, 1967, Data on the rock GSP–1 (granodiorite) and the isotope-dilution method of analysis for Rb and Sr, *in* Geological Survey research 1967: U.S. Geol. Survey Prof. Paper 575–B, p. B181–B186.

Peterman, Z. E., Goldich, S. S., Hedge, C. E., and Yardley, D. H., 1972, Geochronology of the Rainy Lake region, Minnesota-Ontario, *in* B. R. Doe and D. K. Smith, eds., Studies in mineralogy and Precambrian geology: Geol. Soc. America Mem. 135, p. 193–216.

Prince, L. A., and Hanson, G. N., 1972, Rb-Sr isochron ages for the Giants Range Granite, northeastern Minnesota, *in* B. R. Doe and D. K. Smith, eds., Studies in mineralogy

and Precambrian geology: Geol. Soc. America Mem. 135, p. 217–224.

Prinz, W. C., Gair, J. E., and Cannon, W. F., 1975, Greenstone, *in* Inst. on Lake Superior Geology, 21st Ann., Proc.: Marquette, Mich., Northern Michigan Univ., p. 41–85.

Prinz, W. C., and Hubbard, H. A., 1975, Preliminary geologic map of the Wakefield quadrangle, Gogebic County, Michigan: U.S. Geol. Survey Open-File Rept. 75–119.

Schmidt, R. G., 1976, Geology of the Precambrian W (Lower Precambrian) rocks, in western Gogebic County, Michigan: U.S. Geol. Survey Bull. 1407, 40 p.

Schmidt, R. G., and Hubbard, H. A., 1972, Penokean orogeny in the central and western Gogebic region, Michigan and Wisconsin, *in* Inst. on Lake Superior Geology, 18th Ann. Field Guidebook: Houghton, Mich., Michigan Tech. Univ., p. A1–A27.

Sims, P. K., 1972, Vermilion district and adjacent areas, *in* P. K. Sims and G. B. Morey, eds., Geology of Minnesota—A centennial volume: Minnesota Geol. Survey, p. 49–62.

——— 1976a, Early Precambrian tectonic-igneous evolution in Vermilion district, northeastern Minnesota: Geol. Soc. America Bull., v. 87, p. 379–389.

——— 1976b, Precambrian tectonics and mineral deposits, Lake Superior region: Econ. Geology, v. 71, no. 6. (In press.)

Sims, P. K., and Peterman, Z. E, 1976, Geology and Rb-Sr ages of reactivated Precambrian gneisses and granite in the Marenisco-Watersmeet area, northern Michigan: U.S. Geol. Survey Jour. Research, v. 4, no. 4, p. 405–414.

Trent, V. A., 1973, Geologic map of the Marenisco and Wakefield NE quadrangles, Gogebic County, Michigan: U.S. Geol. Survey open-file rept.

Jour. Research U.S. Geol. Survey
Vol. 5, No. 2, Mar.–Apr. 1977, p. 193–205

ELECTRICAL SOUNDINGS NEAR YELLOW CREEK, RIO BLANCO COUNTY, COLORADO

By DAVID L. CAMPBELL, Denver, Colo.

Abstract.—Ten vertical electrical soundings were made in the Piceance Creek Basin in October 1974—5 along Yellow Creek, 2 in Big Duck Creek, and 1 each along Corral Gulch, on the hill in sec. 20, 1 kilometre northwest of 84 Ranch, and along the White River between the mouths of Yellow and Piceance Creeks. Interpretations of these soundings indicate that the anisotropy of the upper oil shales decreases from 2 in the basin center to 1 at a location on its flank. This decrease could result from a greater number of vertical water-filled fractures in the upper shales near the edge of the basin. On the other hand, the anisotropy coefficient for the lower shales increases from 2 to around 9 along the same section, indicating the presence of an increasing number of isolated horizontal aquifers in the lower shales on the basin flank. It is speculated that this trend for the lower shales reverses nearer the basin edge in the area of recharge of these splintered horizontal aquifers.

In October 1974, 10 vertical electrical soundings (VES) were made by the U.S. Geological Survey in the region of Yellow Creek in the Piceance Creek Basin, Rio Blanco County, Colo. (fig. 1). The study area occupies the center and western flank of Piceance Creek Basin, a broad structural basin named after its major drainage system, Piceance Creek. In Eocene time the Piceance Creek Basin contained part of Lake Uinta; the bodies of the organisms deposited on Lake Uinta's floor yield the kerogen that makes the area important today for oil shale deposits. Besides kerogen, many stringers and vugs of alkali salts were precipitated within the marly layers of the lake floor. Abundant deposits of two such salts, nahcolite ($NaHCO_3$) and dawsonite ($NaAl(OH)_2CO_3$), may also prove to be of economic importance someday.

During the past 20 years or so, many wells have been drilled in the Piceance Creek Basin to evaluate its economic potential. Thus, much is already known about the subsurface geology and hydrology of the region. Donnell (1961), Trudell, Beard, and Smith (1974), Dyni (1974), and Hail (1972) describe the geology, and Weeks (1974) and Weeks, Leavesley, Welder, and Saulnier (1974) describe the hydrology of the Piceance Creek Basin. The following summary is based on these publications.

There are three Eocene formations in the basin. The lowest is the Wasatch Formation, consisting of claystones, shales, and mudstones. The middle formation, the Green River, contains the oil shale in seven sequences designated R–1 through R–6 and Mahogany zone. Overlying the Green River Formation is the Uinta Formation, its sandstones and shales extending to the surface. These formations and their subunits show a high degree of lateral continuity throughout the basin, thinning toward the basin's edges. Only a minor amount of faulting, generally of normal dip-slip type, has been mapped in the basin. However, a major graben trending across Dudley Bluffs with some 75 metres of dip slip was mapped by Donnell (1961) where it crosses Piceance Creek and Ryan Gulch. This graben, herein called the Dudley graben, trends toward the study area, but its surface expression ends about 10 kilometres southeast of Yellow Creek.

There are two aquifers in the Piceance Creek Basin (Weeks, 1974). The upper aquifer, which extends from the water table through the Uinta Formation, contains freshwater and is perched on the relatively impermeable Mahogany zone. The lower aquifer contains water which is much saltier than that of the upper aquifer, and, in this zone, the water is actively leaching alkali salts from the Green River Formation. The boundaries of this leached zone may cut the stratigraphic units. The leached zone is thickest in the center of the basin and disappears near its edges. Below it, at least in the center of the basin, are zones (nahcolite and halite zones) of unleached salts (Dyni, 1974).

ANISOTROPY COEFFICIENTS

Bedded formations such as oil shale are often found to be electrically anisotropic; that is, the longitudinal resistivity ρ_l (along the beds) often differs from the transverse resistivity ρ_t (across the beds). When meas-

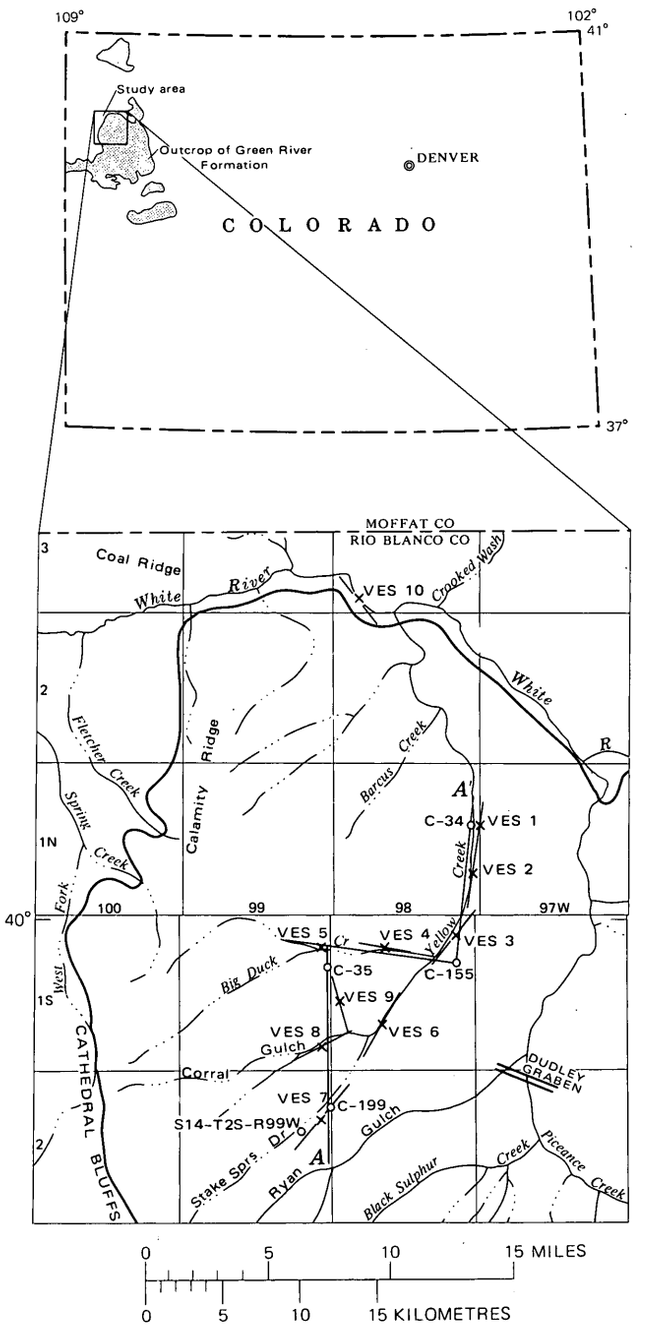

FIGURE 1.—Index map showing locations of VES 1 through VES 10, locations of electrically logged wells sec. 14, T. 2 S., R. 99 W., C–34, and C–35, lithologically logged wells C–199 and C–155, line of section A–A', and geologically mapped Dudley graben. Base from U.S. Geological Survey, Colorado State map, scale 1:500,000, 1969. From Campbell (1975).

ured by a VES, such a sequence of beds will appear to be an isotropic layer with a thickness λ (the "anisotropy coefficient") times its true thickness (as measured, for example, on a well log). As seen by the VES, its apparent resistivity will be the geometric mean

$$\rho_m = \sqrt{\rho_t \rho_l},$$

whereas the apparent resistivity measured on a well log will be only

$$\rho_{log} = \rho_m/\lambda = \rho_l,$$

as stated in the section "Paradox of Anisotropy" in Keller and Frischknecht (1966, p. 103).

A given sequence of beds may have both microanisotropy (due to thin layering within a given lithologic unit—the layering usually can be seen in hand samples) and macroanisotropy (due to interbedding of contrasting lithologies—bed thicknesses are larger than hand-sample size but too small to be distinguished by surface VES). To check for microanisotropy, I measured resistivities on an approximately 3-centimetre cubical prism of oil shale obtained from an outcrop on the Juhan prospect, Roan Cliffs, in a very rich part of the Mahogany zone. The measurement was made using the technique and apparatus described by Scott, Carroll, and Cunningham (1967). Three readings were taken, and the averages are

$$\rho_l = 0.384 \pm 0.030 \times 10^5\ \Omega\cdot\text{m (ohm-metres)},$$

and

$$\rho_t = 1.74 \pm 0.10 \times 10^5\ \Omega\cdot\text{m}.$$

The microanisotropy factor for this sample is

$$\lambda = \sqrt{\rho_t/\rho_l} = 2.13.$$

These measured values of ρ_l, ρ_t are two orders of magnitude higher than those inferred for in situ oil shales, possibly because the sample was very dry; natural shales are water saturated. The microanisotropy factor, on the other hand, is thought to be roughly correct. This impression is borne out by the Water Content Chart (Scott and others, 1967, fig. 6), which indicates that the sample contained about 0.1-percent water when measured and that a water content of 2 to 3 percent may lower the resistivity of the sample by the requisite two orders of magnitude.

Figure 2 shows macroanisotropy coefficients calculated for a sequence of alternating high- and low-resistivity beds. In such a sequence of beds, electric current will be channeled horizontally along the conducting (water-bearing, for example) zones and so the net ρ_t exceeds the net p_l for the total sequence of beds. The anisotropy coefficient λ for the sequence depends on the fraction, f, of its total thickness which is conducting and on the ratio of resistivities of the two types of beds ρ_2/ρ_1, where ρ_2 is the higher resistivity. Figure 2 shows that very large values of λ may result if ρ_2/ρ_1 is large. These values are upper limits because the insulating beds in any real bedded sequence usually contain vertical water-filled cracks which will help

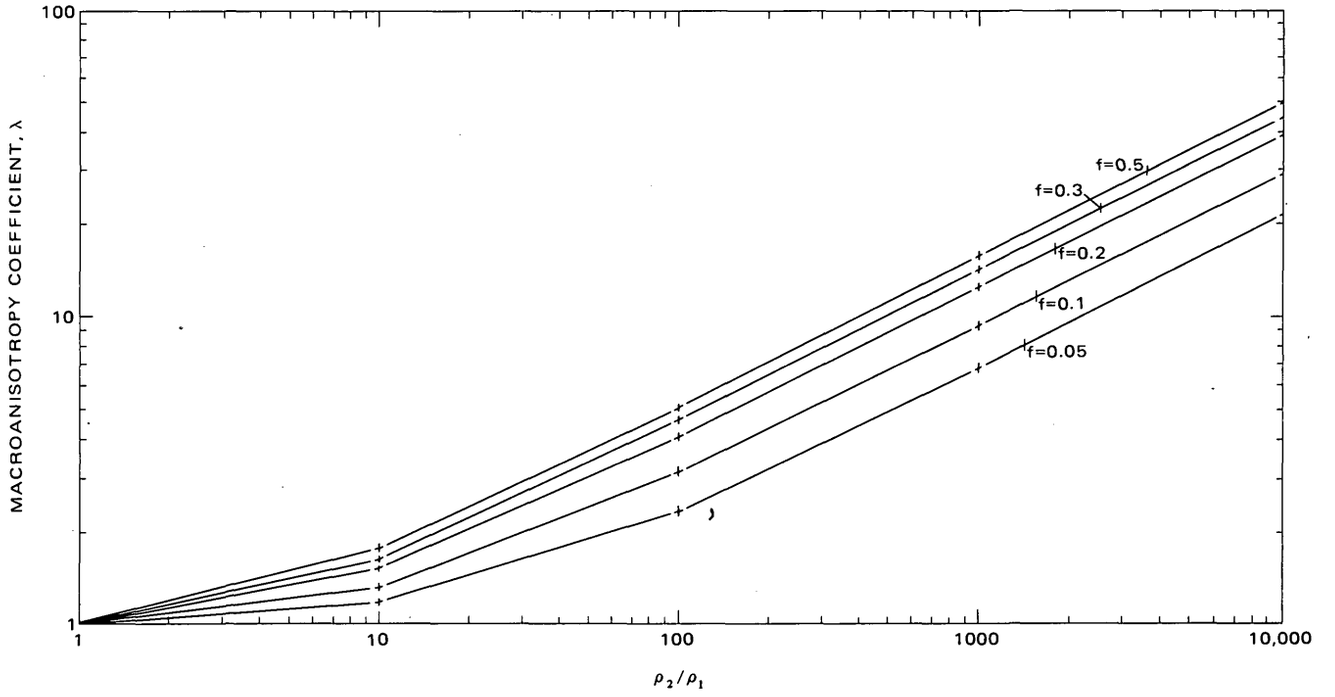

FIGURE 2.—Macroanisotropy coefficient, λ, for a sequence of interbedded layers of resistivities, ρ_1 and ρ_2. The parameter, f, represents either f_1, the fraction of total thickness having resistivity ρ_1, or f_2, the fraction of total thickness having resistivity ρ_2. From Campbell (1977).

electric current to flow vertically and will partially destroy the macroanisotropy calculated for this theoretical case (Campbell, 1977).

DATA COLLECTION AND PRELIMINARY INTERPRETATION

All 10 VES used the Schlumberger configuration (Keller and Frischknecht, 1966). In this symmetrical, four-electrode, in-line configuration, electric current, I, is fed into the ground via the outer electrodes, A and B, and the resulting voltage, V, is measured between two closely spaced inner electrodes, M and N. The spacing $\frac{AB}{2}$ is successively increased between readings and the apparent resistivity $\rho_a = K\frac{V}{I}$, where K is a factor involving the electrode spacings, is calculated for each spacing. Apparently resistivity values versus electrode spacings were plotted on log-log paper to give an apparent resistivity curve. All apparent resistivity curves were calculated and plotted in the field so that operational and instrumental errors could be promptly detected and corrected. To ensure measurable voltage readings at all spacings, the center to potential electrode distance, $\frac{MN}{2}$, had to be expanded from time to time. At changes of $\frac{MN}{2}$, "clutches," readings for both old and new $\frac{MN}{2}$ values were usually taken for two successive $\frac{AB}{2}$ values to make sure the curve segments were tracking each other. The current cables were placed along the road to prevent entanglement in the sagebrush, and the apparent resistivities were corrected for road curvature before interpretation.

By using a standard computer program by Zohdy (1974), the apparent resistivity curves were corrected for jumps due to clutches, smoothed via a spline process, and sampled at a rate of six evenly spaced points per logarithmic cycle. By using another Zohdy program, the smoothed curves were then inverted to give a possible geoelectric section (PGS). That is, for each VES, a model of formation resistivity versus depth was determined; a VES made over a section of flat-lying, isotropic layers having the resistivities and thicknesses specified by the model would resemble the original VES to within characteristic experimental errors.

Original data points (corrected for road curvature), the smoothed VES curve, the PGS found by the Zohdy program, and the calculated sounding curve which would result from that PGS are given for all 10 VES

by Campbell (1975). An example showing these steps for VES 10 is given in figure 3. The geoelectric section for VES 10 involves some 6 m of low-resistivity surficial layers and several deeper, thick layers of moderate resistivity, 9 to 30 Ω·m.

VES 10 differs from all the other VES reported here in that it was made along the White River, on an outcrop of the Wasatch Formation. VES 10 therefore investigates the electrical character of the rocks below the oil shales.Except near the outcrop surface, all these sedimentary rocks are presumably water saturated: The proximity of VES 10 to the White River, and hence, to a shallow water table, should yield resistivity values representative of the deeper buried locations as well.

By using the method described by Keller and Frischknecht (1966, p. 124–5), I calculated that the deepest layer detected by VES 10 must be at least 9,260 ft (2,820 m) thick. Hence, assuming all these layers are electrically isotropic, the minimum depth to (electric; that is, insulating) basement must be 11,630 ft (3,545 m) in the region of VES 10. Given the high degree of lateral continuity of Piceance Creek Basin sediments, I conclude from VES 10 that a very thick sequence of rocks having resistivities near 20 Ω·m underlies the Green River Formation in the study area. These rocks of the Wasatch and underlying formations are much more conductive than oil shales; therefore, a VES that penetrates the entire Green River Formation should end with a descending branch.

The PGS for VES 10 has been assumed to be correct in the absence of contradictory geologic information. When such information is available, however, the PGS must be modified to reflect actual conditions. The method used requires the modification of all PGS's until they (1) resemble the known geologic section, (2) fit any nearby well log data, (3) show a high degree of correspondence from one VES to the next, and (4) match the original observed VES data to an acceptable tolerance.

Comparison of VES 1 and core hole C–34

The center point of VES 1 was about 305 m south of core hole C–34 (=USBM/AEC, core hole 1, described by Carroll, Coffin, Ege, and Welder, 1967), and the current cables passed within 6 m of it. Hence a very close correspondence is expected between the electric logs from C–34 and the interpreted electric section of VES 1.

Table 1 summarizes 6–FF40 electric induction log observations from the depth of 760 ft (232 m), where the casing ended, to its total depth of 3,160 ft (963 m) for C–34. The correlation between well-logged resistivities and lithologies shown in table 1 has been established by Carroll, Coffin, Ege, and Welder (1967) and

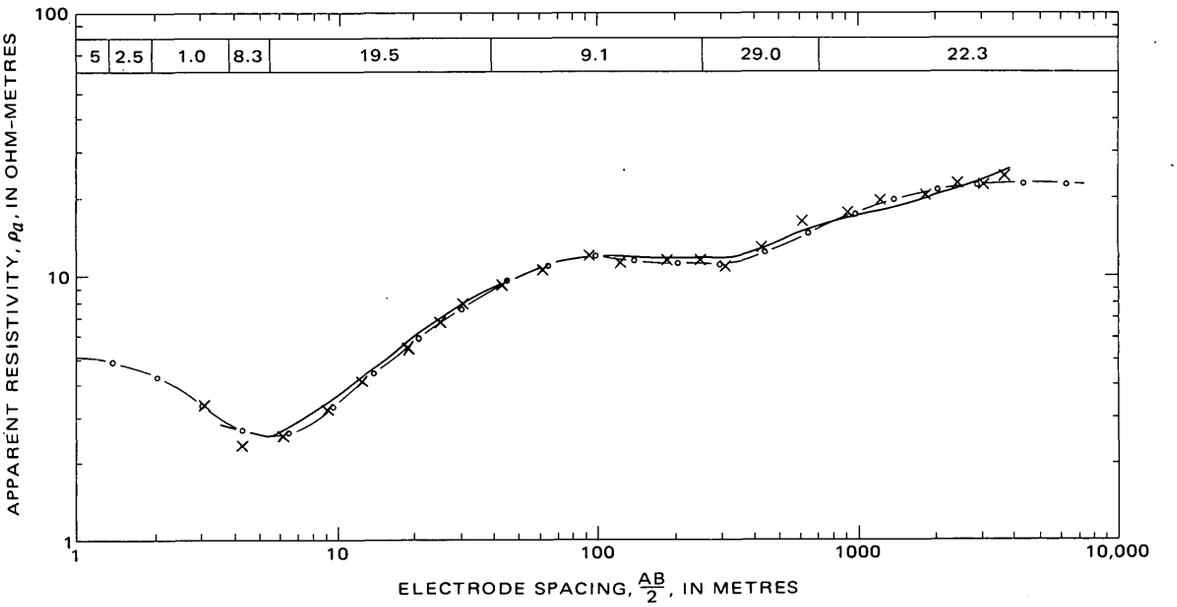

FIGURE 3.—PGS solution for VES 10. The scale at the top shows the PGS model consisting of constant resistivity layers whose depths are to be read off the spacing scale at the bottom of the figure. The resistivity of each layer in ohm-metres is shown on the corresponding part of the top scale. This convention for displaying PGS models is also used in figures 4 through 7. Solid line, computer-smoothed curve; ×, observed value; and, circle-and-dashed line, calculated curve for PGS model.

TABLE 1.—*Description of electric logs from core hole C–34*
[TD (total depth) = 3,160 ft (963 m) : leaders denote no log; sat, saturation value ≧ 600 Ω·m]

Depth interval (metres)	Maximum ρ (Ω·m)	Minimum ρ (Ω·m)	"Average" ρ (Ω·m)	Interpretation
0–232	---	--	----	Casing.
232–247	600	2	10	(?).
247–287	45	5	10	Upper aquifer.
287–390	600	3	500	Mahogany zone.
390–530	sat	2	30	Leached zone.
530–777	sat	40	1,000	Nahcolite zone.
777–TD	150	2	20	Bottom high conductivity zone.

by Coffin, Welder, and Glanzman (1971). Though the scale on the log chart nominally extends to 1,000 Ω·m, Pirson (1963, p. 173) cautioned that quantitative values obtained from such charts are not reliable above about 100 Ω·m. Thus the higher resistivity values read from such charts and reported in the well-log summaries of tables 1 through 3 may be substantially in error. Furthermore, on the C–34 log, there may have been a field adjustment which stopped the recorder pen at a nominal 600 Ω·m on the right-hand side of its excursion. It is not clear whether this adjustment involved only a simple stopping of the pen or a saturation of the logging tool's ability to distinguish between successively higher resistivity layers.

Figure 4 has plots of observed data for VES 1 along with sounding curves calculated for four model geoelectric sections. Each model combines the PGS down to 760 ft (232 m) with various versions of the electric log to total depth. For all models the region below total depth is supposed to be of infinite depth and 20 Ω·m resistivity. Model A treats all logged layers as if they were isotropic. The sounding curve calculated with that assumption falls far below the curve for the observed VES. Model B allows two oil shale strata, the Mahogany zone and the nahcolite zone, to be anisotropic with $\lambda = 2.13$, as measured on our sample. The logged resistivities in these regions were near the right-hand

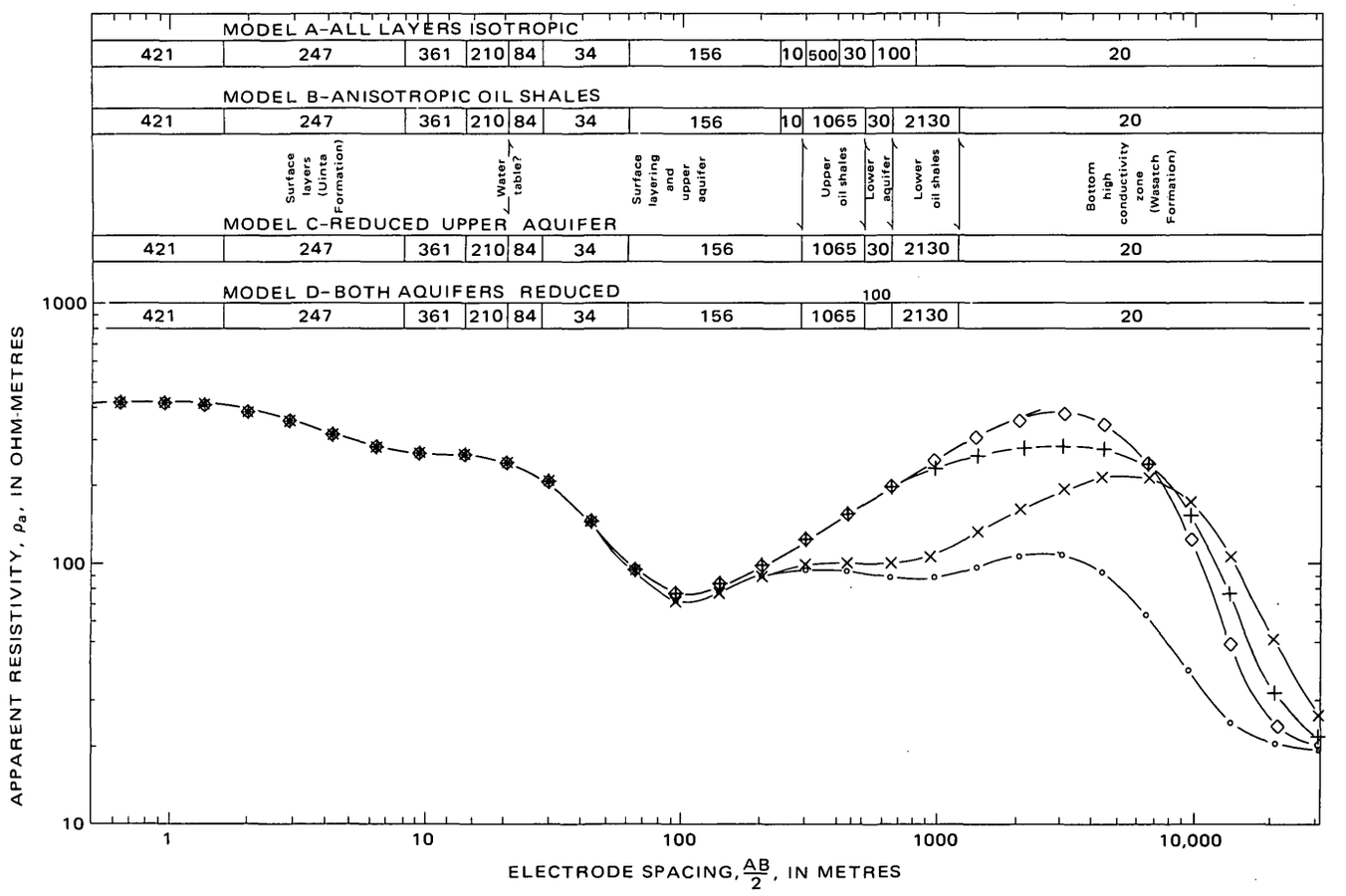

FIGURE 4.—Calculated VES for four models of core hole C–34 compared with observed VES 1. Solid line, observed VES 1. Circle-and-dashed line, calculated curve for model A; ×-and-dashed line, model B; +-and-dashed line, model C; and diamond-and-dashed line, model D. Note that all four models and the observed VES 1 coincide to approximately 100 m on the electrode spacing scale. Only model D is judged to adequately fit the observed VES 1. See figure 3 caption for convention for displaying models.

stop on the 6–FF40 induction log and were, therefore, unreliable. On the log, the Mahogany zone value appeared to hover near the right-hand stop, nominally about 600 Ω·m, whereas the nahcolite zone value was pegged there. Consequently, I assumed the true values for the logged zones to be 500 and 1,000 Ω·m, respectively, and increased these values for the VES calculation to $\rho_m = 1{,}065$ and 2,130 Ω·m, respectively, in accordance with the anisotropy paradox. Nevertheless, the sounding curve calculated for model B still falls below the curve of measured VES 1. The leached zone, though it contains oil shale, was assumed to be isotropic because of the presumed vertical water-bearing cracks and vugs contained in it.

A 10-Ω·m layer is recorded on the C–34 log between 760 ft (232 m) and 940 ft (287 m). This layer probably represents water-soaked sands of the upper aquifer, which is perched directly on the Mahogany zone. I investigated several models of this zone in the lower part of the upper aquifer, but, as long as its resistivity and thickness were kept at 10 Ω·m and 55 m, respectively, an acceptable fit to VES 1 could not be devised. A higher resistivity than that shown on the log is needed for this zone. It seems likely that salty water from the leached zone has moved up the well, contaminating the upper aquifer in a local region around the well. The logging tool, therefore, detected the lower resistivity of the salty water in the contaminated region, while the surface VES measured a higher resistivity value more representative of formation resistivity of the upper aquifer. In model C the 10-Ω·m layer seen on the well log is eliminated, an improved fit to VES 1 results.

The far right-hand branch of VES model C still does not fit the observed data, and, for this reason, model D was devised. An increase from 30 to 100 Ω·m for the resistivity of the lower aquifer (leached zone) gives an excellent match with the VES 1 data. Other interpretations of thickness and resistivity for the leached zone are possible, however. The logged values for this zone may be retained, for example, if the resistivity of the Mahogany zone is increased to 2,000 Ω·m and that of the nahcolite zone to 4,000 Ω·m. Such values are not inconsistent with the C–34 log, because very high logged resistivity values like these are often imprecise.

Comparison of core hole C–35 with VES 5 and VES 9

Core hole C–35 (=USBM/AEC core hole 2) is located on the hill in sec. 20, 1 km northwest of 84 Ranch. It is about 1.6 km south of the center point of VES 5 and 3.2 km northwest of the center point of VES 9. Good correlation can be expected between the C–35 electric log and the interpreted electric sections for VES 5 and VES 9.

Ege, Carroll, and Welder (1967), in discussing core hole C–35, reported oil shale beginning at 1,120 ft (341 m), with the Mahogany zone bounded by the marker A at 1,220 ft (372 m) and marker B at 1,405 ft (428 m). A zone of poor core recovery (leached zone) existed from 1,300 ft (396 m) to 1,450 ft (492 m). The authors placed the top of the nahcolite zone at 1,693 ft (516 m) but reported that some salts remained in place above this level. The hole bottoms in oil shale at 2,214 ft (675 m).

Table 2 summarizes the electric logs for C–35 and gives the extreme and average resistivity values for

TABLE 2.—*Summary of electric logs for core hole C–35*

[TD (total depth) = 2,214 ft (675 m); leaders denote no log; low sat, log hovers near and on saturation value; high sat, log pegged at saturation value; saturation value = 600 Ω·m (nominal)]

Depth interval (metres)	Maximum ρ (Ω·m)	Minimum ρ (Ω·m)	"Average" ρ (Ω·m)	Interpretation
0–122	---	---	----	No log.
122–201	200	10	100	Upper aquifer.
201–235	250	3	5	Do.
235–305	400	40	120	Do.
305–326	Low sat	200	500	Do.
326–341	300	40	130	Do.
341–424	High sat	200	600	Upper oil shale zone.
424–482	Low sat	160	400	Do.
482–524	500+	80	170	Leached zone.
524–619	Low sat	100	500	Upper nahcolite zone.
619–TD	High sat	200	1,000	Lower nahcolite zone.

both the 6–FF40 induction logs and 16-inch normal electric logs. Low-resistivity zones which may represent the upper and lower aquifers are much less apparent on this log than on that for C–34. Except for the narrow zone from 1,580 ft (482 m) to 1,720 ft (524 m), resistivity values are near saturation throughout the oil shale section. Seemingly, the hydrologic definition of upper and lower aquifers is less clear at this location away from the center of the basin.

Figure 5 shows attempts to model VES 5 by using the electric log values from table 2. Again, the models merge the PGS for shallow layering with the core-log thicknesses and resistivities for the oil shale section. The depth to the oil shale section was decreased by 120 ft (37 m), however, because VES 5 was made in Duck Creek Valley at an elevation about 120 ft (37 m) below that of the C–35 site. Because C–35 was still in oil shale when it bottomed, the total thickness of the oil shale there is unknown. Initially, we assumed a total thickness of 1,610 ft (490 m) of oil shale, the thickness

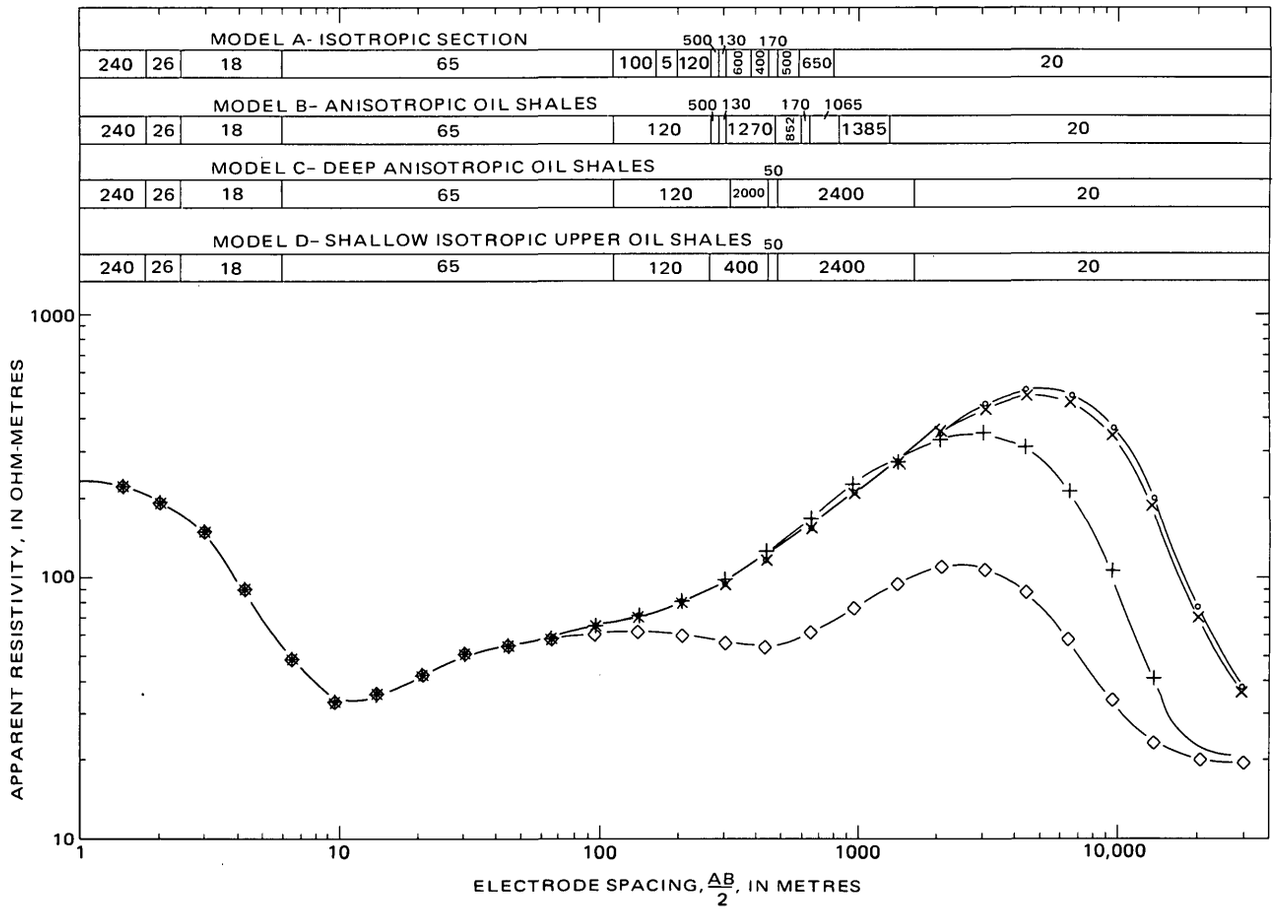

FIGURE 5.—Calculated VES for four model geoelectric sections, compared with observed VES 5. Models A and B are derived directly from the electric log of nearby core hole C–35; models C and D are Dar Zarrouk simplications of a PGS (not shown) which was also based on that log. The upper oil shales at this location are adequately modeled by either a thin high-resistivity zone (model C) or a thick lower-resistivity zone (model D). Heavy line, observed VES 5. Diamond-and-dashed line, calculated VES for model A; plus-and-dashed line, model B; circle-and-dashed line, model C; and ×-and-dashed line, model D. Note that all four models and observed VES 5 coincide to about 70 m on the electrode-spacing scale. Both models C and D are judged to adequately fit observed VES 5. See figure 3 caption for convention for displaying models.

found in hole C–34. Because the section thins towards the basin edge, it was expected that this would be an overestimate.

Model A assumes all layers to be isotropic; the fit fails badly on the right-hand branch. The thick low-resistivity zone between 540 ft (165 m) and 650 ft (198 m) seen on the well logs cannot be present everywhere under VES 5. As at C–34, this zone probably represents only a local contamination of the upper aquifer. Eliminating this zone and consolidating the layers above and below it into a single 120-Ω·m region greatly improves the fit and also provides a layer which is identifiable on the adjacent VES 4.

Model B has this consolidated layer and also supposes all oil shale layers except the 170 Ω·m leached zone to be anisotropic with $\lambda = 2.13$. The fit is improved, but further adjustments are needed because the calculated sounding curve first rises too far above, then falls too far below the observed VES. Apparently the thickness and (or) resistivity of the upper oil shale zone (above the leached zone) should be decreased, and those of the lower oil shale zone (below the leached zone) should be increased.

Models A and B, based on electric log C–35, show electric section details that would never be resolvable by direct interpretation of VES 5. By using the "Dar Zarrouk" technique (Zohdy, 1974), 13 well-logged layers have been reduced to the electrically equivalent 9-layer models C and D. In these models the apparent thickness of the lower oil shale zone has been increased to 3,800 ft (1,160 m) and the leached zone has been

emphasized by decreasing its resistivity to 50 Ω·m. Both adequately fit the observed VES 5.

Models C and D show that the 500-Ω·m layer at 800 ft (268 m) can be interpreted either as an oil shale horizon or not. In discussing core hole C–35, Ege, Carroll, and Welder (1967) place the highest recognizable oil shale at about 1,120 ft (341 m) but do not indicate the lithology of logged units above that level. Model C assumes that the high-resistivity section begins only at that level, decreased by 120 ft (37 m) because of the elevation difference between the sites of VES 5 and C–35, and that it is anisotropic. Model D allows the high-resistivity zone to be shallower, beginning around 800 ft (268 m); consequently, the net resistivity of the thicker zone is lowered somewhat, making it more nearly isotropic. Though it is clear that either interpretation suffices, I prefer model D for three reasons: (1) the oil shales should be shallower at this location on the basin flank, (2) the lower resistivity used for these shales agrees with interpretations of other nearby VES, and (3) an apparent isotropy of these upper oil shales in this location makes sense hydrologically. Somewhere, water from the upper aquifer has to get down to recharge the leached zone; this is most likely near the basin edge where the thinning section and interfingering with other facies impair the rubber-like flexibility of the shales in the basin center (Weeks, 1974). Vertical water-filled cracks and dissolution vugs therefore may be expected in the upper shales under VES 5; the effect of vertical cracks and vugs is to counteract the microanisotropy of the oil shales, making them appear less anisotropic to a surface VES.

In contrast with the upper oil shale zone, the lower oil shales in this location appear very anisotropic, macroanisotropy coefficient λ being on the order of 4.3. Because the microanisotropy of rich oil shale is thought to be only about 2.1, the increased anisotropy of the lower shales may be a macroanisotropy effect due to the inclusion of horizontal water-bearing strata.

VES 9 is also located near core hole C–35 but was terminated at $\frac{AB}{2}$ = 6,000 ft (1,829 m) due to current leakage caused by a rain shower. Because the location was on high ground above the valleys, the oil shale section was deeper than for VES 5. As a result, the resolution of the oil shale part of the present was very weak. The top of the oil shale is at about 1,100 ft (335 m) to 1,200 ft (366 m) in this location. This is almost 200 ft (60 m) deeper than continuity with other nearby VES indicate it should be, so perhaps there is a syncline or down-faulted block under the hill in sec. 20, 1 km northwest of 84 Ranch.

INTERPRETATION OF VES 7

VES 7 was made along Stake Springs Draw just east of Federal Oil Shale Lease Tract C–a. The center of VES 7 was located about 1,509 ft (460 m) west-southwest of core hole C–199. Resistivity logs for C–199 were not available; examining its lithologic log, Marjorie Mullens of the U.S. Geological Survey (written commun., 1974) finds that oil shale extends from 561 ft (171 m) to 1,597 ft (487 m) in C–199 with the base of the leached zone at 1,555 ft (474 m). The 16-in normal log of a well in sec. 14, T. 2 S., R. 99 W., about

TABLE 3.—*Summary of 16-in normal log, sec. 14, T. 2 S., R. 99 W.*

[TD (total depth) = 6,070 ft (1,850 m); datum (Kelly bushing) = 6,741 ft (2,055 m)]

Depth		Thickness		"Average" ρ_1
Feet	Metres	Feet	Metres	(Ω·m)
		261	80	Casing
261	80			
		139	42	125
400	122			
		210	64	390
610	186			
		110	33	170
720	219			
		130	40	90
850	259			
		150	46	240
1,000	305			
		80	24	100
1,080	329			
		130	40	240
1,210	369			
		60	18	100
1,270	387			
		100	31	240
1,370	418			
		310	94	50
1,680	512			
		220	67	20
1,900	579			
		580	177	15
2,480	756			
		450	137	40
2,930	893			
		220	67	160
3,150	960			
		70	21	20
3,220	981			
		100	31	100
3,320	1,012			
		90	27	12
3,410	1,039			
		1,290	393	120
4,700	1,432			
		90	27	450
4,790	1,460			
		330	100	112
5,120	1,560			
		120	37	480
5,240	1,597			
		310	95	140
5,550	1,692			
		550	168	330
TD	TD			

NOTE.—Summary of reported lithology:
Marker A around 520 ft (158 m)
Mahogany marker at 545 ft (166 m)
Marker B around 660 ft (201 m)
Orange marker (in Garden Gulch member of Green River Formation, below oil shales) at 1,600 ft (488 m)
Mesaverde Formation at 5,030 ft (1,533 m)

3,700 m southwest of the centerpoint of VES 7, provided by John Donnell of the U.S. Geological Survey, is summarized in table 3. The values given have been roughly corrected for mud salinity. According to these logs, the oil shale on the basin's edge apparently is shallower, about 500 ft (168 m); thinner, about 1,100 ft (335 m); and much less resistant, ρ_l under 400 Ω·m, than at C–34 in the basin's center.

In figure 6, I consider whether an artificially thickened lower oil shale zone is necessary to produce the monotonically rising apparent resistivity curve we see at VES 7 or whether the effect could arise from a shallow insulating basement. VES 7 is ideally situated for this purpose: (1) it extends to the widest spacing used in this study, $\frac{AB}{2}$=12,000 ft (3,658 m), without leveling off, (2) it is probably located over as thin a section of oil shale as any of the VES in this study, and (3) it is located close to one of the deepest wells in the Piceance Creek Basin, in sec. 14, T. 2 S., R. 99 W. This particular well attained a total depth of 6,070 ft (1,850 m) without reaching basement. In figure 6, the extreme assumption was made that a 5,000-Ω·m basement is located 10 m below total depth. Recall that VES 10 showed a minimum of 11,630 ft (3,545 m) to basement at a location lower in section and only 27 km north of VES 7.

Models A and B in figure 6 are both 28-layer models based on the resistivities reported in table 3. In model A, all layers are assumed isotropic; this puts the presumed basement as shallow as possible. In model B, all oil shale strata were assumed to be microanisotropic, assigned an arbitrary resistivity of 2,000 Ω·m and apparent thicknesses 2.1 times their logged thicknesses. These two models therefore represent opposite extremes, bracketing the probable true case of varying microanisotropy within the oil shale section.

In both models, the high-conductivity zone below the oil shales is too strong, pulling the curves down by very perceptible amounts before they rise again in response to the presumed basement. I conclude that the conducting zone immediately under the oil shales cannot be

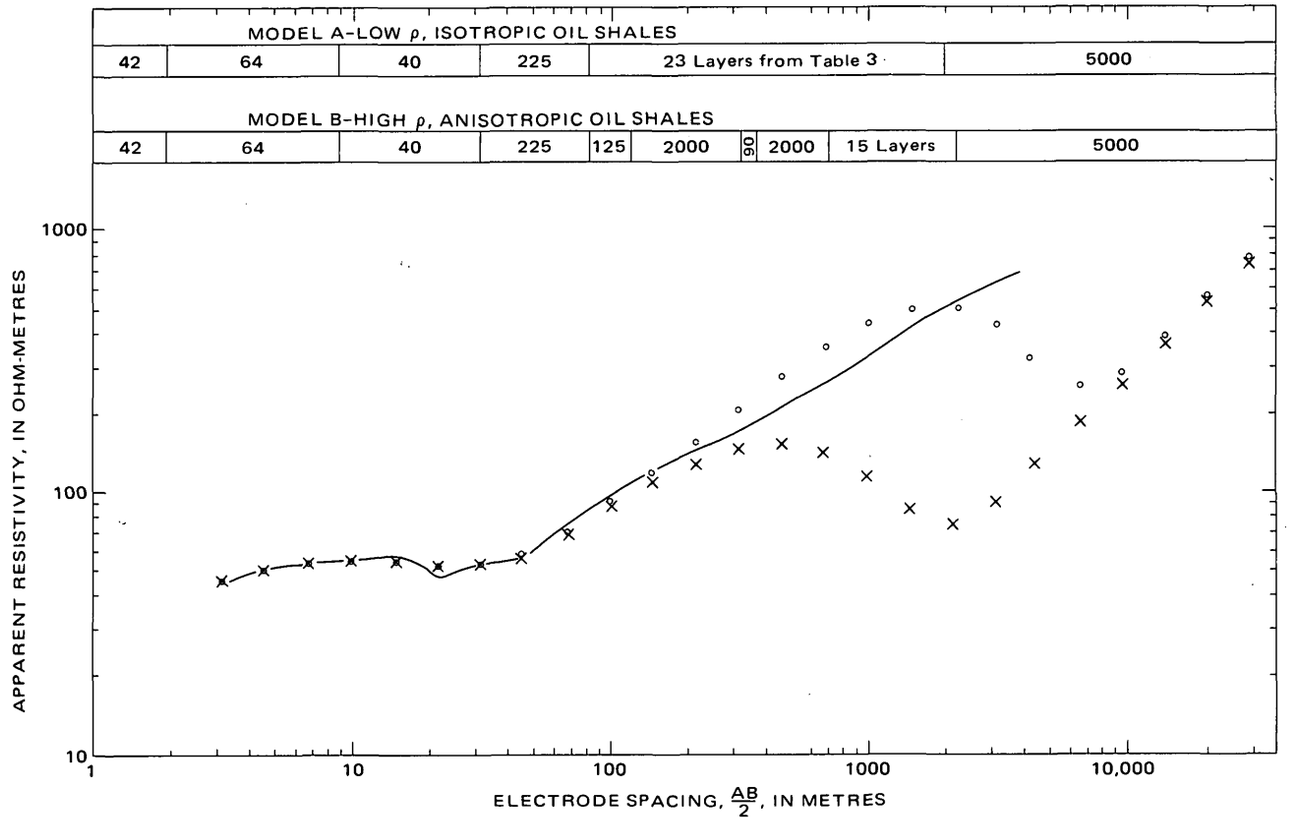

FIGURE 6.—Calculated VES for two model geoelectric sections, compared with observed VES 7. These models represent bounds on the probable true case of varying microanisotropy within the oil shale part of the section. Both models assume a high-restivity basement immediately below total depth of the deepest core hole in the vicinity. This extreme assumption fails to force a fit to the observed VES 7, indicating that the oil shales must be highly macroanisotropic. Solid line, observed VES 7; ×, calculated VES for model A; and, circle, calculated VES for model B. See figure 3 caption for convention for displaying models.

hidden on the VES in such a way that the rising branch at the largest spacings could reflect a deep resistive basement rather than shallower resistive oil shales. The oil shale itself must cause the effect, and so its apparent thickness must be greater than the measured 2.1 microanisotropy would imply.

Figure 7 shows Dar Zarrouk curves (Zohdy, 1974) for three separate models, all of which fit the VES 7 data within experimental error. Several elementary properties of Dar Zarrouk curves are as follows: (1) there is one curve segment for each layer in the model, (2) each curve segment has a right-hand asymptote equal to the resistivity of the corresponding layer, and so rising Dar Zarrouk branches represent higher resistivity layers and falling branches represent lower resistivity layers, and (3) and most relevant here, all models whose Dar Zarrouk curves lie near each other (within about 10 percent) are likely to fit the observations within experimental error. This last statement is from Zohdy (1974), and, when properly qualified with a list of exceptions, it greatly expands our previous knowledge of equivalent models (Zohdy and others, 1974, p. 28).

This "Zohdy criterion" clearly shows that no reliance may be placed on the particular leached zone we have chosen for model B. The short falling branch marked "115" in the Dar Zarrouk figure, which gives rise to the zone, may be moved to the right or to the left, making the zone deeper or shallower, respectively; increasing or decreasing the slope increases or decreases, respectively, the zone's resistivity. The branch may even be broken into several still shorter segments at different depths, giving the rising branch of the Dar Zarrouk curve a sawtoothed appearance without violating the Zohdy criterion.

This last possibility would be the case at a location where the single well-defined leached zone of the basin center has splayed out into a number of water-bearing horizons within the oil shale section. One evidence for this possibility is the large observed anisotropy of the oil shales at this site. Recall that even at the widest spacing, $\frac{AB}{2}$ = 12,000 ft (3,658 m), VES 7 still shows no sign of leveling off in response to the conducting sediments ("bottom high-conductivity zone") which lie below the oil shales at about 1,600 ft (490 m). Model

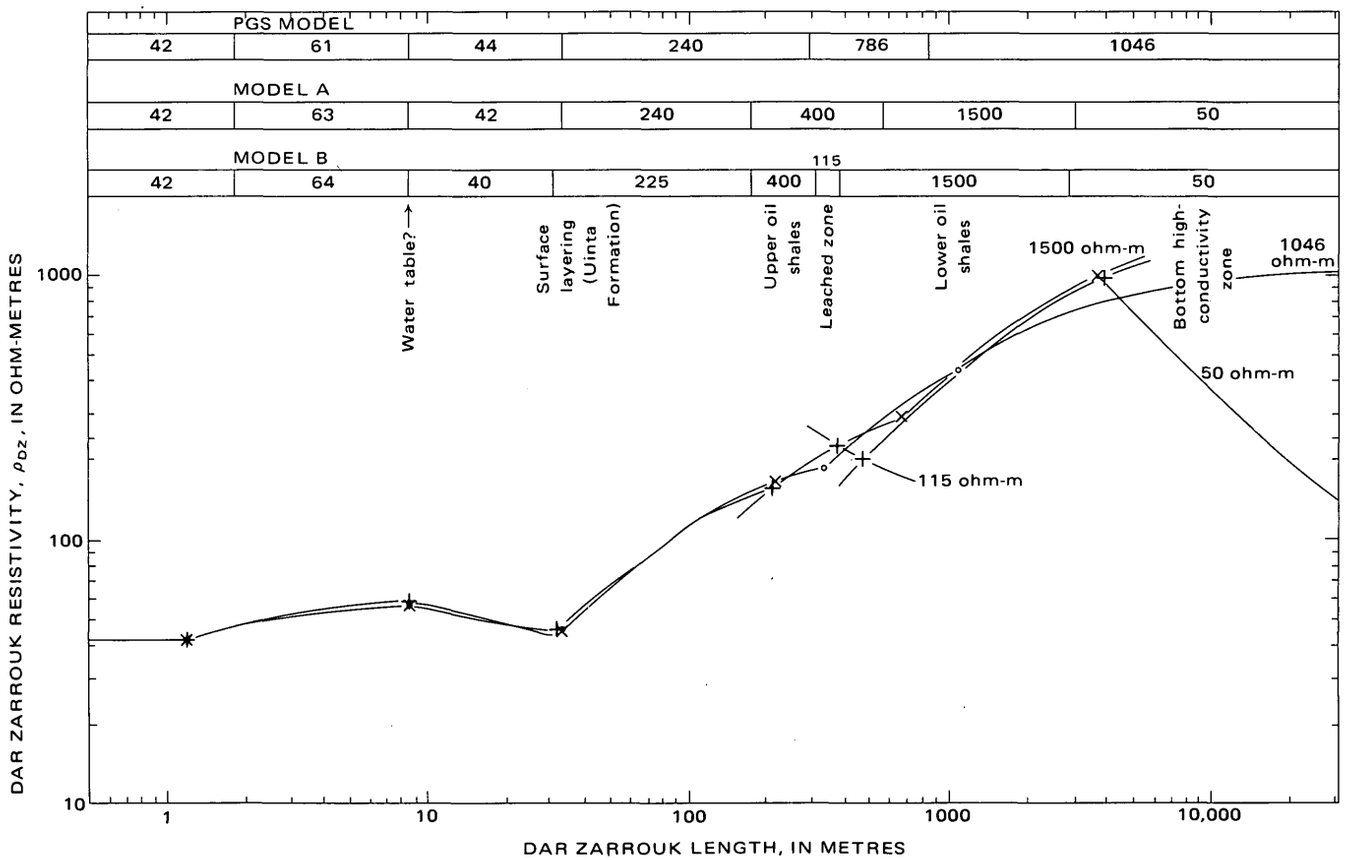

FIGURE 7.—Dar Zarrouk curves for three models of VES 7. All three models give satisfactory fit to the observed VES 7. Circle-and-dashed line, PGS model; X-and-dashed line, model A; and, plus-and-dashed line, model B. See figure 3 caption for convention for displaying models.

B places the top of this high-conductivity zone at 9,500 ft (2,896 m), which is as shallow as possible to avoid contradicting this last data point. By using this figure for depth to top of high-conductivity zone, the macroanisotropy coefficient of the shales must be $(9{,}500-560)/(1{,}600-560)=8.6$. It is likely that this large macroanisotropy is caused by many included conducting horizons with little vertical contact between them. A rough laboratory check has shown the resistivity of a nahcolite sample to be very high, although no quantitative value has been obtained. It therefore appears unlikely that interbedded oil shales and nahcolite horizons are solely responsible for the observed macroanisotropy. The most reasonable interpretation is that the conducting horizons must be water-bearing zones within the lower oil shales. By assuming that the resistivity of those zones is around 2 Ω·m in a matrix of 2,000-Ω·m oil shales, we can infer from figure 2 that only about 7 percent of the section need be water-bearing to produce the observed macroanisotropy.

The ambiguity in defining depth, thickness, resistivity, and number of leached zone(s), which we just have demonstrated for VES 7, carries over to all the VES interpretations of this report. The data often requires a leached zone or complex of horizontal aquifers without specifying their details. All leached zones in our interpreted solutions are therefore to be regarded as symbolic rather than definitive.

OTHER VES

The other VES have been interpreted so as to be consistent with the preferred interpretations we have shown for VES 1, VES 5, and VES 7. For convenience all solutions are listed in table 4. These solutions all fit the observed data within experimental tolerance. Obviously, the listed depths to the bottom high-conductivity zone are very approximate because they are based mainly on the fact that the right-hand branches of VES 1 and 2 in basin center seem to have leveled off and none of the VES curves from the basin flanks do.

TABLE 4.—*Preferred solutions VES 1–10*
[Depth, given in metres; resistance, in ohm-metres]

VES 1											
Depth	1.6	8.4	14	20	28	60	287	507	647	1,197	∞
Resistance	421	247	361	210	84	34	156	1,065	100	2,130	20
VES 2											
Depth	5	15	73	296	518	610	1,524	∞	---	----	--
Resistance	265	120	50	180	1,100	140	2,000	20	---	----	--
VES 3											
Depth	1.5	4.6	12	61	244	457	549	1,615	∞	----	--
Resistance	18	13	200	40	250	1,500	120	2,000	20	----	--
VES 4											
Depth	2.1	7.0	15	61	262	427	518	1,920	∞	----	--
Resistance	122	60	70	50	160	700	100	2,000	20	----	--
VES 5											
Depth	1.8	2.5	6.1	113	267	445	488	2,012	∞	----	--
Resistance	240	26	18	65	120	440	50	2,000	20	----	--
VES 6											
Depth	1.3	2.0	2.7	4.1	34	136	215	∞	---	----	--
Resistance	189	93	35	21	76	133	20	600	---	----	--
VES 7											
Depth	1.8	8.5	30.5	174	305	381	1,905	∞	---	----	--
Resistance	42	64	40	225	400	100	2,000	20	---	----	--
VES 8											
Depth	2.1	4.3	10.7	76	213	335	396	1,524	∞	----	--
Resistance	40	20	60	76	150	400	50	2,000	20	----	--
VES 9											
Depth	2.6	9.1	38.4	96	365	∞	----	----	---	----	--
Resistance	135	238	98	186	66	680	----	----	---	----	--
VES 10											
Depth	1.3	2.0	3.9	5.5	39	256	723	∞	---	----	--
Resistance	5.4	2.5	1.0	8.3	19.5	9	29	22	---	----	--

The depths given are, therefore, a "best guess," calculated under the convention that the resistivity contrast drops from 2,000 to 20 Ω·m. For consistency, the reported VES 5 and VES 7 solutions have been corrected in line with this convention.

Figure 8 projects these solutions onto section line *A–A′* shown in figure 1. True depths to top and bottom of the oil shale have been taken from sections by Dyni (1974), Hail (1972), and stratigraphic descriptions of wells C–34, C–35, C–155, and C–199 (Marjorie Mullens written commun., 1974). Macroanisotropy coefficients, calculated as the ratio of interpreted thickness to true thickness of the unit, are shown on the figure. Though the exact values of these coefficients are not significant, their trends and general magnitudes seem undeniable. The hatching on the sketch shows possible fracture-aquifer patterns that would produce these types of macroanisotropies. In this interpretation, the upper oil shales are increasingly fractured, both horizontally and vertically, near the basin edge and the lower oil shales contain many isolated horizontal aquifers, possibly representing a splintered and diversified leached zone.

In figure 8, a graben is shown under VES 9 in order to explain the deeper oil shales seen there and the lower resistivity right above them. Presumably the shales are deeper at VES 9, and water from the upper aquifer perches in the depression, lowering the resistivity above the shales. A similar effect is seen at VES 6 (not shown in fig. 8). A gentle syncline would fit the data as well as a graben. A graben is indicated because both VES 6 and VES 9 are on strike with the Dudley graben mapped by Donnell (1961) near the mouth of Ryan Gulch. There is no surface indication of faulting near VES 6 or VES 9, however (W. Hail, Jr., oral commun., 1972).

One last question must still be answered: Where does the water in the lower splintered acquifers come from? Following Weeks, Leavesley, Welder, and Saulnier (1974), I conjecture this source to be even nearer the basin edge, in the high country to the west and south. I think that the vertical crack system inferred for the upper shales at the locations of VES 5 through VES 9 intensifies and extends ever deeper near these recharge areas, probably penetrating the entire shale section near the very edge of the basin. Water percolating down these fractures at the basin edge would then recharge the splintered leached zone I have inferred in the lower oil shales in the basin flanks.

REFERENCES CITED

Campbell, D. L., 1975, Schlumberger electric soundings near Yellow Creek, Colorado: U.S. Geol. Survey Open-File Report D–75–354, 28 p.

Campbell, D. L., 1977, A model for electric macroanisotropy coefficient of fractured aquifers: Geophysics, v. 42, no. 1.

Carroll, R. D., Coffin, D. L., Ege, J. R., and Welder, F. A., 1967, Preliminary report on Bureau of Mines Yellow Creek core hole No. 1, Rio Blanco County, Colorado: U.S. Geol. Survey Open-File Report TEI–869, 36 p.

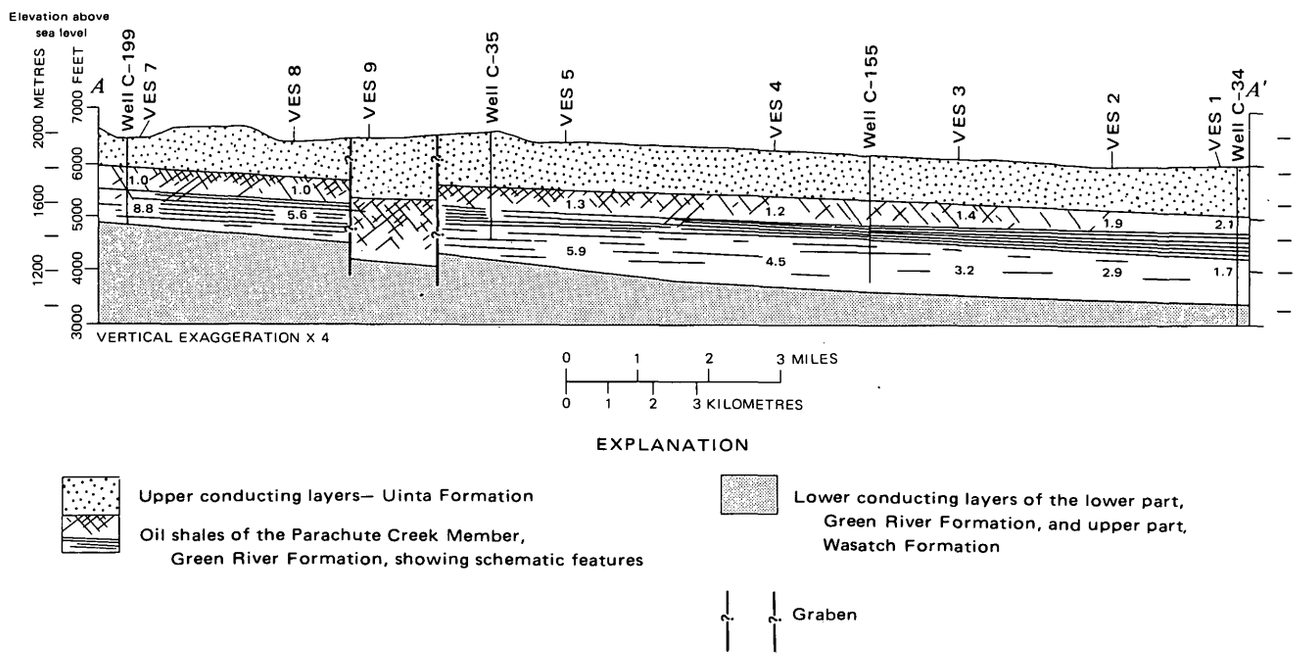

FIGURE 8.—Sketch of geology and fracturing along section *A–A′*. Numbers give macroanisotropy coefficients as inferred from this study. From Campbell (1975).

Coffin, D. L., Welder, F. A., and Glanzman, R. K., 1971, Geohydrology of the Piceance Creek structural basin between the White and Colorado Rivers, northwestern Colorado: U.S. Geol. Survey Hydrol. Inv. Atlas HA–370.

Donnell, J. R., 1961, Tertiary geology and oil-shale resources of the Piceance Creek basin between the Colorado and White Rivers, northwestern Colorado: U.S. Geol. Survey Bull. 1082–L, p. L835–L891.

Dyni, J. R., 1974, Stratigraphy and nahcolite resources of the saline facies of the Green River Formation in northwest Colorado, *in* Murray, D. K., ed., Rocky Mountain Assoc. Geologists, Guidebook to the energy resources of the Piceance Creek Basin, Colorado: p. 111–122.

Ege, J. R., Carroll, R. D., and Welder, F. A., 1967, Preliminary report on the geology, geophysics and hydrology of USBM/AEC Colorado core hole No. 2, Piceance Creek Basin, Rio Blanco County, Colorado: U.S. Geol. Survey Open-File Report TEI–870, 52 p.

Hail, W. J., Jr., 1972, Preliminary geologic map of the Barcus Creek SE quadrangle, Rio Blanco County, Colorado: U.S. Geol. Survey Misc. Field Studies Map MF–347.

Keller, G. V., and Frischknecht, F. C., 1966, Electrical methods in geophysical prospecting: New York, Pergamon Press, p. 90–196.

Pirson, S. J., 1963, Handbook of well log analysis; For oil and gas information evaluation: Englewood Cliffs, N.J., Prentice-Hall, 326 p.

Scott, J. H., Carroll, R. D., and Cunningham, D. R., 1967, Dielectric constant and electrical conductivity measurements of moist rock—A new laboratory method: Jour. Geophys. Research, v. 72, no. 20, p. 5101–5115.

Trudell, L. G., Beard, T. N., and Smith, J. W., 1974, Stratigraphic framework of the Green River Formation oil shales in the Piceance Creek Basin, Colorado, *in* Murray, D. K., ed., Rocky Mountain Assoc. Geologists, Guidebook to the energy resources of the Piceance Creek Basin, Colorado: p. 65–69.

Weeks, J. B., 1974, Water resources of Piceance Creek Basin, Colorado, *in* Murray, D. K., ed., Rocky Mountain Assoc. Geologists, Guidebook to the energy resources of the Piceance Creek Basin, Colorado: p. 175–180.

Weeks, J. B., Leavesley, G. H., Welder, F. A., and Saulnier, G. J., Jr., 1974, Simulated effects of oil-shale development on the hydrology of the Piceance Basin, Colorado: U.S. Geol. Survey Prof. Paper 908, 84 p.

Zohdy, A. A. R., 1974, Use of Dar Zarrouk curves in the interpretation of vertical electrical sounding data: U.S. Geol. Survey Bull. 1313–D, 41 p.

Zohdy, A. A. R., Eaton, G. P., and Mabey, D. R., 1974, Application of surface geophysics to ground-water investigations: U.S. Geol. Survey Techniques Water-Resources Inv., book 2, chap. D1, p. 28.

Jour. Research U.S. Geol. Survey
Vol. 5, No. 2, Mar.–Apr. 1977, p. 207–208

TECHNIQUE FOR CONCENTRATING NANNOPLANKTON FROM THE TERTIARY ROCKS OF THE CALIFORNIA COAST AND PENINSULAR RANGES

By STEVEN W. MOORE, EARL E. BRABB; and A. D. WARREN,[1] Menlo Park, Calif.; San Diego, Calif.

Abstract.—A technique for extracting nannoplankton from marine sedimentary rocks by centrifugation is described in detail. Tests on samples, previously examined using a smear technique, showed that concentration by centrifugation doubled the number of zone-diagnostic nannoplankton assemblages obtainable from the samples.

More than 300 samples of mudstone ranging from Paleocene to Pliocene in age from the California Coast and Peninsular Ranges were examined for nannoplankton using the smear technique of Bukry and Kennedy (1969). About a third of the samples contained nannoplankton and a tenth had age-diagnostic assemblages, according to a preliminary report by Bukry, Brabb, and Vedder (1973). These promising results prompted us to reexamine several of the "undiagnostic" samples to see whether the relative concentration of nannoplankton could be increased on the sample slides. Several months of trial and error using a variety of published and unpublished techniques have led to the method described below, which has significantly increased nannoplankton recovery in terms of abundance and diversity of the assemblages.

Acknowledgments.—Robert G. Coleman and Richard Poore of the U.S. Geological Survey advised us on various aspects of the separation techniques. Anderson, Warren, and Associates kindly arranged for a demonstration of their laboratory techniques. David Bukry determined the ages and relative abundances of the nannoplankton assemblages.

PREVIOUS WORK

Edwards (1963) described a centrifuging technique somewhat similar to ours, and listed several other references for preparing nannoplankton. His technique seems best suited for assemblages smaller than 4 micrometres that are studied by using an electron microscope, whereas ours is designed for assemblages mostly in the 6–9 μm size range to be studied with a high-power polarizing microscope. We have also borrowed many ideas from Funkhouser and Evitt (1959), W. W. Hay (written commun., 1972), Jeffords and Jones (1959), and Barss and Williams (1973, p. 15–18).

[1] Anderson, Warren, and Associates.

PROCEDURE

1. Disaggregate a 2-gram sample in a small mortar by using a pestle and a small amount of pH-adjusted solution. Thoroughly macerate to a slurry.

   The pH of solutions used in this process was kept around 9. A pH below 7 runs the risk of dissolving the calcareous nannoplankton. A solution of a powdered glassware cleaner, such as Alconox, serves to keep pH sufficiently high and also acts to keep clays from flocculating. Care should also be taken here and throughout the process not to contaminate samples. Ideally, raw samples in bags should not be brought into the laboratory, and dust in the air should be minimal.
2. Transfer slurry to a 400-millilitre beaker, adding pH-adjusted solution to 200-ml level.
3. Use an ultrasonic probe for 30 seconds at a middle range setting. This step seems to promote further separation and deflocculation of the particles.
4. Place a 400-mesh sieve over another 400-ml beaker; pour slurry through, gently rinsing with a light spray of pH-adjusted solution. This removes particles larger than 38 μm.
5. Allow slurry to settle for 30 to 45 minutes.
6. Siphon off and discard upper liquid, leaving only bottom sediment and about 40 ml of liquid.
7. Stir the contents of the beaker and pour the slurry into a 50-ml centrifuge tube.
8. Centrifuging:
   (a) Rapidly accelerate centrifuge with slurry to 600 revolutions per minute and hold for 15 seconds, then apply brake. Immediately decant liquid into another centrifuge tube. The settled material contains the relatively "coarse" sediment, minus clay. Any nannoplankton present will generally be 10 μm and larger in size. It may be desirable to make a slide of this fraction for study of any larger forms present.
   (b) Centrifuge the decantate from 8(a) in the same manner, but at 800 r/min, for 30 seconds. Decant and discard the liquid. This decantate contains mostly clay-size particles.

Put settled material and about 5 ml liquid in a small labeled vial. Most of the nannoplankton should be concentrated in this material.

Notes on centrifuging.—The modal size of nannoplankton seems to vary from one interval in geologic time to another. In many of the Oligocene samples in this study, the most common size was 6–9 μm, which the step 8(b) concentrated. On the other hand, many diagnostic Paleocene and Eocene forms are larger and thus tend to be more concentrated in step 8(a). Some modification of given centrifuge rate and time settings may be necessary for samples with nannoplankton varying greatly in size. A quick preliminary smear slide could be made to give a rough approximation of nannoplankton size range in the particular sample.

Also, since variations exist between different models and types of centrifuges, settings stated may not be applicable to other centrifuges and centrifuge heads. The effect of these settings can also be altered by variation in time of acceleration to desired speed and braking. These two factors should remain consistent in order to have more control on the effect of centrifugation. For this study the centrifuge was always rapidly accelerated to the desired rate, held for the specified time, then the brake was applied, stopping the rotation within 5 seconds. By experimentation, different centrifuges can be calibrated to find the right settings needed to extract nannoplankton. Sizes of particles obtained by different settings can be checked using a compound microscope and a micrometer stage.

9. Slide preparation:
   (a) Moisten cover slip with liquid detergent solution. (A solution of approximately 3 ml liquid detergent per litre water.)
   (b) Disperse about 3 drops of sample on cover slip.
   (c) Dry cover slip at low temperature on hotplate.
   (d) Spread a few drops of mounting medium on slide, place cover slip on slide and heat; let the medium "boil" for 5 minutes.
   (e) Gently press out bubbles with a round toothpick.
   (f) Continue heating at low temperature for 30 minutes.
10. Careful cleaning of sieves, glassware, and other equipment is essential to prevent contamination.
   (a) Dipping sieves and the mortar and pestle in a very dilute acid bath (dilute hydrochloric acid or household vinegar) will dissolve any remaining nannoplankton that could later contaminate other samples.
   (b) The equipment should then be rinsed and dipped in dilute sodium bicarbonate solution.

RESULTS

Reexamination of 15 of the original 300 samples indicates that the centrifuge technique doubled the number of assemblages that could be assigned to a specific zone compared to the smear technique. We also estimate that as much as half of the 300 samples may contain nannoplankton assemblages that can be assigned a series age.

The time required to process each sample will vary greatly with operator experience and the equipment available. We are currently processing about 10 samples per day using one centrifuge.

EQUIPMENT USED

International SBV centrifuge with 8-place head (No. IEC 240) and fittings for 50-ml tubes.
50-ml plastic conical-bottom centrifuge tubes.
High-power optical polarizing microscope.
400-ml beakers.
400-mesh sieves, 3-inch diameter.
Acid solution (dilute hydrochloric or vinegar).
Sodium bicarbonate solution (dilute).
Two plastic basins with covers for acid and base baths.
Slide mounting medium:
Pro-texx, R.I. = 1.495 ± 0.005 (Lerner Laboratories).
pH-9-adjusted solution made with Alconox or other suitable low-phosphate wetting agent and cleaner powder; sodium bicarbonate may also be used to adjust pH, but it has less clay dispersing effect.
Litmus paper.
Glass microscope slides and cover slips.
Round toothpicks.
Plastic squeeze bottles.
Labels for slides and vials.
Distilled water.
Capillary tubes.
Liquid detergent (as dispersant on cover slip).

REFERENCES CITED

Barss, M. S., and Williams, G. L., 1973, Palynology and nannofossil processing techniques: Canada Geol. Survey Paper 73–26, 25 p.

Bukry, David, Brabb, E. E., and Vedder, J. G., 1973, Correlation of Tertiary nannoplankton assemblages from the Coast and Peninsular Ranges of California: Latin American Geol. Congress, 2d, Caracas 1973, Preprint, 35 p.

Bukry, David, and Kennedy, M. P., 1969, Cretaceous and Eocene coccolith at San Diego, California: California Div. Mines and Geology Spec. Rept. 100, p. 33–43.

Edwards, A. R., 1963, A preparation technique for calcareous nannoplankton: Micropaleontology, v. 9, p. 103–104.

Funkhouser, J. W., and Evitt, W. R., 1959, Preparation techniques for acid-insoluble microfossils: Micropaleontology, v. 5, no. 3, p. 369–375.

Jeffords, R. M., and Jones, Daniel H., 1959, Preparation of slides for spores and other microfossils: Jour. Paleontology, v. 33, p. 344–350.

Jour. Research U.S. Geol. Survey
Vol. 5, No. 2, Mar.–Apr. 1977, p. 209–215

PLEISTOCENE FISHES FROM ALAMEDA COUNTY, CALIFORNIA

By RICHARD W. CASTEEL and DAVID P. ADAM, Menlo Park, Calif.

Abstract.—Six types of freshwater fishes were recovered from an early Pleistocene (Irvingtonian) locality on the east side of San Francisco Bay, Alameda County, Calif. The fauna includes one centrarchid, one salmonid, three cyprinids, and one catostomid. The fauna indicates fluvial and slow-moving or lacustrine aquatic environments. One of the cyprinids and the catostomid are assigned to provisional genera because of the inadequate amount of material available for study and the obvious differences between these fossils and known fossil or recent fishes. They are new additions to the Pleistocene fish fauna of California. Paleogeographic distribution of some of these fishes indicates former fluvial or lacustrine connections between Utah, Idaho, Oregon, Washington, Nevada, and California. The Pliocene and Pleistocene fossil fish faunas indicate the widespread occurrence of genera now endemic to California. A similar picture is presented by the molluscan evidence.

This paper describes the remains of six freshwater fishes (including two new provisional genera) from the vicinity of Oak Knoll Naval Hospital, Oakland, Alameda County, Calif. (fig. 1) (37°45′45″ N., 122°8′32″ W.), on the east side of San Francisco Bay.

The fishes occur in a deposit of gravel, sand, silt, and clay that overlies and contains pebbles of the Pliocene(?) Leona Rhyolite (Radbruch, 1969, p. 4 of text). The beds are poorly defined and have been tilted and contorted. The Oak Knoll locality is in a small ridge that has produced a faunal assemblage (USGS vertebrate loc. M–1242 and UCMP loc. V–5834) of probable early Pleistocene (Irvingtonian land mammal) age. These localities are shown as Pleistocene locality 22133 on Radbruch's (1969) map. The remains of a freshwater fish, *Orthodon* sp., were described from UCMP loc. V–5834 (Casteel and Hutchison, 1973) and were found in association with the remains of amphibians (*Rana*, *Taricha*), reptiles (*Clemmys*, Colubridae), birds, and mammals (Sciuridae, *Microtus*, *Odocoileus*, *Equus*, ?Proboscidea) that indicate Irvingtonian age.

Two of the fossils are new to the fossil record for California; most, however, are represented in the recent endemic freshwater fish fauna of California. The two new genera are clearly different from existing members of their families, as well as from the known fossil members. At the present time, however, each is known only from a single diagnostic element. Since it it not apparent that species may be separated on the basis of differences in these elements, we have chosen to refer them to provisional genera (α and β) within their respective families. These provisional genera are presented here for the purpose of description. We hope that with the analysis of additional material it will be possible to establish valid specific and (or) generic taxa for these specimens.

The additional material from USGS vertebrate loc. M–1242, as well as the previously undescribed material from UCMP loc. V–5834, indicates a much richer fish fauna than that previously described.

FOSSIL MATERIAL

Family SALMONIDAE

Salmo(?) sp.

Figure 2*B*

Referred material.—UCMP 112742, one nearly complete thoracic vertebra 3.0 millimetres wide.

The vertebra clearly represents a salmonid (*Salmo*, *Salvelinus*, or *Oncorhynchus*) because of the characteristic netlike patterning of its outer surfaces. The specimen is not representative of the genus *Oncorhynchus*, on the basis of the relative sizes of the pores and the intensity of the ribbing on the lateral surface. As it is not possible, with the material available, to distinguish between the thoracic vertebrae of the genera *Salmo* and *Salvelinus* for individuals with vertebrae the size of the specimen in question, the specimen is provisionally assigned to the genus *Salmo*.

This appears to be the first fossil record of this genus or of any salmonid of Irvingtonian age from central California.

Family CYPRINIDAE

Genus α

Figure 3*D–F*

Referred material.—USNM 184077, a right dentary collected by D. P. Adam in April 1972.

Diagnosis.—A cyprinid fish characterized by distinc-

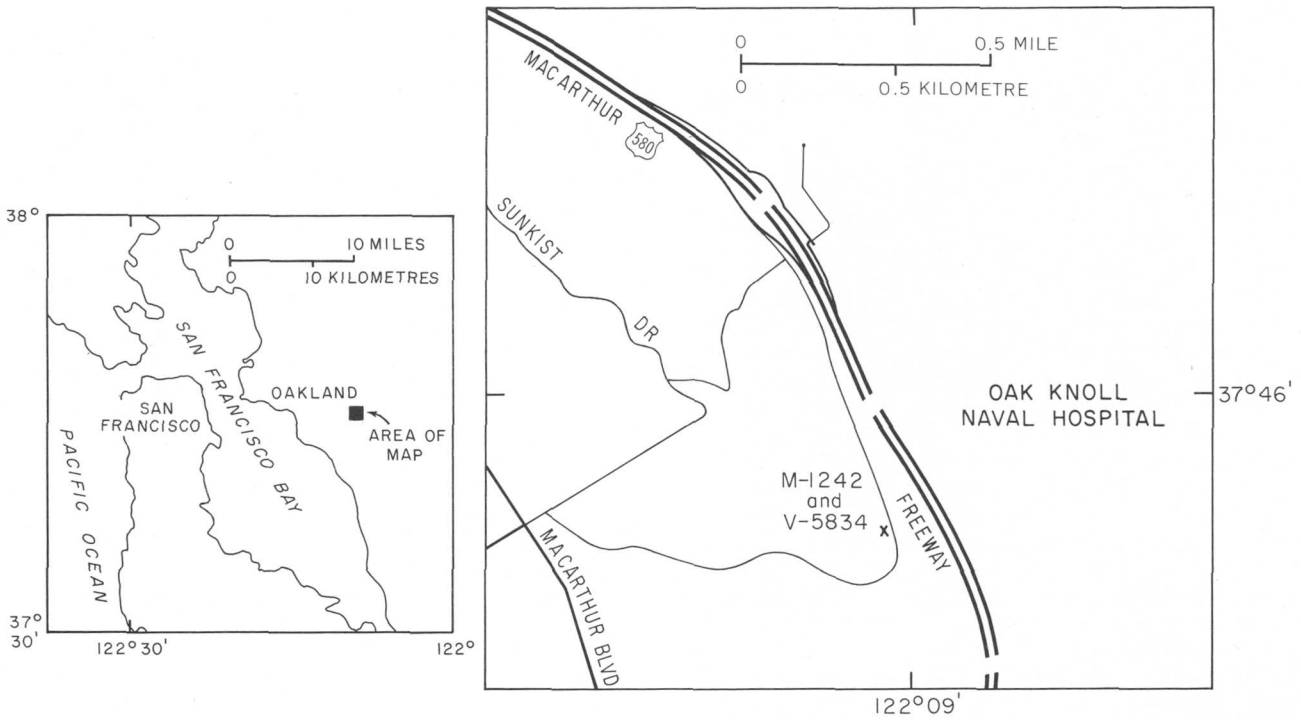

FIGURE 1.—Location of USGS vertebrate loc. M–1242 and University of California Museum of Paleontology loc. V–5834, Oakland, Alameda County, Calif. Base from U.S. Geological Survey Oakland East, 1959; photorevised, 1968.

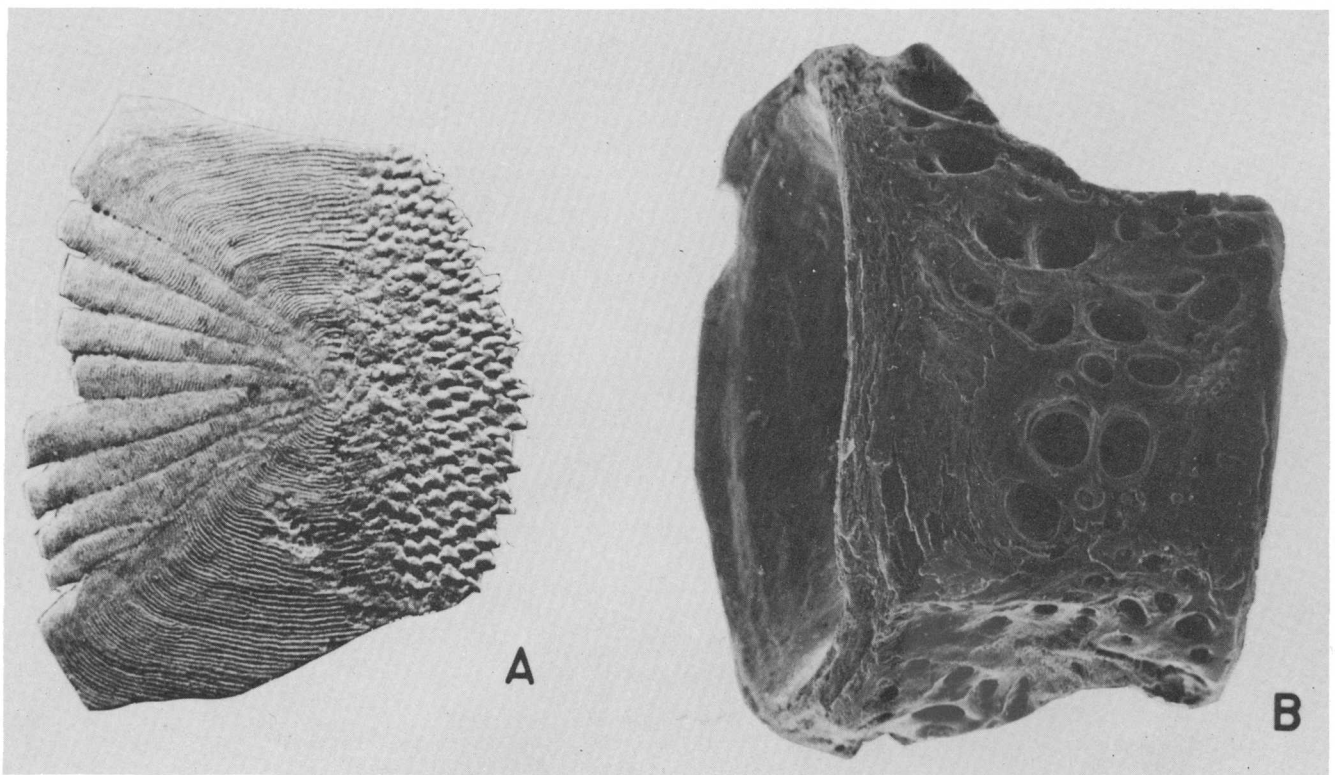

FIGURE 2.—Scanning electron micrographs. *A*, Scale of *Archoplites* cf. *A. interruptus* (Girard); × 25; anterior field to left; U.S. National Museum 184081. *B*, Thoracic vertebra of *Salmo*(?) sp.; × 32; UCMP 112742.

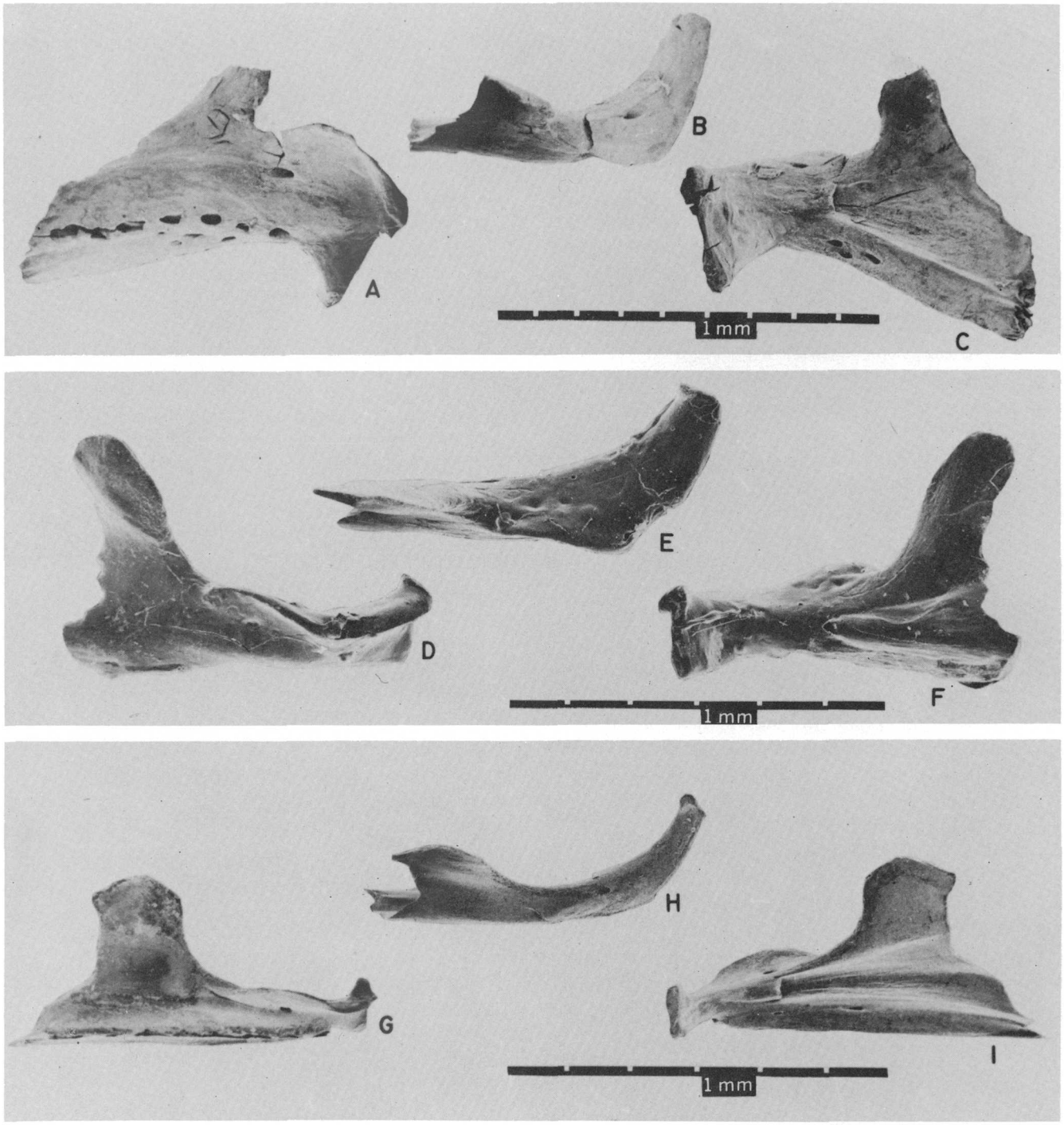

FIGURE 3.—Scanning electron micrographs of right dentaries of three species of crypinids. *A–C.* Right dentary of *Acrocheilus alutaceus* Agassiz and Pickering; specimen 5953. *D–F,* Right dentary of genus *a*; USNM 184077. *G–I,* Right dentary of *Orthodon microlepidotus* (Ayres); specimen 5084.

tive lipping of the dorsolateral margin of the dentary. The dentary is relatively short and very robust. The flange along the dorsolateral surface is oriented dorsally just anterior to the ascending process and then curves laterally toward the anterior and recurves ventrally at the anterior end of the dentary. The ascending process is nearly perpendicular to the long axis of the dentary, and there is a strongly developed symphyseal knob at the anterior end of the dentary.

The specimen is a nearly complete right dentary, lacking the ventral margin and the pores of the anterior part of the preoperculomandibular sensory ca-

nal. A part of the thin posterior margin of the dentary is also probably lacking. The dentary is 6.1 mm long, the symphyseal knob is 1.4 mm high, and the ascending process is 4.3 mm high. The general form of this dentary is not comparable with any of the recent native freshwater cyprinids of California; however, it appears to be matched by a large series of fossil dentaries from Idaho deposits of Pliocene or Pleistocene age in the possession of G. R. Smith (R. R. Miller, written commun., Feb. 10, 1975).

For comparison, figure 3 illustrates the dentary of genus α (fig. 3*D–F*) and the right dentaries of *Orthodon microlepidotus* (Ayres) (fig. 3*G–I*) and *Acrocheilus alutaceus* Agassiz and Pickering (fig. 3*A–C*). As noted by Hopkirk (1974, p. 63), *O. microlepidotus* is characterized by "dorsolateral surface of dentary (anterior to ascending process) strongly flanged and sharp-edged to produce the semi-truncate lower jaw."

The genus *Acrocheilus* is characterized by a highly modified dentary. In this genus the dentary is extremely shortened and robust, and is characterized by a marked development of the flange on the dorsolateral and dorsoanterior margins. The genus is known from fossil material (*A. xestes*) from a fluviatile facies of the Glenns Ferry Formation of late Pliocene and early Pleistocene age in Idaho (Miller and Smith, 1967). This formation also contains a number of freshwater fish presently endemic in the Sacramento–San Joaquin and Salinas–Pajaro drainages in California (Miller and Smith, 1967; Miller, 1958, 1965; Uyeno, 1961). However, genus α does not approach *Acrocheilus* in the extreme degree of its modification (fig. 3). Likewise, the development of the flange along the dorsolateral surface, the sinuous line of this flange, ranging from a dorsal to a ventrolateral orientation, the curvature of the dentary as seen in dorsal aspect, and the robust nature of the dentary itself separate genus α from *Orthodon*, as well as from the other California cyprinids.

Mylopharodon cf. *M. concephalus* (Baird and Girard)

Referred material.—USNM 184078 consists of one left pharyngeal bone and a pharyngeal bone fragment with the anterior edentulous process and last tooth socket, one right pharyngeal bone fragment with the posterior edentulous process and the first two tooth sockets, one molariform pharyngeal tooth (probably III), one fragment of the basioccipital consisting of the posteriorly projecting process, and the masticatory process of the basioccipital.

At the present time this genus is monotypic and is represented by *M. conocephalus* (Baird and Girard), endemic to the California freshwater fauna. This species has been recorded from a fossil assemblage at Potter Creek Cave, Shasta County, Calif., and assigned a Pleistocene (Wisconsin) age (Sinclair, 1904; Jordan, 1907; Uyeno, 1961; Uyeno and Miller, 1963). Other fossil remains of the genus *Mylopharodon* include *M. hagermanensis* and *M.*(?) *condonianus* from Pliocene or Pleistocene Lake Idaho (Miller and Smith, 1967; Uyeno, 1961; Cope, 1883; Miller, 1965). The age of the Lake Idaho fauna is placed at 3.0—3.5 million years (Linder, 1970; Linder and Koslucher, 1974; Miller and Smith, 1967; Evernden and others, 1964).

Orthodon cf. *O. microlepidotus* (Ayres)

Referred material.—USNM 184079, UCMP 77454. A fragment of the posterior edentulous process of a left pharyngeal bone containing the base of pharyngeal tooth I and 115 isolated pharyngeal teeth represent this species.

At the present time the genus *Orthodon* is monotypic, with the single species, *O. microlepidotus* (Ayres), endemic to California. The genus has been reported from fossil freshwater assemblages from central California and the San Francisco Bay area ranging in age from Hemphillian (Pliocene) to Rancholabrean (late Pleistocene) (Casteel and Hutchison, 1973). Remains of this species have also been recovered from Pliocene or Pleistocene lacustrine facies of the Cache Formation of Anderson (1936) near Clear Lake, Lake County, Calif. (Casteel and Rymer, 1975).

Family CATOSTOMIDAE

Genus β

Figure 4*A–D*

Referred materials.—USNM 184080 consists of a complete first vertebra 2.6 mm wide and 2.6 mm high, a complete first vertebra 2.0 mm wide and 2.0 mm high, and a fragment of the left half of a first vertebra collected by D. P. Adam in April 1972. UCMP 112743 consists of two complete first vertebrae 2.5 and 1.9 mm wide and 2.5 and 2.0 mm high, respectively.

Diagnosis.—A catostomid fish characterized by a convex projection of the dorsal and dorsolateral margins of the anterior face of the first vertebra. The dorsolateral surfaces contain a pair of pits for the ventral articulating projections of the scaphia (Nelson, 1948), and the ventrolateral surfaces have rudimentary, laterally projecting transverse processes characteristic of the first vertebra of the catostomids native to western North America.

The first vertebra of genus β possesses relatively large dorsal pits for articulation with the scaphia, as well as rudimentary, laterally projecting transverse processes on the ventrolateral surfaces. The dorsal half

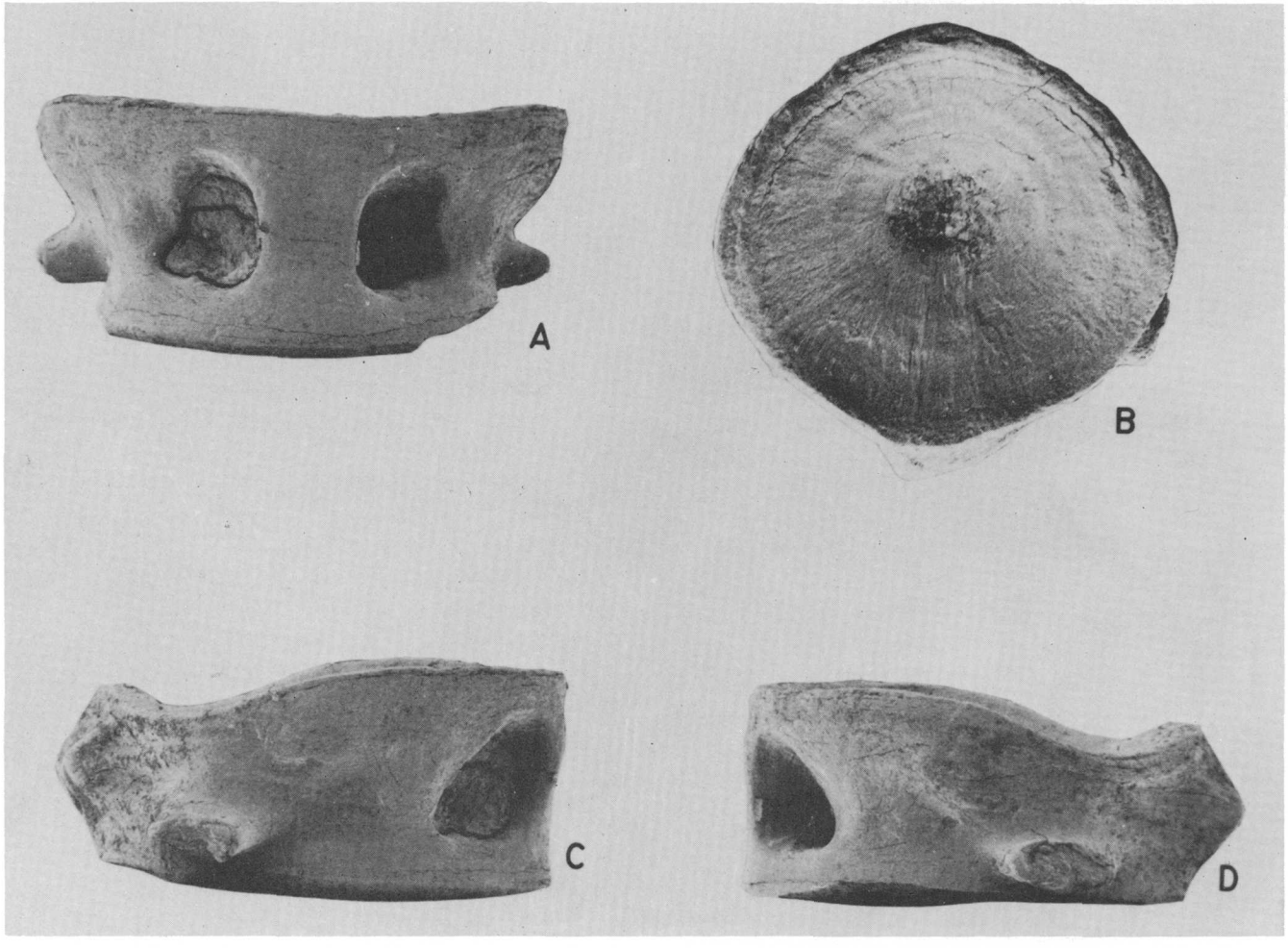

FIGURE 4.—Scanning electron micrographs of first vertebra of genus β; USNM 184080; × 18. *A*, Dorsal aspect. *B*, Posterior aspect. *C*, Left lateral aspect. *D*, Right lateral aspect.

of the anterior margin of the vertebra is markedly convex. The posterior face is flat in lateral view.

Figure 4 illustrates the first vertebra of genus β in dorsal, anterior, and left and right lateral aspects. The occurrence of stublike or rudimentary transverse processes of relatively small diameter on the first vertebra is common among the catostomids native to western North America. The first vertebra of the native catostomids in western North America is presently characterized by anterior and posterior faces that are relatively parallel, and the centrum is relatively thin anteroposteriorly. In contrast, the first vertebra of genus β is more robust, less elongated dorsoventrally and has anterior and posterior faces that are not roughly parallel.

Attempts to identify features similar to those of genus β among other members of the Ostariophysi native to North America have proven fruitless. The closest analog appears among the members of the Catostomidae. It was not possible, however, to establish criteria that could place the specimen unquestionably in one of the three existing genera of catostomids native to California (*Catostomus*, *Chasmistes*, or *Xyrauchen*). Therefore, the genus β was established to reflect the affinities of this material to the Catostomidae, and yet indicate its distinction from the three existing genera of this family native to California.

Family CENTRARCHIDAE

Archoplites cf. *A. interruptus* (Girard)

Figure 2*A*

Referred material.—USNM 184081 consists of numerous ctenoid scale fragments characteristic of *A. interruptus* (Girard) (Casteel, 1972), two fragments of the anterior part of the dentary (one left, one right), one dentigerous fragment of either a premaxillary or a dentary, one first vertebra 2.4 mm wide, one second vertebra 2.3 mm wide, three thoracic vertebra 3.2, 2.1, and 2.2 mm wide, one caudal vertebra 2.0 mm wide,

and one ultimate vertebra 2.0 mm wide. UCMP 113313 consists of one fragment of the anterior articular process of a left operculum and UCMP 113312 is a proximal fragment of a dorsal pterygiophore.

The genus *Archoplites* is represented by a single extant species, *A. interruptus* (Girard), which was restricted to the inland waters of California prior to its introduction by man outside that range (La Rivers, 1962; Moyle and others, 1974; McCarraher and Gregory, 1970).

The genus has been reported as a fossil from the early or middle Pleistocene at Moses Lake, Wash. (Miller, 1965), from Pliocene or Pleistocene Lake Idaho as *A. taylori* (Miller, 1965; Miller and Smith, 1967), and from a late Pleistocene locality near Sacramento, Calif., dated at 103,000 before present (Hansen and Begg, 1970) as *Archoplites* sp. A scale of this genus has also been identified from lacustrine facies of the Pliocene or Pleistocene Cache Formation near Clear Lake, Lake County, Calif. (Casteel and Rymer, 1975).

INDETERMINATE REMAINS

In addition to the above material, the following fish remains (USNM 184082) were also recovered: Indeterminate pterygiophores, indeterminate spiny rays, fragmentary cyprinid pharyngeal arches and teeth, two fragments of the first vertebra of an indeterminate cyprinid, numerous thoracic and caudal vertebrae (ranging in width from 1–3 mm) from indeterminate small cyprinids and (or) catostomids, an indeterminate cyprinid ceratohyal, two cyprinid opercular fragments (one left, one right) each consisting of the opercular arm and the articular process, and numerous scale fragments.

DISCUSSION

This fossil fish fauna probably represents a fluvial and slow-moving or lacustrine aquatic environment. *Archoplites interruptus*, *Orthodon microlepidotus*, and *Mylopharodon conocephalus* presently are found in environments that range from large, sluggish creeks, small rivers, and the upper reaches of large rivers in the Upper Sonoran Life Zone to the fast- and slow-moving and standing waters in the Lower and Upper Sonoran Life Zones (the sucker and hitch zones, respectively, of Hopkirk, 1974). Since none of the remains show marked signs of stream abrasion, it may be assumed that the cyprinid genus α and the catostomid genus β were also inhabitants of this environment and do not represent members of faunas whose remains were deposited after extensive transport. The occurrence of *Salmo*(?) could be interpreted as indicating permanent, cold headwater creeks. However, since this genus presently migrates through all water types, from headwater areas to the open sea, its presence in the Oak Knoll assemblage is not unlikely. It does indicate that active contact did exist between streams of the Transition, Canadian, and (or) Hudsonian Life Zones and the waters in the area of the Oak Knoll Naval Hospital.

The paleogeographic distribution of some of these fishes indicates a close relation between the fish faunas of the Central Valley of California and the fossil fish faunas of Idaho and eastern Washington. *Archoplites* and *Mylopharodon*, both presently endemic to central California, have also been identified in Pliocene or Pleistocene deposits in Idaho and Pleistocene deposits in eastern Washington. Other genera (*Ptychocheilus*, *Chasmistes*, *Acrocheilus*, *Catostomus*) from the Pliocene or Pleistocene Idaho fish faunas indicate former connections with the Colorado, Columbia–Snake, Sacramento–San Joaquin, and Klamath River systems, as well as with lake systems in the Great Basin. A similar pattern, involving the disjunct distributions of the mollusks *Pisidium ultramontanum* Prime, *Ceriphasia acutifilosa* (Stearns), *Carinifex newberri* (Lea), *Valvata utahensis*, *Stagnicola utahensis*, and *Pyrgulopsis* spp., has been described by Taylor (1960). Their distributions appear to extend from Walker Lake, Nev. across Eagle Lake, the upper Pit River, Calif., to Klamath Lake, Fossil Lake, and the Malheur basin, Ore., to the Snake River in southern Idaho and western Wyoming, Gentile Valley and Bear Lake, southeastern Oregon, and, finally, to Utah Lake, Utah. The period of time assigned to these widespread, though not necessarily coeval, connections ranges from Pliocene to early Pleistocene (Taylor, 1960, p. 332).

These disjunct distributions imply an earlier sharing of fish faunas between the major river systems in the West and draw attention to the areas of interior drainage in southeastern Oregon that formerly drained into the Pacific Ocean (Russell, 1903) and parts of the northern and western Great Basin, as well as to questions concerning the course of the pre-Pleistocene ancestral Snake River (Miller, 1965).

The age of the Oak Knoll material is Irvingtonian (early Pleistocene) (Radbruch, 1969; Casteel and Hutchison, 1973). The fish remains indicate species that range from Pliocene through late Pleistocene (Hemphillian through Rancholabrean land mammal ages).

REFERENCES CITED

Anderson, C. A., 1936, Volcanic history of the Clear Lake area, California: Geol. Soc. America Bull., v. 47, no. 5, p. 629–664

Casteel, R W., 1972, A key, based on scales, to the families of native California freshwater fishes: California Acad. Sci. Proc., v. 39, no. 7, p. 75–86.

Casteel, R. W., and Hutchison, J. H., 1973, *Orthodon* (Actinopterygii, Cyprinidae) from the Pliocene and Pleistocene of California: Copeia, no. 2, p. 358–361.

Casteel, R. W., and Rymer, M. J., 1975, Fossil fishes from the Pliocene or Pleistocene Cache Formation, Lake County, California: U.S. Geol. Survey Jour. Research, v. 3, no. 5, p. 619–622.

Cope, E. D., 1883, On the fishes of the Recent and Pliocene lakes of the western part of the Great Basin, and of the Idaho Pliocene lake: Philadelphia Acad. Nat. Sci. Proc., v. 35, p. 134–166.

Evernden, J. F., Savage, D. E. Curtis, G. H., and James, G. T., 1964, Potassium-argon dates and the Cenozoic mammalian chronology of North America: Am. Jour. Sci., v. 262, p. 145–198.

Hansen, R. O., and Begg, E. L., 1970, Age of Quaternary sediments and soils in the Sacramento area, California, by uranium and actinium series dating of vertebrate fossils: Earth and Planetary Sci. Letters, v. 8, no. 6, p. 411–419.

Hopkirk, J. D., 1974, Endemism in fishes of the Clear Lake region of central California: California Univ. Pubs. Zoology 96, 135 p.

Jordan, D. S., 1907, The fossil fishes of California with supplementary notes on other species of extinct fishes: California Univ. Dept. Geol. Bull., v. 5, no. 7, p. 95–144.

La Rivers, Ira, 1962, Fishes and fisheries of Nevada: Carson City, Nevada Fish and Game Commission, 783 p.

Linder, A .D., 1970, Fossil sculpins (Cottidae) from Idaho: Copeia, no. 4, p. 755–756.

Linder, A. D., and Koslucher, D. G., 1974, A partial *Diastichus* (Cyprinidae) skeleton from Plio-Pleistocene Lake Idaho: Northwest Sci., v. 48, no. 3, p. 180–182.

McCarraher, D. B., and Gregory, R. W., 1970, The current status distribution of Sacramento perch, *Archoplites interruptus*, in North America: Am. Fish. Soc. Trans., v. 99, p. 700–707.

Miller, R. R., 1958, Origin and affinities of the freshwater fish fauna of western North America, [chap.] 9 *in* Pt. 1 *of* Hubbs, C. L., ed., Zoogeography: Am. Assoc. Adv. Sci. Pub., no 51, p. 187–222.

——— 1965, Quaternary freshwater fishes of North America, *in* Wright, H. E., Jr., and Frey, D. G., eds., The Quaternary of the United States: Princeton, Princeton Univ. Press., p. 569–581.

Miller, R. R., and Smith, G. R., 1967, New fossil fishes from Plio-Pleistocene Lake Idaho: Michigan Univ. Mus. Zoology Occasional Paper 654, 24 p.

Moyle, P. B., Mathews, S. B., and Bonderson, Noel, 1974, Feeding habits of the Sacramento perch, *Archoplites interruptus:* Am. Fish Soc. Trans., v. 103, no. 2, p. 399–402.

Nelson, E. M., 1948, The comparative morphology of the Weberian apparatus of the Catostomidae and its significance in systematics: Jour. Morphology, v. 83, no. 2, p. 225–251.

Radbruch, D. H., 1969, Areal and engineering geology of the Oakland East quadrangle, Caifornia: U.S. Geol. Survey Geol. Quad. Map GQ–769, scale 1:24,000.

Russell, I. C., 1903, Notes on geology of southwestern Idaho and southeastern Oregon: U.S. Geol. Survey Bull. 217, 83 p.

Sinclair, W. J., 1904, The exploration of the Potter Creek Cave: Calif Univ. Pubs. Am. Archaeology and Ethnology, v. 2, no. 1, p. 1–28.

Taylor, D. W., 1960, Distribution of the freshwater clam *Pisidium ultramontanum;* a zoogeographic inquiry: Am. Jour. Sci., v. 258–A, p. 325–334.

Uyeno, Teruya, 1961, Late Cenozoic cyprinid fishes from Idaho with notes on other fossil minnows in North America: Michigan Acad. Sci., Arts and Letters Papers, v. 46, p. 329–344.

Uyeno, Teruya, and Miller, R. R., 1963, Summary of late Cenozoic freshwater fish records for North America: Michigan Univ. Mus. Zoology Occasional Paper 631, 34 p.

Jour. Research U.S. Geol. Survey
Vol. 5, No. 2, Mar.–Apr. 1977, p. 217–219

BLADES OF OLIVINE IN ULTRAMAFIC ROCK FROM NORTHERN SIERRA NEVADA, CALIFORNIA

By ANNA HIETANEN, Menlo Park, Calif.

Abstract.—Blades of olivine in random arrangement crystallized in a small body of serpentine just north of the Grizzly pluton as a result of contact metamorphism. Interstitial minerals are talc, chlorite, and minor amount of cummingtonite.

A small ultramafic body made up of blades of olivine in random arrangement and interstitial talc is exposed on the west side of Rock Creek about 800 metres south of Spring Valley Lake in the southern part of the Jonesville quadrangle, California (fig. 1, loc. 1245). This rock is along the southern border of a metagabbro mass that has intruded Paleozoic metasedimentary rocks, the Calaveras Formation, 300 m north of the monzotonalitic Grizzly pluton (Hietanen, 1973, pl. 1). The metagabbro consists of inhomogeneous hornblende-plagioclase rock that grades in places to coarse-grained hornblendite. Two other small bodies of ultramafic rock in the metagabbro that are farther from the pluton do not show this uncommon texture.

The ultramafic rock with the blades of olivine was found in a low outcrop about 150 m west of Rock Creek in 1969. It extended over an area of only about 10 m^2 and showed signs of being recently exposed by floodwaters. The outcrop has a very thinly weathered crust in which dark-rust-colored olivine blades contrast with light-brown interstitial areas filled mainly by talc. On a freshly cut surface (fig. 2) the blades of olivine are dark green to black, and the talc is gray. Most olivine blades are 3 to 15 mm long and 0.1 to 2 mm thick. The interstitial areas of talc are polygonal or triangular and 1 to 10 mm in diameter.

MINERAL ASSEMBLAGE AND CHEMICAL COMPOSITION

Thin sections show that in addition to olivine and talc this rock contains serpentine, cummingtonite, chlorite, and magnetite. Olivine blades are elongate parallel to the fast vibration direction and are transected by irregular to subparallel fractures that are 0.01 to 0.05 mm wide and filled by green or rust-colored serpentine minerals, presumably chrysotile. These fractures are similar to the tiny subparallel fractures that lend a slightly foliated structure to large ultramafic masses farther south (Hietanen, 1973, p. 26). No sign of such foliation, however, is visible in the ultramafic rock with blades of olivine, and in many grains another weakly developed set of fractures transects the major set at an angle of 45° to 90°. In a few places the rust-colored chrysotile and disseminated magnetite have replaced as much as 90 percent of the olivine.

The interstitial areas between the olivine blades are filled mainly by talc, chlorite, and cummingtonite. The talc next to the olivine is in larger flakes (0.5 to 2 mm long) than the talc in the centers of the interstitial areas (0.05 to 0.5 mm long). Radiating bundles of long prisms of cummingtonite traverse many of the talc-rich areas. Cummingtonite is transected by fractures that are commonly oriented perpendicular to the length of the prisms and filled by chrysotile. Chlorite is colorless and shows low birefringence. Most of it is in clusters of stubby flakes, 0.01 to 0.05 mm long, between the blades of olivine and areas made up of talc, but some is scattered among talc. Magnetite is in aggregates of tiny grains among talc and chlorite and with serpentine in some of the fractures in olivine.

Chemical analysis (table 1) shows that this ultramafic rock is rich in magnesium (40 percent) and low in silicon (about 42 percent). The alkali content is very low, and the water content is exceptionally high. Spectrographic analysis shows a relatively high amount of chromium and nickel and some boron, cobalt, copper, and vanadium. In the calculation of molecular percentages of minerals (table 1), chromium was calculated as chromite, and aluminum was combined with appropriate amounts of magnesium, silicon, and water to form amesite. The ferric iron and a part of the ferrous iron were combined to form magnetite. The ferrous iron in excess of that in magnetite was calculated as fayalite. Manganese was calculated as tephroite. In the total amount of olivine (52.5 percent) the calculated percentage of forsterite is 93.7. The in-

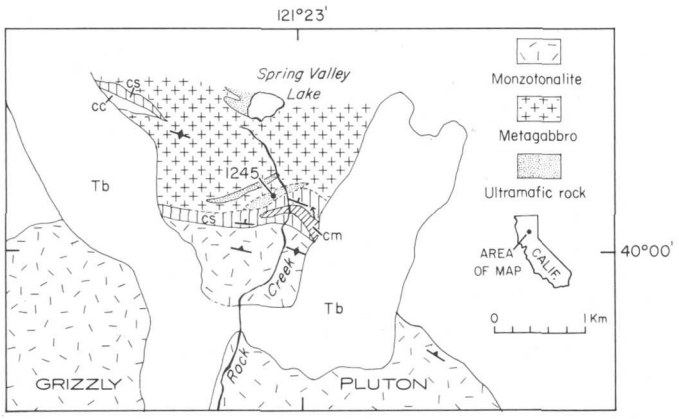

FIGURE 1.—Sketch showing the location 1245 and geologic setting of the ultramafic rock. Metasedimentary rocks north of the Grizzly pluton are schist (cs), metachert (cc), and marble (cm) of the Calaveras Formation (Paleozoic); Tb, Tertiary basalt. From Hietanen (1973).

FIGURE 2.—Photograph of a cut surface of the ultramafic rock showing blades of olivine (dark) in random arrangement. The interstitial areas of talc and chlorite are light gray.

dices of refraction of the olivine, which were $\alpha = 1.652 \pm 0.001$, $\beta = 1.669 \pm 0.001$, and $\gamma = 1.687 \pm 0.001$, support this forsterite content. The percentage of cummingonite estimated in thin sections is about 6.9 and that of talc, about 20.0 After combining the appropriate amounts

TABLE 1.—*Chemical composition, trace elements, and minerals in ultramafic rock with blades of olivine*

[Chemical analysis in weight percent by Elaine Brendt; spectrographic analysis by R. E. Mays]

Chemical composition				*Trace elements in parts per million*		*Minerals, in molecular percent*	
Weight percent		*Cation percent*					
SiO_2	41.84	SiO_2	37.48	B	50	Olivine	52.5
TiO_2	.01	TiO_2	.01	Ba	<4	Talc	20.0
Al_2O_3[a]	2.33	$AlO_{3/2}$	2.46	Co	90	Chlorite	12.3
Fe_2O_3	3.01	$FeO_{3/2}$	2.03	Cr	4,200	Chrysotile	13.6
FeO	4.68	FeO	3.50	Cu	12	Cummingtonite	6.9
MnO	.12	MnO	.09	Mo	<4	Magnetite	3.0
MgO	40.44	MgO	54.01	Ni	2,700	Chromite	1.0
CaO[b]	.10	CaO	.10	Sc	<10	Magnesite	.7
Na_2O	.04	$NaO_{1/2}$	.06	V	43	Subtotal	110.0
K_2O	.01	$KO_{1/2}$	.01			$+H_2O$	9.2
CO_2	.20	CO_2	.24	Not detected: Ag, Be, La, Nb, Pb, Sn, Sr, W, Y, Zn, Zr, P, Ce, Ga, Eu.		Total	119.2
H_2O+	6.62	(H_2O+	19.77)				
H_2O-	.27	Total	99.99			Olivine:	
Total	99.67					Forsterite	93.7
		Total anions	159.7			Fayalite	6.0
						Tephroite	.3
		Mg/Mg+Fe	0.94			Total	100.0

[a] Includes chromium.
[b] Determined spectrographically.

of silicon, magnesium, and water to form these percentages of cummingtonite and talc, the remaining silicon was combined with appropriate amounts of magnesium and water to form serpentine. If amesite is combined with an equal amount of antigorite to form chlorite, the percentages of chlorite (12.3) and remaining serpentine (13.6) are in good agreement with the percentages estimated in thin sections. The mineralogy suggests that the main primary minerals in this ultramafic rock may have been magnesium-rich olivine (about 66 percent), pyroxene (about 27 percent), and amphibole (7 percent).

ORIGIN OF THE BLADES OF OLIVINE

Closely similar textures with randomly oriented blades of olivine have been described from metamorphosed serpentine (Matthes, 1971; Evans and Trommsdorff, 1974) as well as from Archaean ultramafic extrusive rocks, where they formed by rapid cooling of an ultramafic liquid (spinifex texture) (Viljoen and Viljoen, 1969; Naldrett and Mason, 1968; Nesbitt, 1971; Pyke, Naldrett, and Eckstrand, 1973).

The small lens-shaped mass described here was not a surface flow but rather a sill-like body. Most other small bodies of ultramafic rocks in the northern Sierra Nevada are thoroughly serpentinized, consisting mainly of antigorite and talc; primary olivine has been preserved only in the centers of large masses, where it occurs with chrysotile and lizardite (Hietanen, 1973). It is therefore likely that the ultramafic rock near Rock Creek was serpentinized during the first (synkinematic) period of metamorphism and reactions were reversed at elevated temperatures to form olivine and the other minerals from the serpentine during the em-

placement of the pluton. The postkinematic contact metamorphism affected all metasedimentary rocks in a zone, 1 to 2 km wide, around the pluton. Porphyroblasts of cordierite and andalusite and radiating bundles of cummingtonite were formed in pelitic rocks near the contact where temperatures were about 600°C and pressures about 4 kilobars (Hietanen, 1973, p. 33). The assemblage olivine-talc-chlorite-cummingtonite was apparently stable at this temperature and pressure. For comparison, Greenwood (1963) experimentally determined the temperature of reaction of talc + forsterite → anthophyllite at this pressure as 692°C, a somewhat higher temperature than estimated here for the crystallization of the talc-forsterite-cummingtonite assemblage.

The metamorphic origin of the elongate olivine crystals is supported by the very low calcium (Simkin and Smith, 1970) and high magnesium content in the olivine. Magnesium content may have increased because not all of the iron that was separated as magnetite during the serpentinization reentered the secondary olivine. Comparison of the mineralogy of the Rock Creek sample with that of the various metamorphic zones in serpentine around the Bergell tonalite, Italy, as described by Trommsdorff and Evans (1972) shows a close similarity with their two highest grade zones. However, cummingtonite instead of tremolite crystallized in the Rock Creek sample because of the very low calcium content.

REFERENCES CITED

Evans, B. W., and Trommsdorff, Volkmar, 1974, On elongate olivine of metamorphic origin: Geology, v. 2, no. 3, p. 131–132.

Greenwood, H. J., 1963, The synthesis and stability of anthophyllite: Jour. Petrology, v. 4, no. 3, p. 317–351.

Hietanen, Anna, 1973, Geology of the Pulga and Bucks Lake quadrangles, Butte and Plumas Counties, California: U.S. Geol. Survey Prof. Paper 731, 66 p.

Matthes, S., 1971, Die ultramafischen Hornfelse, insbesondere ihre Phasenpetrologie: Fortschr. Mineralogie, Band 48, no. 1, p. 109–127.

Naldrett, A. J., and Mason, G. D., 1968, Contrasting Archaean ultramafic igneous bodies in Dundonald and Clergue Townships, Ontario: Canadian Jour. Earth Sci., v. 5, p. 111–143.

Nesbitt, R. W., 1971, Skeletal crystal forms in the ultramafic rocks of the Yilgarn Block, western Australia: evidence for an Archaean ultramafic liquid, *in* Glover, J. E., ed., Symposium on Archaean rocks: Geol. Soc. Australia, Spec. Pub. 3, p. 331–347.

Pyke, D. R., Naldrett, A. J., and Eckstrand, O. R., 1973, Archean ultramafic flows in Munro Township, Ontario: Geol. Soc. America Bull. 84, no. 3, p. 955–977.

Simkin, Tom and Smith, J. V., 1970, Minor-element distribution in olivine: Jour. Geology, v. 78, no. 3, p. 304–325.

Trommsdorff, Volkmar and Evans, B. W., 1972, Progressive metamorphism of antigorite schist in the Bergell tonalite aureole (Italy): Am. Jour. Sci., v. 272, no. 5, p. 423–437.

Viljoen, M. J., and Viljoen, R. P., 1969, Evidence for the existence of a mobile extrusive peridotitic magma from the Komati Formation of the Onverwacht Group: Geol Soc. South Africa, Spec. Pub. 2, Upper Mantle Project, p. 87–112.

Jour. Research U.S. Geol. Survey
Vol. 5, No. 2, Mar.–Apr. 1977, p. 221–226

MERCURY IN OIL SHALE FROM THE MAHOGANY ZONE OF THE GREEN RIVER FORMATION, EASTERN UTAH AND WESTERN COLORADO

By JOHN R. DONNELL and VAN E. SHAW, Denver, Colo.

Abstract.—Mercury has been reported in concentrations as high as 4 parts per million from oil shale in the Green River Formation near the Federal oil-shale prototype lease-tracts U–a and U–b in eastern Utah. This high concentration of mercury if present throughout a minable zone, would be of concern in commercial oil-shale operations processing large volumes of shale. Using an improved analytical method, surface samples from eastern Utah previously reported to contain high concentrations of mercury were reanalyzed, and an additional 183 drill core samples from the Mahogany zone and adjacent beds were analyzed. The reanalyzed samples averaged slightly more than 0.35 ppm mercury and the drill-core samples averaged 0.37 ppm. The products from a Fischer assay of 100-gram sample of oil shale, found to yield 35 gallons per ton of oil and 43 ppm of mercury, were analyzed for their mercury content. The spent shale contained only 2 percent of the total mercury in the assay products and the gas fraction contained about 58 percent.

The Project Independence blueprint gives several schedules for the development of oil shale (U.S. Federal Energy Administration, 1974, p. 60). Under minimum production, 50,000 bbl (barrels) of oil a day will be produced from oil shale in 1980, increasing to 750,000 bbl a day by 1990.[1] The most optimistic projection postulates a production of 200,000 bbl of oil a day in 1980, increasing to 2.5 million barrels a day by 1990. Even under the most conservative projection of production, large quantities of oil shale may be mined and processed by the year 1990. Because of the large volume of material being processed, metals such as mercury, though present in very minor quantities in the shale, may have an effect on the environment. The amount of these trace metals and their ultimate disposition during and after processing of the shale is of importance.

If a large part of the mercury present in oil shale enters the gas fraction of retorted shale, the mercury may be washed from the atmosphere into streams or may be absorbed by vegetation. It might then travel through the food chain to the grazing animal and ultimately into the human system. Mercury contained in the water produced from the shale in the retorting process will pose a similar hazard to streams and vegetation. Mercury in the oil produced from the shale presumably will be present in quantities no greater than those in most crude oils. Mercury that remains in the retorted residue may be fixed in the inorganic fraction or in the remaining organic carbon, or it may be leached from the tailings and enter the ecosystem.

Four tracts of Federal land in Colorado and Utah totaling slightly more than 20,000 acres (8,100 hectares) were leased in 1974 under the U.S. Department of the Interior's prototype oil-shale leasing program. The potential total productive capacity of these tracts is in excess of 300,000 bbl of oil a day for a period of at least 20 years. Under the terms of the lease the lessees are required to monitor the environment for a period of at least 1 year prior to submitting a final development plan. Core obtained from exploratory drilling, which is part of the monitoring process, is analyzed for trace elements, including mercury. Trace-element analyses done by the lessees are on composite samples from fairly thick oil-shale intervals not necessarily related to minable units.

Core samples from hole C–176 (fig. 1), which penetrated the Mahogany zone, were selected by us for detailed mercury analysis. Core-hole C–176 is southeast of prototype oil-shale test-lease tract C–b.

PREVIOUS WORK

Thus far a systematic analysis of oil shale for mercury has not been undertaken. In 1959 R. A. Cadigan of the U.S. Geological Survey collected eight samples from an 800-foot (244-metre) interval in the Green River Formation in eastern Utah, and had them analyzed for mercury. The samples came from the outcrop in Hells Hole Canyon, sec. 17, T. 10 S., R. 25 E., about 1 mile (1.6 kilometres) east of the east edge of the prototype lease-tract U–b. The analysis indicated a maximum of 4.0 parts per million mercury from the

[1] To convert barrels (1 bbl=42 gal) to cubic metres, multiply by 0.1590; to convert gallons per ton (2,000 lb) to litres per metric ton (1,000 kg) multiply by 4.16.

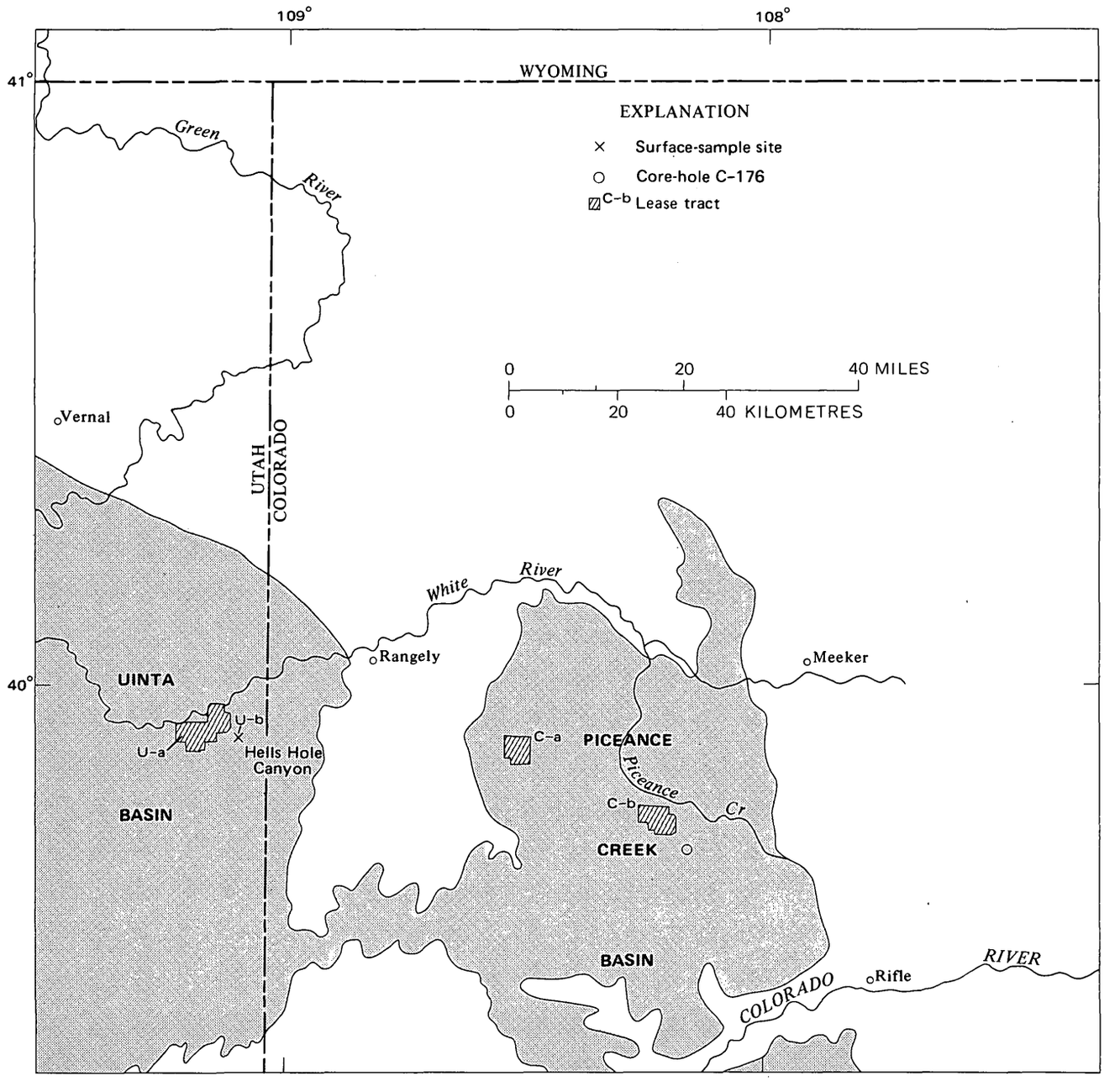

FIGURE 1.—Location of U.S. Department of Interior prototype oil-shale lease tracts and localities sampled for mercury analyses, eastern Utah and western Colorado.

Mahogany bed, an organic-rich shale interval 4 feet (1.2 m) thick in the Mahogany zone. The seven other samples from an 800-foot (244-m)-thick section of the Green River Formation also had anomalously high amounts of mercury (table 1).

In 1972 the part of Cadigan's samples which had not been consumed was reanalyzed by the flameless atomic absorption method described in the section on "Analytical Procedure," and the results are shown in table 1. The amount of mercury found was generally about one-fifth to one-tenth of that originally reported. The high organic content of the samples may have interfered in the determination, in the earlier analyses, resulting in erroneous reports of high mercury concentrations.

Desborough, Pitman, and Huffman (1974) determined mercury concentrations in a total of eight samples from core in the Piceance Creek basin, Colorado, and the Uinta Basin, Utah. The concentration of mercury ranged from 0.07 to 2.9 ppm and averaged 0.48 ppm.

TABLE 1.—*Results, in parts per million, of mercury analyses of surface samples from the Green River Formation, Hells Hole Canyon, Uintah County, Utah*

Stratigraphic position from top of Mahogany bed [1]	1959 analysis	1972 analysis [2]	Rock description
394 feet (120 m) above ----	1.3	0.45	Shale.
269 feet (82 m) above -----	1.8	.29	Oil shale.
152 feet (46 m) above -----	1.6	.38	Do.
14 feet (4 m) above -------	1.1	.48	Zeolite.
2 feet (0.6 m) below -----	4.0	.26	Oil shale.
158 feet (48 m) below -----	1.8	.18	Sandstone (oil impregnated).
378 feet (115 m) below ----	1.6	.30	Oil claystone.
433 feet (132 m) below ----	3.9	.50	Do.

[1] See figure 2 for stratigraphic position of Mahogany bed.
[2] At least three separate determinations were made on each sample.

PRESENT INVESTIGATION

Reanalysis of the samples collected at Hells Hole Canyon indicated that the mercury content of the Green River Formation at that locality averages about 0.36 ppm, in contrast to an average of 2.2 ppm obtained in the previous analysis. Only two samples are from the Mahogany zone and only one of these is an oil shale.

The Mahogany zone is the only unit in the Uinta Basin which is of economic interest to a company using conventional oil-shale mining and extraction methods. The Piceance Creek basin of Colorado contains several rich oil-shale zones, including the Mahogany, that may be economically extracted by conventional mining and retorting methods. Thus far the Mahogany, the uppermost rich zone, has been the only zone mined on a pilot basis and presumably it will be the first one mined in the lease tracts of Colorado.

Core-hole C–176 was drilled by The Oil Shale Corp. (TOSCO) near the center of sec. 21, T. 3 S., R. 96 W., as an exploratory hole on one of the tracts of land nominated for lease during the Department of Interior's 1968 leasing program. The oil content of the core was determined by TOSCO using a modified Fischer-assay method, and the unassayed crushed core residue was stored by the U.S. Geological Survey. Core-hole C–176 is about ½ mile (0.8 km) southeast of the southeast corner of prototype-tract C–b which was leased by Colony Development Operation in 1974. Because of the similarity of mineral composition of the oil shale over large areas and the proximity of C–176 to lease-tract C–b, the mercury content of the core from the Mahogany zone in hole C–176 is assumed to be similar to the Mahogany zone on lease-tract C–b.

SAMPLING

Core was selected for analysis from a 258.5-foot (78.8-m)-interval between the depths of 770.5 feet (234.8 m) and 1,029 feet (313.6 m). Within this interval nine pieces of core having a total footage of 14.6 feet (4.5 m) were missing and no analyses are available for either oil or mercury (a mercury plot of zero on fig. 2 indicates missing samples.) Twelve additional samples of crushed oil shale representing an interval of 11.6 feet (3.5 m) were assayed for oil content but were not available for mercury analysis. In the interval between 799 feet (243.5 m) and 970 feet (295.7 m), which includes the Mahogany zone and overlying beds, most of the samples were selected at 1-foot (0.3-m) intervals. Below the Mahogany zone, in the interval between 970 feet (295.7 m) and 1,029 feet (313.6 m), the samples selected for analysis were composited in intervals ranging from 2 to 18 feet (0.6–5.5 m).

ANALYTICAL PROCEDURE

A split of the crushed material utilized for the Fischer oil assays was used for the analysis. The mercury content was determined by a flameless atomic absorption method used for the determination of submicrograms of mercury in organic and inorganic geologic materials. The analytical procedure is a modification of the method described by Huffman, Rahill, Shaw, and Norton (1972). The major modification is in the sample dissolution technique, and is as follows:

Weigh and transfer 0.2 g of ground organic sample or 0.5 g of inorganic sample to a 250-millilitre Erlenmeyer flask. Add 10 ml of concentrated sulfuric acid, 10 ml of nitric acid, and 10 ml of special-grade perchloric acid to the flask. Cover the flask with a 50-millimetre watchglass and let stand overnight. Place a 150-ml beaker filled with ice water on top of the watchglass, then place the apparatus on a cold hotplate equipped with Variac control. With each suite of samples process a reagent blank and a known standard sample such as NBS–1630 or NBS–1632 completely through the method starting with the dissolution step. Heat the samples slowly so that the surface of the hotplate reaches approximately 170°C in no less than 3½ hours. The samples should then be free of all organic matter; if not, continue heating until all organic matter oxidizes. All the organic matter must be oxidized to prevent frothing in the subsequent aeration step.

The dissolution procedure for samples that contain little organic matter is essentially the same as that for samples containing much organic matter. However, for low-organic-matter samples, the amount of perchloric acid used is 2 ml and the digestion time is usually shortened.

Utilizing the method described by Huffman with the modification described in this report, the deviation from the mean using 40 determinations was ±0.010 on an oil-shale sample containing 0.43 ppm mercury.

ANALYTICAL RESULTS

The results of oil assays and mercury analyses are listed in table 2 and shown by mechanically plotted histograms on figure 2. The oil content of some of the core mentioned as missing in the previous paragraph had been estimated from the amount obtained

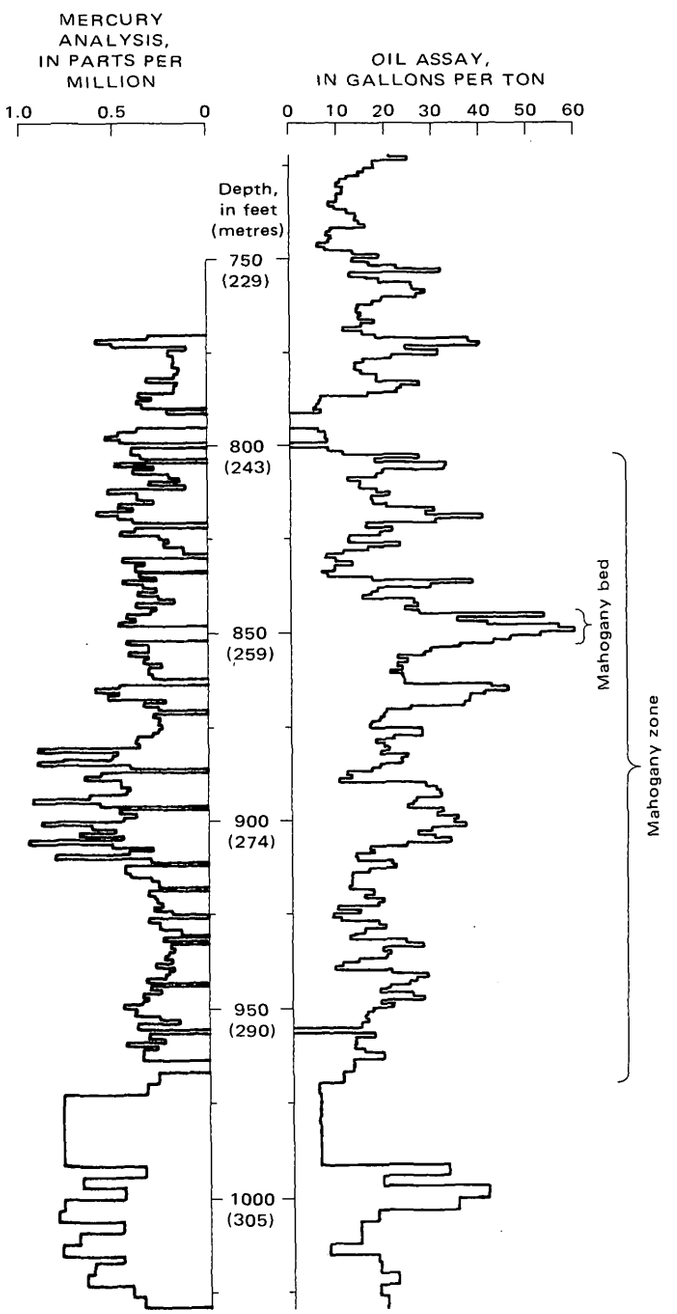

FIGURE 2.—Histograms showing the oil and mercury content of the oil shale in core-hole C–176, TOSCO TG2–1, sec. 21, T. 3 S., R. 96 W., Rio Blanco County, Colo. Mercury content data from U.S. Geological Survey laboratory; oil-assay data from TOSCO Rocky Flats Research Center. 1 gallon per ton equals 4.16 litres per metric ton.

TABLE 2.—*Results of analyses for oil and mercury content of shale in and adjacent to the Mahogany zone (core from hole C–176)*

[Mercury analyses by V. E. Shaw. To convert feet to metres, multiply by 0.3048; to convert gallons per ton to litres per ton, multiply by 4.16]

Lab. No.	Field No. (TG2-1-)	Depth (ft)	Hg (ppm)	Oil yield (gal/ton)
D158985	173	770.5-771.5	0.32	22.6
D158986	174	771.5-772.5	.60	47.6
D158987	175	772.5-773.5	.51	50.6
D158988	176	773.5-774.5	.11	30.7
D158989	177	774.5-776.0	.21	39.4
D158990	178	776.0-777.0	.18	27.0
D158991	179	777.0-778.0	.18	19.3
D158992	180	778.0-779.0	.19	17.1
D158993	181	779.0-780.0	.15	17.2
D158994	182	780.0-781.0	.16	18.7
D158995	183	781.0-782.0	.18	22.9
D158996	184	782.0-783.0	.33	22.8
D158997	185	783.0-784.0	.16	34.5
D158998	186	784.0-785.0	.18	29.5
D158999	187	785.0-786.0	.18	28.3
D159000	188	786.0-787.0	.37	20.5
D159001	189	787.0-788.0	.30	8.0
D159002	190	788.0-789.0	.38	7.4
D159003	191	789.0-790.0	.35	6.7
D159004	192	790.5-791.5	.22	8.1
D159005	193	795.4-796.4	.38	7.2
D159006	194	796.4-797.4	.48	9.1
D159007	195	797.4-798.4	.55	9.1
D159008	196	798.4-799.4	.47	9.7
D159009	197	800.6-801.6	.41	9.9
D158971	198	801.6-802.6	.41	13.8
D159010	199	802.6-803.6	.36	34.4
D159011	201	804.6-805.6	.50	41.5
D159012	202	805.6-806.6	.29	41.0
D159013	203	806.6-807.6	.40	24.3
D159014	204	807.6-808.6	.21	22.7
D159015	205	808.6-809.6	.15	15.0
D159016	206	809.6-810.6	.32	18.3
D159017	207	810.6-811.6	.12	18.0
D159018	208	811.6-812.6	.54	22.6
D159019	209	812.6-813.6	.38	26.2
D159020	210	813.6-814.6	.38	21.2
D159021	211	814.6-815.6	.29	21.7
D159022	212	815.6-816.6	.48	25.4
D159023	213	816.6-817.6	.40	38.3
D159024	214	817.6-818.6	.60	36.0
D158972	215	818.6-819.6	.48	51.3
D159025	216	819.6-820.6	.40	38.6
D159026	217	822.0-823.0	.39	27.0
D159027	218	823.0-824.0	.47	23.7
D159028	219	824.0-825.0	.26	15.4
D159029	220	825.0-826.0	.21	15.2
D159030	221	826.0-827.0	.24	29.0
D159031	222	827.0-828.0	.13	20.3
D159032	223	828.0-829.0	.13	13.7
D158973	225	830.0-831.0	.46	11.8
D159033	226	831.0-832.0	.34	16.2
D159034	227	832.0-833.5	.39	11.5
D159035	228	834.0-835.0	.37	9.6
D159036	229	835.0-836.0	.28	21.5
D159037	230	836.0-837.0	.46	48.4
D159038	231	837.0-838.0	.35	37.1
D159039	232	838.0-839.0	.28	22.9
D159040	233	839.0-840.0	.38	21.1
D158974	234	840.0-841.0	.27	18.8
D159041	235	841.0-842.0	.18	32.8
D159042	236	842.0-843.0	.39	33.8

TABLE 2.—*Results of analyses for oil and mercury content of shale in and adjacent to the Mahogany zone (core from hole C–176)*—Continued

Lab. No.	Field No. (TG2-1-)	Depth (ft)	Hg (ppm)	Oil yield (gal/ton)
D159043	237	843.0-844.0	0.28	30.3
D159044	238	844.0-845.0	.31	34.3
D158975	239	845.0-846.0	.44	67.8
D159045	240	846.0-847.0	.39	44.2
D159046	241	847.0-848.0	.48	52.4
D159047	246	852.0-853.0	.44	54.1
D159048	247	853.0-854.0	.32	45.0
D159049	248	854.0-855.0	.32	37.2
D159050	249	855.0-856.0	.43	35.6
D159051	250	856.0-857.0	.32	28.1
D158976	251	857.0-858.0	.35	31.0
D159052	252	858.0-859.0	.25	28.1
D159053	253	859.0-860.0	.32	29.5
D159054	254	860.0-861.0	.32	26.2
D159055	255	861.0-862.0	.30	29.7
D159056	256	863.7-864.5	.48	53.4
D159071	257	864.5-865.5	.61	58.2
D159058	258	865.5-866.5	.48	51.7
D159059	259	866.5-867.5	.54	47.7
D158977	260	867.5-868.5	.23	47.5
D159060	261	868.5-869.5	.35	46.1
D159061	262	869.5-870.5	.27	31.7
D159062	263	870.5-871.5	(*)	25.1
D159063	264	871.5-872.5	.30	24.6
D159064	265	872.5-873.5	.26	23.4
D159065	266	873.5-874.5	.27	21.1
D158978	267	874.5-875.5	.25	20.7
D159066	268	875.5-876.5	.27	34.9
D159067	269	876.5-877.5	.30	34.9
D159068	270	877.5-878.5	.38	27.1
D159069	271	878.5-879.5	.39	22.3
D159070	272	879.5-880.5	.37	24.6
D159071	273	880.5-881.5	.38	25.7
D159072	274	881.5-882.5	.39	23.3
D159073	275	882.5-883.5	.52	30.8
D159074	276	883.5-884.0	.78	29.0
D159075	277	884.0-885.0	.92	29.5
D159076	278	885.0-886.0	.42	23.3
D159077	280	887.0-888.0	.58	14.5
D159078	281	888.0-889.0	.67	15.9
D158979	282	889.0-890.0	.47	12.4
D159079	283	890.0-891.0	.47	35.9
D159080	284	891.0-892.0	.42	38.7
D159081	285	892.0-893.0	.44	39.6
D159082	286	893.0-894.0	.64	40.0
D159083	287	894.0-895.0	.54	33.3
D159084	288	895.0-896.0	.58	32.5
D159085	290	897.0-898.0	.48	40.5
D159086	291	898.0-899.0	.39	38.5
D159087	292	899.0-900.0	.46	44.2
D159088	293	900.0-901.0	.90	43.2
D158980	294	901.0-902.0	.63	46.3
D159089	295	902.0-903.0	.50	37.2
D159090	296	903.0-904.0	.70	33.6
D159091	297	904.0-905.0	.46	38.1
D159092	298	905.0-906.0	.97	42.5
D159093	299	906.0-907.0	.52	30.5
D159094	300	907.0-908.0	.30	20.6
D159095	301	908.0-909.0	.43	21.7
D158981	302	909.0-910.0	.83	16.7
D159096	303	910.0-911.0	.31	17.4
D159097	305	912.0-913.0	.45	27.6
D159098	306	913.0-914.0	.45	20.5
D159099	307	914.0-915.0	.42	15.9
D159100	308	915.0-916.0	.31	15.8
D159101	309	916.0-917.8	0.27	15.7

TABLE 2.—*Results of analyses for oil and mercury content of shale in and adjacent to the Mahogany zone (core from hole C–176)*—Continued

Lab. No.	Field No. (TG2-1-)	Depth (ft)	Hg (ppm)	Oil yield (gal/ton)
D159102	310	918.7-920.0	.33	21.6
D159103	311	920.0-921.0	.29	19.1
D158982	312	921.0-922.0	.28	24.2
D159104	313	922.0-923.0	.25	22.8
D159105	314	923.0-924.0	.30	11.9
D159106	315	924.0-925.0	.20	17.9
D159107	316	925.0-926.0	.10	10.6
D159108	317	926.0-927.0	.33	12.7
D159109	318	927.0-928.0	.27	22.8
D159110	319	928.0-929.0	.27	24.7
D159111	320	929.0-930.4	.15	19.0
D159112	322	931.0-932.0	.25	15.1
D158983	324	933.0-934.0	.21	35.0
D159113	325	934.0-935.0	.19	23.9
D159114	326	935.0-936.0	.22	26.0
D159115	327	936.0-937.0	.24	25.0
D159116	328	937.0-938.0	.20	17.5
D159117	329	938.0-939.0	.29	13.1
D159118	330	939.0-940.0	.19	11.1
D159119	331	940.0-941.0	.22	26.3
D159120	332	941.0-942.0	.24	36.1
D159121	333	942.0-943.0	.34	32.9
D159122	335	944.0-945.0	.32	25.7
D159123	336	945.0-946.0	.26	23.0
D159124	337	946.0-947.0	.36	32.1
D159125	338	947.0-948.0	.33	35.1
D159126	339	948.0-949.0	.36	23.4
D159127	340	949.0-950.0	.46	26.4
D159128	341	950.0-951.0	.39	21.2
D159129	342	951.0-952.0	.40	19.7
D159130	343	952.0-953.0	.27	19.2
D159131	344	953.0-954.0	.16	19.9
D158984	345	954.0-955.0	.39	18.1
D159132	346	956.7-958.0	.33	21.6
D159133	347	958.0-959.0	.24	16.5
D159134	348	959.0-960.0	.45	16.7
D159135	349	960.0-961.0	.28	16.2
D159136	350	961.0-962.0	.36	18.9
D159137	351	962.0-963.7	.36	24.1
D159138	352	967.0-970.0	.28	13.1
D159139	353	970.0-973.0	.34	6.4
D159140	354	973.0-991.0	.79	6.9
D159141	355	991.0-994.0	.35	41.5
D159142	356	994.0-996.8	.69	23.6
D159143	357	996.8-1000.0	.46	52.1
D159144	358	1000.0-1003.0	.79	44.0
D159145	359	1003.0-1006.0	.82	22.2
D159146	360	1006.0-1009.0	.47	17.6
D159147	361	1009.0-1012.0	.71	17.7
D159148	362	1012.0-1015.0	.80	9.2
D159149	363	1015.0-1017.0	.47	22.3
D159150	364	1017.0-1020.0	.63	23.0
D159151	365	1020.0-1023.0	.67	27.7
D159152	366	1023.0-1026.0	.42	22.6
D159153	367	1026.0-1029.0	.36	24.6

*Concentration less than detectable limit.

for the same interval in nearby cores. These estimated oil amounts have been plotted on the oil-assay histogram, but no attempt was made to estimate mercury amounts for missing intervals. The concentration of mercury in the Mahogany zones averages 0.37 ppm and ranges from less than 0.10 ppm to 0.97 ppm. In

TABLE 3.—*Distribution of 43 ppm mercury in Fischer-assay products from 100 g of sample D159050 (table 2)*

[Modified Fischer assay by I. C. Frost and T. L. Yager, U.S. Geological Survey, Denver, Colo. Mercury analysis by V. E. Shaw, Denver, Colo.]

Product	Product in total sample (wt percent)	Mercury in each product (ppm)	Mercury as part of total mercury (ppm)	Total mercury in each product (percent)
Oil	13.4	0.80	10.72	24.9
Water	1.2	5.57	6.68	15.5
Spent shale	81.5	.01	.81	1.9
Gas plus loss[1]	3.9	6.35	24.77	57.7
Total[1]	100.0	---	42.98	100.0

[1] The percentage of gas plus loss and the percentage of total mercury, derived by use of the modified Fischer assay, are obtained by difference. Approximately 90 percent of the mercury in the gas fraction was deposited on the glass surface of the Allihn condenser of the retort.

the Mahogany zone, a total of 23.6 feet (7.2 m) of core was not analyzed for mercury and therefore was not considered in the averaging.

DISTRIBUTION OF MERCURY IN PRODUCTS FROM A FISCHER OIL-SHALE ASSAY

A 100-g sample of oil shale containing 43 ppm of mercury was retorted using the standard Fischer-assay procedure. The resulting four products and their individual mercury contents are shown in table 3. Different commercial processes may distribute the shale's mercury content among the retort products in different ways. However, the distribution shown on table 3 is a guide, just as the Fischer-assay products are a guide to potential commercial oil recovery.

SUMMARY

Apparently no strong relationship exists between the oil yield of the shale and the mercury content. The high oil-yield shale is generally high in mercury; however, some of the lower yield oil shale contains comparable concentrations. Unfortunately, samples from the Mahogany bed, the most organic-rich interval in the Mahogany zone, were not available for mercury analysis.

The analysis of the Fischer-assay products from a 100-g sample of oil shale that contained 35 gal/ton of oil, 3 gal/ton of water, and 43 ppm mercury indicated that the major amount of mercury was in the gas fraction (58 percent) and the least amount in the spent shale (2 percent).

REFERENCES CITED

Desborough, G. A., Pitman, J. K., and Huffman, Claude, Jr., 1974, Concentration and mineralogical residence of elements in rich oil shales of the Green River Formation, Piceance Creek basin, Colorado and the Uinta Basin, Utah—a preliminary report: U.S. Geol. Survey Open-File Rept. 74–77, 14 p.

Huffman, Claude, Jr., Rahill, R. L., Shaw, V. E., and Norton, D. R., 1972, Determination of mercury in geologic materials by flameless atomic absorption spectrometry, *in* Geological Survey research 1972: U.S. Geol. Survey Prof. Paper 800–C, p. C203–C207.

U.S. Federal Energy Administration, 1974, Potential future role of oil shale—prospects and constraints (Project Independence Blueprint Final Task Force report): Washington, U.S. Govt. Printing Office, 316 p.

U.S. Geological Survey, 1970, Mercury in the environment: U.S. Geol. Survey Prof. Paper 713, 67 p.

Jour. Research U.S. Geol. Survey
Vol. 5, No. 2, Mar.–Apr. 1977, p. 227–233

ACTIVITY-PRODUCT CONSTANTS OF BRUCITE FROM 10° TO 90°C

By K. A. McGEE and P. B. HOSTETLER,[1]
Reston, Va., Columbia, Mo.

Abstract.—The activity-product constant of brucite, $K_B = [Mg^{2+}][OH^-]^2$ (where the brackets denote activities), was determined experimentally at 10°, 25°, 40°, 55°, 70°, and 90°C. The values obtained for $-\log K_B$ are 10.89±0.16 (10°), 10.88±0.10 (25°), 10.90±0.10 (40°), 10.90±0.10 (55°), 10.99±0.14 (70°), and 11.10±0.14 (90°). Using National Bureau of Standards Technical Note 270 data for the ions, the free energy of formation ($\Delta G°_f$) at 25° for brucite is −831.486 joules per mole (−198,730 cal mol^{-1}). Using data compiled by R. A. Robie and D. R. Waldbaum in 1968 for the ions, this $\Delta G°_f$ is −823,323 J mol^{-1} (−198,930 cal mol^{-1}).

Values of $-\log K_B$ are also calculated for the temperature range 0° to 200°C, by using thermochemical data listed by V. B. Parker, D. D. Wagman, and W. H. Evans in 1971 and E. G. King, M. J. Ferrante, and L. B. Pankratz in 1975 and the partial molal heat capacities estimated by C. M. Criss and J. W. Cobble in 1965. The experimental values are similar to the calculated values, especially at lower temperatures.

Brucite ($Mg(OH)_2$) is formed in natural environments mainly as a byproduct of serpentinization, as an alteration product of periclase (MgO) in contact-metamorphosed dolomites, and as a weathering product of ultramafic rocks. Knowledge of the stability of brucite over a range of temperatures is necessary for interpretation of geochemical processes in these environments. For example, activity-product constants of brucite are needed to understand the extremely alkaline waters associated with partially serpentinized alpine-type ultramafic rocks of the Western United States. Barnes and O'Neil (1969) described several springs containing very low amounts of dissolved magnesium, and, because the pH values are greater than 11 in these waters, approximately half of the magnesium in solution is complexed with hydroxyl ion ($MgOH^+$). Because brucite is formed as a reaction product in the serpentinization process, these low magnesium–high pH waters are saturated and possibly supersaturated with respect to brucite. Indeed, Luce (1971) presented evidence for low-temperature precipitation of brucite from one of these springs where the mineral apparently forms as minute tabular crystals embedded in a gel.

Magnesium hydroxide also precipitates as scale on evaporator coils in seawater distillation plants (Hiller, 1952) at temperatures between 85° and 116°C. Recognizing the conditions of brucite stability is, therefore, a matter of significance for both natural and industrial systems.

In a previous study, McGee and Hostetler (1975) determined thermodynamic association constants for the related ion pair $MgOH^+$ over the temperature range of 10° to 90°C. These constants are used in the present study to calculate the amount of uncomplexed magnesium in solution so that the effect of $MgOH^+$ at each temperature of interest can be accounted for in calculations of brucite stability. Several studies have been made in the past to determine activity-product constants for brucite; however, most of the work has been at or near 25°C. Lack of a systematic study of brucite solubility as a function of temperature has prompted the present investigation. We report here experimentally determined values for the thermodynamic activity-product constant of brucite over the temperature range of 10° to 90°C.

Acknowledgments.—We are grateful to J. E. Bauman, Jr., and E. E. Pickett, University of Missouri at Columbia, for helpful discussion during this study and to C. L. Christ and L. N. Plummer, U.S. Geological Survey, for constructive comments during the preparation of this report. This research was supported by the National Science Foundation and the Office of Water Resources Research, U.S. Department of the Interior, through grants GA 31231 and A-043-MO, respectively. Preparation of this report has been supported in part by the Geothermal Research Program of the U.S. Geological Survey.

EXPERIMENTAL METHODS

Forty-two solubility runs of brucite were made; seven runs each at the temperatures 10°, 25°, 40°, 55°, 70°, and 90°C. Eighteen of the runs were made in dilute

[1] P. B. Hostetler, Department of Geology, University of Missouri; present address: School of Earth Sciences, Macquarie University, North Ryde, N.S.W. 2113, Australia.

HCl solutions of varying strength (Br–4, Br–5, and Br–6 series), whereas 24 of the runs were made in pure water. The starting material for all runs was reagent grade $Mg(OH)_2$ (Matheson, Coleman, and Bell Manufacturing Chemists), which has a minimum purity of 98 percent. Maximum impurities are listed as 0.005 percent heavy metals (as Pb), 0.0002 percent arsenic, and 0.5 percent calcium as the oxide. However, X-ray data show the calcium to be present mostly as the carbonate. The material was prepared by first washing it in a concentrated HCl solution for several hours, decanting off the liquid, and rinsing the solid several times with pure water. This slurry was then heated to 90°C and allowed to age for 3 to 4 weeks. The water was then evaporated off, and the remaining powder was used in the runs. This aging process, described by Hostetler (1963), enhances crystal growth and provides more uniformity in the sizes of grains, which in turn causes equilibrium to be attained more rapidly.

The solubility experiments were carried out in temperature-controlled polypropylene water baths. These baths have been described in detail (Hostetler and Christ, 1968).

In all the runs except the Br–7 series, 10.0 grams of $Mg(OH)_2$ was added to 1,800 milliliters of solution (either pure water or HCl solution). In the Br–7 series, 4.0 g of the $Mg(OH)_2$ was added to 550 ml of pure water.

For each run, nitrogen gas, presaturated with water vapor at the temperature of the run, was bubbled through the brucite suspension for the entire length of the run to minimize CO_2 contamination. In addition, the N_2 used for these runs was first scrubbed free of CO_2 by bubbling it through several solutions of concentrated NaOH before reaching the run. All runs were stirred by Teflon-coated magnetic stirring bars resting on the bottom of the reaction vessels.

Each run was sampled periodically for pH and dissolved magnesium. A Beckman Research Model pH Meter (cat. No. 101900) and a Leeds and Northrup Speedomax Type G recorder were used in conjunction with various electrodes to monitor the pH of the runs at random times during the run. Among the electrodes used was a custom-built, combination electrode fabricated by Beckman Instruments, Inc. This electrode uses a large (7-mm) glass pH-sensing bulb to reduce possible electrical effects due to suspended solids and a large ceramic frit to provide a stable liquid junction. The filling solution used was 4 molar KCl saturated with AgCl. To reduce contamination, the electrodes were in contact with the run solution only during actual pH measurements. At other times, the electrodes were maintained at the temperature of the run in various buffers or in pure water. Beckman instant buffer powder was used to make the buffer solutions, which were checked before and after each pH measurement. The electrodes were standardized to the exact listed value of the buffers. The relative accuracy of these buffers is typically ± 0.01 pH units.

After each pH measurement, a sample of the suspension was withdrawn and filtered through a 0.45-μm Millipore filter for analysis of dissolved magnesium. Solids removed during filtration were returned to their respective runs.

Each filtrate was analyzed for aqueous magnesium, using a Perkin-Elmer Model 303 atomic absorption instrument. Before analysis, each sample and standard was made up to be 1,000 ppm in lanthanum to screen out possible interferences. (Note: A lanthanum chloride solution was used.)

When successive pH determinations of a run showed no significant variation (0.01 pH units or less), the run was terminated by filtering the whole volume through a 0.45-μm Millipore filter. The filtrate was saved for analysis of calcium and iron.

SOLUBILITY OF $Mg(OH)_2$ IN PURE WATER

The dissolution of $Mg(OH)_2$ can be represented as

$$Mg(OH)_2 = Mg^{2+} + 2OH^-. \quad (1)$$

Letting brackets denote activities, the activity-product constant of brucite is

$$K_B = [Mg^{2+}]\,[OH^-]^2. \quad (2)$$

In general, the possibility of ion pairing must be considered in solubility studies. In the $MgO-H_2O$ system (at low to moderate temperatures), the complex ion, $MgOH^+$, is apparently the only ion pair that needs to be taken into account (McGee and Hostetler, 1975). Its association reaction is

$$Mg^{2+} + OH^- = MgOH^+, \quad (3)$$

and likewise its association constant is written as

$$K_a = \frac{[MgOH^+]}{[Mg^{2+}]\,[OH^-]}. \quad (4)$$

Two methods are possible for calculating the activity-product constant for $Mg(OH)_2$. One requires independent knowledge of the K_a for $MgOH^+$, whereas the other method includes sufficient data to generate a value for K_a.

Method 1

Electrical neutrality in the system $MgO–H_2O$ (neglecting H^+) indicates that

$$2m_{Mg^{2+}} + m_{MgOH^+} = m_{OH^-}, \quad (5)$$

where m denotes molality.

From analysis of the solution for total magnesium, mass balance gives

$$m_{Mg^{2+}} + m_{MgOH^+} = \text{total Mg molality.} \quad (6)$$

Substituting equation 6 into equation 5 for m_{MgOH^+}, we obtain the expression

$$m_{Mg^{2+}} = m_{OH^-} - \text{total Mg molality.} \quad (7)$$

Knowing the total amount of magnesium in solution by analysis and having calculated m_{OH^-} from pH, K_w, and γ_{OH^-} (values for K_w from Barnes and others, 1966), the molality of uncomplexed magnesium can be calculated from equation 7. This value is then substituted back into equation 6 to obtain m_{MgOH^+}. An initial estimate of ionic strength can be calculated as follows:

$$I = 3 \times \text{total Mg molality.} \quad (8)$$

The activity coefficients for OH^- are then calculated from the extended Debye-Hückel approximation (Garrels and Christ, 1965, p. 61) as follows:

$$-\log \gamma_i = (Az_i^2 I^{1/2})/(1 + \mathring{a}_i B I^{1/2}). \quad (9)$$

For OH^-, $z=1$ and $\mathring{a}_i$ is taken to be 3.5×10^{-8} cm (Klotz, 1964). A and B values for the various temperatures are the same as those used in a previous study (McGee and Hostetler, 1975). Using the molality of the free magnesium and the complexed magnesium, a new ionic strength is calculated and substituted back into equation 9 to generate activity coefficient values for Mg^{2+} and $MgOH^+$.

$$I = \tfrac{1}{2}(4 \times m_{Mg^{2+}} + m_{MgOH^+} + m_{OH^-}) \quad (10)$$

(new values for γ_{OH^-} may also be calculated). For Mg^{2+}, $z=2$ and $\mathring{a}_i$ is taken to be 6.5×10^{-8} cm (Hostetler, 1963). For $MgOH^+$, $z=1$ and 6.5×10^{-8} cm is also used for $\mathring{a}_i$ (McGee and Hostetler, 1975).

Once the molalities and activity coefficients are solved by this iterative procedure, activities are calculated ($[i] = m_i \gamma_i$), and equations 2 and 4 give the activity-product constants.

Method 2

Rearranging equation 4 and expressing activities as the product of molalities and activity coefficients, the association constant of $MgOH^+$ becomes

$$m_{MgOH^+} = \frac{K_a \times [OH^-] \times \gamma_{Mg^{2+}} \times m_{Mg^{2+}}}{\gamma_{MgOH^+}}. \quad (11)$$

Substituting equation 11 into equation 6,

$$m_{Mg^{2+}} + \left(\frac{K_a \times [OH^-] \times \gamma_{Mg^{2+}}}{\gamma_{MgOH^+}} \right) m_{Mg^{2+}} = \text{total Mg.} \quad (12)$$

Equation 12 reduces to equation 13, from which we can calculate uncomplexed magnesium as follows:

$$m_{Mg^{2+}} = \text{total Mg} \Big/ \left(1 + \frac{K_a \times [OH^-] \times \gamma_{Mg^{2+}}}{\gamma_{MgOH^+}} \right). \quad (13)$$

Values for K_a are from McGee and Hostetler (1975).

In a manner analogous to method 1, ionic strength is estimated initially by equation 8. The extended Debye-Hückel approximation (eq 9) is then used to generate activity coefficients, which are used in equation 11. A better ionic strength is then calculated from equation 14, and new activity coefficients are generated as follows:

$$I = 3 \times m_{Mg^{2+}} + m_{MgOH^+}. \quad (14)$$

This cycle can be repeated as many times as necessary until the activity coefficients remain constant. Generally, twice is enough. Equation 2 is used to calculate the activity-product constant for brucite.

It is readily apparent from comparing the results of the two methods that method 2 is far better for calculating brucite solubility than method 1. Method 2 does not require the use of the charge-balance equation; therefore, it is not as sensitive to the presence of other balancing anion impurities (such as HCO_3^-) as method 1. In addition, method 2 is not very sensitive to the numerical value of the association constant used for $MgOH^+$. At 25°C, using 2.60 instead of 2.21 for the log K_{MgOH^+} gives a change of only about 0.01 in the log activity-product constant calculated for brucite. All the activity-product constant calculations reported here were made using method 2. Figure 1 shows the distribution of activity-product constants versus elapsed time in a typical run at 25°C.

DISCUSSION

Table 1 shows typical solubility data for brucite from selected runs in pure water obtained during this investigation. Table 2 gives the remaining data required to calculate activity-product constants for the selected runs. The summarized results for all runs at each temperature are shown in table 3. Using multiple-regression analysis, an equation for the relationship

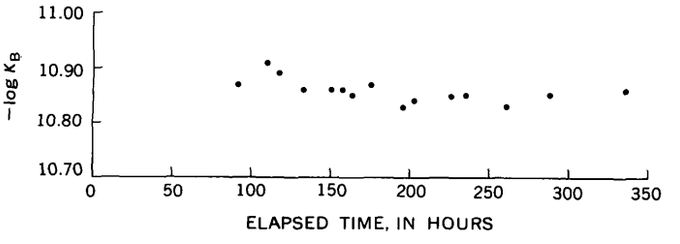

FIGURE 1.—Activity-product constant data for a typical run (2 Br-1 at 25°C). The −log K_B average for this run is 10.86 with a $\pm 2\sigma$ of 0.04.

between $-\log K_B$ and temperature (t=°C) can be derived as follows:

$$-\log K_B = 10.91_8 - 0.00304\ t + 0.0000563\ t^2. \quad (15)$$

As noted in table 3, our average value for the $-\log K_B$ of brucite at 25°C is 10.88±0.10. Several investi-

TABLE 1.—*Typical solubility data for brucite in pure water*

[One run at each temperature. Approximate errors in analysis: Mg^{2+}_{total} ±1 percent; pH reproducible to ±0.02 pH units. The molality of total magnesium in solution can be calculated by using equation 6 and data in this table and table 2]

Sample	Time (hours)	pH	Mg^{2+} ($m\times10^4$)	Time (hours)	pH	Mg^{2+} ($m\times10^4$)
	Run 1Br–2 (10°C)			Run 2Br–3 (25°C)		
1	89	10.64	8.60	72	10.20	5.71
2	97	10.64	8.50	90	10.17	5.80
3	116	10.62	8.61	98	10.17	5.88
4	138	10.64	9.16	114	10.18	5.88
5	162	10.62	9.32	131	10.19	5.99
6	167	10.64	9.51	137	10.18	6.28
7	179	10.62	8.91	143	10.17	6.52
8	191	10.64	9.31	155	10.15	6.85
9	209	10.63	9.31	161	10.17	7.09
10	230	10.60	9.83	169	10.17	7.17
11	239	10.54	10.05	217	10.11	8.69
12	255	10.75	9.74	227	10.10	9.50
13	312	10.62	9.92	255	10.11	9.50
14	348	10.68	10.00	268	10.11	9.50
15	358	10.63	10.48	316	10.11	9.80
16	376	10.68	10.61	---	----	---
17	406	10.68	10.61	---	----	---
18	423	10.68	10.41	---	----	---
19	450	10.57	11.57	---	----	---
20	496	10.69	11.82	---	----	---
	Run 3Br–1 (40°C)			Run 4Br–3 (55°C)		
1	10	9.92	2.24	4	9.55	1.98
2	27	9.92	2.24	21	9.58	2.01
3	49	9.92	2.55	27	9.54	3.35
4	77	9.86	3.12	39	9.50	2.15
5	96	9.81	3.33	44	9.51	2.50
6	129	9.82	4.11	49	9.53	2.77
7	145	9.83	4.05	64	9.50	2.52
8	147	9.82	3.75	67	9.49	2.66
9	150	9.82	4.21	71	9.52	2.81
10	152	9.82	5.84	74	9.52	2.97
11	165	9.81	4.11	88	9.51	2.62
12	170	9.81	4.69	91	9.51	2.87
13	176	9.80	3.94	93	9.51	3.91
	Run 5Br–3 (70°C)			Run 6Br–1 (90°C)		
1	10	9.32	1.22	18	8.75	2.02
2	22	9.28	1.09	24	8.75	2.50
3	27	9.30	1.08	26	8.76	2.21
4	30	9.30	1.65	32	8.80	2.29
5	34	9.29	1.04	42	8.72	1.73
6	48	9.29	1.04	45	8.78	1.53
7	52	9.28	1.80	50	8.80	1.52
8	54	9.27	1.28	115	8.77	1.82
9	61	9.27	1.19	120	8.85	1.70
10	74	9.27	1.38	127	8.85	1.70
11	76	9.26	1.28	139	8.81	1.71
12	79	9.26	2.00	143	8.80	1.52
13	83	9.26	1.71	167	8.82	1.42
14	---	----	----	191	8.81	2.38
15	---	----	----	197	8.81	1.52
16	---	----	----	210	8.81	1.42

TABLE 2.—*Typical data used to calculate apparent activity-product constants of brucite*

[One run at each temperature]

Sample	I ($\times10^3$)	$\gamma_{Mg^{2+}}$	m_{MgOH^+} ($\times10^5$)	γ_{MgOH^+}	$-\log K_B$
	Run 1Br–2 (10°C)				
1	2.59	0.81	1.35	0.95	10.94
2	2.56	.81	1.33	.95	10.95
3	2.59	.81	1.29	.95	10.98
4	2.76	.81	1.43	.95	10.92
5	2.81	.80	1.39	.95	10.95
6	2.87	.80	1.48	.95	10.90
7	2.68	.81	1.33	.95	10.97
8	2.80	.80	1.45	.95	10.91
9	2.80	.80	1.42	.95	10.93
10	2.96	.80	1.39	.95	10.97
11	3.02	.80	1.24	.95	11.08
12	2.93	.80	1.29	.95	11.03
13	2.99	.80	1.47	.95	10.93
14	3.01	.80	1.70	.95	10.80
15	3.16	.80	1.58	.94	10.88
16	3.20	.79	1.80	.94	10.78
17	3.20	.79	1.80	.94	10.78
18	3.14	.80	1.77	.94	10.79
19	3.48	.79	1.51	.94	10.97
20	3.56	.78	2.03	.94	10.72
	Run 2Br–3 (25°C)				
1	1.72	0.84	1.26	0.96	10.91
2	1.75	.84	1.19	.96	10.96
3	1.77	.83	1.21	.96	10.96
4	1.77	.83	1.23	.96	10.94
5	1.81	.83	1.29	.96	10.91
6	1.89	.83	1.31	.95	10.91
7	1.97	.83	1.33	.95	10.92
8	2.07	.82	1.33	.95	10.94
9	2.14	.82	1.44	.95	10.88
10	2.16	.82	1.45	.95	10.88
11	2.62	.81	1.51	.95	10.92
12	2.86	.80	1.61	.95	10.91
13	2.86	.80	1.64	.95	10.89
14	2.86	.80	1.64	.95	10.89
15	2.95	.80	1.69	.94	10.88
	Run 3Br–1 (40°C)				
1	0.68	0.89	1.01	0.97	10.93
2	.68	.89	1.01	.97	10.93
3	.77	.88	1.15	.97	10.87
4	.95	.87	1.21	.97	10.91
5	1.01	.87	1.15	.96	10.98
6	1.24	.85	1.43	.96	10.88
7	1.22	.85	1.44	.96	10.87
8	1.13	.86	1.31	.96	10.92
9	1.27	.85	1.47	.96	10.87
10	1.77	.83	2.00	.95	10.74
11	1.24	.85	1.40	.96	10.90
12	1.42	.84	1.59	.96	10.85
13	1.19	.86	1.31	.96	10.94
	Run 4Br–3 (55°C)				
1	0.61	0.89	1.12	0.97	10.92
2	.62	.89	1.22	.97	10.86
3	1.02	.86	1.81	.96	10.73
4	.66	.89	1.08	.97	10.99
5	.76	.88	1.28	.97	10.91
6	.85	.87	1.48	.97	10.83
7	.77	.88	1.26	.97	10.92
8	.81	.87	1.30	.98	10.92
9	.86	.87	1.47	.97	10.84
10	.91	.87	1.54	.97	10.82
11	.80	.88	1.34	.97	10.89
12	.87	.87	1.46	.97	10.85
13	1.19	.85	1.96	.96	10.73

TABLE 2.—*Typical data used to calculate apparent activity-product constant of brucite*—Continued

Sample	I ($\times 10^3$)	$\gamma_{Mg^{2+}}$	m_{MgOH^+} ($\times 10^5$)	γ_{MgOH^+}	$-\log K_B$
	Run 5Br–3 (70°C)				
1	0.38	0.91	1.11	0.98	10.91
2	.34	.91	.91	.98	11.04
3	.34	.91	.94	.98	11.00
4	.51	.90	1.42	.97	10.82
5	.32	.92	.88	.98	11.04
6	.32	.92	.88	.98	11.04
7	.56	.89	1.47	.97	10.83
8	.40	.91	1.04	.98	10.99
9	.37	.91	.96	.98	11.02
10	.43	.90	1.11	.97	10.96
11	.40	.91	1.01	.98	11.01
12	.62	.89	1.55	.97	10.83
13	.53	.89	1.34	.97	10.89
	Run 6Br–1 (90°C)				
1	0.62	0.88	1.38	0.97	11.09
2	.77	.87	1.70	.97	11.00
3	.68	.88	1.54	.97	11.03
4	.71	.87	1.75	.97	10.94
5	.53	.89	1.12	.97	11.21
6	.47	.89	1.13	.97	11.14
7	.47	.89	1.18	.97	11.10
8	.56	.89	1.31	.97	11.09
9	.53	.89	1.48	.97	10.96
10	.53	.89	1.48	.97	10.96
11	.53	.89	1.36	.97	11.04
12	.47	.89	1.18	.97	11.10
13	.44	.90	1.16	.97	11.09
14	.73	.87	1.86	.97	10.90
15	.47	.89	1.21	.97	11.08
16	.44	.90	1.14	.97	11.11

gators in the past have determined various values for activity-product constants of brucite in the temperature range 16° to 25°C. Many of these were tabulated by Hostetler (1963). Some of this earlier work using conductivity and potentiometric methods is in good agreement with the present study. Gjaldbaek (1925) determined the $-\log K_B$ of brucite to be 10.93 at 18°C. He precipitated $Mg(OH)_2$ by titrating magnesium chloride with sodium hydroxide and then followed the development of the precipitate by conductivity and pH measurements. Krige and Arnold (1948), using the conductivity method, reported a value of 10.85 at 20°C.

Hostetler (1963) determined a value of 11.15 for the $-\log K_B$ of brucite at 25°C. A recalculation of the data from some of his runs, using the approach described herein (method 2) results in a change of approximately 0.02 log units from his calculated values of the activity-product constant. Although the change is in the direction of less stability for brucite, it is not large enough to bring that work into agreement with the results of the present study. Hostetler (1963), using both solubility and precipitation techniques, investigated brucite stability. Each of these experimental approaches depends on an accurate measurement of pH and dissolved magnesium. In the decade or so since that work, considerable refinement has taken place in the methods of pH measurement (discussed in detail in McGee and Hostetler, 1975) and magnesium analysis. These, combined with the development and perfection of the silica-free water baths described by Hostetler and Christ (1968), probably account for the difference between the results of the present study and the earlier work of Hostetler.

Finally, in a recent study on the crystallization of brucite, Liu and Nancollas (1973) reported a value of 10.86 at 25°C for the thermodynamic solubility product of magnesium hydroxide by using crystal-growth experiments to approach equilibrium from saturation. Their value is strikingly close to the value obtained in the present study.

ACTIVITY-PRODUCT CONSTANT FROM THERMOCHEMICAL DATA

As a comparison with the experimental data, values for the activity-product constant of brucite were calculated over a range of temperatures, using recent thermochemical data for brucite (King and others, 1975) and entropy data given by Parker, Wagman, and Evans (1971). (See table 4.) The method is the same as that used by Christ and Hostetler (1970) for magnesite.

TABLE 3.—*Summary of individual run data for* $Mg(OH)_2$

Run series	10°±0.10°C			25°±0.05°C			40°±0.05°C			55°±0.25°C			70°±0.20°C			90°±0.55°C		
	$-\log K_B$	$\pm 2\sigma$	Number of observations	$-\log K_B$	$\pm 2\sigma$	Number of observations	$-\log K_B$	$\pm 2\sigma$	Number of observations	$-\log K_B$	$\pm 2\sigma$	Number of observations	$-\log K_B$	$\pm 2\sigma$	Number of observations	$-\log K_B$	$\pm 2\sigma$	Number of observations
Br–1[a]	10.98	0.18	20	10.86	0.04	15	10.90	0.12	13	10.85	0.18	13	10.93	0.20	13	11.06	0.16	16
Br–2[a]	10.91	.18	20	10.90	.08	15	10.93	.08	13	10.88	.08	13	10.88	.30	13	11.03	.17	16
Br–3[a]	10.97	.16	20	10.92	.06	15	10.92	.10	13	10.87	.15	13	10.96	.16	13	11.02	.16	16
Br–4[b]	10.83	.11	8	10.81	.08	5	10.87	.08	9	10.91	.04	8	11.04	.08	8	11.09	.10	8
Br–5[c]	10.85	.10	8	10.87	.04	5	10.91	.12	9	10.95	.04	8	11.03	.08	8	11.18	.04	8
Br–6[d]	10.94	.13	8	10.94	.04	5	10.99	.15	9	10.96	.03	8	11.09	.07	8	11.10	.06	8
Br–7[a]	10.76	.15	8	10.84	.08	5	10.84	.10	9	10.87	.06	8	10.98	.04	8	11.20	.05	8
Average	10.89	.16	--	10.88	.10	--	10.90	.10	--	10.90	.10	--	10.99	.14	--	11.10	.14	--

[a] Runs made in pure water. [b] Runs made in 0.005 *N* HCl. [c] Runs made in 0.02 *N* HCl. [d] Runs made in 0.08 *N* HCl.

For the reaction

$$Mg(OH)_2 = Mg^{2+} + 2OH^-, \quad (1)$$

the value for K_B can be calculated at any temperature if the free-energy change for the reaction is known at that temperature; that is,

$$\Delta G^\circ_T = -RT \ln K_{BT}. \quad (16)$$

When the free-energy change of the reaction is known at any one temperature T_1, it can be calculated at another temperature, T_2, by using the following equation:

$$\Delta G^\circ_{T_2} = \Delta G^\circ_{T_1} - \Delta S^\circ_{T_1}(T_2 - T_1) - T_2 \int_{T_1}^{T_2} \Delta \bar{C}^\circ_P \, d \ln T + \int_{T_1}^{T_2} \Delta \bar{C}^\circ_P \, dT. \quad (17)$$

T is absolute temperature in kelvins and R is the gas constant. ΔG°, ΔS°, and $\Delta \bar{C}^\circ_P$ are the standard thermodynamic quantities of Gibbs free energy, entropy, and partial molal heat capacity. Equation 17 can be rewritten in a more useful form (Criss and Cobble, 1964) by using average heat capacities between two Celsius temperatures, t_2 and 25°, as follows:

$$\Delta(\Delta G^\circ) = \Delta G^\circ_{t_2} - \Delta G^\circ_{25^\circ} = -\Delta S^\circ_{25^\circ}(t_2 - 25^\circ) + \Delta \bar{C}^\circ_P \Big]^{t_2}_{25^\circ} \times \left[(t_2 - 25^\circ) - T_2 \ln \frac{T_2}{T_1} \right]. \quad (18)$$

T_1 is 298.15 K. The average heat-capacity change for the reaction (eq 1) between temperatures t_2 and 25°C is given by

$$\Delta \bar{C}^\circ_P \Big]^{t_2}_{25^\circ} = \bar{C}^\circ_{P\,Mg^{2+}} \Big]^{t_2}_{25^\circ} + 2\bar{C}^\circ_{P\,OH^-} \Big]^{t_2}_{25^\circ} - C^\circ_{P\,brucite} \Big]^{t_2}_{25^\circ}. \quad (19)$$

The data used to calculate the following results are given in table 4. The average heat-capacity changes ($\Delta \bar{C}^\circ_P \Big]^{t_2}_{25^\circ}$) for the reaction, calculated by using equation 19, are −260.2 (−62.2) at 60°C, −288.3 (−68.9) at 100°C, −308.4 (−73.7) at 150°C, and −319.7 (−76.4) at 200°C joules per mole kelvin (cal mol^{-1} deg^{-1} in parentheses). For the reaction at 25°C, ΔG° is 62,099 J mol^{-1} (14,842 cal mol^{-1}) and ΔS° is −222.76 J mol^{-1} K^{-1} (−53.24 cal mol^{-1} deg^{-1}). The values are then used in equation 18 to determine $\Delta(\Delta G^\circ)$ between 25°C and each of the temperatures 60°, 100°, 150°, and 200°C. The calculated $\Delta(\Delta G^\circ)$ values are 8,309, 19,221, 34,982, and 52,882 J mol^{-1}, respectively (1,986, 4,594, 8,361, and 12,639 cal mol^{-1}). The intermediate values listed in table 5 were obtained by using multiple-regression analysis. The calculated values for $-\log K_B$, as well as the experimental values determined in this study, are plotted against temperature in figure 2. The estimated error in the experimental values, taken to be at least twice the standard deviation, ranges from ±0.10 to ±0.16. As a comparison, Robie and Waldbaum (1968) list free-energy data for the dissolution of brucite that result in a total uncertainty of ±3,975 J (±950 cal). The uncertainty associated with the values given by Parker, Wagman, and Evans (1971) is probably similar. This uncertainty translates to ±0.7 in the calculated value for $-\log K_B$ at 25°C.

The $-\log K_B$ determined in this study at 25°C is 10.88. Using equation 16 and converting 10.88 to free energy gives $\Delta G^\circ_{r,\,298K}$ of 62,099 J mol^{-1} (14,842 cal mol^{-1}). Using this value and the values listed in Parker and others (1971) for magnesium ion and hydroxyl

TABLE 4.—*Thermochemical data used to calculate the activity-product constant of brucite*

[Temperatures in degrees Celsius. ΔG°_f in J mol^{-1}, cal mol^{-1} in parentheses. S° and $\bar{C}^\circ_p$ in J mol^{-1} K^{-1}, cal mol^{-1} deg^{-1} in parentheses]

Quantity	Brucite (1)	$Mg^{+2}{}_{aq}$ (2)	$OH^-{}_{aq}$ (3)
ΔG°_f (25°)	−831486	−454801	−157293
	(−198730)	(−108700)	(−37594)
S° (25°)	63.18	−138.1	−10.75
	(15.10)	(−33.0)	(−2.57)
$\bar{C}^\circ_p \Big]^{60^\circ}_{25^\circ}$	80.25	213	−197
	(19.18)	(51)	(−47)
$\bar{C}^\circ_p \Big]^{100^\circ}_{25^\circ}$	83.22	280	−243
	(19.89)	(67)	(−58)
$\bar{C}^\circ_p \Big]^{150^\circ}_{25^\circ}$	86.53	289	−255
	(20.68)	(69)	(−61)
$\bar{C}^\circ_p \Big]^{200^\circ}_{25^\circ}$	89.37	314	−272
	(21.36)	(75)	(−65)

1. ΔG_f° (25°) calculated from activity-product constant data determined in this study (eq 16) plus free-energy data for the ions given in Parker and others (1971). S° (25°) from Parker and others (1971). Average heat-capacity data graphically calculated from data in King and others (1975). Parker and others (1971) listed a value of −199,-230 cal mol^{-1} for the ΔG°_f (25°) of brucite.
2. ΔG°_f (25°) and S° (25°) from Parker and others (1971). Robie and Waldbaum (1968) listed a value of −108,900 cal mol^{-1} for $\Delta G^\circ_{f,Mg^{2+}}$ at 25°C. Average heat capacities from Criss and Cobble (1964).
3. ΔG°_f (25°) and S° (25°) from Wagman and others (1968). Average heat capacities from Criss and Cobble (1964).

TABLE 5.—*Values of −log* K_B *calculated from data in table 4*

t°C	$\Delta(\Delta G^\circ)$ J mol^{-1}	$\Delta(\Delta G^\circ)$ cal mol^{-1}	ΔG°_f J mol^{-1}	ΔG°_f cal mol^{-1}	−log K_B
0	−5,230	−1,250	56,869	13,592	10.88
10	−3,222	−770	58,877	14,072	10.86
20	−1,088	−260	61,011	14,582	10.87
25	0	0	62,099	14,842	10.88
30	1,109	265	63,208	15,107	10.89
40	3,389	810	65,488	15,652	10.92
50	5,816	1.390	67,915	16,232	10.98
60	8,309	1,986	70,408	16,828	11.04
70	10,920	2,610	73,019	17,452	11.11
80	13,598	3,250	75,697	18,092	11.20
90	16,401	3,920	78,500	18,762	11.29
100	19,221	4,594	81,320	19,436	11.38
120	25,209	6,025	87,308	20,867	11.60
140	31,631	7,560	93,730	22,402	11.85
150	34,982	8,361	97,081	23,203	11.98
160	38,388	9,175	100,487	24,017	12.12
180	45,501	10,875	107,600	25,717	12.40
200	52,882	12,639	114,981	27,481	12.69

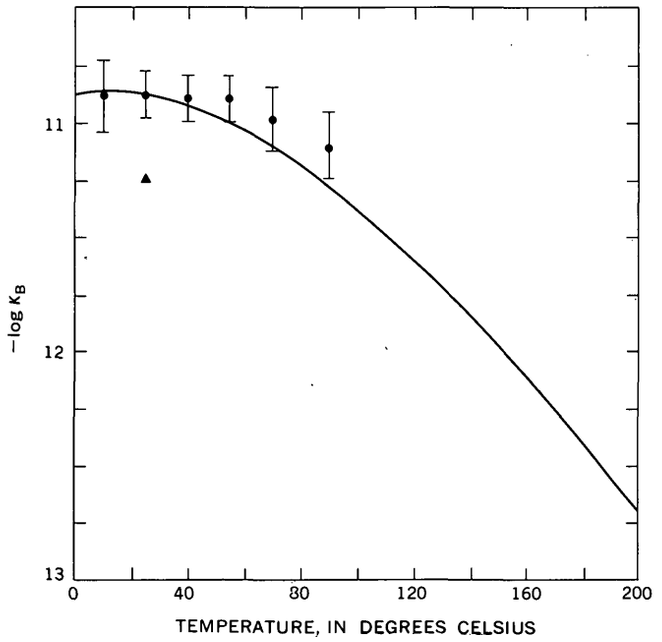

FIGURE 2.—Calculated and experimental values for $-\log K_B$ plotted against temperature. Solid circles with bars represent experimental values of $-\log K_B$ from this study and associated uncertainties ($\pm 2\sigma$). The solid curve represents calculated $-\log K_B$ values as a function of temperature based on a $\Delta G°_r$ (25°) of 14,842 cal mol^{-1}. The triangle represents $-\log K_B$ at 25° calculated from data in the National Bureau of Standards Technical Note 270 series (Wagman and others, 1968; Parker and others, 1971).

ion gives a free energy of formation for brucite of $-831{,}486$ J mol^{-1} ($-198{,}730$ cal mol^{-1}). This compares with their listed value of $-833{,}578$ J mol^{-1} ($-199{,}230$ cal mol^{-1}), a difference of some 2,092 J (500 cal). Using Robie and Waldbaum's (1968) data for the ions plus our converted activity-product constant listed above gives a free energy of formation for brucite of $-832{,}323$ J mol^{-1} ($-198{,}930$ cal mol^{-1}). The difference here is all due to a change in the value for magnesium ion. In either case, our experimental value for the dissociation reaction is only a small percentage of the total. When the free energy of formation for brucite is calculated, the biggest contributor is the magnesium ion, and differences here should be carefully examined when the $\Delta G_f°$ for brucite is calculated from dissolution reaction data.

REFERENCES CITED

Barnes, H. L., Helgeson, H. C., and Ellis, A. J., 1966, Ionization constants in aqueous solutions, *in* Clark, S. P., Jr., ed., Handbook of physical constants [rev. ed.]: Geol. Soc. America Mem. 97, p. 401–413.

Barnes, Ivan, and O'Neil, J. R., 1969, The relationship between fluids in some fresh alpine-type ultramafics and possible modern serpentinization, western United States: Geol. Soc. America Bull., v. 80, no. 10, p. 1947–1960.

Christ, C. L., and Hostetler, P. B., 1970, Studies in the system MgO-SiO_2-CO_2-H_2O, [Pt.] 2, The activity-product constant of magnesite: Am. Jour. Sci., v. 268, no. 5, p. 439–453.

Criss, C. M., and Cobble, J. W., 1964, The thermodynamic properties of high temperature aqueous solutions. V. The calculation of ionic heat capacities up to 200°C: Am. Chem. Soc. Jour., v. 86, no. 24 p, 5390–5393.

Garrels, R. M., and Christ, C. L., Solutions, minerals, and equilibria: New York, Harper and Row, 450 p.

Gjaldbaek, J. K., 1925, [An investigation of the solubility of magnesium hydroxide. I. The existence of different modifications of magnesium hydroxide. II. The solubility product and the dissociation constant of magnesium hydroxide]: Zeitschr. Anorg. u. Allg. Chemie, v. 144, no. 3, p. 145–168, 269–288. [In German.]

Hillier, H., 1952, Scale formation in sea-water distilling plants and its prevention: Inst. Mech. Engs. (London), Proc. 1B, p. 295–322.

Hostetler, P. B., 1963, The stability and surface energy of brucite in water at 25°C: Am. Jour. Sci., v. 261, no. 3, p. 238–258.

Hostetler, P. B., and Christ, C. L., 1968, A temperature-controlled water bath for mineral solubility studies: U.S. Geol. Survey Prof. Paper 600-D, p. D217–D221.

King, E. G., Ferrante, M. J., and Pankratz, L. B., 1975, Thermodynamic data for $Mg(OH)_2$ (brucite): U.S. Bur. Mines Rept. Inv. 8041, 13 p.

Klotz, I. M., 1964, Chemical thermodynamics: New York, W. A. Benjamin, 468 p.

Krige, G. J., R., and Arnold, R., 1948, The ageing of aqueous suspensions of magnesium hydroxide: South African Chem. Inst. Jour., v. 1, no. 2, p. 61–75.

Liu, S-T, and Nancollas, G. H., 1973, The crystallization of magnesium hydroxide: Desalination, v. 12, p. 75–84.

Luce, R. W., 1971, Brucite identified as crystallizing from a natural cold alkaline spring gel: Clays and Clay Minerals, v. 19, no. 5, p. 335–336.

McGee, K. A., and Hostetler, P. B., 1975, Studies in the system MgO-SiO_2-CO_2-H_2O, [Pt.] 4, The stability of $MgOH^+$ from 10° to 90°C: Am. Jour. Sci., v. 275, no. 3, p. 304–317.

Parker, V. B., Wagman, D. D., and Evans, W. H., 1971, Selected values of chemical thermodynamic properties: U.S. Natl. Bur. Standards Tech. Note 270–6, 106 p.

Robie, R. A., and Waldbaum, D. R., 1968, Thermodynamic properties of minerals and related substances at 298.15°K (25.0°C) and one atmosphere (1.013 bars) pressure and at higher temperatures: U.S. Geol. Survey Bull. 1259, 256 p.

Wagman, D. D., Evans, W. H., Parker, V. B., Halow, Iva, Bailey, S. M., and Schumm, R. H., 1968, Selected values of chemical thermodynamic properties: U.S. Natl. Bur. Standards Tech. Note 270–3, 264 p.

Jour. Research U.S. Geol. Survey
Vol. 5, No. 2, Mar.–Apr. 1977, p. 235–242

REMOVAL OF FLUORINE AND LITHIUM FROM HECTORITE BY SOLUTIONS SPANNING A WIDE RANGE OF pH

By HARRY C. STARKEY, WAYNE MOUNTJOY, and
JOHNNIE M. GARDNER, Denver, Colo.

Abstract.—One-gram samples of hectorite were treated with 40 millilitres each of hydrochloric acid (6 *N*), acetic acid (4.5 *N*), distilled water, natural seawater, sodium chloride (0.6 *N*), and sodium hydroxide (2.5 *N*) for 10 days in stoppered plastic centrifuge tubes. X-ray diffraction patterns show that the structure was virtually destroyed by the hydrochloric and acetic acids. Analyses of the supernatant liquids were made to determine amounts of the elements removed by the various treatments. All treatments removed at least some SiO_2, MgO, CaO, Li_2O, and F. The acids removed most of the lithium and magnesium after 3 days. The fluorine and the magnesium released by the acetic acid began to form sellaite (MgF_2). After 5 days, sufficient sellaite was produced to be discernible by X-ray diffraction. The loss of silica from the sample when it was treated with sodium hydroxide amounted to about 10 percent of the total sample.

Lithium is absorbed by many plants. Bertrand (1943) listed 43 species of plants that contained lithium but he did not say whether the lithium affected plant growth. Aldrich, Vanselow, and Bradford (1951), however, showed that lithium, when present in amounts of at least 13.5 parts per million in the leaves of several citrus plants, was toxic to those plants.

Lithium is widespread in the conterminous United States, especially in the western areas (Shacklette and others, 1973). Wells and Whitton (1972) noted that organic acids leach lithium from soils during podzolization. Lithium is not found on the exchange sites of clays but is found in the octahedral layer of 2:1 layer silicates such as hectorite, other smectites, and some micas. Apparently lithium becomes available to plants only through the dissolution of these lithium-bearing minerals. Because of the wide variations in the compositions of both soils and organic acids, the present authors decided to investigate the release of lithium from hectorite under stated pH conditions.

Fluorine is often present in lithium-bearing clays in which it proxies for hydroxyl ions. The effects of fluorides in drinking water on dental caries and tooth mottling are well known. The amounts of fluorine released from hectorite under given pH conditions may indicate how fluorine from soils could enter the ground water.

Hectorite, $(Mg_{2.67}Li_{0.33})Si_4O_{10}(F, OH)_2Na_{0.33}\cdot nH_2O$, was chosen for this study because, even though it is not a common soil mineral, it contains large amounts of lithium and fluorine, it can be made fairly pure by use of water only, and the magnesium in it can be easily removed by acids. Other processes may remove lithium and fluorine from the structures of clays, but this report will be restricted to the study of the amounts released by solutions of different pH.

PREVIOUS WORK

The relative ease with which hectorite can be decomposed by hydrogen ions has been known for some time, but most investigators have been concerned with measuring the removal of silicon and magnesium only. Nutting (1940) treated hectorite with hydrochloric acid solutions ranging in concentrations from 0.001 to 4.00 percent and applied 90°–92°C heat for 24 hours. He measured only the removal of silicon and magnesium, noting that more silicon was removed in pure water than in dilute acids (0.025 percent and less). Above this concentration the amounts of silicon and magnesium removed varied directly with, but not proportional to, the concentration of the hydrochloric acid except that between the concentrations of 0.1 and 0.25 percent hydrochloric acid the pH of the solutions remained relatively stable and the amounts of silicon and magnesium in the filtrates decreased. Nutting theorized that this pH stability was due to the inactivation of the hydrogen ions by physical adsorption or chemical reaction, or to the release of hydroxyl ions over that particular range. He also stated that magnesium could be completely removed from hectorite by electrodialysis leaving pure silica. He made no mention of the solubility of lithium or fluorine.

Caldwell and Marshall (1942) attempted to produce a hydrogen clay by dialysis in a sample which they termed "saponite," and which Marshall (1964) later termed hectorite, but concluded that the hydrogen form could not be produced by that method because all the

MgO, 25.08 percent, was removed as was 15.6 percent SiO_2. About 0.7 percent Li_2O was removed from the sample. No analysis was given for the total sample used in this study, but calculations based on the analyses of the various size fractions of the sample indicate that the original Li_2O content was about 0.78 percent. Therefore, approximately 90 percent of the Li_2O was removed. The amount of released fluorine was not measured.

Kerr and others (1956) concluded that the attack by hydrogen ions begins at the edges of the hectorite crystal rather than on its silicate surfaces because the release of magnesium ions precedes the release of the silicon ions. Their samples were prepared by passing the clay suspensions through both hydrogen and hydroxyl forms of Amberlite. They reported that the anion exchanger removed sulfate ions, which were probably present as gypsum, from the clay but they, evidently, did not test for fluoride ions. Lithium ions were also not determined.

Faust, Hathaway, and Millot (1959) treated hectorite with hot 10 *N* hydrochloric acid for 6 hours which destroyed the structure and removed 19.2 percent MgO of the original 25.03 percent MgO in the sample.

Using weakly acidic solutions to more nearly approximate natural conditions, Tiller (1968a) demonstrated that for each 2 micromoles of H^+ added to hectorite, 0.95 ± 0.01 μmol Mg and 0.93 ± 0.025 μmol Si were released. This constant ratio between the amounts of released silicon and magnesium, together with X-ray data, suggested that the edges rather than the octahedral layers were the first to undergo attack. Tiller did not determine lithium but he assumed that it was released in the same manner as the magnesium and in the same ratio as was present in the original sample. In a companion paper, Tiller (1968b) concluded that the dissolution of hectorite in weakly acidic solutions may take place in two consecutive reactions: the displacement of octahedral cations by protons and the dissociation of silicic acid from the tetrahedral layer. The first reaction was considered to be reversible, whereas the second was only partly so.

The release of fluorine from hectorite has not been determined to the authors' knowledge. However, fluorine which could have come from soil clays has been detected in natural waters. Vinogradov (1959) stated that alkaline waters contribute to the washing of fluorine from the soil. He had not studied in what form the fluorine occurred but assumed that the soluble part must be very small and that the major part of the fluorine occurred in the fine fraction of the soil.

Wood (1973), in reporting the reactions of a sample of earth material with natural water from the Canadian River north of Amarillo, Texas, and with distilled water, stated that fluoride entered water by exchange reaction as well as by solution. The sample of earth material, obtained from the Ogallala Formation contained mixed-layer illite–montmorillonite, quartz, calcite, and traces of potassium and plagioclase feldspars. X-ray analysis revealed no fluoride minerals in the sample although Wood stated that the volcanic ash from the Ogallala Formation could furnish small quantities of fluoride-rich minerals to the samples. He pointed out that the fluoride went into solution very rapidly when the sample was treated with distilled water and suggested the possibility that the fluoride might all have come from mineral dissolution.

SAMPLE PREPARATION

The sample used in this study from the type locality at Hector, Calif., was furnished to the authors by A. J. Gude 3d of the U.S. Geological Survey. The sample, as obtained, contained about 30 percent calcite. Chunks that appeared to have less calcite than the rest of the sample were hand picked and soaked overnight in water. The resulting suspension was stirred by mechanical stirrer after which it was fractionated by centrifugation. The <1 micrometre fraction showed no trace of calcite either by X-ray diffraction or by treatment with dilute hydrochloric acid and was, therefore, dried and used for experimentation. Chemical analysis later confirmed the absence of calcite (table 1). After the fine fraction (<1 μm) was dried, the aggregates formed during the drying process were reduced to approximately 40 mesh by a ball mill and then were hand ground to pass a 60-mesh sieve before they were weighed.

EXPERIMENTAL PROCEDURE

Six 1-gram samples were weighed out into 50-millilitre polypropylene centrifuge tubes after having been dried for several hours at 80°C and after standing overnight in a desiccator containing calcium chloride. Forty millilitres each of 6 *N* hydrochloric acid (pH not measured), 4.5 *N* acetic acid (pH 1.80), 0.6 *N* sodium chloride solution (pH 5.80), distilled water (pH 6.05), natural seawater (pH 7.68), and 2.5 *N* sodium hydroxide solution (pH 13.90) were added to the respective tubes. A like amount of each liquid was placed in similar containers as control samples.

The samples were retained in the centrifuge tubes with polyethylene stoppers for 10 days during which time they were shaken each day. At the end of 10 days

TABLE 1.—*Amounts of elements, in milligrams, removed from 1 gram of purified hectorite*

[L.O.I., loss on ignition, determined gravimetrically by Wayne Mountjoy. CO_2 determined gasometrically by I. C. Frost. SiO_2 and Al_2O_3 determined colorimetrically and total Fe, MgO, CaO, Na_2O, K_2O, and Li_2O determined by atomic absorption by Wayne Mountjoy. F determined by specific ion electrode after 5 ml solution was diluted to 100 ml with ammonium citrate; analyst, J. M. Gardner. HAc, acetic acid. Dash leaders, no determination made]

	Purified hectorite (percent)	Amount of elements (milligrams) removed from hectorite by					
		6 N HCl solution	4.5 N HAc solution	H_2O	NaCl solution	Sea water	NaOH solution
SiO_2 ------	55.4	19.71	7.67	1.76	1.52	1.1	57.00
Al_2O_3------	<.3	.54	.05	.00	.00	.00	.03
Fe_2O_3------	.03	.43	.01	.00	.00	.00	.00
MgO -------	24.5	238.99	182.95	.22	1.53	15.00	.01
CaO -------	1.15	12.03	11.54	.05	9.75	6.9	.76
K_2O -------	.05	.47	.53	.06	.06	(1/)	.61
Na_2O ------	.90	8.86	8.33	2.21	(1/)	(1/)	(1/)
Li_2O ------	1.03	10.33	9.47	.03	.08	.09	.08
CO_2 -------	<.01	---	---	---	---	---	---
F ---------	4.60	19.95	3.73	.21	.14	.10	.47
L.O.I.-----	14.6	---	---	---	---	---	---
Subtotal-	102.57	---	---	---	---	---	---
O = F----	-1.94	---	---	---	---	---	---
Total----	100.63	---	---	---	---	---	---

1/ Negative values were obtained for these figures which indicates the exchange of the alkalis for some of the calcium but these values are questionable because the experimental errors in determining the large amounts of alkalis were greater than the exchange values.

the supernatant liquids were removed by centrifugation. The samples were washed twice with 10-ml portions of distilled water which were then added to the supernatant liquids. The samples were then washed several times with methyl alcohol to remove any occluded liquids.

A partial chemical analysis of the solid residue is shown in table 1. Only those elements were sought that one would expect to find in a hectorite that had a possible calcite impurity. Nevertheless, the sum of the determined elements added up to 100.63 percent, indicating that all the major elements had been determined and that any undetermined elements would be present only in minor or trace amounts. The same elements were sought in the supernatants as were found in the original hectorite. The results of the analysis of the various control solutions were subtracted from those of the corresponding leachates.

Another sample of the material was used for a cation exchange determination by leaching it overnight with 1 *N* ammonium chloride adjusted to pH 7 with ammonium hydroxide. The leachate obtained was analyzed in the same manner as the other solutions, and this analysis is shown in table 2.

TABLE 2.—*Analysis of the ammonium chloride ion exchange solution*

[SiO_2 and Al_2O_3 determined colorimetrically. Fe_2O_3, MgO, CaO, Na_2O, K_2O, and Li_2O determined by atomic absorption; analyst, Wayne Mountjoy. F determined by specific ion electrode method by J. M. Gardner. Dash leaders, ions not exchangeable]

Oxide	Weight percent	Millequivalents/100 grams of exchangeable cations
SiO_2 ----------	0.55	---
Al_2O_3----------	.01	---
Fe_2O_3----------	<.02	---
MgO ----------	.40	9.8
CaO ----------	1.35	48.1
Na_2O ----------	.90	29.0
K_2O ----------	.07	1.5
Li_2O ----------	.01	1.9
F ---------	.04	---

X-ray diffraction patterns were run of the original material and each of the residues.

Because sellaite had been found in the residue of the hectorite treated by acetic acid, further experiments were designed to determine when the precipitation of sellaite began and to study the effects of acetic acid on the clay since acetic acid is often used for the removal of carbonates from clay samples. Samples were therefore leached for periods of from 1 to 10 days in 1:3 acetic acid (pH 1.80). The samples were then treated in

the same way as the previous ones and the residues were analyzd by X-ray diffraction. The leachates, however, were analyzed for magnesium, lithium, and fluorine content only (table 3).

TABLE 3.—*Analysis of acetic acid (pH 1.80) leachates*

[MgO and Li_2O determined by atomic absorption by Wayne Mountjoy. F determined by specific ion electrode method by J. M. Gardner].

Number of days treatment	MgO	Li_2O	F
	Weight percent of the original sample		
1	5.15	0.26	0.85
2	9.50	.46	1.58
3	11.70	.57	1.88
4	13.25	.65	1.49
5	14.65	.72	1.23
6	15.50	.78	1.14
7	16.00	.82	1.12
8	16.50	.84	1.04
9	16.90	.86	.91
10	17.50	.93	.80

To determine the effect of the use of a weak acid to remove carbonates from hectorite, a 1-gram mixture of 70 percent of the previously purified hectorite and 30 percent calcite was made up to approximate the original sample. The procedure used was designed to simulate that which might be used in carbonate removal. Ten millilitres of 1:3 acetic acid (pH 1.80) was added to the mixture. When the escape of CO_2 bubbles subsided, another aliquot was added. This second addition also produced CO_2 bubbles. When the bubbling stopped, a third aliquot was added that produced no new bubbling, indicating that the calcite had been removed. The supernatant was immediately removed and saved for analysis. The sample was washed several times with the washings being added to the supernatant. The residue was dried and analyzed by X-ray diffraction.

EXPERIMENTAL RESULTS

The octahedral layer was readily attacked by the acid solutions with all the lithium and almost all the magnesium being removed by the hydrochloric acid. The analysis of the acetic acid solution showed that at least 75 percent of the original magnesium and more than 90 percent of the lithium were removed. A small amount of the magnesium that had been released by the acetic acid solution combined with fluorine that also had been released to form sellaite (MgF_2).

The 6 *N* hydrochloric acid removed about one-third weight percent of the original hectorite and the 4.5 *N* acetic acid removed about one-fourth of the original sample.

The distilled water (pH 6.05), the sodium chloride solution (pH 5.80), and the seawater (pH 7.68) had little effect on the structure of the hectorite, as shown by X-ray analysis of the residues. Only 0.18, 0.15, and 0.11 percent SiO_2, respectively, was removed by these solutions. The amounts of alkalis and alkaline earths reported in the analyses for these three solutions appear to be largely the result of cation exchange rather than attack of the mineral itself, although some extremely small particles could have been attacked and would thus account for the presence of silica in the solutions. In view of the slight removal of the various elements by the distilled water, the possibility must be considered that some of the hectorite went into solution during the removal of calcite from the original sample by centrifugation in which many litres of distilled water were used.

The sodium hydroxide solution had no more effect on the alkalis and alkaline earths than did the distilled water, the seawater, or the sodium chloride solution, but it did release about 10 percent of the silica present by attacking the tetrahedral layer. More fluorine was released by the sodium hydroxide than was released by the above-named solutions but not as much as was released by the two acids.

Figure 1 shows the results of the treatment of hectorite with acetic acid for varying lengths of time. Magnesium and lithium were apparently released at a constant ratio, through attack on the octahedral layer. Fluorine was also released. At about 3 days the solution became saturated with sellaite (MgF_2), which had begun to precipitate, producing a decided drop in the fluorine content of the solution (fig. 2).

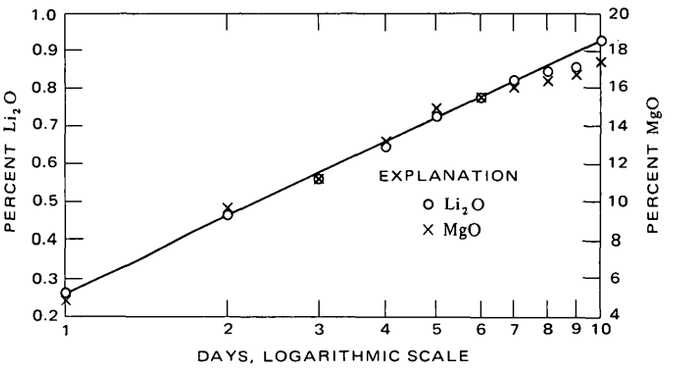

FIGURE 1.—The release of lithium and magnesium from hectorite by 4.5 *N* acetic acid over a period of 10 days.

The solubility product calculated from these data, $[Mg^{2+}][F^-]^2$, is $10^{-6.7}$ as opposed to a value of $10^{-10.1}$ calculated from the thermodynamic data (Parker and others, 1971). The discrepancy is presumably due to the formation of the $Mg(Ac)^+$ complex in the solution.

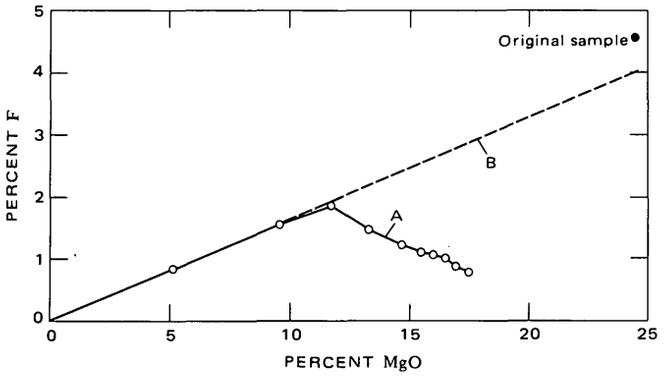

FIGURE 2.—Comparison of the amounts of F and MgO released from hectorite by 4.5 *N* acetic acid over 10 days with the amount of each in the original sample. A, amounts determined in solution; B, amounts assumed to be leased from hectorite. The difference is due to the precipitation of sellaite after 3 days.

The X-ray diffraction patterns (fig. 3) show a decrease of the intensity of the peaks after 3 days of the acetic acid treatment. After the fifth day enough sellaite had been precipitated to produce some diffraction peaks from this phase. The reflections produced by the sellaite were broad and ill defined at first but after 10 days they were reasonably well developed. By that time the hectorite peaks had nearly disappeared, except for the 060 which was still fairly well defined although the area under the peak had been reduced by 80 percent. Centrifugation produced a concentration of the sellaite which gave a stronger diffraction pattern, thus confirming the identification. The data from this diffraction pattern are compared with those of a synthetic sellaite (Swanson and others, 1955) in table 4.

TABLE 4.—*Comparison of X-ray diffraction data of sellaite precipitated in acetic acid solution with those of a synthetic sellaite*

Acetic acid precipitate		Synthetic sellaite[1]		
dA	I/I_1	dA	I/I_1	hkl
3.276	100	3.265	100	110
2.537	30	2.545	22	101
		2.310	1	200
2.231	82	2.231	96	111
2.089	33	2.067	34	210
1.716	65	1.711	73	211
1.640	35	1.635	31	220
1.513	25	1.526	19	002
1.465	10	1.462	6	310

[1] Data from Swanson, Fuyat, and Ugrinic (1955).

The procedure previously described for removing calcite from a prepared calcite-clay sample required less than 3 hours. However, even this relatively brief time was sufficient for the acetic acid to attack the hectorite. Only MgO, Li_2O, and F were determined in the supernatant liquid, and the weight percentages of these are 0.72, 0.03, and 0.07, respectively.

The free-swelling volume of hectorite in water, determined by Foster's (1953) method, is 39 ml/g. This swelling volume made it impossible to handle the sample treated by distilled water in the same manner as the other samples, inasmuch as it formed a hydrogel which completely filled the centrifuge tube when the water was added. Therefore, it was necessary to use larger volumes of water to wash the sample. Even then, it is doubtful that all the elements removed from the structure of the mineral were determined because the water occluded in the gel must have contained some ions in solution.

Each of the elements found in the reacting solutions were sought in the NH_4Cl exchangeable cation solution, also. The amounts of Ca, Na, and K found to be exchangeable account for all these elements found in the original sample. The sum of these three elements present in the original sample plus 5.7 milliequivalents/100 g Mg satisfies the determined exchange capacity of 76.8 meq/100 g and it is thought, therefore, that the remainder of Mg in the exchange solution was actually released by dissolution of the sample. This assumption is further strengthened by the fact that overnight leaching for 16 hours in the NH_4Cl solution for exchange determination was long enough to remove measurable amounts of SiO_2, Li_2O, and F from the sample also. The percentages of the original amounts of these elements and the nonexchangeable Mg removed were: Li_2O, 1.0; MgO, 1.2; SiO_2, 1.0; and F, 0.9.

Fluoride was found in all the solutions although, in some solutions, the amounts were very small. The presence of small amounts of silica in the same solutions in which fluoride was minimal indicates that some fine particles of the mineral were dissolved.

DISCUSSION AND CONCLUSIONS

Hectorite is readily attacked by both strong and weak acids with the octahedral layer being attacked first and being almost completely destroyed before any significant attack occurs on the tetrahedral layer. The lithium and magnesium are removed at a constant weight ratio of about 1:20 although they are present in the sample in a ratio of about 1:24. The 6 *N* hydrochloric acid released considerable fluorine; more than 40 percent of the original amount was found in solution after the 10 days of this experiment.

The amounts of the cations released by the distilled water, seawater, and sodium chloride solution are very small, and the actual amounts are obscured by the ef-

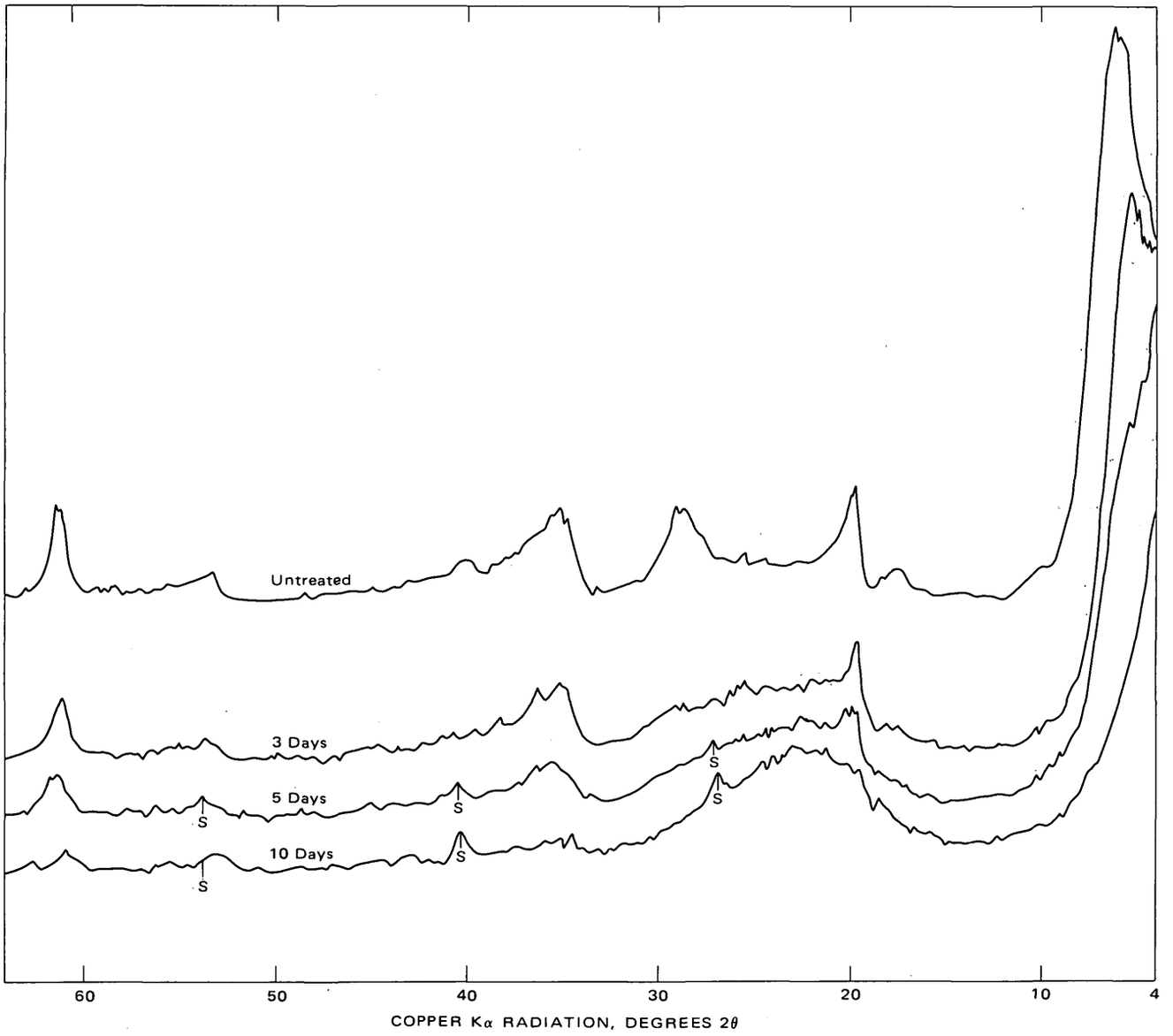

FIGURE 3.—Smoothed X-ray diffraction patterns of hectorite before and after treatment with 4.5 *N* acetic acid at 3, 5, and 10 days. S, sellaite.

fects of cation exchange. These amounts, determined after 10 days of the solution experiments, are in the same range as those obtained from the cation exchange reactions that occurred over a period of 16 hours.

The amount reported for magnesium released by the sodium hydroxide is low as compared with the amount of lithium released by the same treatment. In such a strong basic solution, it is possible that the magnesium was precipitated as $Mg(OH)_2$.

All the elements that were determined in the reacting solutions were sought in the ammonium chloride leachate but only those elements that could be considered exchangeable were converted to meq/100 g (table 2). The presence of silica and fluorine in the ammonium chloride solution indicates that some of the very fine material must have been taken into solution; this addition could account for the presence of lithium, which is not ordinarily exchangeable in ammonium chloride solutions.

X-ray diffraction patterns indicate that the hectorite structure was destroyed by both the 6 *N* hydrochloric and the 4.5 *N* acetic acid solutions. Sellaite (MgF_2) was found, however, in the pattern produced by the acetic acid residue. It is obvious that the sellaite was precipitated from the solution rather than having been present in the original sample because (1) no trace of it was seen in the X-ray pattern of the original material or in the patterns of any of the other residues,

and (2) if sellaite had been present in the original sample, it would have been removed during the centrifugation because of the differences in specific gravity. The specific gravity of sellaite is 3.15 as compared to that of hectorite which is about 2.70. The precipitation of sellaite reduced the amount of both fluorine and magnesium in the acetic acid leachate; therefore, the amounts of these two elements shown in table 1 are slightly lower than the amounts actually removed from the hectorite.

Results of the first 3 days of the daily experiment with the acetic acid indicate that the fluorine and magnesium were removed at a constant ratio as illustrated in figure 2. The broken line of the graph shows that the continued removal of lithium and magnesium at that ratio would come close to removing all of both elements, but the precipitation of sellaite after 3 days makes this only a conjecture. If this is true, all the fluorine (4.6 percent) should have been removed by the hydrochloric acid treatment, but only 2 percent was found in solution and no sellaite was observed in the residue. If all the fluorine had been removed by the hydrochloric acid, some of it could have combined with hydrogen to form hydrofluoric acid which could be lost by vaporization; or the hydrofluoric acid could have combined with the silica to form silica tetrafluoride and thus escape into the atmosphere.

Wilson, Bain, and Mitchell (1968) concluded that the removal of carbonates by the use of 1:3 acetic acid to water solution had no effect upon saponite from the Dalradian metalimestones of northeast Scotland. This clay contained only a trace of lithium and therefore was not considered by those authors to be hectorite. Their conclusion was based on the fact that no differences were noted in the X-ray diffraction patterns of samples treated by acetic acid and of samples from which the carbonates had been removed by the (ethylenedinitrilo)tetraacetic acid disodium salt and by ion-exchange resins. Figure 3 shows that a sample of hectorite treated in the same way does begin to show a loss of intensity in the diffraction peaks after the third day, and the analysis of the supernatant liquid obtained by the removal of calcite from the hectorite shows that about 2.9 percent of the MgO and Li_2O present in the hectorite was removed by the 1:3 acetic acid in less than 3 hours.

Lithium is released from hectorite by attack of the octahedral layer and is in proportion to the amount of magnesium released, but the two elements not necessarily released in the same ratio as they are present in the sample.

Very little fluoride was removed by the sodium hydroxide which attacked the tetrahedral layer and removed 5.70 percent of the silica. The small amount of fluorine that was found in the sodium hydroxide solution could have been removed by anion exchange near the edges of the particles. Some dissolution of the octahedral layer occurred as shown by the presence of lithium in the solution.

Nutting (1940), Caldwell and Marshall (1942), Kerr, Zimmerman, Fox, and Wells (1956), Faust, Hathaway, and Millot (1959), and Tiller (1968a, b) have shown that hectorite is subject to attack by hydrogen ions which release magnesium. The present study has demonstrated that lithium and magnesium are released coincidently from hectorite when acids attack the octahedral layer. Hectorite, especially from the type locality, is associated with calcite. Removal of this calcite by chemical means should be approached with caution. Even the weak acids which are normally considered to have minimal effect on clay minerals could alter hectorite by removal of magnesium, lithium, and fluorine. Removal of the calcite by physical methods is to be preferred. If the physical methods do not entirely remove the calcite, they should at least reduce the amount present so that less acid is necessary.

The amounts of silicon, magnesium, lithium, and fluorine removed by distilled water, though small, suggest that hectorite would be slightly soluble in rainwater which, in equilibrium with atmospheric carbon dioxide, has a pH of 5.7 at 25°C (Carroll, 1962). The effects of rainwater on hectorite would be extremely difficult to assess because of the seasonal and regional variations in the composition of rainwater. However, long-term exposure of hectorite to seawater, which also removed only a small amount of the above elements, and to rainwater, could have considerable effect on the structure of the minerals because the water would be continuously renewed and the dissolution products would be removed.

REFERENCES CITED

Aldrich, D. G., Vanselow, A. P., and Bradford, G. R., 1951, Lithium toxicity in citrus: Soil Sci., v. 71, p. 291–295.

Bertrand, Didier, 1943, Sur la diffusion du lithium chez les vegetaux: Acad. Sci. [Paris] Comptes Rendus, v. 217, p. 707–708.

Caldwell, O. G., and Marshall, C. E., 1942, A study of some chemical and physical properties of the clay minerals nontronite, attapulgite, and saponite: Missouri Univ. Agr. Expt. Sta. Research Bull. 354, 51 p.

Carroll, Dorothy, 1962, Rainwater as a chemical agent of geologic processes—a review: U.S. Geol. Survey Water-Supply Paper 1535–G, p. G1–G18.

Faust, G. T., Hathaway, J. C., and Millot, Georges, 1959, A restudy of stevensite and related minerals: Am. Mineralogist, v. 44, nos. 3–4, p. 342–370.

Foster, M. D., 1953, Relation between ionic substitution and swelling in montmorillonites pt. 2 *of* Geochemical studies of clay minerals: Am. Mineralogist, v. 38, nos. 11–12, p. 994–1006.

Kerr, G. T., Zimmerman, R. H., Fox, A. J., Jr., and Wells, F. H., 1956, Degradation of hectorite by hydrogen ions: Clays and Clay Minerals, v. 4, p. 322–329.

Marshall, C. E., 1964, Soil materials, v. 1 *of* The physical chemistry and mineralogy of soils: New York, John Wiley and Sons, Inc., 388 p.

Nutting, P. G., 1940, A study of the association of magnesia with silica in a pure magnesium clay: Washington Acad. Sci. Jour., v. 30, no. 6, p. 233–237.

Parker, V. B., Wagman, D. C., and Evans, W. H., 1971, Selected values of thermodynamic properties—tables for alkaline earth elements: Natl. Bur. Standards Note 270-6, 106 p.

Shacklette, H. T., Boergnen, J. G., Cahill, J. P., and Rahill, R. L., 1973, Lithium in surficial materials of the conterminous United States and partial data on cadmium: U.S. Geol. Survey Circ. 673, 8 p.

Swanson, H. E., Fuyat, R. K., and Ugrinic, G. M., 1955, Magnesium fluoride (sellaite), MgF_2 (tetragonal), *in* Standard X-ray diffraction powder patterns: U.S. Natl. Bur. Standards Circ. 539, v. 4, p. 33–34.

Tiller, K. G., 1968a, A chemical study of the dissolution of hectorite with special reference to the release of silica, pt. 1 *of* Stability of hectorite in weakly acidic solutions: Clay Minerals, v. 7, no. 3, p. 245–259.

——— 1968b, Studies of the chemical equilibrium and the calculation of free energy, pt. 2 *of* Stability of hectorite in weakly acidic solutions: Clay Minerals, v. 7, no. 3, p. 261–270.

Vinogradov, A. P., 1959, The geochemistry of rare and dispersed chemical elements in soils: New York, Consultants Bur. Enterprises, Inc., 209 p.

Wells, N., and Whitton, J. S., 1972, Lithium, pt. 1 *of* A pedochemical survey: New Zealand Jour. Sci., v. 15, no. 1, p. 90–106.

Wilson, M. J., Bain, D. C., and Mitchell, W. A., 1968, Saponite from the Dalradian meta-limestone of north-east Scotland: Clay Minerals, v. 7, no. 3, p. 343–349.

Wood, W. W., 1973, Rapid reaction rates between water and a calcareous clay as observed by specific-ion electrodes: U.S. Geol. Survey Jour. Research, v. 1, no. 2, p. 237–241.

Jour. Research U.S. Geol. Survey
Vol. 5, No. 2, Mar.–Apr. 1977, p. 243–251

EFFECTS OF DREDGED CHANNELS ON TRACE-METAL MIGRATION IN AN ESTUARY

By CHARLES W. HOLMES, Corpus Christi, Tex.

Abstract.—Determination of trace-metal levels in the sediments of the Matagorda Bay system revealed anomalously high mercury values. The distribution of the mercury-rich sediment deposits is the result of the sedimentological regime of the bay system produced by the tidal currents in the dredged channel. According to this model, the oxygenated open gulf water pushed into the bay by tidal currents activates the mercury and reintroduces it into the sediment regime of the bay in an area where the turbidity maximum is most prevalent. Within this region, the absorption sites are at a maximum, tying up the mercury. The mercury-enriched suspended material is then transported and deposited according to the hydraulic regime within the bay system.

A survey of the distribution of 31 elements in the sediments of the Matagorda estuarine system revealed abnormally high levels of mercury present in the southern part of the system (C. W. Holmes, unpub. data, 1975). High mercury levels were previously known to exist (Corpus Christi Caller, 1971); however, it was assumed to be confined to the immediate vicinity of a chloralkali plant on Point Comfort. This report examines the physical and chemical parameters of Lavaca and southern Matagorda Bays and presents a model that may account for the transportation and deposition of mercury within this estuarine system.

The Matagorda Bay system, on the southeastern Texas Coastal Plain, is a drowned valley complex separated from the Gulf of Mexico by a postglacial barrier spit and island, the Matagorda Peninsula (fig. 1). The rather smooth bottom of the bay averages about 3.3–3.6 meters in depth and has a maximum depth of 4.5 m. Like most estuaries of the western Gulf Coast, the central parts of the bay are floored monotonously by fine sediment surrounded by a rim of sandy sediment. Extremely fine sediment is found in the deepest parts of the basins (Byrne, 1975). Despite constant influx of sediment, this system appears to be maintaining a constant depth because of an established dynamic equilibrium by the wave action and sediment transportation (W. A. Price, oral commun., 1972).

Communication between the Gulf and Matagorda Bay before 1965 was wholly through Pass Cavallo. However, since the completion of the 13-m-deep ship channel to Point Comfort in 1965, significant exchange flows through this channel. Before 1964, little or no exchange took place via the shallow channel extending from Matagorda Bay to a small turning basin at Point Comfort. This basin was enlarged and the present configuration developed during the construction of the present channel in 1964–65 (see fig. 1).

Acknowledgments.—I wish to thank the General Land Office and the Bureau of Economic Geology of the State of Texas for their support in the initial phase of this study, and to acknowledge the assistance in the field of Dr. Joseph McGowen and E. A. Slade. I wish to thank Paul Kuchinski of the Texas Water Quality Board, Corpus Christi, Tex., for making the data available.

HYDROLOGY

Data obtained during this study, supplemented by data gathered by the U.S. Geological Survey (Hahl and Ratzlaff, 1969, 1971, 1972), indicate that the combination of the low tidal ranges (0.5–1.5 m) of the western Gulf of Mexico and the shoalness of the system create a condition in which wind-generated forces drive the water circulation. The circulation pattern thus formed is greatly modified during high freshwater runoff, which takes place predominantly during late winter to early summer. During this period, the freshwater influx has a pressure head high enough to drive the estuarine brackish water from Lavaca Bay and parts of southwestern Matagorda Bay.

Within the channel, however, the wind-generated forces and the freshwater runoff have only a secondary influence on circulation compared with the tidal-dominated circulation. The degree of tidal domination is clearly manifested by the current and salinity data.

The current direction and relative strength in the channel were determined by drogues deployed at various depths during the peak ebbtides and floodtides. Although this method of measuring currents does not allow for measurement of the current velocity, subjective estimates can be made by the relative speed of

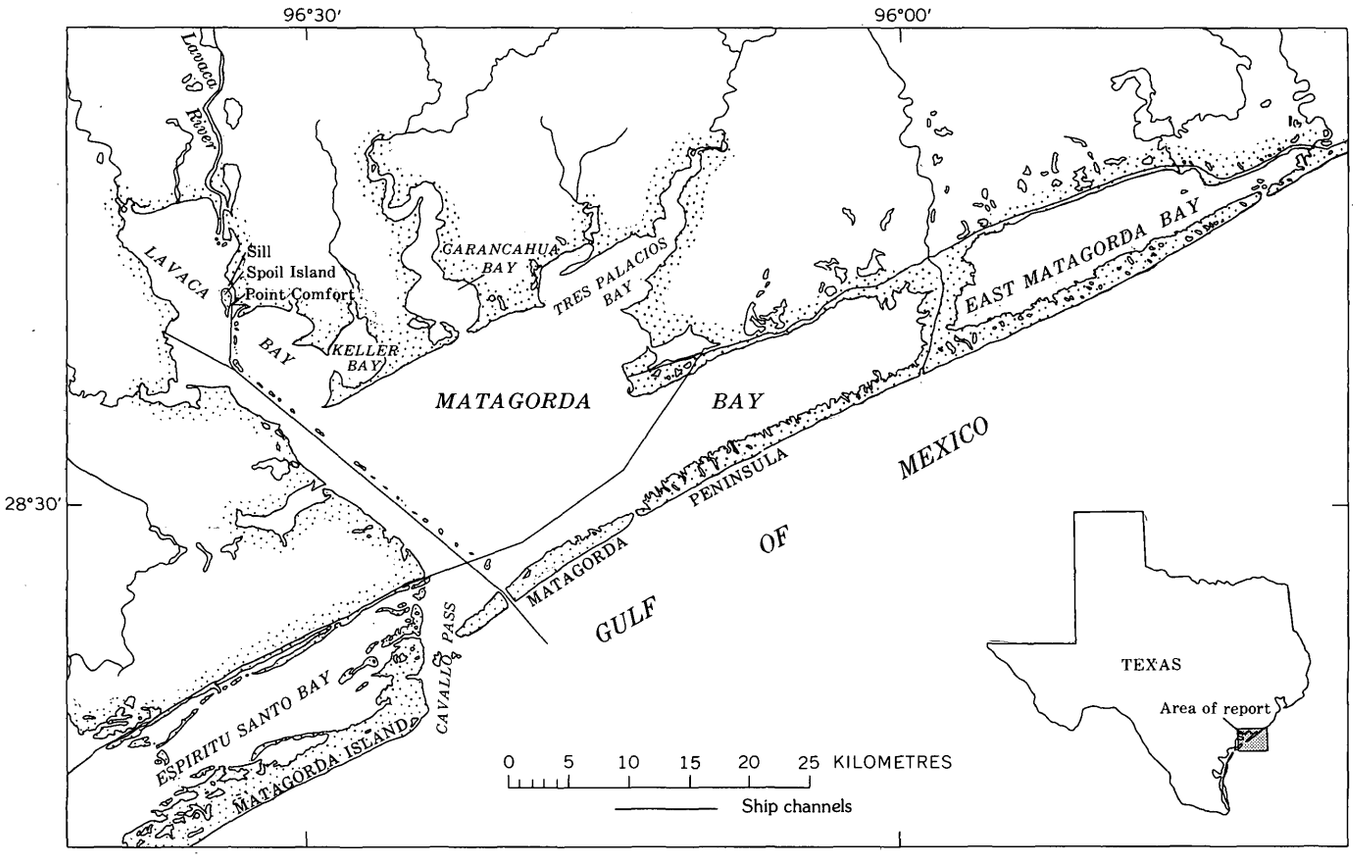

FIGURE 1.—Location of Matagorda Bay.

the surface buoys attached to the drogues. Samples for suspended sediment mass and salinity determinations were taken simultaneously with drogue measurements. The samples were taken by lowering the sample intake to the desired level and pumping for 2 minutes, the length of time determined to clear the hose and pump, before the sample was retained. The suspended sediments were collected in polyethylene containers and kept agitated until filtered on a preweighed acid-washed 0.4 micron Nuclepore filter, air dried, and weighed. The salinity was determined by refractometer (Behrens, 1965).

These observations show that a strong outward current at lower levels and a weak but definite outgoing surface current are present during the ebbtide in the lower reaches of the channel (fig. 2). In the part of the channel near Point Comfort, no distinct current is evident. Thus, during maximum ebbtide, the estuarine water on the surface extends to the channel mouth and an outward-moving wedge of gulf water is present in the deeper parts of the channel.

At the time of the maximum floodtide, however, a very strong inward current exists at the lower levels of the channel. This current pushes gulf water some 32 kilometers to the head of the channel. At this point, the water upwells, and a significant fraction flows over the sill that stretches between the spoil island and the mainland. Scour channels in the sill suggest that the flow is occasionally strong (James Bowman, oral commun., 1973). Near the mouth of the channel, a distinct inward flow of water exists in the surface layers. However, in this upper section of the bay, the wind-derived currents dominate (fig. 3). Thus, over a full tidal cycle, the effect of the circulation in the channel is a net movement inward in lower levels of the channel, upwelling and mixing at the head of the bay, and a net seaward transport of surface water.

DISTRIBUTION OF MERCURY IN MATAGORDA BAY

Total mercury content from 800 bottom sediments sampled from Lavaca and Matagorda Bays ranged from near 10 micrograms per gram to a background level of less than 0.02 μg/g. These samples were collected in small van Veen sediment samplers and represent the top 6–10 centimeters of bottom sediments. (J. R. Byrnes, oral commun., 1971). The mercury content was determined by the mercury vapor detector method (Vaughn, 1967). Supplemental mercury data for sedi-

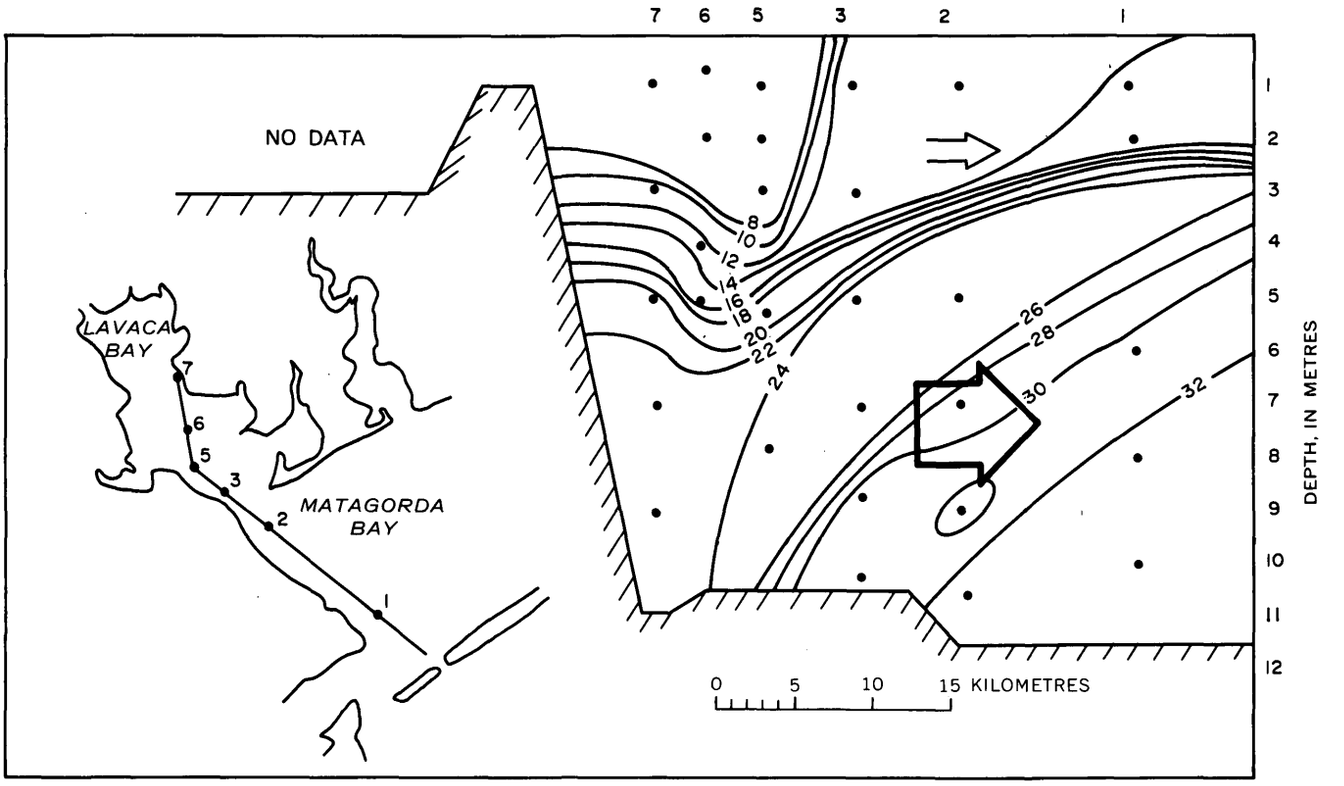

FIGURE 2.—Cross section along the ship channel, showing the distribution of salinity during the ebbtide phase, October 1, 1973. Isopleths are given in parts per thousand. Arrows, current direction (size represents relative current strength); dots, sample sites (number represents sample station and corresponds to number on the sketch map).

ments from cores, suspended sediment, and water were determined by flameless atomic absorption (Hatch and Ott, 1968). Replicate analysis of selected samples suggests a precision of less than 10 percent for both methods. The results of these analyses showed that two regions of mercury-rich sediment exist in the system—one in Lavaca Bay, which extends from the northwest side of the spoil-settling island southeastward toward the junction of Lavaca and Matagorda Bays, and the second along the north side of the channel in Matagorda Bay (fig. 4). This latter area corresponds to the deepest part of the bay and that part which contains the finest sediment.

In order to ascertain a three-dimensional aspect of the mercury distribution in the sediment, a series of 1-m cores was taken across the regions of high surficial mercury content. The cores were taken by divers in such a way that the sediment-water interface remained intact and undisturbed. Immediately upon retrieval, the cores were sampled continuously at 2-cm intervals. The cores at many sites near the spoil banks penetrated through spoil cover (easily recognized by its color and texture) to normal bay sediment. No matter where the core was taken, whether in spoil or nonspoil, the vertical distribution of mercury was similar; that is, highly concentrated in the top 5–7 cm, decreasing to background levels below 7 cm, suggesting that the mercury distribution is only a recent event and postdates the dredging of the channel.

In 1971, mercury concentrations ranging from 7 to 22 μg/g were found by the Texas Water Quality Board in the sediments on the floor of the turning basin that contained the outlet from the plant. After maintenance dredging, in which the dredged materials were placed in the pond constructed on the spoil island, and after corrective procedures were applied to the effluent, the mercury content of the sediment from the floor of the turning basin was found to be 1.8 μg/g. During this dredging, daily monitoring of the effluent in the spoil-settling pond indicated that the mercury concentration of the water was maintained at less than 1 μg/l. There was one exception; that is, when the effluent reached 800 μg/l and the dredging activity was stopped. No data are available to explain the high value, but as is often found, the outfall pipe from the dredge was probably jetting water directly toward the effluent point.

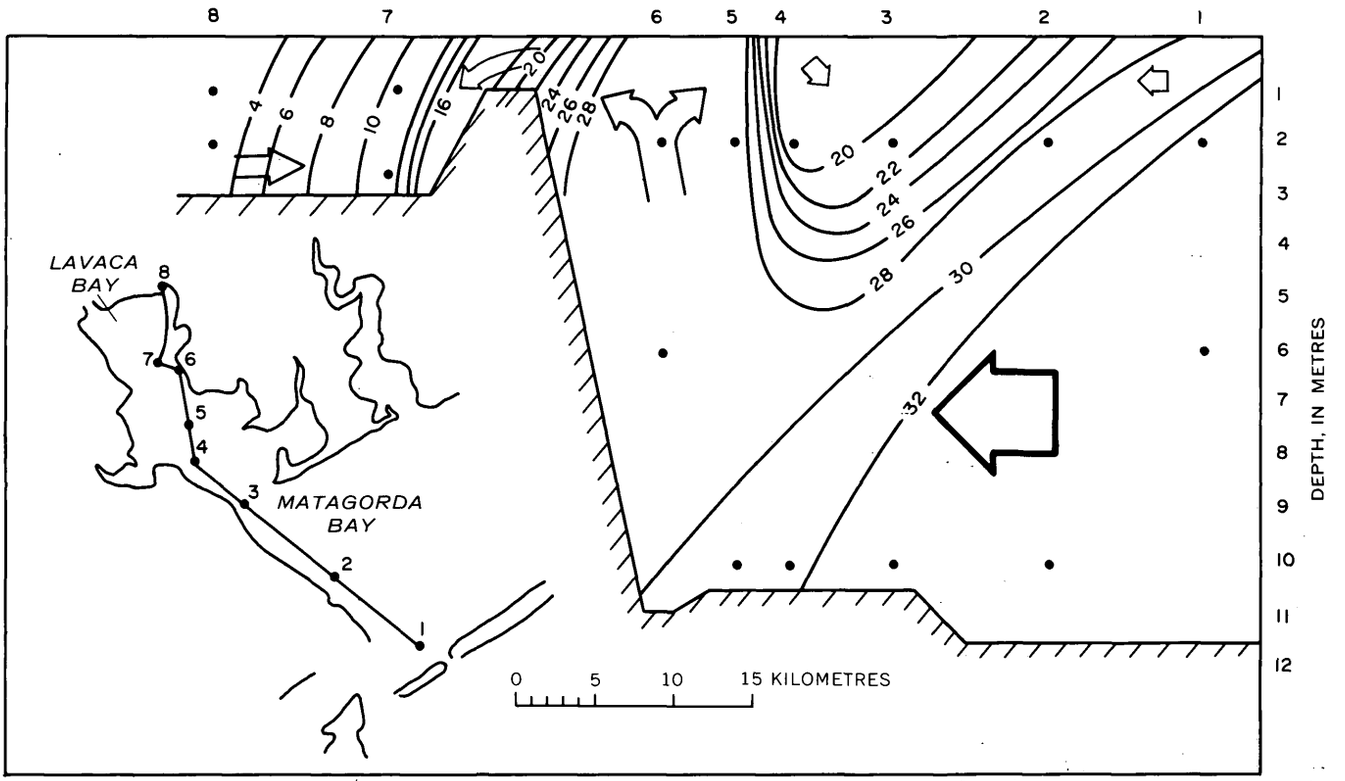

FIGURE 3.—Cross section of the ship channel, showing the distribution of salinity during the floodtide phase, December 1, 1973. Isopleths are given in parts per thousand. Arrows, current direction (size represents relative current strength); dots, sample sites (number represents sample station and corresponds to number on the sketch map).

SUSPENDED MATERIAL

The concentration of suspended particulate material in the channel during ebbtide was found to be highest in Lavaca Bay (fig. 5). During this phase of the tidal cycle, the suspended material ranged from 52 mg/l to 6 mg/l. In the floodtide phase of the tidal cycle, the strong bottom current stirs the bottom, increasing the suspended material concentration within the water column near the bay mouth (fig. 6). The suspended material concentration in the upper reaches of the channel, however, increased only slightly. This material was also different from the material in the lower reaches of the channel in that it appears, by visual inspection, to have a higher organic content. Mercury concentrations of the particulate matter ranged from less than 10 μg/g to greater than 100 μg/g. The lower concentrations were observed near the mouth of the channel during the ebbing of the tide (fig. 7), whereas the higher values were observed in the upper reaches of the channel near maximum floodtide (fig. 8). The water associated with the suspended material in both places had less than 1 μg/l.

We also noted at the time of sampling (December 1973) that during the floodtide phase, a turbidity maximum of 150 mg/l was present in the upper reaches of Lavaca Bay. Such a turbidity maximum develops best in a partly mixed estuarine system and where the salinity gradient starts (Schubel, 1971). In such an estuary, fresh, less dense water flows downstream (seaward), and the saline (higher density) water flows upstream. Sedimentary particles that settle from the freshwater into the lower layers are carried back upstream by the upstream flow, where part of the sediment settles. Some of the particles may be transported into the upper layers, and a turbidity maximum may be formed in the water column. The seaward boundary of the turbidity maximum can be readily seen by the steep gradient of total suspended material. This front moves up and down the estuary in response to changes in river flow and wind-driven circulation. In Lavaca Bay, hydrologic data (Hahl and Ratzlaff, 1969, 1971, 1972) and Landsat-A photos show such a turbidity maximum ranging the length of Lavaca Bay and sometimes extending into Matagorda Bay proper.

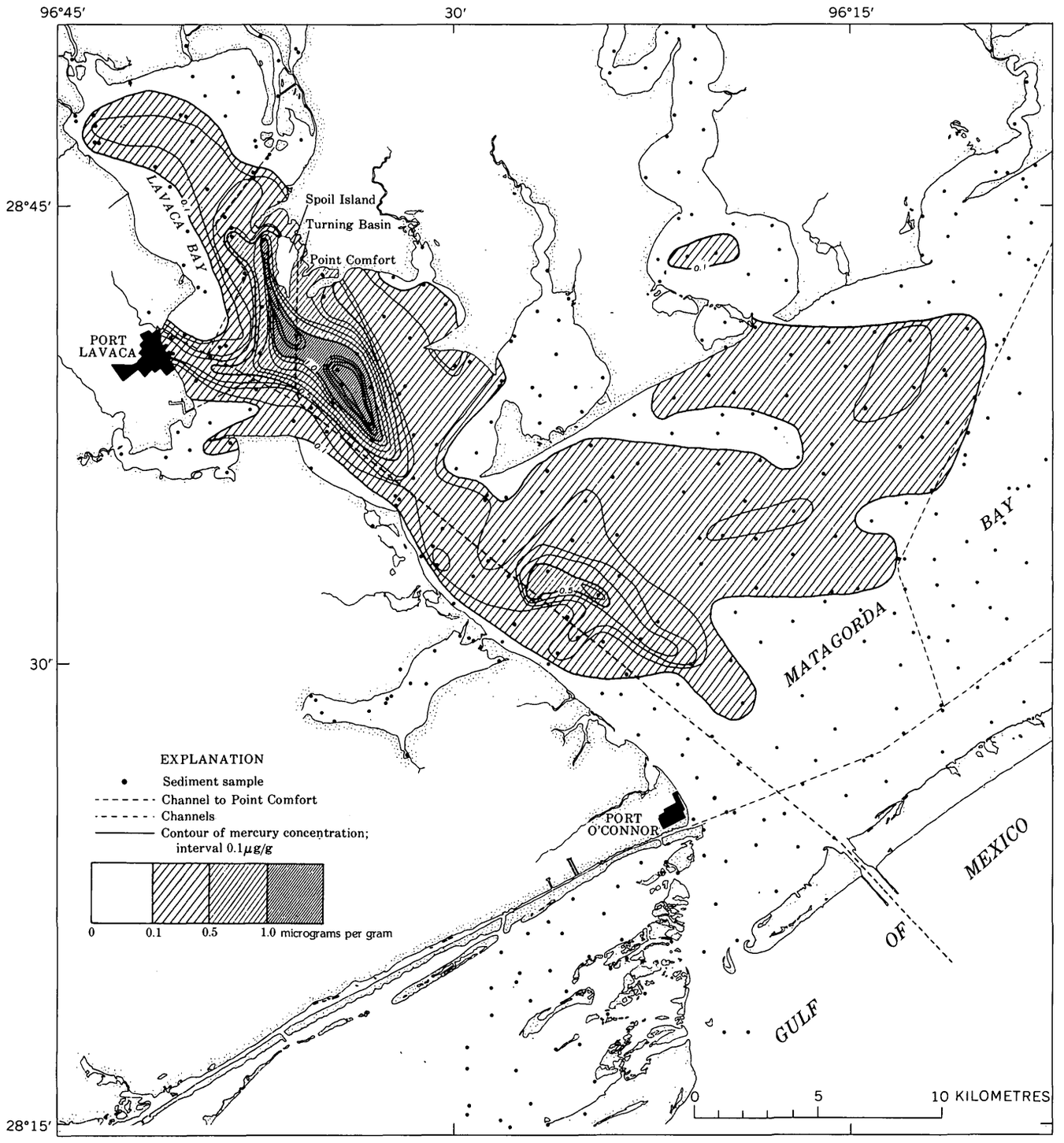

FIGURE 4.—Distribution of total mercury in the sediments of Lavaca Bay and the southern section of Matagorda Bay.

WATER QUALITY OF THE CHANNEL AND TURNING BASIN

The chemical nature of the water in the channel and the turning basin varies with the seasons and with the phases of the tide (Hahl and Ratzlaff, 1969, 1971, 1972). From late winter to early summer, the channel and the turning basin are well mixed with respect to chemical constituents. In the summer, the water in the turning basin becomes highly stratified, the deep water being nearly depleted of dissolved oxygen. Thus it appears that within the turning basin, the bottom waters trend toward stagnation during the summer, possibly forming an anoxic wedge similar to that formed in the harbor at Corpus Christi (Holmes and others, 1974).

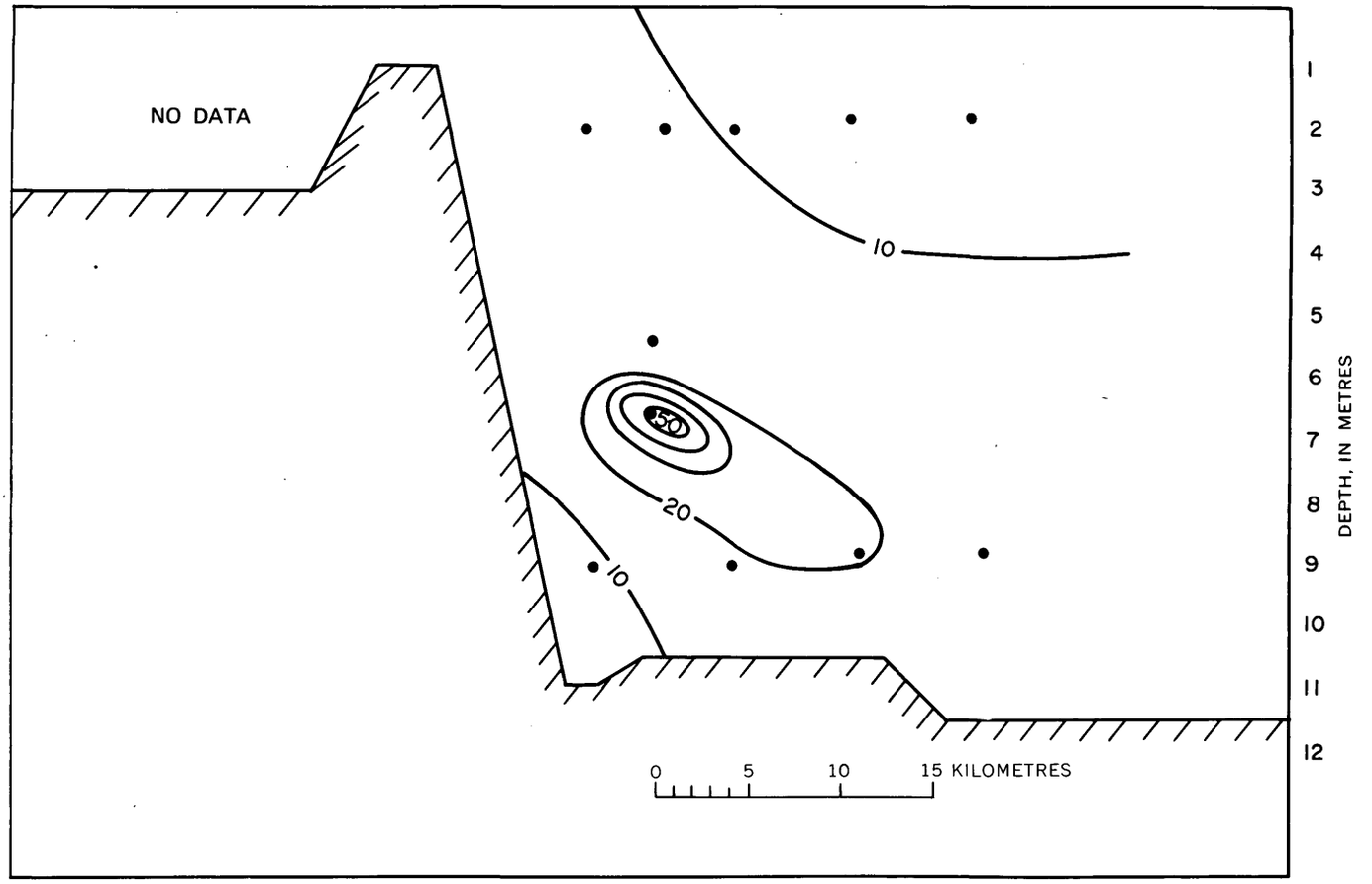

FIGURE 5.—Cross section of the ship channel, showing the distribution of the suspended material during the ebbtide phase, October 1, 1973. Isopleths are given in milligrams per litre. Dots, sample sites.

During this period, the upwelling, as described above, shifts toward the mouth of Lavaca Bay. Further evidence of this anoxic bottom condition is suggested by the slightly negative (—80 to —40 mV) Eh (reduction-oxidation potential) of the bottom sediments.

CHEMISTRY OF MERCURY IN ESTUARIES

Data on the chemistry of mercury in aqueous media (Hem, 1970) suggest that the dissolved mercury entering the turning basin should be in some form of an hydroxide or chlorohydroxide complex, depending on the salinity of the water. When the system contains an oxygen-poor, low-salinity water mass, mercury would possibly be precipitated into the mud as a sulfide, probably as a hydrated sulfide complex. These same conditions would also lead to methylation of mercury, an important step leading to significant bioaccumulation. If mercury were introduced into an oxygenated, low-salinity, turbid water mass (for example, during the winter), a significant part would be adsorbed on suspended material (Cranston and Buckley, 1972) and a significant fraction would probably be associated with material of a molecular weight less than 500 (Lindberg and Harris, 1974). Increasing the salinity of such a water would shift the equilibrium of the mercury complex to the stable chloride side (Anfalt and others, 1968). Thus, if an oxygen-rich, highly saline water mass displaced an oxygen-depleted water mass from which mercury was being precipitated, a significant part of the precipitated element could be resolubilized, aided by aerobic bacteria acting upon the sulfide substrate (Wood, 1974). If this water mass is turbid, the mercury would be adsorbed onto the particulate material and transported with this material.

MODEL OF MERCURY MOVEMENT

The data and observations presented here suggest that the tidal action in the dredged channel has played an important role in the processes by which mercury is distributed within the bay system and that this action is solely the result of channelization. Since the construction of the channel to Point Comfort, the

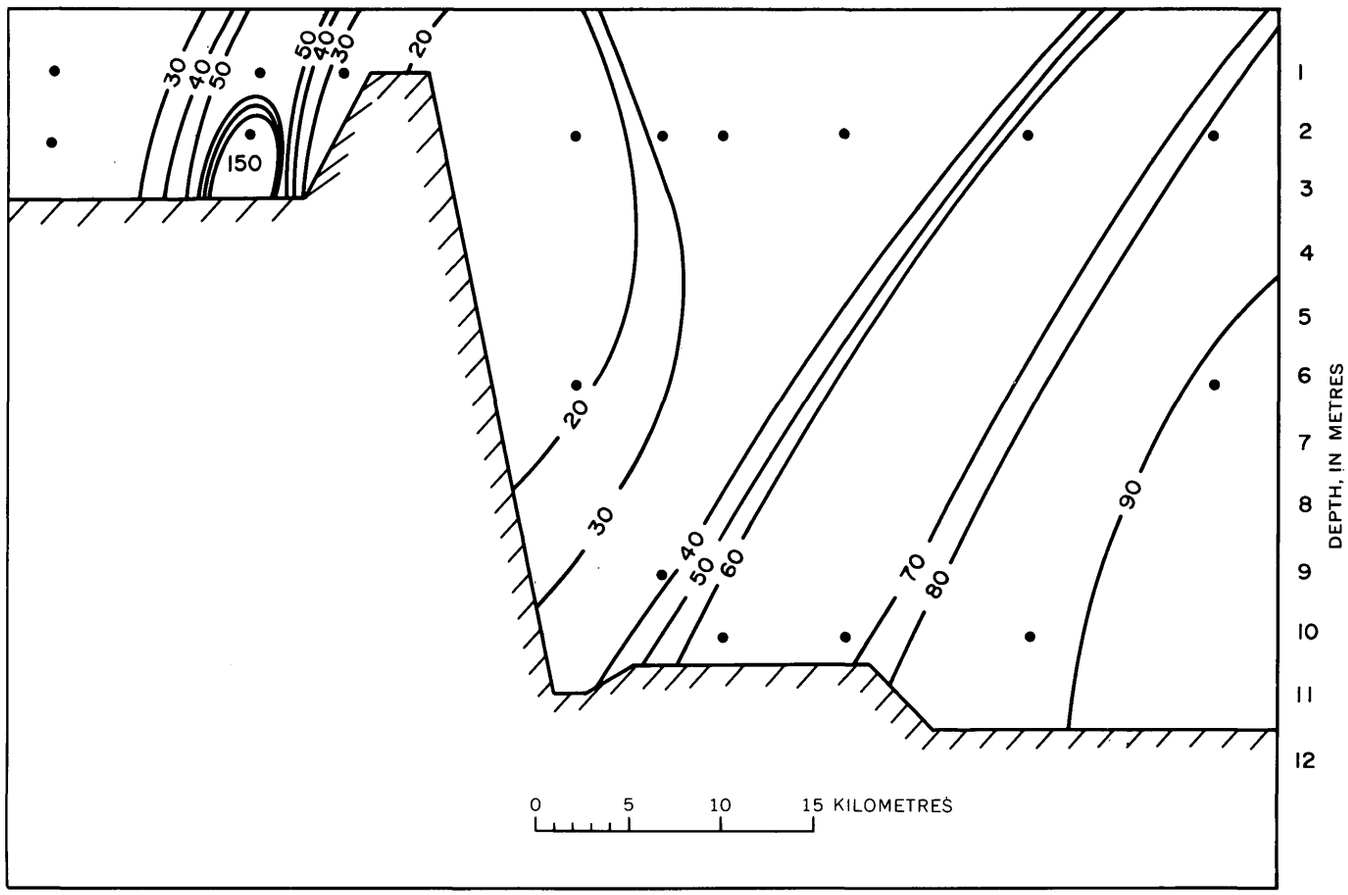

FIGURE 6.—Cross section of the ship channel, showing the distribution of suspended material during the floodtide phase, December 1, 1973. Isopleths are given in milligrams per litre. Dots, sample sites.

basin has been periodically flushed by saline waters that have a high oxygen content. This influx of gulf water has had two major effects. First, mercury, which may have been precipitated in the turning basin when it was more or less closed, is probably undergoing solubilization, reentering the system, and immediately being adsorbed on particulate material. A similar phenomenon has been observed for zinc and cadmium in Corpus Christi Harbor (Holmes and others, 1974). The second effect is that new mercury entering the system is immediately adsorbed on the particulate matter (Cranston and Buckley, 1972) and is flushed from the turning basin by the current.

The low concentration of mercury dissolved in the water supports the contention that most of the mercury is immediately sorbed into suspended matter, a phenomenon also noted by Cranston and Buckley (1972). The particulate material is transported from the turning basin and immediately trapped in the zone of maximum turbidity. As this zone migrates up and down the bay, the mercury-laden suspended material is deposited. This explains the deposit of mercury-rich sediment within Lavaca Bay. This presence of slightly lower concentrations of mercury in sediments in the upper reaches of Lavaca Bay in southern Matagorda Bay reflects such deposition during extremes in the hydraulic cycle, drought conditions causing the sediment trap to move into the upper reaches of Lavaca Bay, and flood conditions pushing this zone into Matagorda Bay. The distribution toward northern sections of Matagorda Bay is a result of the prevailing southeasterly winds. Thus, I suggest that the tidal forces conducted upchannel in Matagorda Bay are ultimately responsible for the introduction of mercury-rich suspended material into the bay. Once trapped within the sediment regime of the estuary, the mercury-rich suspended material is deposited in accordance with the forces acting within the system.

The introduction of open marine water from the gulf via the channel plays an important role in the mercury distribution in this system. In Corpus Christi Bay, a similar phenomenon (Holmes and others, 1974) played a significant role in the transport of metals to the bay system from the harbor area. In both places,

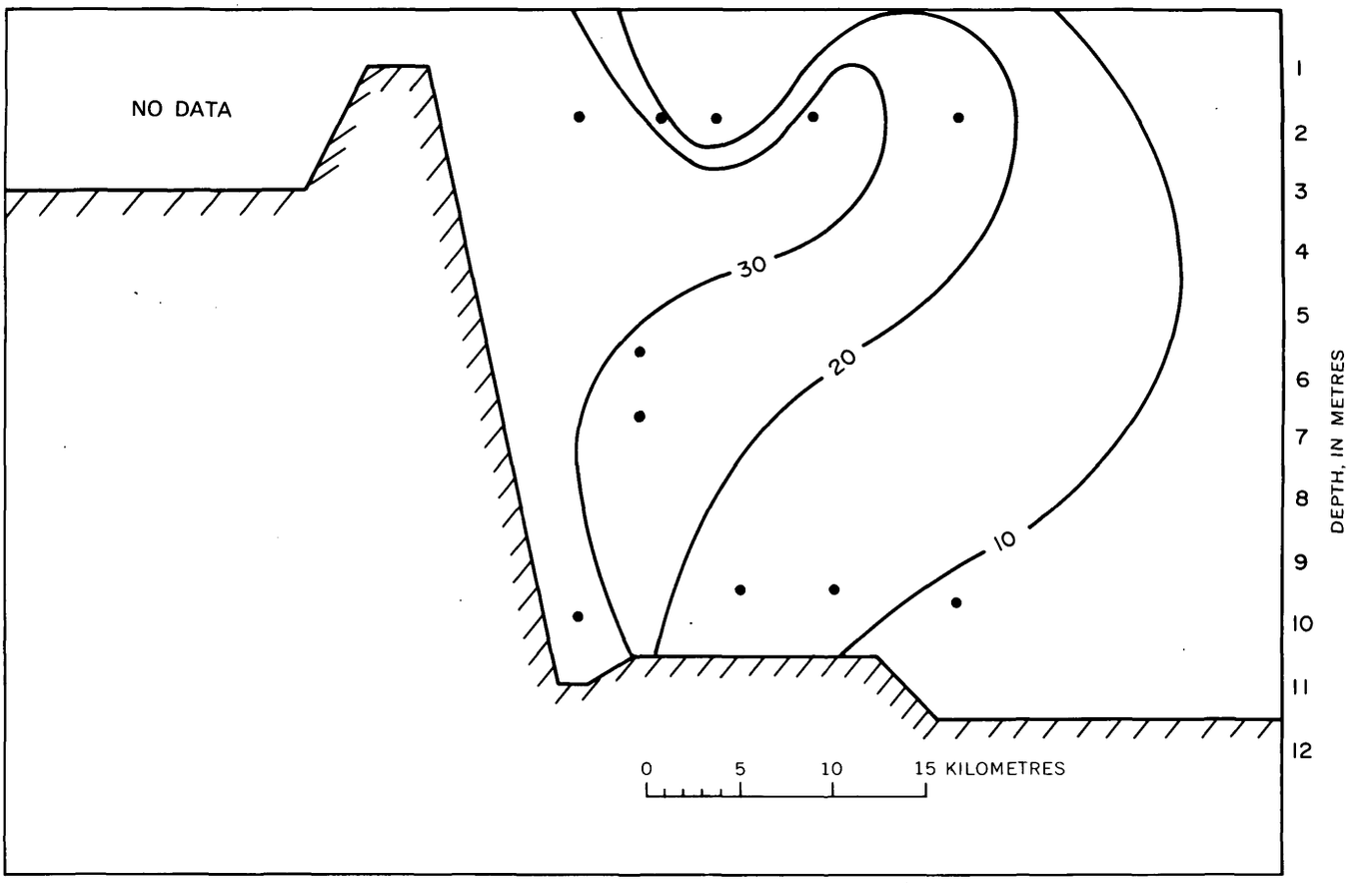

FIGURE 7.—Cross section of the ship channel, showing the distribution of mercury associated with the suspended material dur- the ebbtide phase, October 1, 1973. Isopleths are given in micrograms per gram. Dots, sample sites.

the distributive phenomenon can be directly related to dredge channels. These channels introduce marine waters that have a strong hydraulic head in sufficient strength to disrupt any equilibrium that may have been established and to become a significant factor in the chemistry of the estuarine system.

REFERENCES CITED

Anfalt, Torbjorn, Dyressen, David, Ivanora, Elena, and Jagner, Daniel, 1968, State of divalent mercury in natural waters: Svensk. Kem. Tidsskr., v. 80, no. 10, p. 340–342.

Behrens, E. W., 1965, Use of the Goldberg refractometer as a salinometer for biological and geological field work: Jour. Marine Research, v. 23, no. 2, p. 165–177.

Byrne, J., 1975, Holocene depositional history of Lavaca Bay, Texas Gulf Coast: Austin, Texas, Univ. Texas, Ph. D. dissert., 125 p.

Corpus Christi Caller, 1971, Alcoa removes mercury-laden silt: Corpus Christi Caller, Dec. 29, 1971, p. 12D.

Cranston, R. E., and Buckley, D. E., 1972, Mercury pathways in a river and estuary: Environmental Sci. and Technology, v. 6, no. 7, p. 274–278.

Hahl, D. C., and Ratzlaff, K. W., 1969, Chemical and physical characteristics of water in estuaries of Texas, Sept. 1967–Sept. 1968: Texas Water Devel. Board Rept. [117], 96 p.

——— 1971, Chemical and physical characteristics of water in estuaries of Texas, Oct. 1968–Sept. 1969: Texas Water Devel. Board Rept. [144], 162 p.

——— 1972, Chemical and physical characteristics of water in estuaries of Texas, Oct. 1969–Sept. 1970: Texas Water Devel. Board Rept. [171], 152 p.

Hatch, W. R., and Ott, W. L., 1968, Determination of submicrogram quantities of mercury by atomic absorption spectrophotometry: Anal. Chemistry, v. 40, no. 14, p. 2085–2087.

Hem, J. D., 1970, Chemical behavior of mercury in aqueous media, *in* Mercury in the environment: U.S. Geol. Survey Prof. Paper 713, p. 19–24.

Holmes, C. W., Slade, E. A., McLerran, C. J., 1974, Migration and redistribution of zinc and cadmium in marine estua-

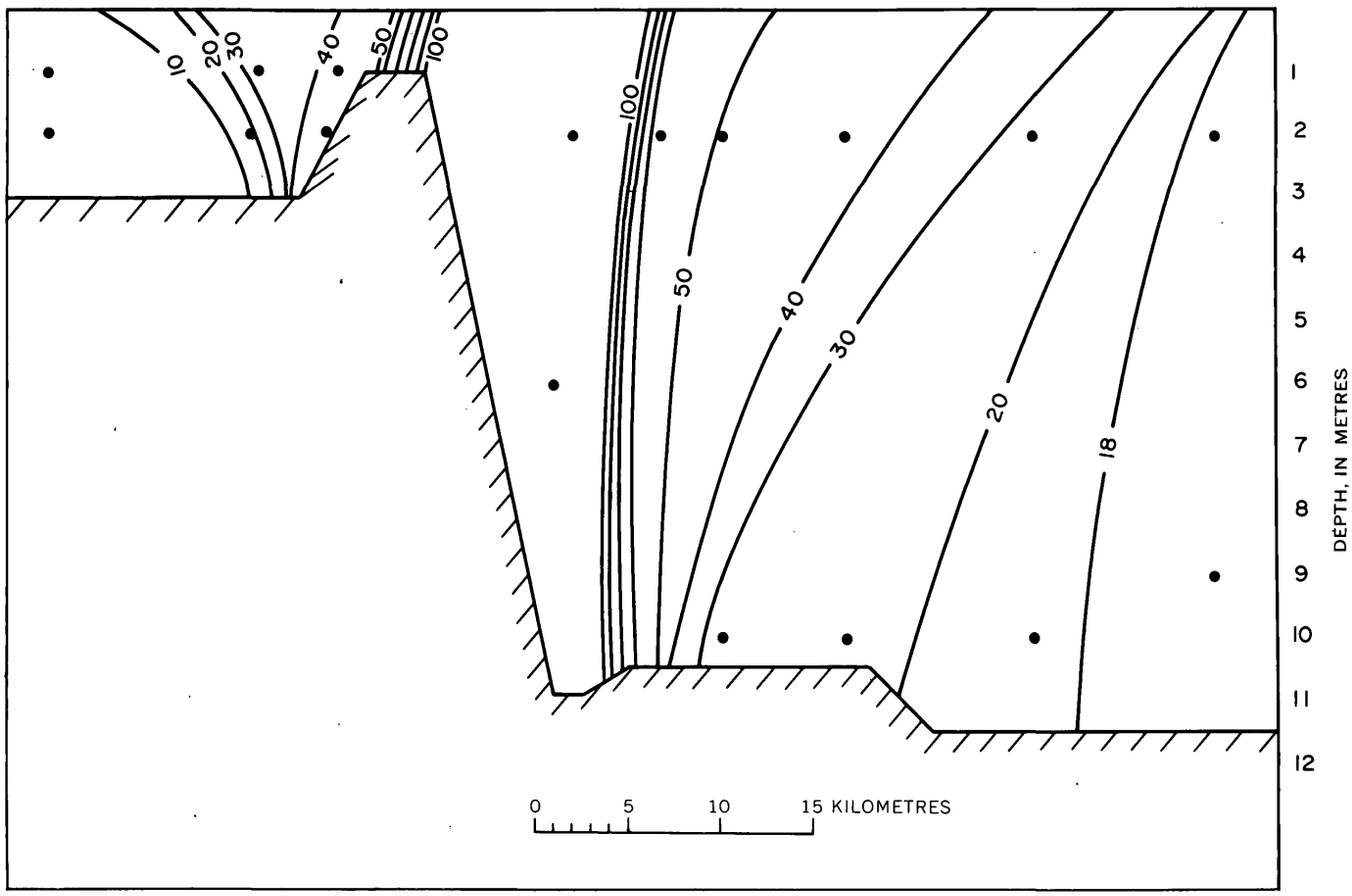

FIGURE 8.—Cross section along the channel, showing the distribution of mercury associated with suspended material during floodtide, December 1, 1973. Isopleths are given in micrograms per gram. Dots, sample sites.

rine system: Environmental Sci. and Technology, v. 8, no. 3, p. 255–259.

Lindberg, S. E., and Harriss, R. C., 1974, Mercury-organic matter associations in estuarine sediments and interstitial water: Environmental Sci. and Technology, v. 8, no. 5, p. 459–462.

Schubel, J. R., 1971, The estuarine environment; estuaries and estuarine sedimentation: Am. Geol. Inst. Short Course Lecture Notes, Wye Inst., Maryland, p. 331.

Vaughn, W. W., 1967, A simple mercury vapor detector for geochemical prospecting: U.S. Geol. Survey Circ. 540, 8 p.

Wood, J. M., 1974, Biological cycles for toxic elements in the environment: Science, v. 183, no. 4129, p. 1049–1052.

Jour. Research U.S. Geol. Survey
Vol. 5, No. 2, Mar.–Apr. 1977, p. 253–262

POSSIBILITY OF TRIGGERING EARTHQUAKES BY INJECTION OF RADIOACTIVE WASTES IN SHALE AT OAK RIDGE NATIONAL LABORATORY, TENN.

By R. J. SUN, Reston, Va.

Work done in cooperation with the U.S. Energy Research and Development Administration

Abstract.—Most investigators generally agree that the conditions for producing earthquakes by fluid injection through wells and by reservoir construction are (1) the presence of an underlying rock that is stressed to the verge of fracturing by tectonic stresses and (or) is on the brink of sliding on preexisting fault planes, (2) the presence of potentially active faults(s), and (3) an increase of pore pressure in the rock caused by fluid injection or seepage from reservoir(s), which is probably the triggering force. The mechanism of disposal of radioactive wastes in shale by grout injection and hydraulic fracturing, which has been used at ORNL (Oak Ridge National Laboratory, Tenn.) is different from injection of fluid. The injected grout is in its liquid phase only during the injection period and, it is to be hoped, is confined in the hydraulically induced bedding-plane fractures. The grout is then allowed to solidify under pressure after termination of the injection, and, after solidification, it becomes an integral part of the shale. Significant characteristics of the disposal method and the site are as follows: (1) Because of the low permeability of shale and high viscosity of the injection grout, pore pressure in the rock, beyond the region of induced fractures, does not increase due to the injections; the injected grout enters newly formed bedding-plane fractures, (2) the injection site is free of local faults and of major interconnected joints and fractures; accordingly, injected grout in its liquid state is expected to be confined principally in the induced nearly horizontal bedding-plane fractures, and (3) due to low tensile strength along shale bedding planes, the energy needed to induce bedding-plane fractures is small; experiments made at ORNL indicate that the energy released during hydraulic fracturing in shale is so small that seismic signals generated by grout injections cannot be differentiated from ambient ground vibrations. In view of the fact that an increase of pore pressure in rock (the triggering force) and association with potentially active fault(s) do not occur at the proposed site at ORNL and that the disposal method does not produce an increase in pore pressure, it can reasonably be concluded that neither the method nor the site has the characteristics for triggering earthquakes during and after grout injections.

The Oak Ridge National Laboratory (ORNL) is selecting a site in Melton Valley, Oak Ridge, Tenn. (fig. 1), within the reservation of the U.S. Energy Research and Development Administration (ERDA), to dispose of radioactive wastes in shale by grout injection and hydraulic fracturing. Because injection of fluid at the U.S. Army's Rocky Mountain Arsenal well, Denver, Colo., from 1962 through 1965, appears to have triggered earthquakes (Evans, 1966), ERDA is interested in knowing whether grout injection and hydraulic fracturing at the selected site has the potential to trigger earthquakes. The U.S. Geological Survey was asked by ERDA to evaluate the possibility of inducing earthquakes by the grout-injection method in general, and, specifically, whether or not the use of this waste-disposal method at the proposed site at ORNL would trigger earthquakes. This paper presents the results of these evaluations.

The mechanism of disposal of radioactive wastes by grout injection and hydraulic fracturing is different from injection of fluid. Radioactive waste is mixed in a cement grout and injected into thick, poorly permeable shale by means of hydraulic fracturing. The injected liquid grout moves radially from the injection well through induced, nearly horizontal bedding-plane fractures in the shale. Upon completion of grout injection, the well-head is sealed, and the injected grout is allowed to solidify under pressure. After solidification, the grout becomes an integral part of the shale (fig. 2). Ideally, during injection, when the grout is still in the liquid state, it is confined to a small part of the shale body. The criteria for disposal of wastes by grout injection and hydraulic fracturing should include the following: (1) well-bedded shale should be at least several hundred feet thick, with nearly horizontal bedding planes, without known faults, and (or) major interconnected joints and fractures and (2) the least principal stress, which is the sum of Earth stress and

FIGURE 1.—Map showing location of the proposed hydraulic-fracturing site and the present hydraulic-fracturing facility site.

tensile strength of shale, should be normal to the nearly horizontal bedding planes so that bedding-plane fractures are induced hydraulically (Sun, 1973).

It should be mentioned at this point that most of the experience of hydraulic fracturing in oil wells indicates that hydraulically induced fractures are generally

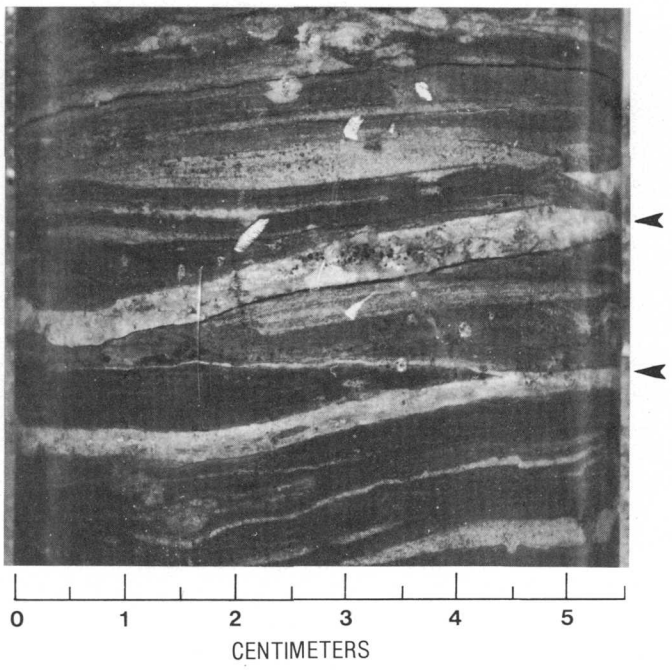

FIGURE 2.—Core showing grout sheet integrated with shale after solidification. Arrowheads indicate grout sheets.

vertical (Hubbert, 1971). However, at particular locations and at a relatively shallow depth, for example, above 2000 ft (600 m), bedding-plane fractures are more easily induced in thick shale than in other formations (Sun, 1973; Sun and Mongan, 1974).

Because only nearly horizontal bedding-plane fractures are to be induced at a site, the dominant waste-injection force applied to the rock during injection should be in a nearly vertical direction. No significant fluid is expected to leak out of the induced fractures during injection, and the fractures will not be closed completely by overburden pressure after solidication of the injected grout. Uplift of the ground surface is expected to result from the injections.

Experiments made at the ORNL site and the site at West Valley, N.Y., indicate that the ground surface had been uplifted by the injections (de Laguna and others, 1968; Sun, 1969; Sun and Mongan, 1974; Weeren, 1974). From 1964 through 1972, a total volume of 2 150 000 gallons (8100 cubic meters) of grout containing 1 345 000 gal (5100 m^3) of wastes had been injected (Sun, 1975, table 11) at the present fracturing facility site at ORNL (fig. 1). The observed maximum ground uplift near the injection well was 0.20 feet (0.06 meters) (Weeren, 1974). Because no visual differences in land surface could be detected, this small amount of uplift could only be determined by precise leveling. As indicated by core drilling, the injected grout is probably confined within a radial distance of 600 ft (190 m) from the injection well (de Laguna and others, 1968, 1971; Weeren, 1974; Sun, 1975).

HISTORY OF MANMADE EARTHQUAKES

In November 1965, Evans (1966) showed a correlation between pressure of fluid injection, the volume of waste injected into a 12 000 ft (3 658 m) disposal well at the Army's Rocky Mountain Arsenal, Denver, Colo., and the number of earthquakes reported in the Denver area. He suggested publicly that the waste injection at the Arsenal well had caused the Denver area earthquakes. Evans' pronouncement created considerable public interest and concern. In December 1965, the U.S. Geological Survey, in cooperation with the Colorado School of Mines, Regis College, and the University of Colorado, undertook a series of studies to determine the relationship, if any, between the disposal of wastes in the arsenal well and the location and frequency of earthquakes. The results of these studies supported Evans' conclusion (Healy and others, 1966).

Because of the strong possibility that waste injection was triggering the earthquakes, the Army decided to shut down the waste disposal well in February 1966. Despite the cessation of deep-well injection, earthquakes continued to plague the Denver area through August 1967. Two earthquakes (magnitude 5.0, April 10, 1967, and magnitude 5.3, August 9, 1967, at a depth of 3 miles or 5 kilometers), the largest in Denver since 1882, were strongly felt throughout the Denver metropolitan area. Because these seismic events occurred 14 to 18 months after termination of the deep-well injection, Major and Simon (1968) concluded that the correlation between fluid injection and earthquake occurrence upon which Evans based his view had been reduced. The overall number of earthquakes in the Denver area, however, has declined exponentially since 1967 (M. W. Major, Colorado School of Mines, oral commun., Feb. 9, 1976). This reduction of earthquake occurrence suggests that tremors in the Denver area were caused by the release of tectonic stresses and that deep-well injection was simply the triggering force.

Since Evans' initial thesis was announced, interest in the triggering of earthquakes by fluid injection has increased. A detailed study at the Rangely Oil Field, Rio Blanco County, Colo., was conducted by the Geological Survey in cooperation with the Chevron Oil Co., regarding the relation between fluid injection for waterflood of the oil field and the number of earthquakes in the area.

In 1969, the Geological Survey installed 16 seismographs around the Rangely Oil Field to obtain detailed data and concluded that (1) there is an apparent cor-

relation between the number of earthquakes and the annual volume of injected fluid, (2) changes in the quantity of injection of fluid are related to changes in the number of earthquakes recorded, and (3) parts of the field without natural faults do not produce earthquakes even when the pore pressures in the rock are quite high (Gibbs and others, 1972). In November 1970, four injection wells straddling a fault zone were backflowed to reduce the pore pressure in the hypocentral region. The wells were backflowed and pumped for a period of 6 months. Within a very short time following the initiation of backflowing, earthquake occurrence within about a 3000-ft (915-m) radius of the wells decreased markedly in frequency and ultimately almost ceased (Raleigh, 1972).

Carder (1945, 1970) associated earthquakes near Hoover Dam, Boulder City, Nev., with the filling of Lake Mead. He suggested that the earthquakes around Lake Mead were directly or indirectly a result of fluctuations in surficial crustal loading. Anderson and Laney (1975), however, offered a different explanation. They suggested that a hydraulic connection between the lake water and the deep aquifer system, which includes buried faults, is needed to cause the release of seismic energy in the Lake Mead area. Where hydraulic connection between the lake and aquifer is prevented by strata of low permeability (evaporites), as in the eastern basin, seismicity does not occur despite the large volume of impounded water in the area.

Schleicher (1975) indicated that the Palisades Reservoir in southeast Idaho also triggers earthquakes. Epicenters are concentrated near the reservoir, and the number of earthquakes is related to water fluctuations in the reservoir. He suggested that the area around the Palisades Reservoir would almost certainly be subject to earthquakes even if the reservoir were not there. The effect of construction of the reservoir was to trigger faulting when tectonic stresses were on the verge of causing it anyway.

Earthquakes attributed to fluctuation of water level and filling of reservoirs are also reported in other parts of the world. For example, Marathon and Kremasta Lakes in Greece, Vajont Dam in Italy, Lake Eucumbene of Snowy Mountains in Australia, Kariba Dam in Rhodesia, and Koyna Dam in India reported small to moderate earthquakes that began a few months after river closure (Carder, 1970). Although all these reservoirs are located in areas that were generally considered aseismic, potentially active or active faults are found in all these reservoirs (Carder, 1970).

Even such events as river flooding have been related to the occurrence of earthquakes. McGinnis (1963) observed that an abnormally high number of earthquake epicenters have been detected within 200 mi (322 km) of New Madrid, Mo. This area is composed of extensive alluvial valleys, is extensively fractured, and shows evidence of many major and minor faults. McGinnis concluded that the correlation of the mean monthly river stage and the earthquake frequency in the alluvial valleys indicates that an increase in the rate of change of water-load variation tends to increase earthquake activity.

TRIGGERING MECHANISM

From the foregoing discussion, it is apparent that the injection of fluid and the construction of dams do have the potential to trigger earthquakes, if rocks are stressed and pore pressure in rock is increased. The mechanism by which earthquakes are triggered is not clearly known. However, most investigators (Healy and others, 1966; Carder, 1970; Gibbs and others, 1972; Schleicher, 1975) generally agree that the following conditions are associated with manmade earthquakes: (1) Rock at the site must be under high stress and near its breaking strength or on the brink of sliding on preexisting fault plane(s), (2) rock is possibly associated with potentially active fault(s), and (3) change of pore pressure in the rock is probably the triggering force. The following is a simple model of rock failure or sliding on a preexisting fault plane due to increase of pore pressure in rock.

Let σ_1, σ_2, and σ_3 be three principal stresses acting mutually at right angles in the Earth's crust. The order of magnitude is represented by subscript number, σ_3 representing the least stress. In such a system, it can readily be seen that, except under conditions of hydrostatic loading (that is, $\sigma_1=\sigma_2=\sigma_3$), there will be three planes of "maximum" shear stress.

The total stress state can be represented by three Mohr circles on the shear (τ) and normal (σ) stress axes (fig. 3), each circle representing the stress state on a different plane. The maximum shear stress in each plane is respectively $(\sigma_1-\sigma_2)/2$, $(\sigma_2-\sigma_3)/2$, and $(\sigma_1-\sigma_3)/2$, of which the latter is the greatest (Farmer, 1968). From the three Mohr circles shown in figure 3, it is concluded that (1) the value of the intermediate principal stress σ_2 does not affect rock failure and (2) the plane of shear fracture passes through the direction of the intermediate principal stress, σ_2; and the normal stress, σ, on the fracture plane makes an angle of α with the plane normal to the principal stress σ_1 (fig. 4).

By equilibrium of forces, the normal and shear stresses shown in figure 4 are given by

$$\sigma=\frac{\sigma_1+\sigma_3}{2}+\frac{\sigma_1-\sigma_3}{2}\cos 2\alpha \qquad (1)$$

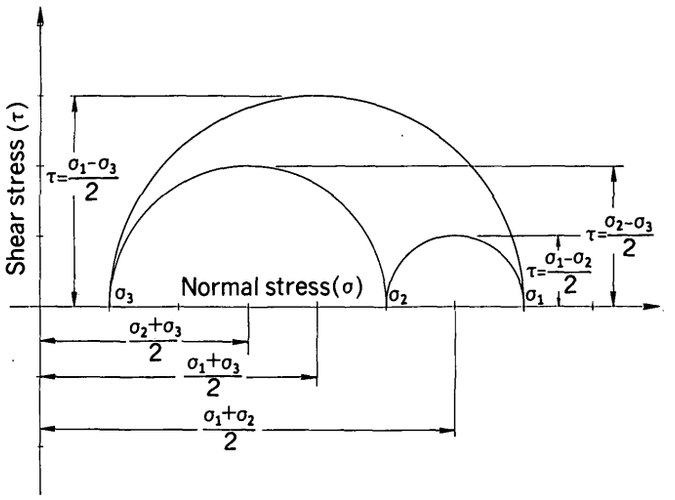

FIGURE 3.—Mohr circles for triaxial stress at a point.

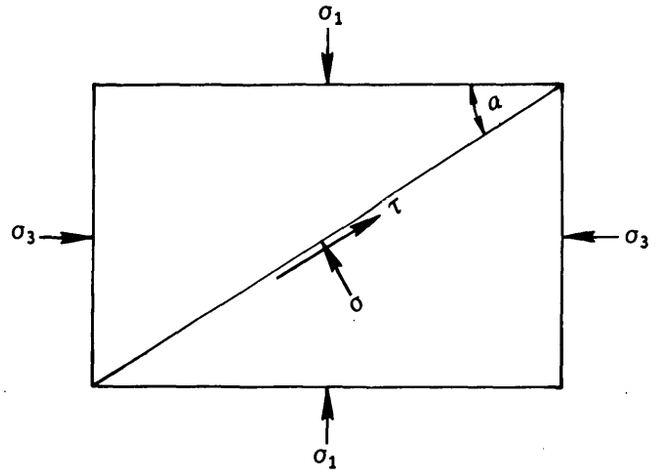

FIGURE 4.—Stresses in a plane.

and

$$\tau = \frac{\sigma_1 - \sigma_3}{2} \sin 2\alpha. \qquad (2)$$

Many investigators (Hubbert, 1951; Anderson, 1951; and Sanford, 1959) used the Coulomb-Navier fracture criteria successfully to explain the mechanics of faulting. The equation for this criterion (fig. 5) is

$$\tau = \tau_0 + \sigma \tan \phi, \qquad (3)$$

where τ_0 is the shear strength of the rock due to cohesion, and ϕ is the angle of internal friction. Both τ_0 and ϕ are characteristics of the rock.

If the rock pores are saturated with water, then the rock is also subject to a hydraulic pressure, p, throughout the interconnected pore space. Thus, the principal stresses in the rock will be decreased to $\sigma_1 - p$, $\sigma_2 - p$, and $\sigma_3 - p$ (Hubbert and Rubey, 1959). By substituting

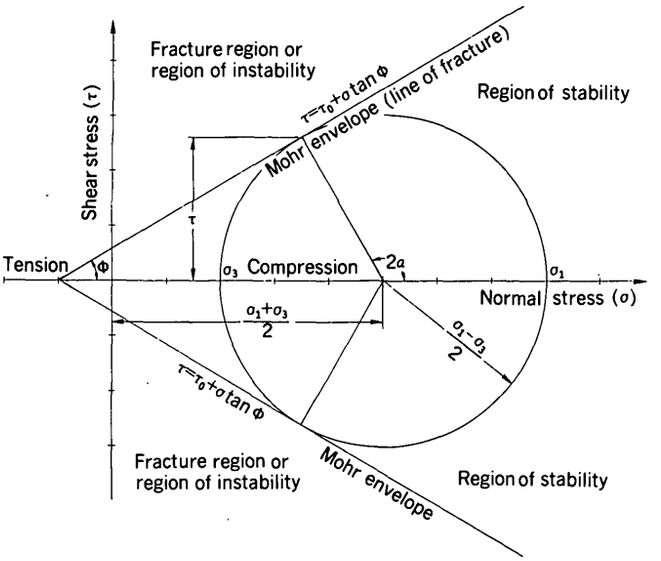

FIGURE 5.—Coulomb-Navier fracture criterion under triaxial stress conditions.

these principal stresses into equations 1 and 2, the effective normal and shear stresses are

$$\sigma = \frac{(\sigma_1 - p) + (\sigma_3 - p)}{2} + \frac{(\sigma_1 - p) - (\sigma_3 - p)}{2} \cos 2\alpha \qquad (4)$$

and

$$\tau = \frac{\sigma_1 - p) - (\sigma_3 - p)}{2} \sin 2\alpha \qquad (5)$$

After simplification, equations 4 and 5 are reduced to

$$\sigma = \frac{(\sigma_1 + \sigma_3)}{2} + \frac{(\sigma_1 - \sigma_3)}{2} \cos 2\alpha - p \qquad (6)$$

and

$$\tau = \frac{\sigma_1 - \sigma_3}{2} \sin 2\alpha. \qquad (7)$$

The relation of pore pressure to rock failure and stability is shown in figure 6. Here, for a rock having no pore pressure (dry) and the constant principal total stresses σ_1, σ_2, and σ_3, a Mohr circle for the stress state, which is within the Mohr envelope, is shown. The rock is, therefore, not subject to fracture and is stable.

Now, without changing the total principal stresses, let the pore pressure in the rock be increased from 0 to p. From equations 6 and 7 it is seen that the diameter of the Mohr circle remains constant but the center of the Mohr circle is moved to the left along the normal-stress axis by a distance equal to the pore pressure, p. In addition, by increasing the pore pressure from p to $p + \Delta p$, the Mohr circle still remains constant in diameter but is translated further to the left by a distance equal to the increase in pore pressure Δp (fig. 6). Obviously, if the pore pressure in the rock increases sufficiently, the Mohr circle will be continuously moved to

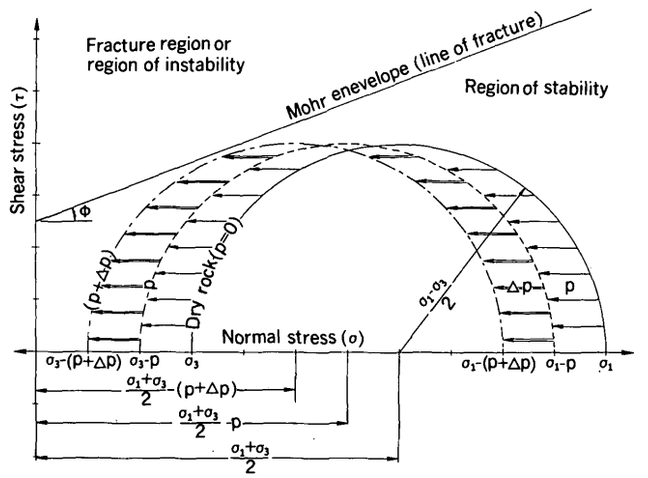

FIGURE 6.—Coulomb-Navier fracture criterion showing how rock failure can be affected by increase of pore pressure (principal stresses are kept constant).

the left until it touches the Mohr envelope and rock failure takes place (Hubbert and Rubey, 1960; Jaeger, 1962). The result of the failure is rock fracturing and (or) sliding on preexisting fault planes.

Injection of fluid and seepage from reservoirs certainly will increase pore pressure in the rock. If rock in the area of potentially active fault(s) has been stressed to the verge of breaking, then the increase of pore pressure would contribute to fracturing or slippage of the rock. Fracturing and (or) slippage of rock would release elastic energy which had already been stored in the rock and could cause earthquakes. Thus, the relation of fluid injection and reservoir seepage to manmade earthquakes is simply that they can trigger faulting—that is, they can modify its timing, intensity, or location—when rock is already stressed to the verge of breaking by tectonic stresses or has the potential to slide on preexisting fault planes.

POSSIBILITY OF TRIGGERING EARTHQUAKES BY GROUT INJECTION AND HYDRAULIC FRACTURING

It is of significance in this evaluation to determine if the disposal of radioactive wastes in shale by grout injection and hydraulic fracturing has the potential to trigger earthquakes such as those caused by fluid injection and reservoir construction. As mentioned before, the mechanism of grout injection and hydraulic fracturing is generally different from injection of fluid. In addition to this difference, it is understood that the disposal sites are to be located only in shale which is locally free of faults and extensive natural fractures and joints. For background information, a brief discussion of suggested procedures for investigating a site and a description of injection techniques that have been used at ORNL and that form a basis for the conclusions drawn herein follow.

During evaluation of a disposal site, at least one core hole should be drilled at the site to obtain geophysical logs and onsite subsurface geologic information including frequency and condition of natural joints and fractures, as well as information on the natural characteristics of rock such as elastic constant and directional tensile strengths. Detailed surface studies of joints and faults in the vicinity of the proposed site are also required.

In addition to the injection well, which should be constructed with a strong steel casing and be pressure grouted from bottom to top, at least four observation wells should be constructed. They should also be constructed with strong casings and should be pressure grouted from bottom to top. These observation wells are located at a radial distance of about 200 ft (60 m) from the injection well and are used to locate the position of induced fractures after each injection test.

At least one water injection and one grout injection should be made at the site to determine whether the site is feasible for disposal of radioactive wastes by grout injection and hydraulic fracturing. Each of the injections should be made with a gamma-energy radioactive isotope as a tracer. The altitude and orientation of induced fractures can be determined by gamma-ray logs of the observation wells before and after the injection, as well as by an analysis of injection pressures. Pressure decay of a water injection can be used to judge whether injected grout can be contained in the induced bedding-plane fractures during its liquid state. The longer the pressure is maintained in the injection well after termination of the water injection, the smaller is the indication that the system is leaking. The absence of fast leakage would suggest that no major interconnected joints and fractures exist in the vicinity of the injection well. One of the site requirements for disposal of radioactive wastes by grout injection is the local absence of faults and of extensive fractures and joints.

Waste injection has been made repeatedly at ORNL at different depths in an injection well, starting near the bottom and moving upward. A 360-degree slot is made in the casing by a hydraulic-jet tool before injection. The slot extends about 12 inches (300 millimeters) into the shale. Several injections can be made through the same slot. After several injections, the injection well is cemented to a new injection depth. A new slot is then made, and the process is repeated.

The injected grout becomes an integral part of the shale after solidification which occurs within 2 to 3

days. Owing to the low permeability of shale and quick solidification of the grout, pore pressure in the shale beyond the induced fracture zone is unlikely to be increased by grout injections. Even during the injection period when the grout is in its liquid state, it is believed that the grout is confined in hydraulically induced bedding-plane fractures because of the low permeability of shale and high viscosity of the grout.

Because the two required and necessary conditions for triggering earthquakes—potentially active fault(s) and an increase of pore pressure—are not associated with the grout-injection method, it is concluded that the possibility of triggering earthquakes by grout injection is very remote. A logical question then is whether earthquakes can be triggered by hydraulic fracturing during grout injections. A discussion of this question follows.

In 1971, the ORNL presented a proposal to the U.S. Atomic Energy Commission (AEC, presently ERDA) that the direction, depth, and extent of hydraulically induced fractures resulting from grout injections could possibly be determined by seismic mapping techniques. The seismic mapping was scheduled to be accomplished by seismic monitoring prior to, during, and following pressure injection. The concept of this technique assumes that rock failure results in strain release of energy which is dissipated by parting failure, or fracturing, thereby causing vibration, or sound waves. These vibrations, when transmitted through the Earth, can be detected by sensitive instruments (large gain and dynamic range). The instruments are tuned for these seismic signals, if the signals are of sufficient magnitude and their spectral content or frequency signature is unique in comparison with ambient vibration noise. The AEC requested the Geological Survey to review the ORNL proposal (Dennis T. Wong, ERDA, oral commun., Aug. 1972). After reviewing the proposal, the author of the present report questioned whether the seismic mapping technique could achieve the goal stated in the proposal. The basis for questioning the usefulness of the technique was that cohesive forces of shale along bedding planes are small; therefore, the energy required to fracture shale is negligible (Sun and Mongan, 1974). Also, the magnitude of ambient ground vibration would be at least as large as the seismic signals, if any, generated by fracturing of shale during injection.

The seismic mapping technique was tested in ORNL by four injections made through a casing slot at a depth of 832 ft (254 m) (Weeren, 1974). An array of six seismometers was installed to obtain seismic signals.

During the first two injections, the seismometer array was approximately 1500 ft (457 m) in diameter; during the last two injections, the diameter was increased to 2000 ft (610 m). A downhole seismometer was installed during the fourth injection to reduce surface noise and to improve sensitivity. The results of the seismic mapping study were inconclusive. As expected, no meaningful seismic signals were obtained from any of the four injections (Weeren, 1974). This indicates that seismic signals generated by hydraulic fracturing are, if they exist at all, so small that they can not be differentiated from ambient ground noise.

POSSIBILITY OF TRIGGERING EARTHQUAKES BY GROUT INJECTIONS AT THE PROPOSED ORNL SITE

Available information from 1699 through 1973 indicates that no earthquake has been reported within 10 mi (16 km) of Oak Ridge (McClain and Myers, 1970; National Oceanic and Atmospheric Administration and U.S. Geological Survey, 1975); however, earthquakes have been reported in the area predominantly to the south and east (fig. 7). The largest earthquake (intensity VII) was recorded near Luttrell, Tenn., on March 28, 1913. Despite this minor seismic activity, no field evidence or documented information on active or potentially active faults in the vicinity of the proposed site can be found.

The proposed new waste disposal site is located about 800 ft (244 m) south of the present fracturing facility site (fig. 1), where 23 grout injections and hydraulic fracturing had been made from 1964 through 1972. No seismicity was observed during these injections at the ORNL seismograph station, which is located about 0.5 mi (0.8 km) east of the present hydraulic fracturing facility site (R. A. Robinson, ORNL, oral commun., Mar. 1976).

The proposed disposal site was tested by one grout injection and one water injection in 1974 and 1975, respectively. Formation of bedding-plane fractures during the injection tests was interpreted from injection pressures and confirmed by gamma-ray logs made in observation wells (Sun, 1975). Pressure decay-time data observed during the water injection in 1975 indicated that no major interconnected fractures and joints exist at the disposal site and that at the injection depth the shale permeability is very low. The shut-in well-head pressure of the water injection was about 2300 pounds-force per square inch (162 kilograms-force per square centimeter); 18 days after termination of the injection, 590 lbf/in^2 (41 kgf/cm^2) of pressure was still recorded at the well head (Sun, unpub. data, 1976). If the shale contains major interconnected joints and fractures at the injection depth, no well-head pressure would have been observed at that time. On the basis of

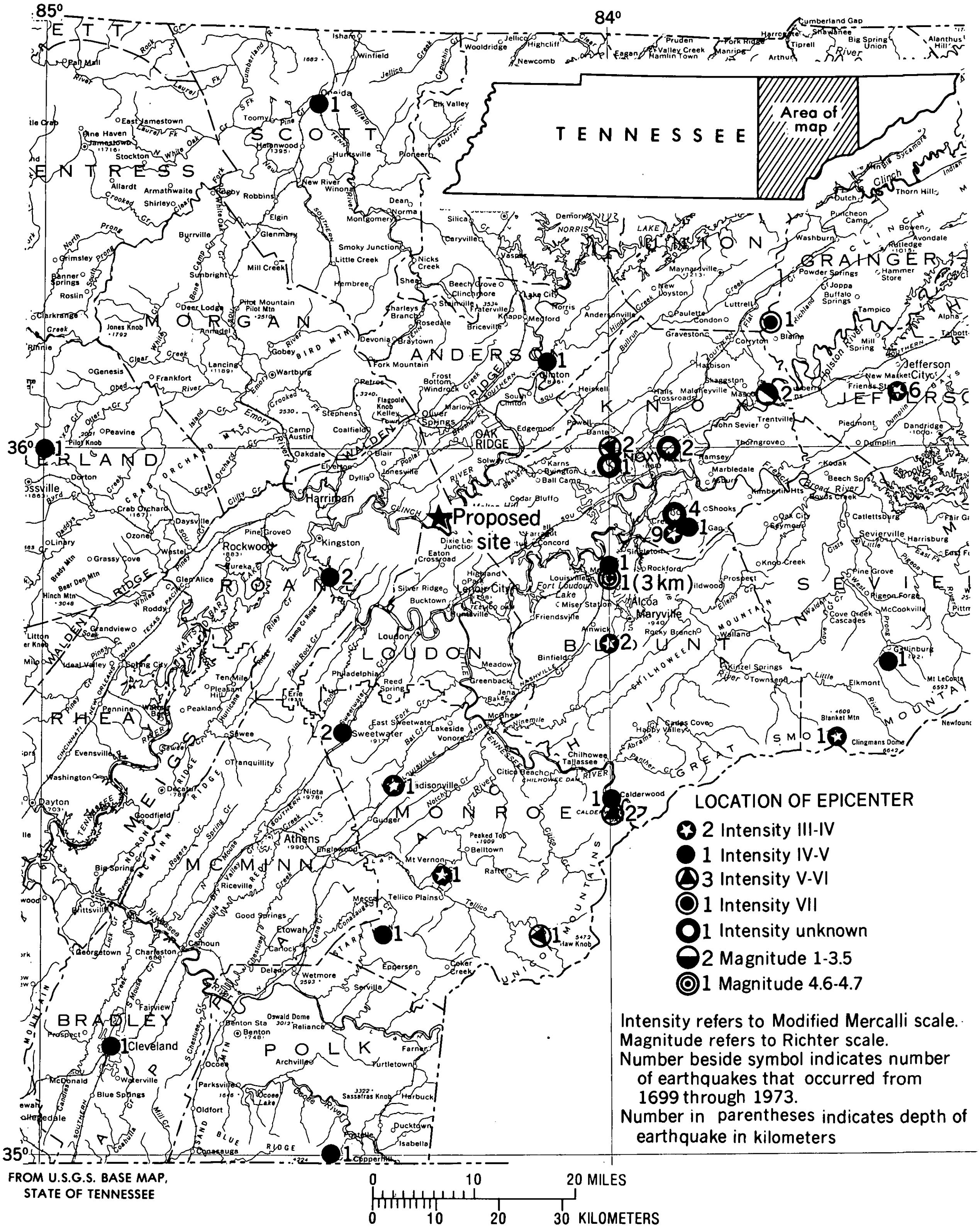

FIGURE 7.—Map showing location of epicenter in the vicinity of Oak Ridge, Tenn., on the basis of available information from 1699 through 1973 (McClain and Myers, 1970).

this information, it is concluded that the proposed site is probably suitable for the purpose of disposal of radioactive wastes by grout injection and hydraulic fracturing using the methods described herein without the risk of triggering earthquakes.

CONCLUSION

Because of the low permeability of shale and high viscosity of the waste-grout mixtures that have been used in waste-disposal operations at ORNL, the injected grout even in its liquid state is believed to be confined within induced horizontal bedding-plane fractures. After solidification, the injected grout is completely integrated with the shale. Therefore, it is concluded that beyond the region of induced fractures, pore pressures in shale would not be increased by grout injection and hydraulic fracturing.

The extension of hydraulically induced fractures is dependent on the applied hydraulic loads; fractures will cease extending when applied pressure falls below a critical level. Thus, the extension of induced fractures is a stable propagation with no dynamic characteristics (Sun and Mongan, 1974). Because of low tensile strength along shale bedding planes, the energy needed to induce bedding-plane fractures in shale is very small; therefore, elastic energy released by hydraulic fracturing during grout injection would be negligible.

The proposed waste disposal site at ORNL has been tested by one grout injection and one water injection. Bedding-plane fractures were induced, and there were no indications of major interconnected joints and fractures. In addition, no field evidence indicates that the injection formation contains faults on the site.

In view of the fact that an increase of rock pore pressure (the triggering force) by fluid injection and association with potentially active fault(s) do not occur at the proposed site at ORNL and that an increase in pore pressure does not result from disposal of radioactive wastes by grout injection and hydraulic fracturing, it can reasonably be concluded that neither the method nor the site has the potential to trigger earthquakes during and after grout injections. The validity of the conclusion is strengthened by the fact that no seismic activity (above ambient noise level) was observed at a seismograph station 0.5 mi (0.8 km) east of the present hydraulic fracturing facility site where 23 grout injections were made from 1964 through 1972.

A precaution, however, can be taken, as suggested by Raleigh (1972), to place seismograph stations near the injection site. If the seismicity increases above the ambient noise level at the site, grout injection should be terminated and further study initiated.

REFERENCES CITED

Anderson, E. M., 1951, The dynamics of faulting: London, Oliver and Boyd, 206 p.

Anderson, R. E., and Laney, R. L., 1975, The influence of late Cenozoic stratigraphy on distribution of impoundment-related seismicity at Lake Mead, Nevada-Arizona: U.S. Geol. Survey Jour. Research, v. 3, no. 3, p. 337–343.

Carder, D. S., 1945, Seismic investigation in the Boulder Dam area, 1940–1944, and the influence of reservoir loading on local earthquake activity: Seismol. Soc. America Bull., v. 35, p. 175–192.

——— 1970, Reservoir loading and local earthquakes: Geol. Soc. America Eng. Geology Case Histories, no. 8, p. 51–61.

de Laguna, Wallace, Tamura, Tsuneo, Weeren, H. O., Struxness, E. G., McClain, W. C., and Sexton, R. C., 1968, Engineering development of hydraulic fracturing as a method for permanent disposal of radioactive wastes: Oak Ridge Natl. Lab. ORNL–4259, 261 p.

de Laguna, Wallace, Weeren, H. O., Binford, F. T., Witkowski, E. J., and Struxness, E. G., 1971, Safety analysis of waste disposal by hydraulic fracturing at Oak Ridge: Oak Ridge Natl. Lab. ORNL–4665, 41 p.

Evans, D. M., 1966, The Denver area earthquakes and the Rocky Mountain Arsenal disposal well: Mtn. Geologist, v. 3, no. 1, p. 23–26.

Farmer, I. W., 1968, Engineering properties of rocks: London, E. & F. N. Spon Ltd., 180 p.

Gibbs, J. F., Healy, J. H., Raleigh, B. C., and Coakley, John, 1972, Earthquakes in the oil field at Rangely, Colorado: U.S. Geol. Survey open-file report, 27 p.

Healy, J. H., Jackson, W. H., and Van Schaack, J. R., 1966, Microseismicity studies at the site of the Denver earthquakes in geophysical and geological investigations relating to earthquakes in the Denver area, Colorado: U.S. Geol. Survey open-file report, pt. 5, 19 p.

Hubbert, M. K., 1951, Mechanical basis for certain familiar geologic structures: Geol. Soc. America Bull., v. 62, no. 4, p. 355–372.

——— 1971, Natural and induced fracture orientation: Am. Assoc. Petroleum Geologists Mem. 18, p. 235–238.

Hubbert, M. K., and Rubey, W. W., 1959, Role of fluid pressure in mechanics of overthrust faulting, part 1: Geol. Soc. America Bull., v. 70, no. 2, p. 155–166.

——— 1960, Role of fluid pressure in mechanics of overthrust faulting—A reply: Geol. Soc. America Bull., v. 71, no. 5, p. 617–628.

Jaeger, J. C., 1962, Elasticity, fracture and flow—with engineering and geological applications: New York, John Wiley, 208 p.

Major, M. W., and Simon, R. B., 1968, A seismic study of the Denver (Derby) earthquakes: Colorado School Mines Quart., v. 63, no. 1, p. 9–55.

McClain, W. C., and Myers, H. O., 1970, Seismic history and seismicity of the southeastern region of the United States: Oak Ridge Natl. Lab. ORNL–4582, 46 p.

McGinnis, L. D., 1963, Earthquakes and crustal movement as related to water load in the Mississippi Valley Region: Illinois State Geol. Survey Circ. 344, 20 p.

National Oceanic and Atmospheric Administration and U.S. Geological Survey, 1975, United States Earthquakes, 1973: U.S. Dept. Commerce and U.S. Dept. Interior, 112 p.

Raleigh, B. C., 1972, Earthquakes and fluid injection: Am. Assoc. Petroleum Geologists Mem. 18, p. 273–279.

Sanford, A. R., 1959, Analytical and experimental study of simple geologic structures: Geol. Soc. America Bull., v. 70, no. 1, p. 19–52.

Schleicher, David, 1975, A model for earthquakes near Palisades Reservoir, southeast Idaho: U.S. Geol. Survey Jour. Research, v. 3, no. 4, p. 393–400.

Sun, R. J., 1969, Theoretical size of hydraulically induced horizontal fractures and corresponding surface uplift in an idealized medium: Am. Geophys. Union Jour. Geophys. Research, v. 74, no. 25, p. 5995–6011.

——— 1973, Hydraulic fracturing as a tool for disposal of wastes in shale, *in* Braunstein, Jules, ed., Underground waste management and artificial recharge—2d International Symposium, New Orleans, La., Sept. 26–30, 1973: Internat. Assoc. Sci. Hydrology Pub. 110, v. 1, p. 219–270.

——— 1975, Geohydrologic evaluation of a site for disposal of radioactive wastes by grout injection and hydraulic fracturing at Holifield National Laboratory (formerly Oak Ridge National Laboratory), Oak Ridge, Tennessee: U.S. Geol. Survey Open-File Rept. 75–671, 77 p.

Sun, R. J., and Mongan, C. E., 1974, Hydraulic fracturing in shale at West Valley, New York—A study of bedding-plane fractures induced in shale for waste disposal: U.S. Geol. Survey Open-File Rept. 74–365, 152 p.

Weeren, H. O., 1974, Shale, fracturing injections at Oak Ridge National Laboratory—1972 series: Oak Ridge Natl. Lab. ORNL–TM–4467.

Jour. Research U.S. Geol. Survey
Vol. 5, No. 2, Mar.–Apr. 1977, p. 263–264

THE QUANTITATIVE DETERMINATION OF CHLOROPHYLLS *A* AND *B* FROM FRESHWATER ALGAE WITHOUT INTERFERENCE FROM DEGRADATION PRODUCTS

By W. THOMAS SHOAF and BRUCE W. LIUM, Doraville, Ga.

Abstract.—Chlorophyll was efficiently extracted from freshwater algae with dimethyl sulfoxide. The extract was chromatographed on commercially available thin-layer cellulose sheets, 2 percent methanol and 98 percent petroleum ether being used as the solvent. Chlorophylls *a* and *b*, and phaeophytins *a* and *b* were cleanly separated from each other and other degradation products. No artifacts were formed. Recoveries of chlorophylls *a* and *b* were 98 and 96 percent as measured by spectrophotometry or fluorometry.

Chlorophyll in natural waters is frequently estimated by trichromatic spectrophotometry of algal extracts. When no interfering compounds are present, these trichromatic equations are good estimates. The major criticism is that in natural plankton extracts, spectrally similar chlorophyll breakdown products are frequently present (Jeffrey, 1968; Daley and others, 1973; Daley, 1973). Thus, chlorophyll cannot be accurately determined by this method. One way to avoid the problem is to chromatographically separate the breakdown products from the chlorophylls before measurement. Separation of the spectrally similar chlorophylls *a* and *b* (as well as degradation products) will result in a more accurate determination of the chlorophylls.

Several chromatographic methods have been published, and most of these utilize thin-layer chromatography to separate the chlorophylls. Thin-layer materials employed have included the following: layers of Kieselguhr G impregnated with triolein, castor oil, or paraffin oil (Daley and others, 1973), layers prepared from glucose shaken with ether (Madgwick, 1965), plates coated with Kieselguhr G impregnated with peanut oil dissolved in isooctane (Jones and others, 1972), and layers of powdered confectioners icing sugar containing 5 percent cornflour suspended in light petroleum (Jeffrey, 1968). These methods apparently work well and are free of artifacts, but the ability to prepare these special thin-layer plates and equipment needed are not present in many laboratories involved in chlorophyll determinations for ecological purposes. The need then exists for a method which can produce good artifact-free separations of the chlorophylls by using inexpensive commercially available materials. The following method utilizes a commercially available precoated cellulose sheet to achieve these results and obtain a high recovery. The method is also compatible with the use of dimethyl sulfoxide, a more efficient chlorophyll extractant than acetone for green algae (Shoaf and Lium, 1976).

DESCRIPTION OF METHOD

Algae (both pure laboratory cultures and natural samples) are filtered through a glass-fiber capable of retaining particles whose diameter is 0.45 micrometre or greater. Each filter is then rolled and placed into a glass tissue grinder; 3 to 4 ml (millilitres) of dimethyl sulfoxide is added, and the sample is ground with a Teflon pestle for 3 min at 500 r/min (revolutions per minute). The sample is transferred to a 15-ml screw-cap graduated centrifuge tube, and the pestle and grinding vessel are rinsed with dimethyl sulfoxide, which was added to the sample. An equal volume (approx 6 ml) of diethyl ether is added, the cap is screwed on, and the sample is shaken vigorously for 10 s (seconds). After waiting an additional 10 s, the sample is again shaken vigorously for 10 s. The cap is removed, and distilled water equal to 25 percent of the total volume is added slowly, almost drop by drop. As the water is added, the dimethyl sulfoxide–diethyl ether solution separates into two immiscible liquids, the dimethyl sulfoxide–water solution on the bottom and the diethyl ether layer containing the green chlorophylls above. The tube is capped and shaken well so that all the chlorophyll migrates into the diethyl ether layer. The sample is centrifuged at $1{,}000 \times g$ (gravity) for 10 min to cleanly separate the two layers and to sediment

the glass filter and algal cell debris. After centrifugation the upper diethyl ether layer containing all the chlorophyll is pipetted off and placed into a 15-ml screwcap graduated centrifuge tube. An equal volume of distilled water is added, and the tube is shaken vigorously for 10 s. The distilled water is added to remove traces of dimethyl sulfoxide dissolved in the diethyl ether layer. The addition of the water will isolate the dimethyl sulfoxide in the water phase where it can be removed. If the dimethyl sulfoxide is not removed, serious trailing will result in the thin-layer chromatography step. The sample is again centrifuged at $1{,}000 \times g$ for 5 min. After centrifugation the upper diethyl ether layer is pipetted off and placed in a 15-ml graduated centrifuge tube. The tube is placed in a 25°C (Celsius) water bath, and the solution is evaporated almost to dryness by blowing nitrogen over the ether surface. When the sample is almost dry, the total volume is brought up to 0.5 ml by the addition of acetone, and the sample is mixed until a uniform solution is obtained. The solvent change from ether to acetone is necessary because of the difficulty in quantitatively removing a given volume from a highly volatile ether solution (low boiling point of 34.6°C).

An aliquot of the acetone solution is removed with a microlitre syringe and streaked onto a thin-layer cellulose sheet (Bakerflex, No. 0–4468) 50×200 mm (millimetres), approximately 15 mm from one end and 6 mm from each side. The thin-layer sheet is then placed in a chromatography tank containing 98 percent petroleum ether (30°–60°C fraction) and 2 percent methanol and allowed to develop in the dark. The approximate time for the solvent to travel to about 20 to 30 mm from the top of the sheet is 30 min. The ratio of petroleum ether to methanol is very critical, and this is the factor most likely to affect the migration rate and separation of the chlorophylls. This solution should be prepared fresh daily because the ratio of the solvents will change as a result of evaporation. After development, spots or streaks of chlorophyll are removed by scraping the cellulose containing the chlorophyll into a screwcapped centrifuge tube and adding 3 ml of 90 percent acetone and mixing. After centrifuging to remove the cellulose, the concentration in the supernatant is determined with a spectrophotometer or spectrofluorometer.

RESULTS AND DISCUSSION

Typical *Rf* (distance traveled by the chlorophyll from the point of application divided by the distance traveled by the solvent from the point of application) values for chlorophylls and degradation products are shown in table 1. Recoveries of pure chlorophylls *a* and *b* were 98 and 96 percent, respectively. Thus chlorophylls *a* and *b* and their phaeophytins may be readily separated and determined by this method. It is not possible to accurately determine chlorophyll *c* by using this method with natural samples for two reasons. In some samples other degradation products of chlorophyll *a* and *b* and phaeophytin *a* and *b* (apparently chlorophylides and phaeophorbides; that is, chlorophylls or phaeophytins missing part or all of the phytol tail) do not migrate but remain at the origin with chlorophyll *c* and phaeophytin *c*, each of which also lacks a phytol tail. Chlorophyll *c* is only sparingly soluble in diethyl ether or acetone. (Merck Index, 1968, p. 245; Jeffrey, 1972), so that total recovery is not possible.

Chlorophyll *a* and *b* are accurately determined by this method without interference from degradation products. The method utilizes commercially available precoated cellulose sheets to achieve separations and obtain a high recovery.

TABLE 1.—*Rf values for chlorophylls and degradation products*

Compound	*Rf*	Color
Phaeophytin *a*	0.89	Gray.
Chlorophyll *a*	.76	Blue green.
Phaeophytin *b*	.61	Greenish yellow.
Chlorophyll *b*	.34	Yellowish green.
Phaeophytin *c*	0	Yellowish green.
Chlorophyll *c*	0	Yellowish green.

NOTE.—Highly purified chlorophylls *a* and *b* were purchased from a commercial source. Chlorophyll *c* was extracted from a freshwater species of *Cyclotella*. The phaeophytins were formed by acidification of the chlorophylls with HCl.

REFERENCES CITED

Daley, R. J., 1973, Experimental lacustrine chlorophyll diagenesis: Archives Hydrology, v. 72, p. 409–439.

Daley, R. J., Gray, C. B. J., and Brown, S. R., 1973, Reversed-phase thin-layer chromatography of chlorophyll derivatives: Jour. Chromatography, v. 76, p. 175–183.

Jeffrey, S. W., 1968, Quantitative thin-layer chromatography of chlorophylls and carotenoids from marine algae: Biochim. Biophys. Acta, v. 162, p. 271–285.

——— 1972, Preparation and some properties of crystalline chlorophyll c_1 and c_2 from marine algae: Biochim. Biophys. Acta, v. 279, p. 15–33.

Jones, I. D., Butler, L. S., Gibbs, E., and White, R. C., 1972, An evaluation of reversed phase partition for thin-layer chromatographic identification of chlorophylls and derivatives: Jour. Chromatography, v. 70, p. 87–98.

Madgwick, J. C., 1965, Quantitative chromatography of algal chlorophylls on thin layers of glucose: Deep-Sea Research, v. 12, p. 233–236.

Merck Index, 1968, The Merck Index [8th ed.]: Rahway, N. J., Merck and Co., 1,713 p.

Shoaf, W. T., and Lium, B. W., 1976, Improved extraction of chlorophyll *a* and *b* from algae using dimethyl sulfoxide: Limnology and Oceanography, v. 21, no. 6, p. 926–928.

Jour. Research U.S. Geol. Survey
Vo. 5, No. 2, Mar.–Apr. 1977, p. 265–276

PHYTOPLANKTON DISTRIBUTION AND PRIMARY PRODUCTIVITY IN DONNER LAKE, CALIFORNIA

By ALEX E. DONG and ROBERT C. AVERETT, Sacramento, Calif.

Prepared in cooperation with the California Department of Water Resources

Abstract.—Donner Lake is an unenriched system in the Lake Tahoe basin of the Sierra Nevada of California. The lake has a surface area of 1.5 square miles (3.9 square kilometres) and a drainage area of 14 mi² (36 km²). The maximum depth is about 200 feet (60 metres). Between May and December 1973, the phytoplankton in Donner Lake was represented by 6 classes and at least 25 genera. The dominant green alga was the desmid *Cosmarium staurastroides*, which comprised about 25 percent of the total phytoplankton collected. The dominant diatom was *Asterionella formosa*, which comprised about 13 percent of the total phytoplankton. Blue-green algae were represented by *Chroococcus* sp., but were never abundant and constituted only 1.5 percent of the total organisms sampled. The depth of the euphotic zone from May through September ranged from 35 to 93 feet (11 to 28 metres). Thermal stratification was strong throughout the summer with a maximum temperature difference between the surface and bottom water of 17° Celsius in July. Average phytoplankton concentrations were often greater below the euphotic zone than in the euphotic zone. This pattern of phytoplankton distribution is similar to nearby Lake Tahoe and other oligotrophic lakes. Three primary productivity measurements were made during the study using the carbon-14 method. The primary productivity values were 93, 64, and 56 milligrams of carbon per cubic metre per day for May 17, August 13, and October 16, respectively. The productivity profile in May was shallow and unimodal, whereas the August and October profiles were deeper and biomodal. Dissolved-oxygen concentrations were maximum at the same depths as maximum primary productivity. On the basis of phytoplankton types and their vertical distribution patterns, and upon primary productivity measurements, Donner Lake is considered oligotrophic.

Lakes in the Tahoe Basin of the Sierra Nevada of California are used heavily throughout the year for recreation. Many of the lakes in the basin have summer homes and commercial establishments along their shorelines. The increased use of these lakes has resulted in a renewed interest by regulatory agencies to assess changes in water quality and protect the lakes from excessive enrichment from sewage disposal.

Donner Lake in the Tahoe Basin is a small lake that has become a popular recreation area in recent years. Along the shoreline of Donner Lake are a number of private dwellings, commercial establishments, and a large state-operated campground. Until recently, domestic wastes in the Donner Lake basin received only septic tank treatment. A sewage system has been constructed and waste material is now transported out of the basin.

As part of a comprehensive lake study program in cooperation with the California Department of Water Resources, the California district of the U.S. Geological Survey made a water-quality study of Donner Lake from May through December, 1973. The study of Donner Lake not only offered an opportunity to evaluate water-quality conditions in a small basin undergoing extensive shoreline development, but also an opportunity to gather basic limnological information on a high-altitude dilute-solution system (Dong, 1975).

This paper is concerned with phytoplankton types and distribution and primary productivity in Donner Lake.

DESCRIPTION AND PHYSICAL SETTING

Donner Lake is about 80 miles (130 kilometres) northeast of Sacramento and about 12 mi (20 km) northwest of Lake Tahoe. The lake is adjacent to Interstate Highway 80, the main northern California trans-Sierra highway, and is easily accessible from San Francisco and Sacramento in California, Reno, Nev. and Lake Tahoe recreation areas (fig. 1).

The surface area of Donner Lake is 1.5 mi² (3.9 km²). The altitude of the lake is 5,933 feet (1,808 metres) above mean sea level. The lake volume is regulated by a small dam on the outlet, Donner Creek, resulting in a usable capacity of 9,500 acre-ft (11.7 cubic hectometres) of water. The 14 mi² (36 km²) drainage area of the Donner Lake basin is covered by coniferous forests. Three tributaries, Lakeview Creek, Billy Mack Creek, and Negro Creek enter at the west end of the

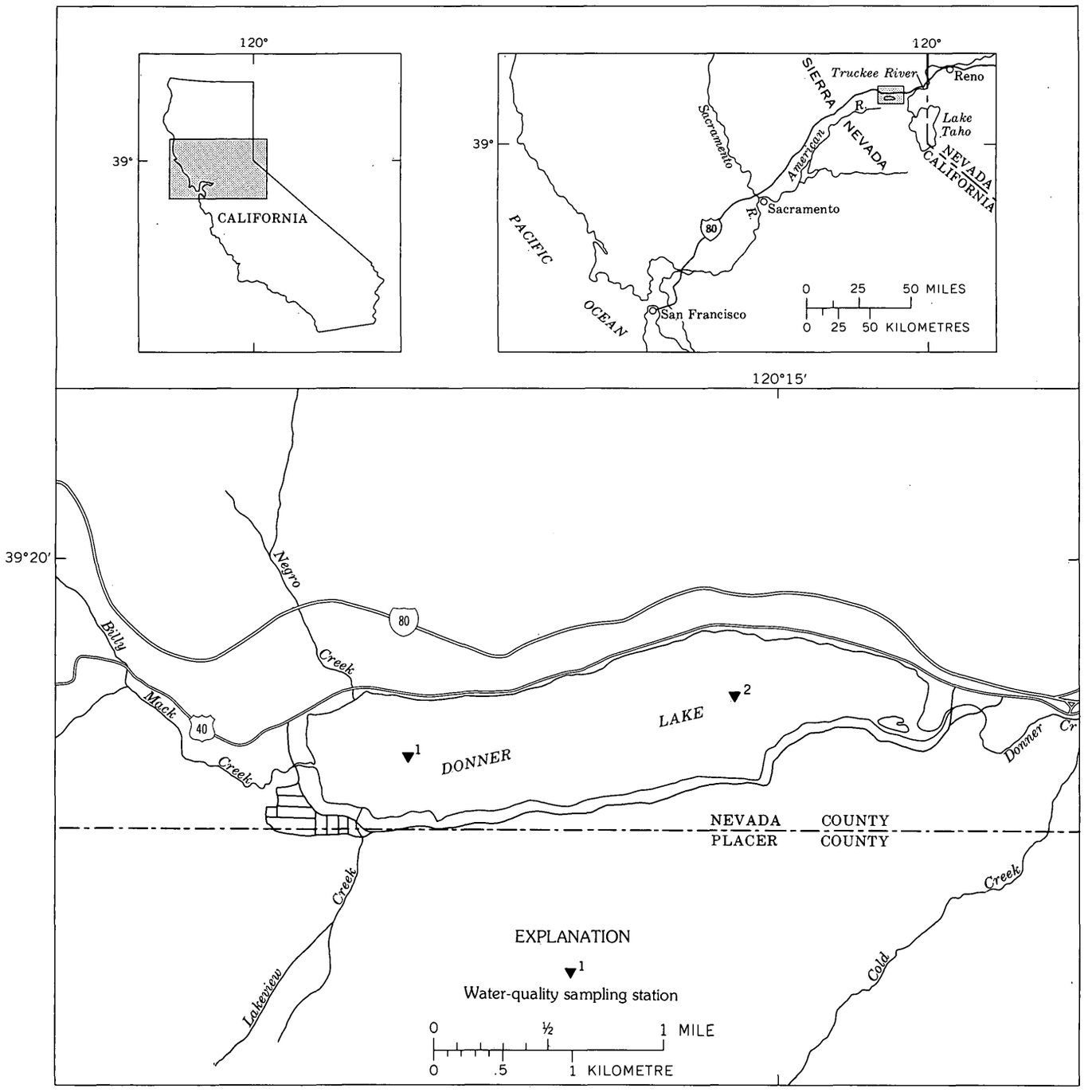

FIGURE 1.—Index map showing location of study area.

lake. Donner Creek, the outlet, flows eastward into the Truckee River.

Donner Lake was formed in volcanic and glacial deposits. The west end of the watershed consists of recent surficial undifferentiated deposits of silt, clay, and fine sand. The north, east, and south shores of the lake consist of various types of Pleistocene glacial deposits, namely unsorted boulders, gravel moraines, sand and gravel outwash, and minor alluvial deposits. Underlying the Holocene and Pleistocene deposits are an andesite breccia, tuff breccia, and andesite flows, (R. W. Birkeland, written commun., 1961).

Abundant snowfall and subzero temperatures are common in winter. The lake is usually ice covered from January to April. The long-term average January air temperature is 27°F (−3°C). Summers are

cool and dry with a long-term average July temperature of 61°F (16°C). Long-term average annual precipitation is about 45 inches or 1,143 millimetres (California Region Framework Study Committee, 1971, Map 37). Average annual evaporation from the lake is estimated to be 36 in or 914 mm (California Region Framework Study Committee, 1971, May 7).

METHODS

Water samples were collected for phytoplankton analyses at stations 1 and 2 (fig. 1). Samples were collected once monthly during May, August, October, and December, and twice monthly in June and July. Carbon-14 primary productivity measurements were made and water samples for chlorophyll analyses were collected at station 1 on May 17, August 13, and October 16, 1973. Samples were not collected between January and April when the lake surface was frozen.

Water samples for phytoplankton analyses were collected with a 1-gallon (4-litre) PVC (polyvinyl chloride) water sampler at depths near or within 0, 12–16, 28–33, 82–98, and 147–180 ft (0, 4–5, 9–10, 25–30, and 45–55 m) ranges. The intermediate depths were immediately above, at, and below the metalimnion at the period of sampling. The 147–180 ft (45–55 m) range corresponded to depths near the lake bottom at the two sampling stations. Water samples for chlorophyll-*a* analyses and carbon-14 primary productivity measurements were collected with a PVC water sampler at depths corresponding to light transmission values of 60, 30, 20, 10, 5, and 1 percent of the surface light. Carbon-14 primary productivity measurements were made using the method described by Slack and others (1973, p. 99). Sample filters were counted using a liquid-scintillation apparatus at the U.S. Geological Survey Radiochemical Laboratory.

Water samples containing phytoplankton were preserved by addition of 2.5 ml of Lugol's solution to every 250 ml of sample. Chlorophyll-*a* samples were frozen from the time of collection until analyzed by personnel of the U.S. Bureau of Reclamation in Sacramento. Analyses were made using the methods described by Strickland and Parsons (1968, p. 188).

Phytoplankton was identified to genus, and when possible, to species, using the inverted microscope method described by Slack and others (1973, p. 72).

Measurements of water temperature and dissolved oxygen were made using a multiparameter instrument. Light transparency was measured with a submarine photometer.

RESULTS

Physical measurements

The temperature of the lake water and the depth of the euphotic zone (that part of the lake from the surface to the depth at which 1 percent of the surface light is present; also known as compensation depth) were measured during all visits at each station. These measurements were made because one of the study objectives was to relate phytoplankton distribution and abundance to the position of the metalimnion and to the euphotic zone.

Thermal pattern

In 1973, thermal stratification in Donner Lake probably began in late April. By mid-May a weak metalimnion was present (fig. 2, graphs *A* and *B*). By July 31 there was a 17°C temperature difference between the top and bottom water of the lake and a well-pronounced metalimnion extending from about the 23- to 72-ft (7- to 22-m) depth (fig. 2, graphs *I* and *J*). The bottom water of the lake was consistently about 5°C, but occasionally 4°C was recorded. Beginning in September the surface water of the lake began to cool, resulting in a reduction in the temperature difference between the surface and bottom water (fig. 2, graphs *M* and *N*). By mid-October, the temperature difference between the surface and bottom water had been reduced to about 7°C and the metalimnion was between the 50- to 98-ft (15- to 30-m) depth (fig. 2, graph *P*). Autumn overturn apparently occurred in November because by early December the lake was homothermous (fig. 2, graphs *Q* and *R*). The depth of the metalimnion at the two sampling sites is given in table 1.

Depth of euphotic zone

The euphotic zone ranged from 35 to 93 ft (11 to 28 m) in depth (table 1). There was little difference

TABLE 1.—*Approximate depth of metalimnion and compensation level*

[See figure 1 for location of stations]

Date (1973)	Depth below water surface, in metres			
	Station 1		Station 2	
	Metalimnion	Compensation level	Metalimnion	Compensation level
May 16–17	1–10	11	1–10	11
June 7	1–10	18	1–10	17
June 21	1–15	11	1–15	11
July 11	5–25	21	5–25	26
July 31	8–20	24	7–22	24
Aug. 13	8–20	24	8–20	24
Sept. 13	12–22	24	12–25	24
Oct. 16	15–30	27	15–30	28
Dec. 6	None	15	None	12

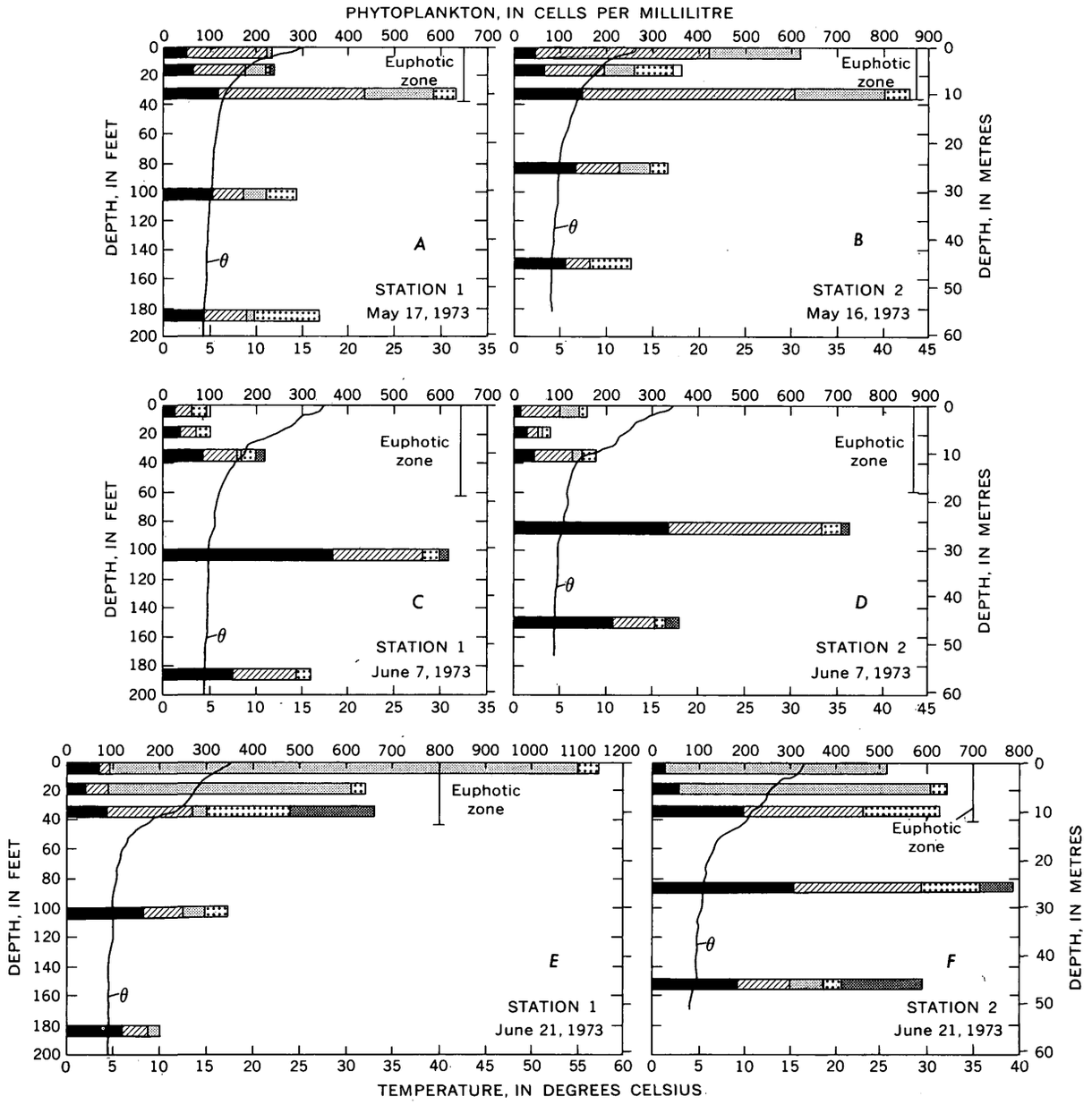

FIGURE 2.—Water-temperature profiles and vertical distribution of phytoplankton by class.

in the depth of the zone between the two sampling stations at any sampling period. Maximum depths were recorded in summer and early autumn when phytoplankton numbers were low in the surface water of the lake.

Phytoplankton species composition

The phytoplankton in Donner Lake was represented by six classes and at least 25 genera (table 2). The percentage values given in table 2 are derived from all samples collected between May and December 1973 (Dong, 1975).

The green algae (Class Chlorophyceae) were dominated by the desmid *Cosmarium staurastroides*, which comprised about 99 percent of the green algae and about 26 percent of the total cells of all groups. Although *C. staurastroides* was found in all samples, it was particularly abundant from July through September.

The dominant diatoms (Class Bacillariophyceae) were *Asterionella formosa*, followed by *Synedra tenera* and *Rhizosolenia* sp. The 9 species of diatoms comprised about 30 percent of the total phytoplankton in all the samples.

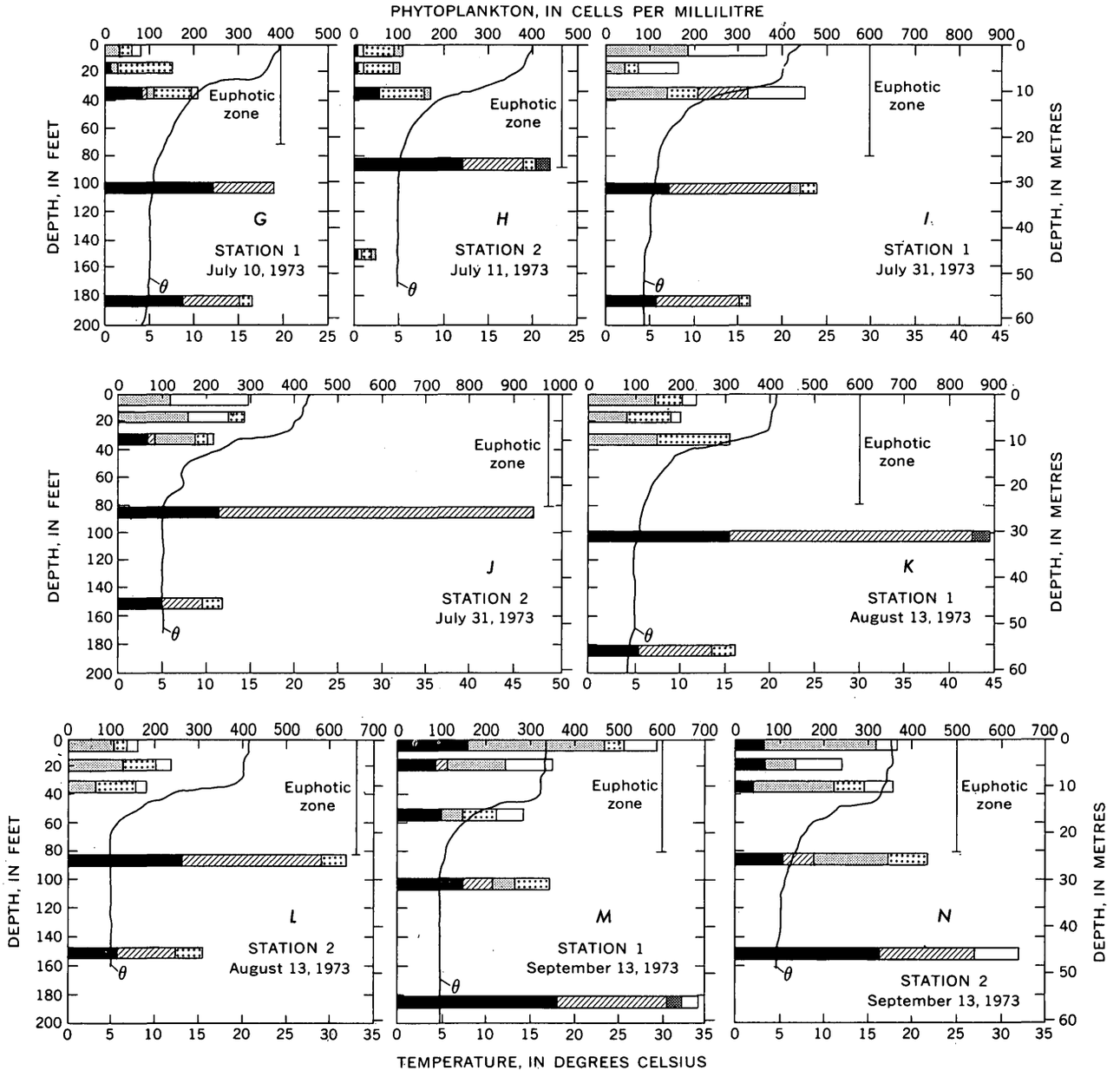

FIGURE 2.—Continued

The yellow-brown algae (Class Chrysophyceae) were represented by at least five genera. A group of unidentified forms were included in this class. The unidentified forms comprised about 13 percent of the Chrysophyceae, but only about 3 percent of the total phytoplankton in all the samples.

The flagellates (Class Cryptophyceae) in Donner Lake were extremely difficult to identify, and the taxonomy of most of the flagellates is still unknown. The unidentified group, seemingly of a single genus, comprised about 95 percent of the flagellates. Flagellates were present in every sample, but were never abundant.

Blue-green algae (Class Myxophyceae) were sparse in the Donner Lake samples. The class was dominated by *Chroococcus* sp., but overall the class comprised only about 2 percent of the total organisms collected. Blue-green algae were found only in the June 7 and August 13 samples.

The dinoflagellates (Class Dinophyceae) were dominated by an unknown genus having *Peridinium*-like characteristics and were thus designated as such in table 2. Dinoflagellate occurrence was erratic and members of the class were not found on all sampling dates.

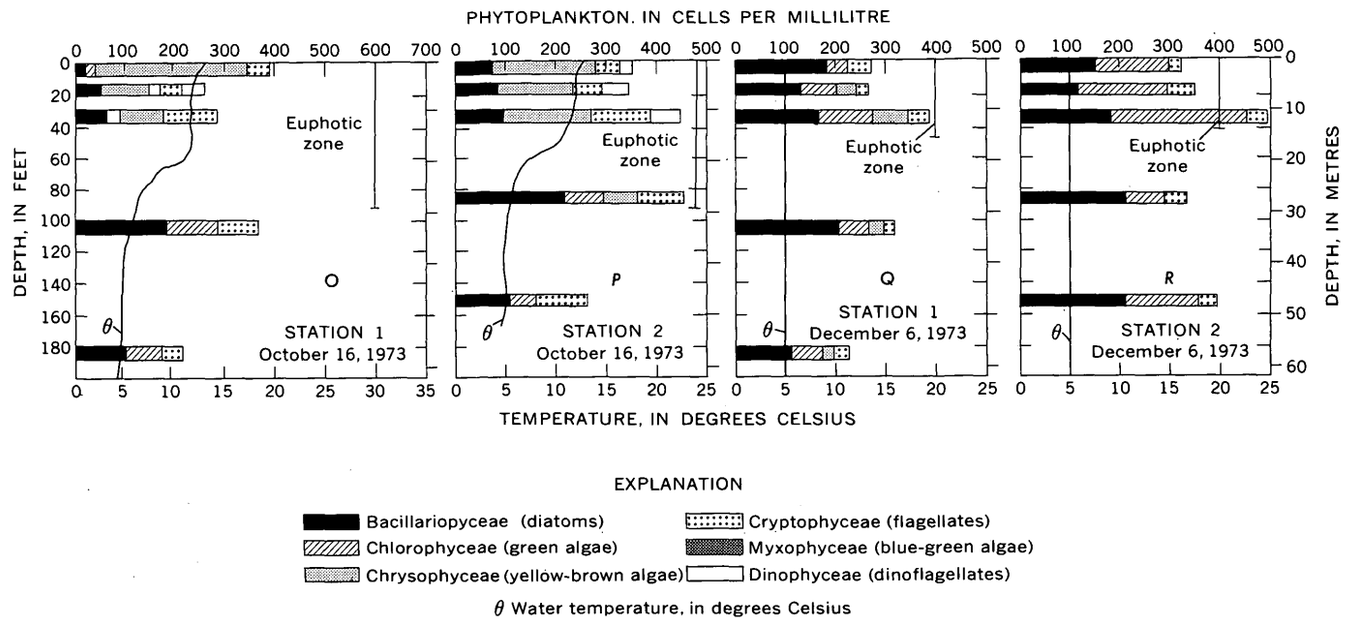

FIGURE 2.—Continued

Depth distribution of phytoplankton

The depth distribution of phytoplankton in Donner Lake was similar at the two sampling stations throughout the entire sampling periods (fig. 2). The influence of thermal stratification on the vertical distribution of phytoplankton was apparently insignificant because the distribution of algal cells varied with depth; whereas the thermal pattern remained approximately the same throughout the summer and autumn. Note, however, that phytoplankton concentrations were measured at discrete depths (point samples) rather than continuously with depth. The abundance of phytoplankton at particular depths could have been missed with this sampling scheme.

In May the greatest concentration of phytoplankton was between the surface and the 32-ft (10-m) depth. On June 7, phytoplankton numbers were highest at the 98-ft (30-m) depth, but on June 21 the phytoplankton was again concentrated between the surface and 32-ft (10-m) depth at station 1 (fig. 2, graph *E*). However, at station 2 there was a rather large concentration of cells at the 82- and 148-ft (25- and 45-m) depths (fig. 2, graph *F*). The phytoplankton concentration was relatively low on July 10 and 11, when the greatest concentration (about 400 cells/ml) was found near the 98-ft (30-m) depth (fig. 2, graphs *G* and *H*). On July 31 and August 13, cell densities were again highest at the 98-ft (30-m) depth (fig. 2, graphs *I*, *J* and *K*). The phytoplankton concentrations on September 13 were highest at the surface and near the bottom. The September maximum was near the 185-ft (56-m) depth at station 1 and the 147-ft (45-m) depth at station 2 (fig. 2, graphs *M* and *N*). On October 11, the greatest concentrations were at the surface, 32- and 98-ft (10- and near 30-m) depths. The December 6 samples, the last collected for the study, contained the greatest number of phytoplankton at the 32-ft (10-m) depth. Cell concentrations at the 148-ft (45-m) depth were also relatively high at station 2 in December.

Phytoplankton concentration and the euphotic zone

The comparison of the depth distribution of phytoplankton to the location of the euphotic or lighted zone is informative. Phytoplankton require light for photosynthesis; however, the organisms are not always most abundant in the euphotic zone. In Donner Lake, the average concentration of phytoplankton above and below the euphotic zone varied erratically between sampling periods, but only slightly between the two sampling stations (fig. 3).

The results in figure 3 are average values, based on three discrete depth samples from the euphotic zone and two discrete depth samples below the euphotic zone. This sampling scheme is biased because the depth of the euphotic zone was always less than one-half and often less than one-third of the depth of the lake at the sampling sites. Consequently, more intensive sampling per unit was made in the euphotic zone than below the euphotic zone. The results are useful, however, because they illustrate that at times more phytoplankton was found below than in the euphotic zone.

TABLE 2.—*Types and abundance of phytoplankton, May–December 1973*

Types	Abundance Percentage of class	Percentage of total
Chlorophyceae (green algae):		
Cosmarium staurastroides	99.0	26.0
Cosmocladium sp.	<1	<1
Unidentified	1.3	<1
Total	----	26.0
Bacillariophyceae (diatoms):		
Asterionella formosa	43.0	13.0
Fragilaria crotonensis	<1	<1
Melosira granulata	<1	<1
Melosira italica	4.3	1.3
Nitzschia sp	<1	<1
Rhizosolenia sp	22.0	6.7
Synedra delicatissima	<1	<1
Synedra tenera	30.0	8.8
Synedra sp	<1	<1
Total	----	30.0
Chrysophyceae (yellow-brown algae):		
Chrysochromulina parva	26.0	6.7
Chrysochromulina sp	17.0	4.5
Dinobryon sertularia	1.6	<1
Dinobryon sp	43.0	11.0
Unidentified	13.0	3.3
Total	----	26.0
Cryptophycaea (flagellates):		
Cryptomonas sp	4.0	<1
Unidentified	95.0	12.0
Total	----	13.0
Myxophyceae (blue-green algae):		
Chroococcus sp	80.0	1.5
Unidentified	20.0	<1
Total	----	1.9
Dinophyceae (dinoflagellates):		
Glenodinium sp	14.0	<1
Gymnodinium sp	12.0	<1
Peridinium sp	24.0	1.2
Peridinium-like	50.0	2.4
Total	----	4.8
Miscellaneous group ciliates	100	<1

The average number of phytoplankton in and below the euphotic zone was approximately equal at station 1 on May 17, but was greater than below the euphotic zone at station 2. The samples obtained on June 7 contained more phytoplankton below than in the euphotic zone. On June 21, the average number of phytoplankton in the euphotic zone at station 1 was three times the average number below the euphotic zone. In July and August, the average number of phytoplankton was greatest below the euphotic zone, whereas in September, October, and December the average number of phytoplankton in and below the euphotic zone was about equal. The phytoplankton below the euphotic zone probably was passively sinking, and was the result of previous algal production in the euphotic zone. Sample collection periods for this study were not spaced closely enough to follow the biomass of a particular type from the euphotic to the noneuphotic zone.

When the composition of phytoplankton found in and below the euphotic zone is examined, the relation between classes of phytoplankton and relative abundance in the euphotic zone shows no recurring pattern (fig. 4). For example, on June 7, the Chrysophyceae (yellow-brown algae) made up only 4 percent of the phytoplankton in the euphotic zone. None were found in water samples collected below the euphotic zone. Two weeks later (June 21) the Chrysophyceae made up 64 percent of the phytoplankton in the euphotic zone, and 15 percent of the phytoplankton below the euphotic zone. On July 11, 20 days later, the Chrysophyceae were found only in the euphotic zone, where they made up 18 percent of the total phytoplankton. Although the Chrysophyceae were usually found in the euphotic zone, the Chlorophyceae (green algae) were most frequently found below the euphotic zone throughout the study. In May when thermal stratification was weak, and in December when the lake was homothermous, the percentage composition of phytoplankton above and below the euphotic zone was nearly equal.

PRIMARY PRODUCTIVITY

Primary productivity in Donner Lake was measured only at station 1. Measurements were made on May 17, August 13, and October 16, 1973. Paired incubation bottles were suspended at depths corresponding to light transmissions values of 60, 30, 20, 10, 5, and 1 percent of the surface light. The 1-percent light value was considered the compensation depth. The actual depths corresponding to these light values for the three sampling periods are shown in table 3. As mentioned in "Methods," water samples for chlorophyll-*a* analysis were collected at the same depths that primary productivity was measured. The dissolved-oxygen concentration was determined at 1-m intervals.

Primary productivity profiles, as well as chlorophyll-*a* and dissolved-oxygen profiles, are shown in figure 5. Phytoplankton concentration and depth distribution taken from figure 2 (graphs *A*, *K*, and *O*) also are included in figure 5. Water samples for phytoplankton

TABLE 3.—*Light transparency at station 1*

Transparency, in percentage of surface light	Depth, in metres		
	May 17, 1973	Aug. 13, 1973	Oct. 16, 1973
60	1.4	1.0	1.0
30	3.0	6.0	5.8
20	3.9	9.0	8.0
10	5.4	13.5	12.5
5	7.2	17	16.5
1	11	24.0	27

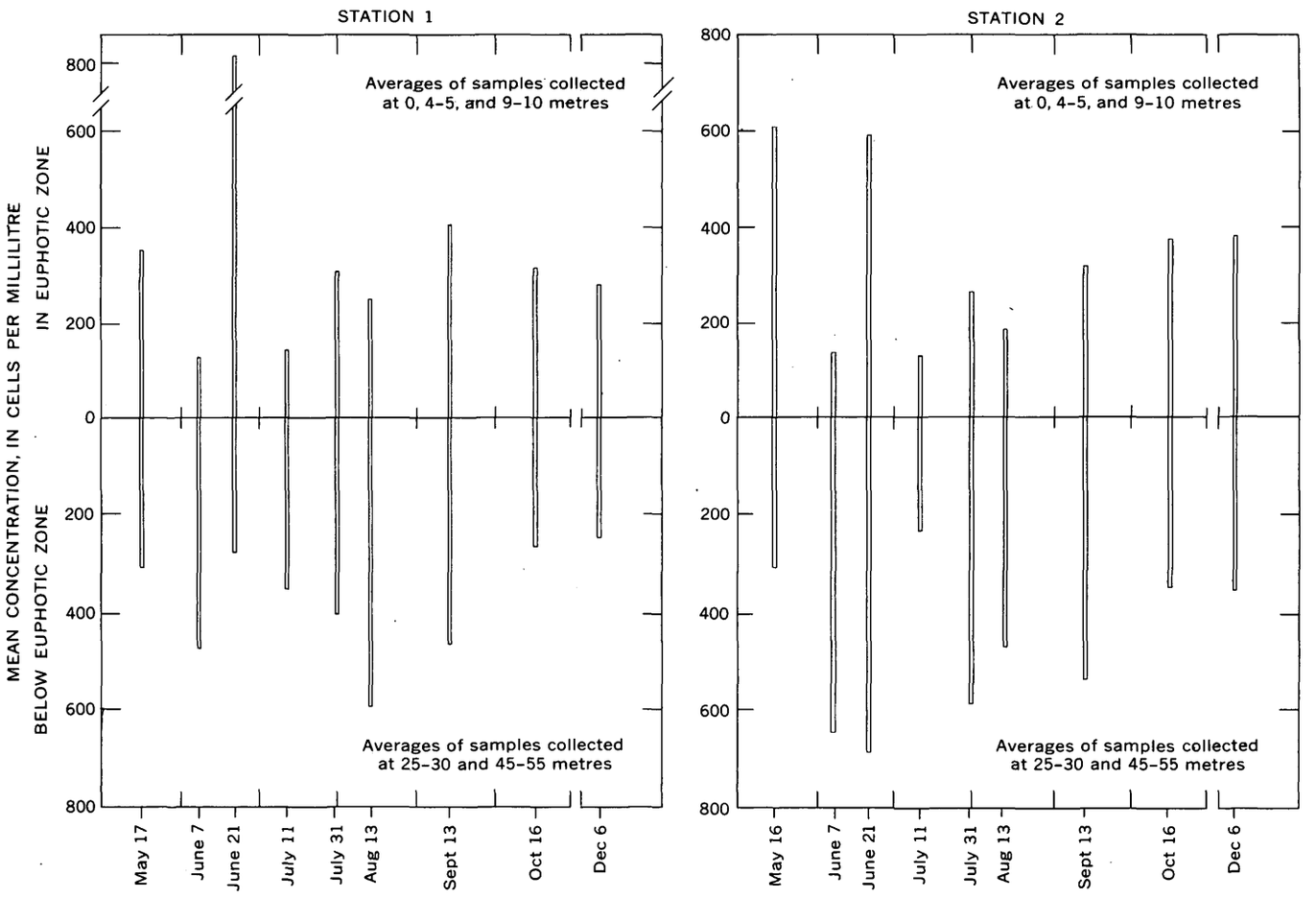

FIGURE 3.—Average phytoplankton concentration in and below the euphotic zone, 1973

concentration and types were not collected at the same depths that the primary productivity or chlorophyll-*a* measurements were made. However, in several instances the depths of collection were the same, permitting an analysis of phytoplankton concentration and primary productivity.

On May 17, the compensation depth (level) was 36 ft (11 m), resulting in a relatively shallow euphotic zone. The primary productivity profile for this date was markedly sharp, having a maximum rate of about 14 $(mgC/m^3)/d$ (milligrams of carbon per cubic metre per day) at the 16-ft (5-m) depth. A total of 93 $(mgC/m^2)/d$ (milligrams of carbon per square metre per day) was assimilated during the 24-hour period (table 4).

TABLE 4.—*Primary productivity (carbon assimilation rate)*

Date of measurement	Total carbon assimilation rate	
	$(mgC/m^2)/d$	$(mgC/m^2)/h$
May 17, 1973	93	9.5
Aug. 13, 1973	64	7.1
Oct. 16, 1973	56	7.7

Chlorophyll *a* sometimes may be correlated with phytoplankton biomass but in this study no relation could be found.

On May 17, a large amount of pollen, probably from the coniferous trees (primarily *Pinus* sp.) which surround the lake, was found on the water surface. Large concentrations of pollen also were found in water samples collected at several depths in the lake. The pollen could have had a shading effect and thus could be in part responsible for the shallow euphotic zone in the lake on May 17. Chlorophyll-*a* concentrations determined May 17 averaged three times higher than those obtained on the following two sample dates, indicating the presence of a large phytoplankton biomass in the euphotic zone.

The shapes of the primary productivity profiles for August 13 and October 16 are similar to each other. On August 13, the euphotic zone extended to the 80-ft (24-m) depth, which was twice the May 17 depth. The total carbon assimilated on August 13 was 64 $(mgC/m^2)/d$ (table 4). There were two primary pro-

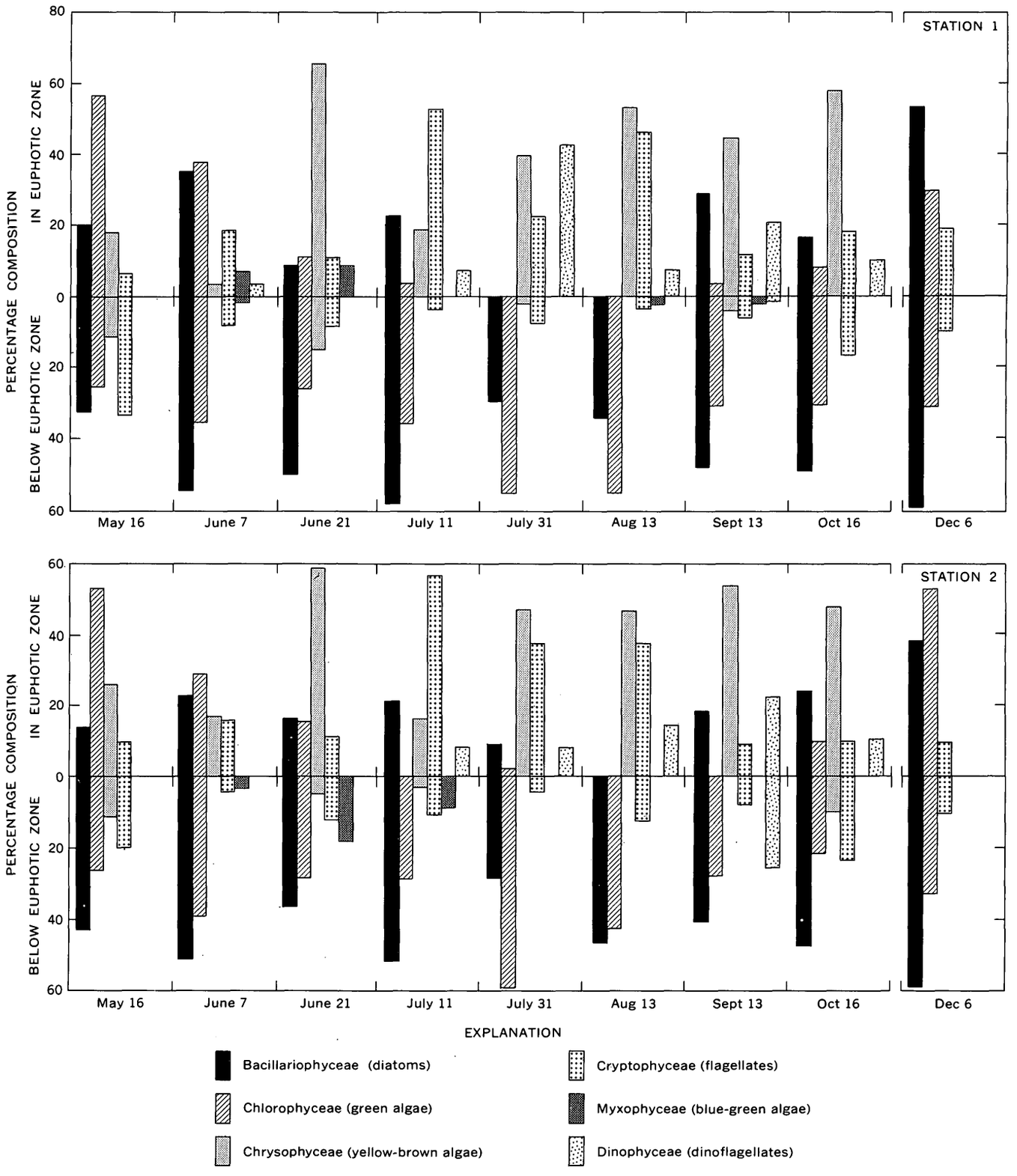

FIGURE 4.—Percentage composition of phytoplankton by class, in and below the euphotic zone, 1973.

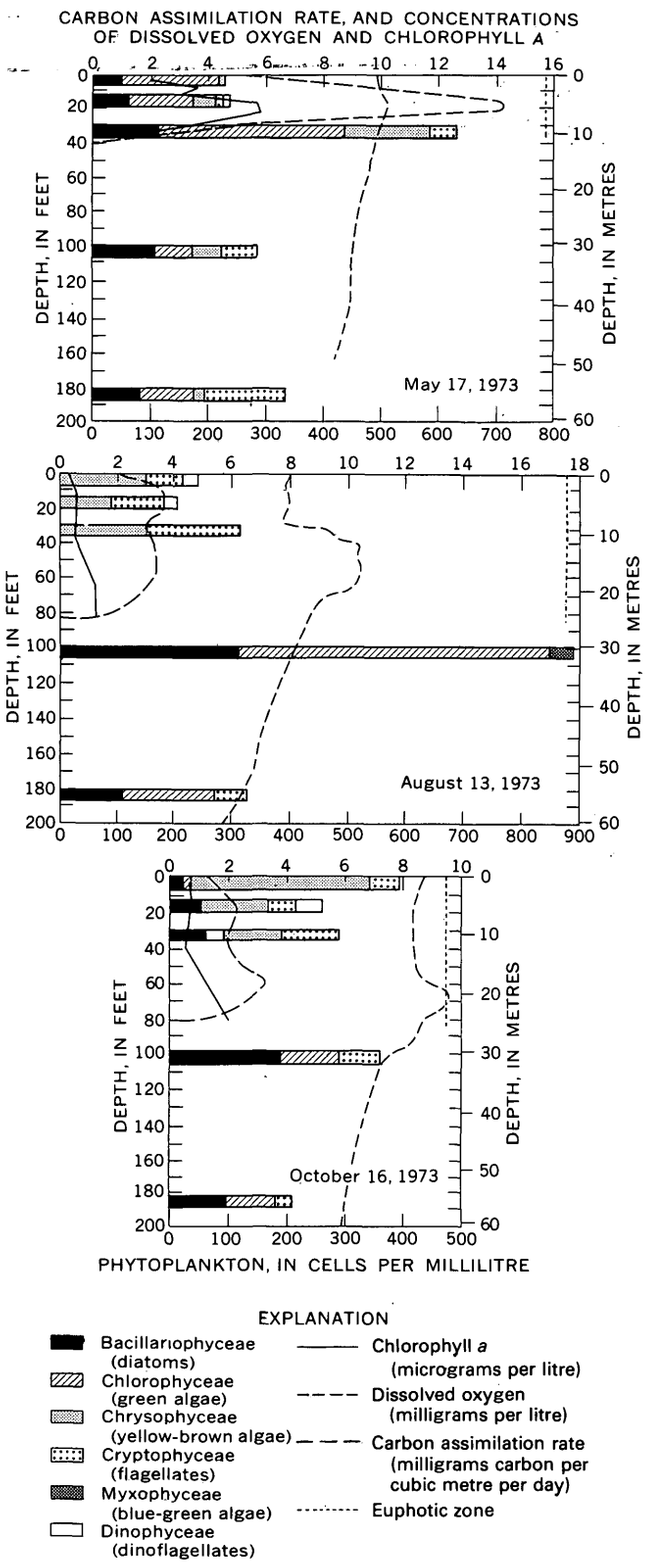

FIGURE 5.—Primary production (carbon assimilation rate), dissolved-oxygen and chlorophyll-*a* profiles, and phytoplankton concentrations, 1973.

duction peaks, the uppermost near the 16-ft (5-m) depth and the lowermost near the 60-ft (18-m) depth. The maximum chlorophyll-*a* concentrations were closely related to the maximum peaks of primary productivity, with a maximum chlorophyll-*a* concentration near the 68-ft (21-m) depth. The dissolved-oxygen maximum on August 13 corresponded closely to the lowermost primary productivity peak (near 60 ft or 18 m) but only slightly to the upper primary productivity peak (near 16 ft or 5 m).

The October 16 primary productivity profile also had two peaks, the uppermost near the 20-ft (6-m) depth, and the lowermost near the 58-ft (18-m) depth. Both peaks correlated with the chlorophyll-*a* curve. However, the maximum chlorophyll-*a* concentration was at the 79-ft (24-m) depth, which was near the compensation depth. Thus, though a high concentration of phytoplankton may have been present at this depth, low light levels reduced primary productivity. The maximum dissolved-oxygen value was at the 66-ft (20-m) depth, about 10 ft (3 m) below the depth of maximum primary productivity.

The total carbon assimilated on October 16 was 56 $(mgC/m^2)/d$. This value was similar to the August 13 primary productivity measurement of 64 $(mgC/m^2)/d$ (table 4), but only two-thirds the value of May 17.

DISCUSSION

The algal types in any lake may vary with season, and population shifts may take place gradually when a lake becomes enriched. The 1973 sampling of Donner Lake revealed some 25 or more phytoplankton genera and six classes. The samples probably included all the major classes present in the lake during the study period, but probably not all the genera.

In nearby Lake Tahoe, Goldman (1974, p. 129) listed over 160 species of phytoplankton, of which 129 species were routinely collected at an index sampling station. Of the 160 species, 112 were diatoms. The diatom *Asterionella formosa* was listed by Goldman (1974) as one of the 10 dominant species found in Lake Tahoe between 1967 and 1971. This species was also the most abundant diatom in Donner Lake. *Fragilaria crotonensis* was a dominant diatom in Lake Tahoe, but comprised less than 1 percent of the diatoms in Donner Lake. Of the nine diatoms found in Donner Lake, only five have been found in Lake Tahoe.

Neither the dominant green alga of Donner Lake, *Cryptomonas* sp., nor the two blue-green types have been reported in Lake Tahoe.

Overall, of the 25 algal genera found in Donner Lake, only 9 were reported to be present in Lake Tahoe

(Goldman, 1974). There is, of course, no compelling reason why the plankton flora of Donner Lake should duplicate that of Lake Tahoe. The results of this study indicate that Donner Lake has its own species composition of phytoplankton.

The lack of a significant number of blue-green algal taxa could indicate that Donner Lake is not eutrophic at this time (Edmondson, 1967), and the presence of the desmid *Cosmarium staurastroides* as a dominant phytoplankter in Donner Lake could support the contention that the Lake is oligotrophic (Nygaard, 1949). However, as Brook (1965) has warned, desmids have a wide rather than a narrow tolerance range of habitats, and may not always indicate unenriched conditions.

While Donner Lake is shallower, the ratio of depth of the euphotic zone to the maximum lake depth is similar to that reported by Kiefer and others (1972) for Lake Tahoe. Examination of the depth distribution of phytoplankton in Donner Lake above and below the euphotic zone indicates that the species composition was similar. This fact is shown in figures 3 and 4, especially in May and December, when the depth of the euphotic zone was similar (table 1). In May, thermal stratification in the lake was weak, and in December the lake was homothermous. Under these conditions there would be no thermal-density barrier to influence the vertical distribution of phytoplankton.

Gessner (1948) concluded that turbulence of water is the dominant factor in determining the sinking rate of phytoplankton cells. Under nonturbulent conditions, phytoplankton will sink much more rapidly than under turbulent conditions. Gessner also found that in the nonturbulent hypolimnion (neglecting internal waves), phytoplankton cells sink about ten times faster than in the wind-mixed and hence turbulent epilimnion. In a study of the vertical distribution of phytoplankton in the German Königsee, a deep but protected lake, Gessner (1948) found that most of the phytoplankton was below the metalimnion. In contrast, in the Würmsee, a large German lake unprotected from the wind, the phytoplankton populations were always greatest in the epilimnion, the zone of turbulence.

Donner Lake is probably between the Königsee and the Würmsee types of lakes from the standpoint of exposure to wind-induced mixing. Periods of calm occur at Donner Lake in the morning hours, a time when the phytoplankton cells could sink below the euphotic zone and into and below the metalimnion. In midafternoon, at least during the spring and summer, easterly winds are commonplace, causing turbulence in the epilimnetic water.

The vertical distribution of phytoplankton in Donner Lake was determined by collecting water samples at discrete depths. As a result, particular water masses having large concentrations of phytoplankton could have been missed. Nevertheless, the vertical distribution pattern was like that reported by Kiefer and others (1972) for Lake Tahoe; they found that the bulk of Lake Tahoe's phytoplankton crop was below the euphotic or lighted zone and below the metalimnion. At the time of their study, the euphotic zone in Lake Tahoe extended to the 280-ft (85-m) depth; the phytoplankton maximum was at the 330-ft (100-m) depth. A second phytoplankton mass was found at the 1,150-ft (350-m) depth.

Kiefer and others (1972) proposed that deep-water phytoplankton populations in Lake Tahoe (populations well below the euphotic zone) result from periods of high primary productivity in the euphotic zone, after which the cells gradually sink. This conclusion is based on the lack of productivity at a depth of 1,150 ft or 350 m (because light was limiting), low concentrations of organic substances in the deeper water, and the similarity of phytoplankton species in and below the euphotic zone. Oligotrophic lakes usually are cooler than eutrophic lakes, and have lower rates of secondary production. Consequently, the phytoplankton decomposition rate would be slow, and grazing by zooplankton would be lessened. As a result, a greater percentage of phytoplankton would be expected to sink in an oligotrophic lake.

From the work of Kiefer and others (1972) and Gessner (1948), the vertical phytoplankton distribution in Donner Lake can be explained by rather simple events—phytoplankton produced in the euphotic zone passively sinking below the euphotic zone and into the hypolimnion during periods when the water is calm.

On the basis of findings in known oligotrophic lakes (for example, Crater Lake, Ore. and Lake Tahoe), Kiefer and others (1972) mentioned and provided support for the contention that the presence of maximum phytoplankton populations in deep water is a common feature of oligotrophic lakes. If this is true, Donner Lake would be considered unenriched or oligotrophic from the standpoint of the vertical distribution of phytoplankton.

Primary productivity profiles for Donner Lake (fig. 5), except for the May 17 profile, are similar to other oligotrophic or mesotrophic lakes. Goldman and others (1973), Goldman (1974), Kiefer and others (1972), and Goldman and Armstrong (1969) described similar primary productivity profiles for Castle Lake and Lake Tahoe. A bimodal productivity profile as found

in Donner Lake on August 13 and on October 16 (fig. 5) is also found on the primary productivity profiles for Castle Lake and Lake Tahoe. The shape of the productivity profile on May 17 was similar to that of an enriched or eutrophic lake such as Clear Lake (Goldman, 1968). In Clear Lake, the productivity profile resulted from the presence of high concentrations of suspended inorganic sediment that restricted light penetration. In Donner Lake, pollen probably reduced light penetration during the May 17 sampling period and caused the shallow peak in the primary productivity profile.

Primary productivity rates in Donner Lake were 9.5, 7.1, and 7.7 $(mgC/m^2)/h$ on May 17, August 13, and October 16, respectively. Using the criteria presented by Goldman (1968) for assigning the trophic state of a lake based upon primary productivity measurements, Donner Lake would be considered unenriched or oligotrophic. Goldman (1968) considered Lake Vanda in Antarctica with a primary productivity rate of $1(mgC/m^2)/h$ as ultraoligotrophic. Castle Lake, Calif., had a primary productivity rate of about $70(mgC/m^2)/h$ and was considered as mesotrophic, or partly enriched (Goldman and others, 1973). In Castle Lake, the dissolved oxygen in the hypolimnion often becomes depleted in late summer, an event that does not occur in Donner Lake. Primary productivity values on an hourly basis were not given by Goldman (1968) for Lake Tahoe. However, on a daily basis, Goldman (1974) gives a range from 42 to 259 $(mgC/m^2)/d$ in Lake Tahoe. Daily primary productivity in Donner Lake ranged from 56 to 93 $(mgC/m^2)/d$, a range similar but perhaps slightly less than Lake Tahoe. In comparing the values of the three measurements made in Donner Lake to those in the literature, Donner Lake can be considered oligotrophic from the standpoint of primary production.

REFERENCES CITED

Brook, A. J., 1965, Planktonic algae as indicators of lake types, with special reference to the desmidiaceae: Limnology and Oceanography, v. 10, p. 403–411.

California Region Framework Study Committee, 1971, Comprehensive Framework Study, California Region; Appendix V—Water Resources: Pacific Southwest Inter-Agency Committee, Water-Resources Council, 339 p.

Dong, A. E., 1975, Limnological data for Donner Lake, California, November 1972 through December 1973: U.S. Geol. Survey open-file rept., 51 p.

Edmondson, W. T., 1967, Why study blue-green algae? *in* Environmental requirements of blue-green algae: U.S. Environmental Protection Agency, p. 1–6.

Gessner, Fritz, 1948, The vertical distribution of phytoplankton and the thermocline: Ecology, v. 29, p. 386–389.

Goldman, C. R., 1968, Aquatic primary productivity: Am. Zoologist, v. 8, p. 31–42.

——— 1974, Eutrophication of Lake Tahoe emphasizing water quality: U.S. Environmental Protection Agency Ecol. Research Ser., EPA–660/3–74–034, 408 p.

Goldman, C. R., and Armstrong, Richard, 1969, Primary productivity studies in Lake Tahoe, California: Verh. Internat. Ver. Limnologie, v. 17, p. 49–71.

Goldman, C. R., Stull, E. A., and de Amezaga, Evelyne, 1973, Vertical patterns of primary productivity in Castle Lake, California: Vehr. Internat. Ver. Limnologie, v. 18, p. 1760–1767.

Kiefer, D. A., Holm-Hansen, Osmund, Goldman, C. R., Richards, Robert, and Berman, Thomas, 1972, Phytoplankton in Lake Tahoe—Deep-living populations: Limnology and Oceanography, v. 17, no. 3, p. 418–422.

Nygaard, G., 1949. Hydrobiological studies of some Danish ponds and lakes II. The quotient hypothesis and some new or little known phytoplankton organisms: Kgl. Danske Vidensk. Selsk. Biol. Skr., v. 7, no. 1, 293 p.

Slack, K. V., Averett, R. C., Greeson, P. E., and Lipscomb, R. G., 1973, Methods for collection and analysis of aquatic biological and microbiological samples: U.S. Geol. Survey Techniques Water-Resources Inv., book 5, chap. A4, 165 p.

Strickland, J. D. H., and Parsons, T. R., 1968, A practical handbook of seawater analysis: Fisheries Research Board Canada Bull. 167, 311 p.

RECENT PUBLICATIONS OF THE U.S. GEOLOGICAL SURVEY

(The following books may be ordered from the Branch of Distribution, U.S. Geological Survey, 1200 South Eads Street, Arlington, VA 22202 (an authorized agent of the Superintendent of Documents, Government Printing Office). Prepayment is required. Remittances should be sent by check or money order payable to U.S. Geological Survey. Give series designation and number, such as Bulletin 1368–A, and the full title. Prices of Government publications are subject to change. Increases in costs make it necessary for the Superintendent of Documents to increase the selling prices of many publications offered. As it is not feasible for the Superintendent of Documents to correct the prices manually in all the previous announcements and publications stocked, the prices charged on your order may differ from the prices printed in the announcements and publications)

Professional Papers

P 576–D. Sedimentary rock alteration in the Slick Rock district, San Miguel and Dolores Counties, Colorado, by D. R. Shawe. 1976. p. D1–D51; plates in pocket. $3.

P 680–F. Late Cenozoic Ostracoda from Midway Island drill holes, by J. C. Holden. 1976. p. F1–F43; 17 plates. $1.90.

P 729–E. Late Quaternary vegetation history of the Yellowstone Lake basin, Wyoming, by R. G. Baker. 1976. p. E1–E48; 10 plates. $1.90.

P 813–H. Summary appraisals of the Nation's ground-water resources—Arkansas-White-Red Region, by M. S. Bedinger and R. T. Sniegocki. 1976. p. H1–H31. 85¢.

P 840. Descriptions and analyses of eight new USGS rock standards, compiled and edited by F. J. Flanagan. 1976. 192 p. $3.10.

P 882. Recent surface movements in the Baldwin Hills, Los Angeles County, California, by R. O. Castle and R. F. Yerkes. 1976. 125 p.; plates in pocket. $7.50.

P 899. The karst landforms of Puerto Rico, by W. H. Monroe. 1976. 69 p.; plate in pocket. $1.80.

P 907–D. Fluid-inclusion petrology—Data from porphyry copper deposits and applications to exploration, by J. T. Nash. 1976. p. D1–D16. 65¢.

P 911. Historical review of the international water-resources program of the U.S. Geological Survey 1940–70, by G. C. Taylor, Jr. 1976. 146 p. $2.90.

P 915. Plutonic rocks of the Santa Rita Mountains, southeast of Tucson, Arizona, by Harald Drewes. 1976. 75 p. $1.95.

P 919. Volcanic suites and related cauldrons of Timber Mountain–Oasis Valley caldera complex, southern Nevada, by F. M. Byers, Jr., W. J. Carr, P. P. Orkild, W. D. Quinlivan, and K. A. Sargent. 1976. 70 p. $1.90.

P 929. ERTS–1, a new window on our planet, edited by R. S. Williams, Jr., and W. D. Carter. 1976. 362 p. $13.

P 931. Geology of the northern part of the Toquima Range, Lander, Eureka, and Nye Counties, Nevada, by E. H. McKee. 1976. 49 p.; plates in pocket. $1.45.

P 969. Some engineering geologic factors controlling coal mine subsidence in Utah and Colorado, by C. R. Dunrud. 1976. 39 p. $1.25.

P 972. Correlation of late Cenozoic tuffs in the central Coast Ranges of California by means of trace- and minor-element chemistry, by A. M. Sarna-Wojcicki. 1976. 30 p. 85¢.

P 974. Type sections and stratigraphy of the members of the Blackleaf and Marias River formations (Cretaceous) of the Sweetgrass Arch, Montana, by W. A. Cobban, C. E. Erdmann, R. W. Lemke, and E. K. Maughan. 1976. 66 p. $1.70.

P 976. Molluscan paleontology of the lower Miocene Clallam Formation, northwestern Washington, by W. O. Addicott. 1976. 44 p., 9 plates. $1.75.

P 983. The structure of a turbulent flow in a channel of complex shape, by H. J. Tracy. 1976. 24 p. 65¢.

P 990. Numerical model of the salt-wedge reach of the Duwamish River estuary, King County, Washington, by E. A. Prych, W. L. Haushild, and J. D. Stoner. 1976. 34 p. $1.05.

P 1002. The Guatemalan earthquake of February 4, 1976, A preliminary report, by A. F. Espinosa, editor. 1976. 90 p. $2.20.

P 1005. Lithium resources and requirements by the year 2000, edited by J. D. Vine. 1976. 162 p. $2.90.

P 1006–A,B. Demand and supply of nonfuel minerals and materials for the United States energy industry, 1975–90–A preliminary report. A, Demand for nonfuel minerals and materials by the United States energy industry, 1975–90, by J. P. Albers, W. J. Bawiec, and L. F. Rooney. p. A1–A19. B, Supply of nonfuel minerals and materials for the United States energy industry, 1975–90, by G. H. Goudarzi, L. F. Rooney, and G. L. Shaffer, 1976. p. B1–B37. $1.70.

Bulletins

B 1385–E. Mineral resources of the Eagle Cap Wilderness and adjacent areas, Oregon, by P. L. Weis, J. L. Gualtieri, W. F. Cannon, E. T. Tuchek, A. B. McMahan, and F. E. Federspiel, *with a section on* Aeromagnetic survey, by W. E. Davis. 1976. p. E1–E100; plates in pocket. $1.60.

B 1405–I. Paleozoic and Mesozoic stratigraphy of the northern part of the Ruby Range, southwestern Montana, by R. G. Tysdal. 1976. p. I1–I26. 55¢.

B 1413. The Columbia River basalt group in the Spokane quadrangle, Washington, Idaho, and Montana, by A. B. Griggs, *with a section on* Petrography, by D. A. Swanson. 1976. 39 p.; plate in pocket. $1.95.

B 1419. Annotated bibliography of the geology of selenium, 1958–74, by C. A. Gent. 1976. 49 p. 80¢.

Water-Supply Papers

W 1817–F. Organic carbon and nitrogen concentrations and annual organic carbon load of six selected rivers of the United States, by R. L. Malcolm and W. H. Durum. 1976. p. F1–F21. 45¢.

W 2038. Hydrology and environmental aspects of Erie Canal (1817–99), by W. B. Langbein. 1976. 92 p. $1.20.

W 2039–B. An appraisal of ground water for irrigation in the Appleton area, west-central Minnesota, by S. P. Larson. 1976. p. B1–B34; plates in pocket. $2.60.

W 2130. Surface-water supply of the United States, 1966–70—Part 11., Pacific slope basins in California—Volume 3. Southern Central Valley basins. 1976. 670 p. $5.25.

U.S. GOVERNMENT
PRINTING OFFICE
PUBLIC DOCUMENTS DEPARTMENT
WASHINGTON, D C 20402

OFFICIAL BUSINESS
PENALTY FOR PRIVATE USE $300

POSTAGE AND FEES PAID
U.S. DEPARTMENT OF THE INTERIOR
INT 413

U.S.MAIL

Special
fourth-class
rate books

CHIEF PLANS & PROGRAMS DEV
TOPO DIVISION USGS
NATIONAL CENTER STOP 512
RESTON VA 22092

D